Modeling of ultrafast laser-induced magnetization dynamics within the Landau-Lifshitz-Bloch approach

Unai Atxitia Macizo

Advisor: Dr. Oksana Fesenko Morozova (Chubykalo-Fesenko)

Department Condensed Matter, Universidad Autonoma de Madrid

Tutor: Dr. Farkhad Aliev Kazanski

A thesis submitted for the degree of

PhilosophiæDoctor (PhD), in Physics,

2012 June

To my parents.

Resumen

La tecnología actual de almacenamiento magnético requiere de avanzados dispositivos basados en complejas nanoestructuras, diseñadas para alcanzar campos suficientemente bajos de conmutación manteniendo la estabilidad térmica. Uno de los mayores problemas es la velocidad de escritura de la información. En las conmutaciones convencionales basadas en la aplicación de un campo magnético externo, el tiempo de conmutación es una función lineal de dicho campo. En principio podríamos pensar que la velocidad de la conmutación está, entonces, limitada por la magnitud máxima del campo externo que pueda conseguirse. Sin embargo, recientemente se ha demostrado que la inversión de la imanación determinista mediante campo externo no es posible por debajo de los 2 picosegundos [156].

Los recientes experimentos con potentes pulsos láser de anchuras temporales de varias decenas de femtosegundos [19] han abierto la puerta a inversiones de imanación por debajo del picosegundo [134, 157]. En aleaciones de GdFeCo se ha observado una inversión lineal de la imanación [157]. Así es como se ha denominado al nuevo mecanismo responsable de la inversión en un tiempo de 700 femtosegundos. Este nuevo límite ha impulsado el desarrollo de complejos modelos númericos capaces de describir la respuesta magnética de este tipo de materiales. Estos modelos han permitido la predicción de un estado transitorio de orden ferromagnético en estas aleaciones que están acopladas antiferromagnéticamente [134], así como la inversión de la imanación sin ningún tipo de estímulo externo diferente del calentamiento producido por el láser [**?**].

Sin embargo, los mecanismos fundamentales detrás de estos nuevos fenómenos siguen aun sin ser completamente comprendidos. El conocimiento de tales mecanismos es crucial para el control de tan interesantes procesos y por tanto el desarrollo de tecnología basada en ellos. Uno de los objetivos de esta tesis es el desarrollo de modelos teóricos más descriptivos que ayuden a la comprensión de los mecanismos detrás de este tipo de fenomenos.

Desde el punto de vista fundamental, el proceso de desimanación en femtosegundos ocurre en condiciones extremas de desequilibrio, implicando a los electrones, fonones y espines. Los modelos fenomenológicos que implican ecuaciones en términos de las temperaturas correspondientes a las distribuciones transitorias de los electrones, fonones y sistema de espines han sido muy exitosos a la hora

de describir la desimanación en escalas de tiempos ultrarrápidas. El modelo que describe la dinámica de no equilibrio entre los electrones y fonones, denominado modelo de 2 temperaturas (2T), es muy sólido, y ha sido comprobado experimentalmente múltiples veces. Sin embargo, los cambios de imanación en estas escalas de tiempo muchas veces no pueden ser descritos por una temperatura del sistema de espines [95]. La dinámica de la imanación deber ser, entonces, descrita por modelos termodinámicos apropiados acoplados al modelo de 2T.

En la descripción "coarse-grain", las fluctuaciones del sistema de espín están incluidas en el macroespín térmico. En esta tesis introducimos un novedoso modelo micromagnético basado en la ecuación de Landau-Lifshitz-Bloch (LLB) [64]. En este modelo se ha obtenido analíticamente el promedio térmico de las fluctuaciones de espín de alta energa en frecuencias de THz mediante la aproximación de campo medio. En la presente tesis se ha propuesto por primera vez el acoplo del modelo de 2T a la ecuacion de LLB. Actualmente, este el único modelo capaz de simular computacionalmente desimanaciones ultrarrápidas en nanoestructuras magnéticas, es decir hasta varias micras de dimensiones espaciales. Esto modelo ha demostrado esencialmente que la desimanación ultrarrápida puede verse como un proceso termodinámico donde los electrones y los fonones son interpretados como baños térmicos que intercambian energía con el sistema de espines.

Antes de lidiar con la modelización de las aleaciones ferrimagnéticas GdFeCo, compuestas de dos redes ferromagnéticas (Gd y FeCo) antiferromagnéticamente acopladas, hemos comenzado estudiando materiales en principio más simples como son los metales ferromagnéticos Ni, Fe o Co [19]. En esta tesis nos hemos centrado en el metal de transición Ni, ya que gracias a una colaboración internacional con el grupo liderado por el Prof. M. Münzenberg en la Universidad de Göttingen (Alemania) hemos tenido acceso a datos experimentales con los que comprobar la validez de nuestro modelo. Experimentalmente, en estos metales de transición sólamente se ha observado una desimanción ultrarrápida del orden de cientos de femtosegundos seguida de una reimanación a su estado inicial de equilibrio. Nuestro modelo ha sido capaz de describir ambas dinámicas dando sentido físico a las observaciones experimentales.

Por otro lado, en tierras raras, como el Gd o el Tb se ha observado que la desimanación procede en dos etapas, una ultrarrápida con un tiempo característico de 1 picosegundo seguida de una más lenta, de decenas de picosegundos, es decir, mucho más lenta que en los metales de transición [169]. En el estudio de tierras raras, del mismo modo que hicimos con los metales de transición, hemos escogido modelar la tierra rara Gd, dado que gracias a una colaboración con el grupo liderado por el Prof. U. Bovensiepen en la Universidad de Duisburg-Essen

(Alemania) hemos tenido acceso a datos experimentales con los que comparar y validar nuestro modelo.

Debe mencionarse que sólo en algunos materiales ferrimagnéticos como el CoFeGd se ha descrito el control de conmutación (y no de desimanación) en la escala de tiempo del femtosegundo [157]. Lamentablemente, la ecuación de LLB para materiales ferromagnéticos no puede describir materiales compuestos por dos redes magnéticas, como por ejemplo la aleación ferrimagnética GdFeCo, donde, además de la conmutación ultrarrápida, se ha observado una dinámica distinta para cada red. En esta tesis hemos derivado, de manera similar al caso ferromagnético, una ecuación de LLB para materiales ferrimagnéticos. Este modelo nos ha permitido estudiar los tiempos característicos de estos sistemas y lo hemos propuesto como modelo para la dinámica ultrarrápida en sistemas compuestos de dos redes magnéticas.

El objetivo de esta tesis ha sido por tanto, avanzar en el conocimiento de los procesos microscópicos relevantes que se producen en la escala de tiempo del femtosegundo incluyendo la dinámica de los electrones, fonones y las ondas de espines de frecuencia THz. Esto nos ha permitido comprender las velocidades de desimanación ultrarrápidas: la desimanación a fs, la recuperación a ps y la amortiguación precesional a 100 ps.

En resumen, en la presente tesis hemos realizado el siguiente trabajo:

- Desarrollo de modelos de la dinámica de la imanación válidos en todo el rango de temperaturas. El modelo está basado en la ecuación LLB para materiales ferromagnéticos y en el modelo 2T para la evolución temporal de las temperaturas electronicas y de la red.

- Comparación del modelo con experimentos de velocidad de desimanación ultrarrápida en Ni y Gd, permitiendo dar sentido físico a las velocidades de desimanación ultrarrápidas.

- Desarrollo del modelo macroscópico para materiales ferrimagnéticos y antiferromagnéticos. El modelo está basado en los mecanismos térmicos; está derivado de forma similar a la ecuación LLB para materiales ferromagnéticos y verificado mediante simulaciones atomísticas, para después aplicarlo los parametros especificos del material ferrimagnético GdFeCo.

- Introducimos el modelo de calculos atomísticos correlaciones temporales en el ruido térmico (ruido coloreado). A partir de este nuevo modelo atomístico generalizamos el modelo micromagnético basado en la ecuación LLB para ruido blanco en un modelo LLB para ruido coloreado.

Contents

1 Introduction and Motivation **1**

1.1 Introduction 1
1.2 Ultrafast magnetization reversal 7
1.3 The challenge of modeling of ultrafast magnetization dynamics . . 10
1.4 About this thesis 12

2 Modeling of ultrafast laser-induced magnetization dynamics: Theoretical Background **15**

2.1 Modeling of electron and phonon dynamics 16
2.2 Magnetization dynamics: Landau-Lifshitz-Gibert equation 24
2.2.1 LLG-Langevin equation: stochastic magnetization dynamics 25
2.2.2 Atomistic LLG Langevin simulations 27
2.3 Magnetization dynamics: Landau-Lifshitz-Bloch equation 28
2.3.1 Dynamics of a macrospin 29
2.3.2 Stochastic LLB equation 32
2.3.3 Multi macro-spin micromagnetic model 34
2.4 Multiscale modeling of magnetic materials 35
2.5 Ultrafast laser-induced demagnetization within the LLB model . . 37
2.6 Ultrafast laser-induced magnetization precession 38

3 Modeling of ultrafast magnetization dynamics in Nickel **41**

3.1 Introduction and Motivation 41
3.2 Absorbed power as a function of film thickness 42
3.3 Magnetization dynamics model 45
3.4 Two temperature model parametrization from experimental reflectivity 47
3.5 Comparison between experiment and modelling 51
3.6 Discussion 53
3.7 Conclusions 54

4 Ultrafast magnetization dynamics using the quantum version of LLB equation **57**
4.1 The Landau-Lifshitz-Bloch model with quantum spin number S. . 59
4.2 Modeling of the laser-induced ultrafast demagnetization within the quantum LLB 61
4.2.1 M3TM versus LLB model 62
4.2.2 Diversity of magnetization dynamics within the LLB model 64
4.3 Linking different timescales 67
4.4 Discussion 69
4.5 Conclusions 70

5 Modeling of laser-induced demagnetization in Gd **73**
5.1 Experiment 75
5.2 Model Hamiltonian 77
5.2.1 Two temperature model: electron and phonon temperature dynamics 77
5.2.2 Many LLB-macrospin model 78
5.2.3 Spin-phonon interaction Hamiltonian 81
5.2.4 Spin-carriers interaction Hamiltonian 84
5.2.5 Demagnetization via electron scattering in Gd: phenomenological model 86
5.2.6 Inclusion of spin-phonon interaction 88
5.2.7 Comparison with M3TM model 90
5.2.8 Long timescale demangetization 90
5.3 Discussion and outlook 91
5.4 Conclusions 93

6 The Landau-Lifshitz-Bloch equation for ferrimagnet **95**
6.1 Introduction 95
6.2 Atomistic model 97
6.3 Mean Field Approximation for Ferrimagnet 98
6.4 LLB equation for classical ferrimagnet 103
6.4.1 Temperature dependence of damping parameters 106
6.4.2 Longitudinal relaxation parameters 109
6.4.3 The LLB equation and the Baryakhtar equation 113
6.4.4 Relaxation of sublattices 115
6.4.5 Ultrafast precessional switching 117
6.4.6 On the possibility to derive LLB equation above T_c 117
6.5 Conclusions 119

7 Temperature-dependent Normal Modes in a Two-component Magnet 121
7.1 Introduction . . . 121
7.2 Precession modes in Ferrimagnets . . . 125
7.2.1 Zero damping approximation . . . 126
7.2.2 Damping contribution to transverse mode frequency . . . 128
7.3 Longitudinal modes in two-component systems . . . 131
7.3.1 Eigenproblem for longitudinal motion in ferrimagnets . . . 131
7.3.2 Eigenvalues for longitudinal motion in ferrimagnets . . . 133
7.3.3 Comparison with atomistic simulations . . . 140
7.4 Conclusions . . . 142

8 Ultrafast spin dynamics: the effect of colored noise 143
8.1 Ornstein-Uhlenbeck process . . . 144
8.2 Atomistic colored noise approach . . . 146
8.3 Relaxation times . . . 149
8.4 Generalized macroscopic equation . . . 151
8.5 Conclusions . . . 156

Appendix 143

A Heisenberg Hamiltonian and the mean field approximation 159
A.1 Heisenberg Magnetic Hamiltonian . . . 159
A.2 Mean-Field Approximation for the Heisenberg model . . . 160

B Stochastic Methods 163
B.1 General case . . . 163
B.2 Dynamical equations for the averages: macroscopic equation . . . 164
B.3 FPE for the classical LL Langevin equation. . . . 165

C One Spin LLB equation 167

D Micromagnetic exchange stiffness 175

References 179

List of publications of U. Atxitia 194

Acknowledgement 198

1

Introduction and Motivation

1.1 Introduction

The dynamical change of magnetization can take place in a very wide range of time scales. The Earth has a magnetic field which polarization reverses in a time scale of billion of years (1 billion year $\approx 3 \times 10^{16}$ seconds) due to geological events while the exchange interaction between spins leads to the femtosecond (10^{-15} seconds) spin dynamics. Though both of them have time scales far beyond the human sensitivity, the science has made possible the measurement of these two extreme types of **magnetization dynamics**. At the same time the Earth is like a magnet, and can orient a compass needle leading to one of the most old and well-known magnetization dynamics examples. Incredible as it may seem actual magnetic data recording in hard-drive disks is still based in the same mechanism as a compass does. Thus, the application of an external magnetic field is an easy way to manipulate and, in particular, to reverse the magnetization of a medium, from a needle to a nanometer size magnetic bit.

When an external magnetic field $\mathbf{H}$ is applied non-collinear to the magnetic moment direction $\boldsymbol{\mu}$ then a torque $\mathbf{T} = \boldsymbol{\mu} \times \mathbf{H}$ acts upon the magnetic moment so we may write the rate of change of angular momentum with time,

$$\frac{d\boldsymbol{\mu}}{dt} = -\gamma \boldsymbol{\mu} \times \mathbf{H}. \tag{1.1}$$

The value of $\gamma = 1.76 \times 10^7 \text{rad s}^{-1}\text{Oe}^{-1}$ is defined as the ratio of the magnetic moment to the angular momentum and it is called the **gyromagnetic ratio**. The solution of equation (1.1) describes the so-called **precession motion** of the magnetization around the direction of the applied field with the Larmor frequency $\omega_{\text{Larmor}} = \gamma H$, thus, the magnetic field driven magnetic precession has a GHz time scale for achievable magnetic fields. As example, in actual magnetic devices the

magnetization is reversed using magnetic fields as large as $1T = 10^4$Oe with a characteristic timescale of nanoseconds [153].

Although it has been shown that adequate magnetic field pulses can fast up this process down to hundred picosecond time scale via the so-called precession switching [14], recent experiments using relativistic electron bunches from Standford Linear Accelerator (SLAC) to generate short magnetic field pulses up to 3T showed that deterministic magnetization reversal does not take place if the pulse is shorter than 2ps (3T strength) [156]. Moreover, a well defined and strong enough magnetic field pulse generation with duration below 100 ps is still a challenge in nowadays devices.

In this limit, around 100 ps, the excitation of faster magnetic response requires the excitation of the spin-orbit coupling. The spin-orbit interaction is the responsible of the coupling between the orbital angular momentum **L** and the spin **S** (LS coupling). The LS coupling mediates the spin-lattice interaction, i.e. the angular momentum transfer between them. Thus, promoting the transfer of angular momentum from the spin to orbital degree of freedom a faster magnetization loss could be achieved. Unfortunately, the spin-orbit coupling time scale ranges from tens of picosecond to hundreds of picoseconds.

Therefore, the investigations of fundamentally different mechanisms to modify magnetization faster than sub-nanosecond time scale are actively conducted. For example, the excitation of the magnetization by a spin-polarized current was proposed by Berger [20] and Slonczewski [145], the so-called spin-torque transfer effect. Data storage devices based on this effect have become very promising because they get rid of mechanical spinning of conventional magnetic hard-disk devices and the speed of magnetization manipulation is fasten up to sub-nanosecond timescale. Nevertheless, the magnetization reversal time is still far above 100 ps. The latter timescale has been proposed [153] to be the limit below which the processes in a magnetic medium can be referred to as **ultrafast magnetization dynamics**.

In 1996 Beaurepaire *et al.* [19] have shown that Ni could be demagnetized by a 60 fs laser pulse (see Fig. 1.2) showing the magnetic response on timescale below 1ps, i.e. beyond the timescale of the spin-orbit interaction. Since then, manipulating and controlling magnetization with ultrafast laser pulses have become a new field in modern magnetism that is referred to as **femtosecond magnetism** [3, 19, 82, 142, 173].

After this first observation, many experimental efforts were done to confirm this finding in Nickel [82, 142] as well as in very wide range of magnetic materials, for example, other transition metals (Fe [36] or Co [162]), magnetic semiconductors [167], dielectrics [101] and half-metals [63]. However, the work done by

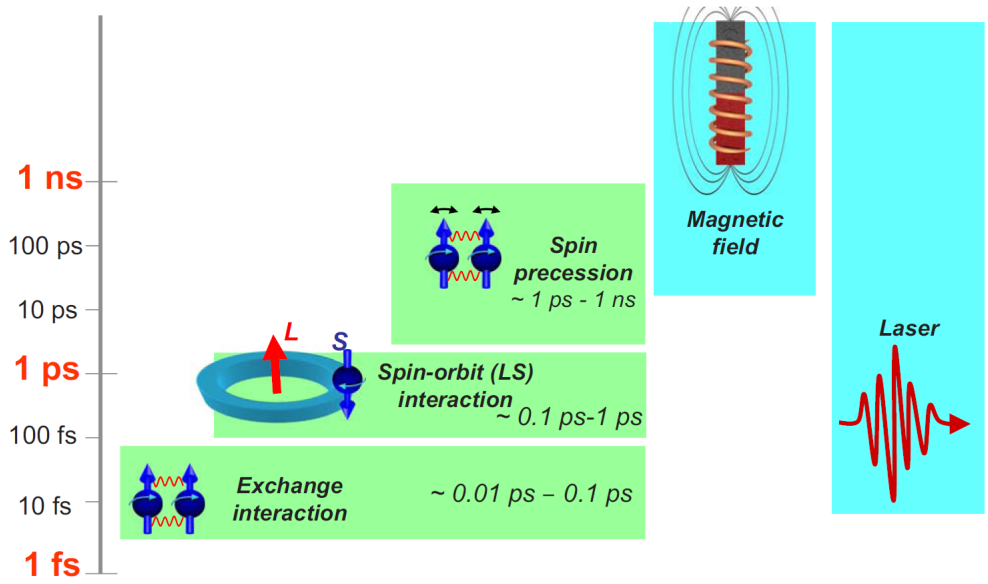

Figure 1.1: Time scales in magnetism as compared to magnetic field and laser pulse excitation. Figure taken from Ref. [102].

Beaurepaire *et al.* [19] was not the first attempt to excite and probe the spin system dynamics using fast laser pulses. In 1984 Agranat *et al.* [5] were not successful in observing any magnetic effect in Ni using sub-nanosecond laser pulses. Nowadays, it seems obvious that the problem was that the laser pulse was of the same duration or even longer that the characteristic timescales. Although this limitation was present, it was possible to estimate that the spin-lattice relaxation time in Gd thin films was around 100 ± 80ps [160] in agreement with theoretical estimations [86]. At this time scales all the subsystems were in thermodynamics equilibrium with each other and therefore the system response followed the excitation profile. Consequently, a much shorter excitation and probe were required to observe the ultrafast magnetization dynamics.

The femtosecond manipulation of the magnetization makes use of powerful femtosecond laser pulses to induce an instantaneous change of the magnetization of both the length and orientation of the magnetization vector [24, 158, 162]. The measurement of theses magnetization changes are probed with a much less powerful second laser pulse which defines the temporal resolution, using pump-probe magneto-optical techniques [19] based on Kerr or Fadaray effects. Other time-resolved techniques are also employed: second harmonic generation [72, 82,

135], photo-emission [3, 142] and more recently x-ray magnetic circular dichroism [148].

These experiments have attracted many researchers with the aim of understanding both the fundamental mechanisms and the control of the magnetic properties of materials on the femtosecond timescale [102]. However, even for the simplest itinerant ferromagnets, such as Ni, the underlying elementary mechanisms leading to the macroscopic demagnetization on the femtosecond time scale have not yet been identified. The challenge lies in the complexity of a parallel, dynamic treatment of photons, electrons, phonons and the spins on various length and time scales.

Beaurepaire and co-workers [19] explained the observed loss of the magnetic order caused by the interaction of a laser pulse with Ni thin films on the basis of a so-called phenomenological **three temperature model** (3TM). The 3TM assumes that the energy from the laser pump pulse is mainly absorbed by the electron system which is described by a temperature T_e. This is a reasonable assumptions: first, in the spectral range where the laser pulse works the direct deposition of photon energy is only efficient in electron system [153], direct excitation of phonons would require far infrared spectral range [**?**], and second, femtosecond pump-probe photo-emission experiments have showed that the hot electrons follow a quasi equilibrium Fermi distribution [26]. The excess of energy in the electron system is then redistributed into the phonon and spin systems also described in terms of temperatures. Within this model the magnetization reduction is considered in terms of an increase of the spin temperature due to energy transfer to the spin system via electron-spin or/and phonon-spin interactions.

It has been shown that the introduction of the spin temperature is not adequate [97] since the spin system is not in the quasi-equilibrium on the femtosecond timescale. It has been suggested to couple the spin dynamics to the two-temperature (2T) model for phonon and electron temperatures [10, 11, 95, 96, 97]. These models are also based on the energy flow picture and leave unidentified the angular momentum transfer mechanism and the underlying quantum mechanism responsible for the spin flip [11]. However, the thermal excitations which disorder the spin system have to arise from a microscopic spin-flip process, acting on a femtosecond timescale.

Several contributions are currently under debate: (i) phonon-assisted spin flips (phonon mediated Elliott-Yafet (EY) processes) that transfer angular momentum from the magnetization to the lattice [105]; (ii) hot electron mediated spin flips at hot spots of the electronic band structure originating from spin-orbit interaction [11, 130, 140, 166] and electron-electron EY scattering [109]; (iii) laser-induced transport processes that essentially drive spin polarization of the

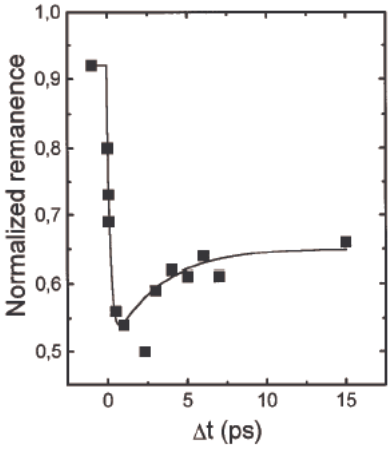

Figure 1.2: Ultrafast demagnetization in ferromagnetic Nickel induced by a 60 fs laser pulse. Figure taken from seminal work of Beaurepaire *et al.* [19].

conduction electrons [18, 121]. The spin system also contributes to the observed demagnetization rates, slowing them down at elevated temperatures $T \to T_C$ (T_C is the Curie temperature) via the spin-spin interaction and critical slowing down effects [97].

Depending on the characteristics of the system the demagnetization can occur via electron-spin, lattice-spin or electron-lattice-spin coupling. In transition metals, the elementary scattering events in a quantum description can be divided into two processes, sketched in Fig. 1.3, that are seen to be the most relevant. The first candidate is the Elliott-Yafet [56, 109, 152, 171] process. It makes use of the fact that due to spin-orbit interaction the spin of the electron is not a good quantum number anymore and, as a consequence, intermixes the spin channels at some high symmetry points of the band structure. If the electrons, heavily excited by the energy input of the intense femtosecond laser pulse, are scattered into these spin hot spots in the Fermi surface (by defects, phonon scattering events etc.), the final state has a certain probability to be of opposite spin direction. A spin-mixing can be calculated and is a factor of twenty higher in Ni than in Cu, which explains the observed time scales in femtosecond spin dynamics [152]. This first elementary scattering mechanism reduces the total magnetization. The first theoretical calculations of such EY scattering events in transition metals performed by Steiauf and Fahnle in Ref. [152] suggested that EY was a sufficient mechanism to explain the observed magnetization loss but recently Karva *et al.* [**?**] using a more accurate approach have concluded that the EY process is clearly inefficient mechanism. This particular contradiction indicates that the degree of understanding nowadays is insufficient to get a valid response.

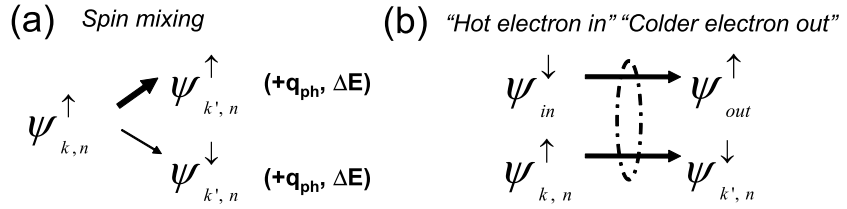

Figure 1.3: Schematics of the spin-flip processes. (a) Elliott-Yafet process of an electron-scattering event with a phonon to an unoccupied intraband band state is depicted. The spin-orbit interaction intermixes the spin channels in some points of the band structure. In the final state a certain probability of a reversed spin is given. The phonon takes energy and momentum from the electron system. (b) Exchange scattering of a hot electron which in effect exchanges the spin orientation of the hot electron and the locally remaining electron at lower energy. Figure taken from Ref. [11].

The second process which is currently discussed is the electron-electron scattering mediated by exchange interaction [15, 85]. It is suggested to be a dominant spin-scattering contribution at higher energies [85]. An electron at around the Fermi level is excited by an incoming hot electron of opposite spin direction. While the hot electron relaxes to an unoccupied state at the Fermi level, the second electron takes up the energy of the hot electron. After the scattering process both have exchanged their spin orientation, a process well known from spin-polarized electron energy loss spectroscopy (SPEELS) [132]. In this second case, as long as the hot electron remains in the ferromagnet, the total magnetization is not reduced as can be seen in Fig. 1.3. However in both cases an electron with opposite spin remains at around the Fermi level. The excited spin state will not be stable in its environment and will further decay into spin excitations of lower energy [**?**]. The subsequent relaxation path of this Stoner-like excitation can be pictured as follows: from the localized Stoner process, described in a Hubbard-like model band, a propagator can be constructed equivalent to a delocalized magnon and both can be transformed into each other [55]. This results into multiple interaction channels and allows different relaxation paths in a broad energy range where both the spin-wave dispersion and the single particle excitation spectrum overlap (for energies larger than $\Delta_{\mathrm{ex}} - E_{\mathrm{F}}$), suggesting an important role in the spin relaxation process.

The rare-earth metal Gd is an important example of the diversity of different materials since its response to fs laser excitation has been experimentally reported to be slower than in transition metals [160, 169]. Several mechanisms for ultrafast demagnetization in Gd have been discussed on theoretical background: the EY

phonon-mediated scattering [105]; the diffusion mechanism [18] and the direct spin-phonon interaction caused by the spin-orbit coupling such as the Raman processes [86]. However, the experimental results suggest that the scattering of conduction band electrons is also relevant [169]. The predicted timescale associated with the Raman processes of the order of 100 ps does not account for all observed demagnetization at the femto- and picosecond range.

Basing on these different experimentally observed demagnetization time scales Koopmans *et al.* [105] have proposed the classification of ferromangets in two types: (i) "fast" ferromagnets which demagnetization timescale is of the order of femtoseconds as transition metals, and (ii) "slow" ferromagnets with several picosecond demagnetization characteristic times, e.g. Gd ∼100ps or Tb ∼10ps [169]. The figure of merit that has been proposed is based on the ratio between the atomic magnetic moment and the Curie temperature μ_0/T_C [105]. The explanation of the diversity of ultrafast demagnetization process requires a good understanding of the time scales and the relative weight of the elementary spin-flip processes. We conclude that the femtosecond laser induced demagnetization has rich phenomenology which is far from being completely understood and is a very hot topic.

Furthermore there also exist the subsequent magnetization dynamics and the total response has now been shown to proceed with several important characteristic timescales [106] as sketched in Fig. 1.4: (i) the femtosecond demagnetization with timescale τ_M (ii) the picosecond recovery with timescale τ_E and (iii) the hundred picoseconds -nanosecond magnetization precession and relaxation, traditionally characterized by the ferromagnetic resonance frequency ω_{FMR} and the Landau-Lifshitz-Gilbert damping parameter α_{LLG}. The laser induced magnetization precession provides an easy experimental method to study the magnetic precession with results comparable to FMR experiments [147, 165]. This technique has the advantage that it can be used to probe small structures and to optically excite spin waves [158].

1.2 Ultrafast magnetization reversal

Besides the new fundamental questions that the femtosecond laser pump-probe experiments pose about the nature of the spin dynamics in pico- and sub-pico second regimes they also open new perspectives for applications in magnetic storage devices.

In the last few decades a control of the magnetization dynamics demanded by the magnetic data storage industry has triggered the development of the field of magnetization dynamics. Several years of magnetic data storage thermal stability

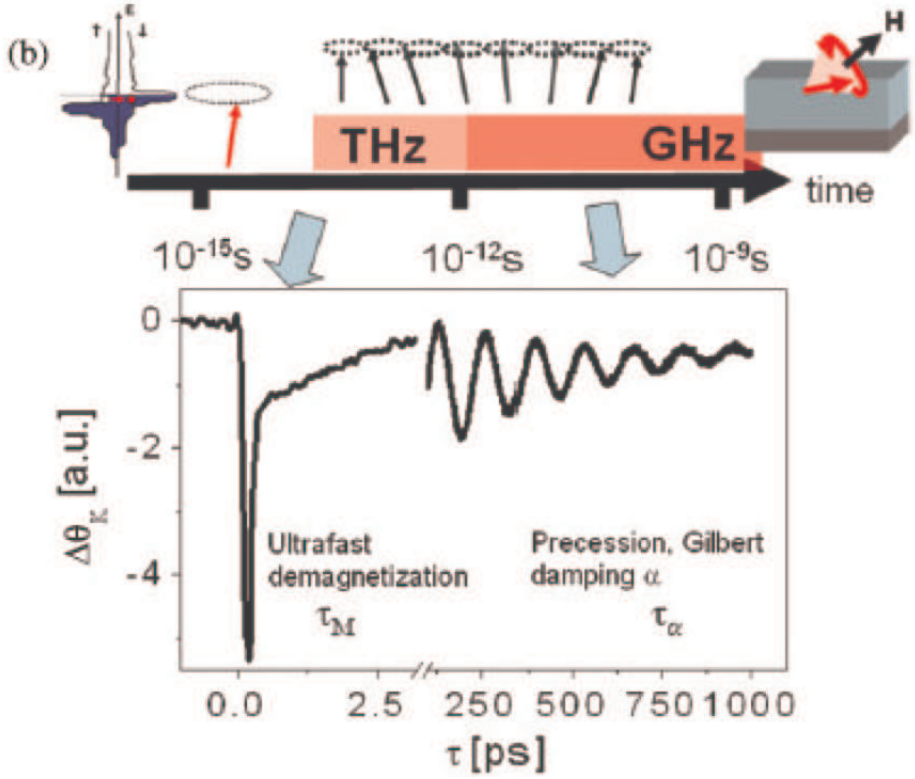

Figure 1.4: Sketch of the three characteristic timescales excited by the powerful femtosecond laser pulse. Figure taken from Ref. [165].

are required in actual hard-disk drives (HDD) and at the same time as fast as possible magnetic recording is desired. The actual magnetic data storage in HDD is composed of oppositely oriented domains in magnetically ordered materials representing bits of information where an external magnetic field can be applied to reverse the orientation of the magnetization of such domains. The application of an external magnetic field to reverse the magnetization is the conventional way to record a magnetic bit but, as we have already mentioned, this recording technology has a limited speed of several nanoseconds. Alternative ways to overcome this limit has been proposed, among them we can cite, for instance, the use of spin polarized currents which make use of the so-called spin-torque transfer effect [20, 145] or the ultrafast magnetic vortex switching using magnetic field pulses [**?**]. The switching timescale in this case is normally limited to 100ps.

Pump-probe experiments with powerful femtosecond lasers have pushed this limit down to the femtosecond time scale in the past decade, and opened new possibilities to control the magnetization. Among these, it was demonstrated the possibility to optically generate coherent magnetic precession [90, 158], laser-

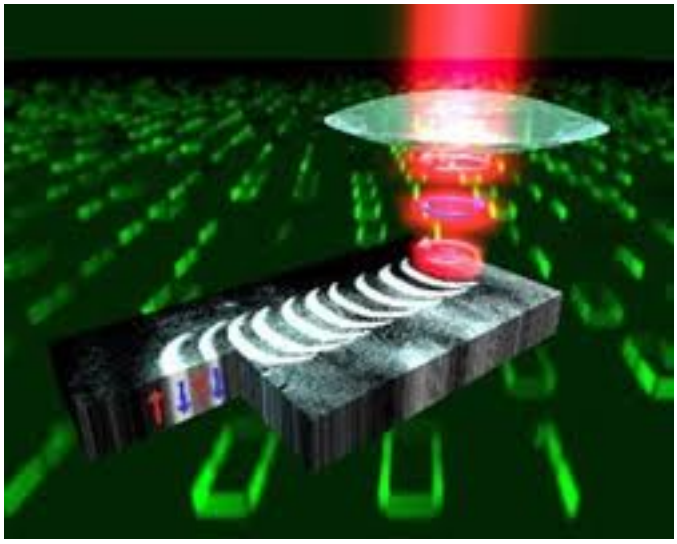

Figure 1.5: Demonstration of all-optical recording of magnetic bits. Figure taken from Ref. [149].

induced spin reorientation [24, 100] or the ultrafast generation of ferromagnetic order in antiferromagnetic FeRh [89]. However, technologically speaking it is more exciting the question of how fast the magnetization can be reversed using fs laser pulses? The first demonstration of all-optical switching was performed by Stanciu *et al.* [149] using 40 fs circularly polarized laser pulses in GdFeCo metallic ferrimagnets, see Fig. 1.5. In our days this material remains the only one where not only ultra-fast demagnetization but also the controlled switching has been reported.

Far before this finding, rare-earth 3*d*-transition metal (RE-TM) ferrimagnetic compounds were well-known materials in the magneto-optical recording. Such ferrimagnetic compounds are very interesting due to the possibility to tune the magnetization compensation temperature T_M where the magnetizations of the RE and TM sublattices cancel each other as well as the angular momentum compensation temperature T_A where the total angular momentum is zero. Basing in the theory of ferrimagnetic resonance [168] which predicts a strong temperature dependence of the frequency and the damping parameter a precession free magnetization reversal is expected to be possible near T_A. The ferrimagnetic resonance theory is derived in equilibrium conditions, thus the applicability to non equilibrium situations can be doubtful.

In 1990 Aeschlimann *et al.* [4] proposed a thermomagnetic writing process in ferrimagnetic GdTbFe alloys using laser pulses. They showed that working in temperatures around T_M the reversal of magnetization occurs faster than laser

pulse duration 16 ns, at this time a quite fast process. Moreover, at this timescale the system is in internal quasi equilibrium therefore the ferrimagnetic resonance theory is still applicable. But several years passed until femtosecond laser pulses were used to study ultrafast spin dynamics across compensation temperatures [150] in GdFeCo. In Ref. [150], high-speed and strongly damped spin dynamics in the vicinity of T_A were observed using the laser induced magnetization precession technique, i.e. dynamical properties in the pico- to nanosecond time scale. In a posterior work [151], the same authors observed a subpicosecond magnetization reversal after the application of a fs laser pulse and applying an external magnetic field. There, it was discussed that the possible mechanism behind this ultrafast switching was related to the combined action of the field and the high speed properties of GdFeCo across the compensation temperatures. The validity of this explanation is still under debate.

Differently to the mentioned works and as we mentioned above, the use of a circularly polarized fs laser pulse was experimentally proved to be enough to provide a deterministic magnetization reversal [149]. Thus, it removes the external magnetic field limitation and is a completely optical process. Here, the proposed reversal mechanism was the combined action of the laser heating up to Curie temperature and the inverse Farady effect (IFE) [**?** **?**]. It has been suggested that due to the IFE a magnetic field up to 20 Teslas is created in GdFeCo ferrimagnetic metal due to its strong magneto-optical properties [157]. More accurate estimations suggest that the IFE field can not be so large and let the correct description of the process as an open question.

Moreover, more recently, in collaboration with several theoretical and experimental groups we have shown [**?**] that a linearly polarized fs laser pulse is a sufficient stimulus to reverse the magnetization of micrometer GdFeCo structures where neither compensation temperatures nor the IFE are present during the process. However, the microscopic mechanism driving this switching is still unclear, thus, the understanding of the fundamental physics behind it is quite important from the fundamental point of view and further experimental and theoretical advances are required.

1.3 The challenge of modeling of ultrafast magnetization dynamics

The correct account for the physics of the magnetization changes on femtosecond time scales is obviously not trivial and requires the time-dependent relativistic quantum mechanics within a many-body approach. Nevertheless, currently even

ab-initio models rest on some approximations and suppositions. W. Hübner and G. P. Zhang have put forward the first-principle model [173] of the excitation of non-magnetic states under the laser-field mediated by the enhanced spin-orbit interaction. Alternatively the enhancement of the exchange interactions have been considered [**?**]. These models, however, strongly underestimate the experimentally observed demagnetization timescales. On the other hand, K. Carva *et al.* [**?**] have proposed that the super diffusive spin transport can be a sufficient mechanism to explain the observed demagnetizations. M. Fähnle *et al.* have introduced the breathing and bubbling Fermi-surface models [**?**] to describe the electron-hole scattering events. While some degree of understanding has been achieved in *ab-initio* modeling of the ultrafast demagnetization scale [173**?** **?**], the direct comparison with experiments and the modeling of all three ultrafast magnetization dynamics time scales, see Fig. 1.4, within the same approach is outside the possibilities of quantum-mechanical approaches.

A simplified statistical approach to model the ultrafast laser induced magnetization dynamics is using the stochastic Landau-Lifshitz-Gilbert (LLG) equation for atomistic spins [96, 97, 134]. The exchange between classical spins is modeled in the Heisenberg Hamiltonian framework and the thermal fluctuations are introduced as standard random Langevin fields, i.e the LLG equation is augmented by a random field to mimic the temperature. This approach has proven to model the main features of the laser induced magnetization dynamics [96, 97]. More interestingly it has been capable to predict a new transient laser induced ferromagnetic state in antiferromagnetically coupled two lattice system such as GdFeCo [134]. The advantage of this technique is that the thermal magnetic fluctuations are correctly described and it can be used up to and above the Curie temperature T_C. Additionally, the *ab-initio* calculations can provide information into the atomic scale parameters entering into the Heisenberg Hamiltonian as, for example, it has been done in FePt by N. Kazantseva *et al.* [95]. Thus, classical spin models have demonstrated their potential to reproduce the main features of the magnetization dynamics in pump-probe experiments [96]. However, due to their atomistic nature, the total simulated size in these models constitutes several tens of thousands of cubic nanometers at most. Larger simulation scale is the province of micromagnetics.

In magnetism, micromagnetic modeling has proved to be a very useful tool, complementary in many respects to experimental measurements, especially for calculations of hysteresis and dynamics of magnetic nanoelements such as magnetic grains, dots, stripes, etc[30, 37, 62]. Nowadays the micromagnetic approach is used as a design tool, for example, for the evaluation of novel magnetic recording

media performance. The importance of micromagnetics can hardly be overestimated since a huge amount of experimental work in nanomagnetism relies on the physical insights provided by the micromagnetic modeling, based, for example, on open source programs such as OOMMF [1]. Micromagnetic modeling needs as input the micromagnetic parameters: effective crystalline anisotropy K, exchange stiffness A and saturation magnetization M_s. These are provided normally by experimental measurements as spatially averaged quantities. The dynamics is based on the integration of the classical Landau-Lifshitz-Gilbert (LLG) equation of motion [68, 111].

At the same time, standard micromagnetics is also essentially zero-temperature, although the micromagnetic parameters could be taken as experimentally measured values at a given temperature T. In thermal micromagnetics the fluctuations are introduced as additional random fields acting on each discretization element [31, 40]. It has been shown that this approach is correct only for low temperatures [71] due to the fact that the standard micromagnetic approach considers constant magnetization length in each element. Thus high-frequency spinwaves, responsible for longitudinal magnetization fluctuations near the Curie temperature T_C are cut and the value of the Curie temperature is strongly overestimated. We have proposed [10] an improved micromagnetic approach for higher temperatures based on the Landau-Lifshitz-Bloch (LLB) equation [41, 47] which removes the condition of the conservation of the magnetization magnitude at each discretization element and introduce longitudinal fluctuations. Thus, the LLB equation is a good candidate to model the ultrafast magnetization dynamics because it takes correctly into account the thermal fluctuations produced by the laser pulse energy deposited into the magnetic system via interaction with electrons or phonons.

1.4 About this thesis

While a full first-principles description of the laser induced magnetization dynamics that takes correctly into account all the processes, starting from an exact electron, lattice and spin structure, correct elemental excitations as well as the coupling between them in highly non-equilibrium situations is highly desirable, at the moment it is impossible. Nowadays a more phenomenological models have been proven its usefulness in the description of the observed ultrafast induced magnetization dynamics. In this thesis we have focused our effort in the development of a phenomenological model for the simulation of laser induced magnetization dynamics based on the micromagnetic LLB equation. In Ref. [10] we have suggested the use of the LLB equation to model the ultrafast magnetization

dynamics. The consequent comparisons with experiment presented in this thesis have proved the validity of this approach.

Chapter 2 The models which build the basis for this thesis are introduced in this chapter. The electron and lattice temperature dynamics is described by the widely used two temperature model (2TM). The microscopic origins of such a model are discussed in detail. The Landau-Lifshitz-Bloch (LLB) is presented as well as the micromagnetic model based on it. Some examples of laser induced magnetization dynamics using the 2TM and the LLB model are given.

Chapter 3 We apply the theoretical approach presented in the previous chapter to investigate the femtosecond laser induced magnetization dynamics in ferromagnetic Ni thin films. We quantitatively compare our model and the experimental results which are provided by Prof. M. Münzenberg's group in the University of Göttingen (Germany). Both experimental and theoretical results are in a very good agreement giving proof of thermal magnetization mechanism based on electron-spin interaction.

Chapter 4 This chapter extends the LLB model for classical spins to the quantum version. We investigate the influence of the finite spin number and the scattering rate parameter λ on the ultrafast magnetization dynamics. The relation between the femtosecond demagnetization rate and the perpendicular picosecond-nanosecond damping, provided by the LLB theory, is checked based on the available experimental data. We discuss the possibility that the same elementary processes act on femto- and nanosecond time scales.

Chapter 5 This chapter deals with the ultrafast magnetization dynamics of rare-earth Gd which we investigate as a function of equilibrium temperature by employing the quantum LLB approach presented in the previous chapter in combination with the two-temperature model. Here we have modeled the experimental results provided by Prof. U. Bovensiepen's group in Duisburg-Essen University (Germany). In the picosecond regime the demagnetization time determined from the experiment increases with temperature from 0.8 ps at 50 K to 1.5 ps at 280 K. A successful description of this observation is achieved by considering the dynamics of $4f$ spin system coupled to $5d$ conduction electrons within two coupling mechanisms: (a) through electronic scattering and (b) spin-flip scattering mediated by phonons.

In the next two chapters we deal with the modeling of the macroscopic magnetization dynamics of the two sublattice magnet based on the LLB approach:

Chapter 6 Similar to the ferromangetic LLB derivation we derive novel dynamical LLB equations for each sublattice in a ferrimagnetic material.

Chapter 7 We study the magnetization dynamics of GdFeCo ferrimagnetic alloys using the previously derived ferrimagnetic LLB equation. For the transverse motion we generalize the ferrimagnetic resonance theory to high temperatures. For the longitudinal motion we study the different dynamics of each sublattice.

Chapter 8 In this chapter we introduce a new method to take into account the noise memory effects into atomistic simulations which ca be necessary to model materials containing slow-relaxing rare-earth impurities. We introduce a thermodynamically correct phenomenological Landau-Lifshitz-Miyasaki-Seki (LLMS) approach. We demonstrate the effect of the noise correlation time on the ultrafast demagnetization rate. Starting from the LLMS equations we also derive the corresponding LLB-type equation with memory effects.

We also include four appendix sections.

Appendix A In this first appendix we present the Heisenberg Hamiltonian for localized classical spins. We also present the mean-field approximation (MFA) which is widely used through this thesis.

Appendix B This appendix present a brief introduction to the general stochastic methods. The Fokker-Planck equation (FPE) is defined and the FPE for the classical Landau-Lifshitz equation is calculated in detail as example.

Appendix C Here a detailed calculation of the Landau-Lifshitz-Bloch equation for ferromagnets is presented.

Appendix D A method to calculate the micromagnetic exchange stiffness as a function of the temperature is presented.

2

Modeling of ultrafast laser-induced magnetization dynamics: Theoretical Background

A starting point for modeling the evolution of the highly non equilibrium situation induced after a powerful femtosecond laser pulse hits a magnetic sample can be to follow the flow of angular momentum and/or the flow of energy among the different systems involved in the process [153]. Although the role of angular momentum transfer is undoubtedly important and is a fundamental question in the femtosecond spin dynamics [25, 148], little understanding has been achieved so far. Theoretical approaches beyond Born-Oppenheimer approximation to trace ultrafast angular momentum transfer are out of reach and novel theoretical approaches have to be developed [60]. The correct account for the physics of the magnetization changes on femtosecond time scales is obviously not trivial and requires the time-dependent relativistic quantum mechanics within a many-body approach [23]. An important problem is the open question of the role of different subsystems; photons, phonons, electrons, and spins, in the ultrafast angular momentum transfer. While some degree of understanding has been achieved in *ab-initio* calculations of the ultrafast demagnetization [173], modeling all three ultrafast magnetization dynamics rates that can be induced by the laser pulse within the same approach is outside the possibilities of quantum mechanical approaches.

This chapter introduces the basic theoretical concepts for the present work on the ultrafast magnetization dynamics in ferromagnetic compounds. We will outline the general features of the laser induced electron, phonon and magnetization

dynamics in metals after the application of a femtosecond laser pulse. All three subsystems will be treated phenomenologically but under strong microscopic basis. First, the discussion focuses on the electron and phonon systems interaction with the laser pulse and between them. At first stages, the coupling of the femtosecond laser pulse electromagnetic field to the metal electron system [23, 83] leads to the formation of a coherent collective polarization of the electron gas which is almost instantaneously lost (< 10 fs) [19]. A thermalized electron distribution [26] is then reached through inelastic electron-electron scattering events [131]. After the thermalization of the electron gas, there still exists a thermal non-equilibrium between the electrons and the lattice. The electron-phonon coupling [6, 70] allows the transfer of the excess of energy in the electron system to the phonon system. Except for the initial coherent coupling between the laser electromagnetic field and electrons, the rest of the sequence may be described within a so-called two temperature model (2TM) [92].

Secondly, the macroscopic magnetization dynamics is considered. Here, several descriptions of the magnetization have been previously used in different approaches. For instance; (i) the three temperature model (3TM) where a spin temperature is coupled to 2TM rates equations [19], (ii) a modified classical Bloch equation taking into account the temperature variation of the magnetization modulus and the effective field [24] and, (iii) more recently the Koopmans' M3TM approach, a Bloch-type equation derived from microscopic basis for a two level ($S = 1/2$) system using Boltzmann rate equations [105].

Differently to the macroscopic models presented above, we propose to use the Landau-Lifshitz-Bloch (LLB) equation for the dynamics of the average spin polarization. It contains the dynamics of both the modulus and the orientation of the macroscopic magnetization. In this chapter we discuss that the introduction of longitudinal relaxation makes this equation suitable to describe the temperature induced demagnetization on the time scales below 100 ps. We show [10] that this equation is particularly important when the experimental conditions allow to induce a motion of damped precession of the magnetization [158]. Additionally, we show that the LLB equation is an excellent candidate for multiscale modeling capable of describing thermodynamic equilibrium and non equilibrium properties of magnetic materials on length scales up to micrometers [95].

2.1 Modeling of electron and phonon dynamics

In the pump-probe experiments an intense femtosecond pump pulse is focused on the sample. The absorption of the energy carried by the laser pulse induces a sudden non equilibrium state between the involved subsystems: electrons, phonons

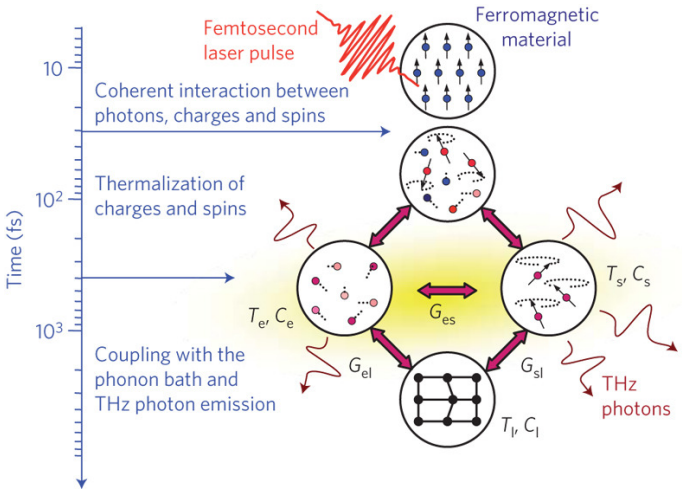

Figure 2.1: Schematic representation of mechanisms taking place in ultrafast magnetization dynamics. Figure taken from Ref. [23].

and spins. A schematic representation of the whole sequence of processes generated after the laser pulse interacting with a ferromagnetic material is shown in Fig. 2.1. In this section we focus our attention on the non equilibrium dynamics between electron and phonon systems.

Collective electron dynamics

In thermal equilibrium, before arrival of the pump laser pulse, the electron distribution within a metal is characterized by the Fermi-Dirac distribution with a well defined electronic temperature T_e. This temperature coincides with the macroscopic sample temperature $T_e = T_0$. The absorption of a femtosecond laser pulse produces a **coherent collective polarization** of the electron population [23]. This collective electron motion is destroyed by electron-electron, electron-thermal phonons or electron-defect elastic scattering events [131]. As a consequence, a highly excited ensemble of incoherent electron-hole pairs which do not obey the Fermi-Dirac statistics is created. Fig. 2.2 shows a schematic example of the resulting non-Fermi distribution [26]. The total number of non-thermal excited electrons is determined by the energy of the exciting laser pulse and the absorbed energy density.

Electronic thermalization

After some time τ_{th} (thermalization time) the optically excited conduction electrons thermalize through electron-electron interaction and excitation of secondary

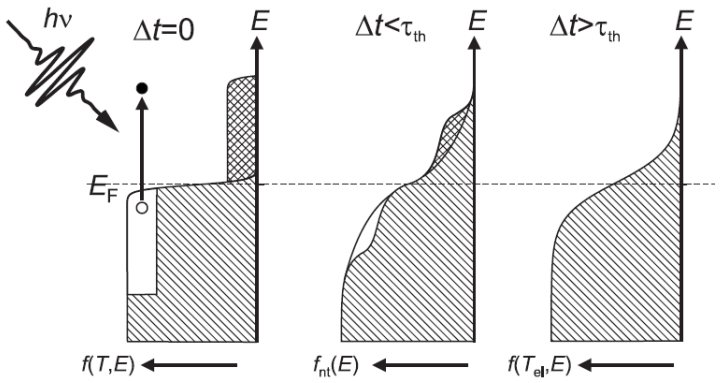

Figure 2.2: Schematic relaxation of the electron system in a metal after excitation by laser pulse. Starting from a Fermi-Dirac distribution $f(E,T)$ in equilibrium, the intense laser pulse generates a strongly non-thermal electron distribution f_{nt}, which thermalizes within the thermalization time τ_{th} through electron-electron interaction and excitation of secondary electrons. Figure taken from Ref. [26].

electrons. This process, sketched in Fig. 2.2, is known as the **electronic thermalization** and results in a Fermi distribution of hot electrons characterized by an electronic temperature T_e. Electronic temperatures T_e of the order of a few 1000 K can be achieved before a significant energy transfer due to coupling to phonons can occur. These high electronic temperatures are developed due to small heat capacity of the electronic system compared to phonons.

The absorption of a laser pulse energy is not homogeneous within the sample but it exponentially decays from the surface [84]. This inhomogeneous excitation results in a spatial energy gradient which is the source of efficient transport effects that dissipate the energy out of the excited region. This transport process is the so-called **ballistic** transport and it evolves at Fermi velocity competing with $e-e$ and $e-p$ scattering events in the redistribution of the photo-injected energy within the excited region. Moreover, due to the ballistic transport, the energy can be rapidly distributed over large distances to deeper regions of the sample [29]. Furthermore, the temperature gradient drives the hot electrons into deeper parts of the sample with a slower speed than ballistic transport. Recently it has been suggested that the hot electrons superdiffuse [18].

The above described electronic thermalization processes take place in a timescale of the order of 10-100 fs, see Fig. 2.1, depending on the specific material, after which the electron system can be described by a time dependent temperature $T_{\mathrm{e}}(t)$.

Two-temperature model

In the following picoseconds (the typical time scale for metals), there is still a non-equilibrium between electrons and lattice, also assumed to be in local thermal equilibrium with temperature T_{ph}. The electron-phonon coupling permits the exchange energy between hot electrons and phonons. This lowers the electronic temperature and raises the lattice temperature such that both subsystems have equilibrated. The strength of the coupling between these subsystems governs the time interval on which the energy transfer evolves. The whole sequence of excitation and thermalization may be described within a so-called **two temperature model** that treats the electronic and phononic systems as coupled heat baths [92]. This model takes the generation of non-thermal hot electrons and the subsequent relaxation to thermalized electrons as infinitely fast.

The 2TM was derived by Kaganov [92] starting with a general electron and phonon Hamiltonian. For completeness we present the derivation in order to better understand the approximations which have been done.

Electron and phonon Hamiltonian

We explicitly write a standard Hamiltonian for electron and phonon system,

$$\mathcal{H} = \mathcal{H}_e + \mathcal{H}_{ee} + \mathcal{H}_{ph} + \mathcal{H}_{e-ph}. \tag{2.1}$$

The **electron system** is described by

$$\mathcal{H}_e = \sum_k \frac{k^2}{N D_F} c_{\mathbf{k}}^{\dagger} c_{\mathbf{k}}, \tag{2.2}$$

where $c_{\mathbf{k}}^{\dagger}\,(c_{\mathbf{k}})$ describes creation (annihilition) of electrons in state $\mathbf{k}$, $k = |\mathbf{k}|$. N electrons are thus described as spinless particles obeying Fermi-Dirac statistics with a constant density of states D_F around the Fermi level [103]. For the electronic specific heat C_e we will keep the free electron approximation along the manuscript. Within this approximation, according to the Fermi-Dirac distribution the following relation between C_e and D_F holds

$$C_e = \frac{1}{3}\pi^2 D_F k_B^2 T_e = \gamma T_e. \tag{2.3}$$

where k_B is the Boltzmann constant. The second term $\mathcal{H}_{ee}$ describes the interaction within the electron subsystem for example, the (screened) Coulomb $e-e$ interaction that takes care of thermalization of optically excited carriers towards

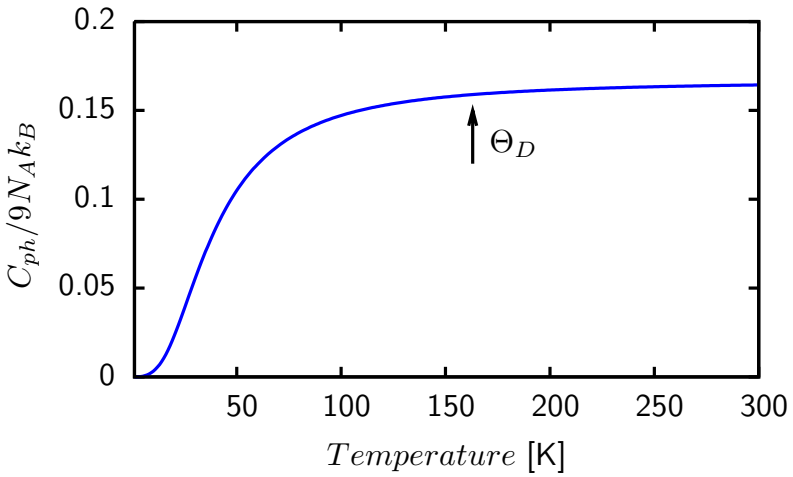

Figure 2.3: Phonon system specific heat as a function of temperature within the Debye model for Gd.

a Fermi-Dirac distribution at T_e. Throughout this study, this interaction is supposed to be efficient enough to cause an instantaneous electron thermalization to a well-defined electron temperature T_e.

The phonon system is described by the harmonic-phonon Hamiltonian

$$\mathcal{H}_{ph} = \sum_{\mathbf{k}} a^{\dagger}_{\mathbf{k}} a_{\mathbf{k}} \hbar\omega_{\mathbf{k}}, \tag{2.4}$$

where $a^{\dagger}_{\mathbf{k}}$ ($a_{\mathbf{k}}$) is the $\mathbf{k}$ state phonon creation (annihilition) operator. We will use the Debye model in which the phonon spectrum continues in the same form up to the Debye frequency Ω_D that is the upper bound of integration. Within the Debye model one assumes that the relation $\omega_{\mathbf{k}} = \upsilon k$ (υ is the speed of sound) holds everywhere in the Brillouin zone that is approximated by a sphere bound by the Debye wave vector k_D. The latter is defined by the requirement that total number of phonon modes is N, this yields $k_D = (6\pi^2/\upsilon_0)^{1/3}$, where υ_0 is the unit-cell volume. One can introduce the Debye temperature Θ_D as $k_B\Theta_D = \hbar\Omega_D$. This approximation gives the following expression for the specific heat $C_{ph}(T_{ph})$ [129]:

$$C_{ph}(T_{ph}) = 9N_Ak_B \left(\frac{T_{ph}}{\Theta_D}\right)^3 G_4\left(\frac{\Theta_D}{T_{ph}}\right) \tag{2.5}$$

where N_A is the Avogrado number and

$$G_4\left(\frac{\Theta_D}{T_{ph}}\right) \equiv \int_0^{\frac{\Theta_D}{T_{ph}}} dx \frac{x^4 e^x}{(e^x-1)^2}. \tag{2.6}$$

At low temperatures, $T \ll \Theta_D$, Eq. (2.5) yields the well-known scaling law with temperature $C_{ph}(T_{ph}) \sim (T/\Theta_D)^3$, and at high temperatures Eq. (2.5) gives the saturation value $C_{ph} = 3k_B$ [7]. The low temperature approximation does not smoothly join with the high temperature approximation at $T \sim \Theta_D$. For $T \gg \Theta_D$ we get $C_{ph} \to C_{ph,\infty} = 25\text{Jmol}^{-1}\text{K}^{-1}$ [7]. In the calculations along the present thesis we will use both a constant value or the integral expression (2.5) depending on the temperature regimes we will be working in. For example in Ni the phonon temperature in fs laser pump-probe experiments is always close or above the Debye temperature $\Theta_D = 375\text{K}$ [19], thus, we are allowed to use a constant value in the 2TM to simulate Ni. However, in Gd and for the particular experimental set-up of our experimental partners [154] which allows an initial temperature variation between low temperatures $T_0 = 50\text{K}$ up to the Curie temperature $T_0 = T_C = 293\text{K}$ we will use the integral expression given by Eq. (2.5) because it crosses the low and high temperature regimes for the phonon temperature, see Fig. 2.3.

As we have already mentioned, the excess of energy in the electronic system is transferred to the lattice via **electron-phonon** interaction described by $\mathcal{H}_{e-ph}$, The electron-phonon coupling term is modeled with an energy-transfer rate $H_{\text{e-ph}}$ that was derived by Kaganov [92] by summation of all one-phonon emission and absorption processes assuming thermal electron and phonon distributions.

$$\mathcal{H}_{e-ph} = \sum_{\mathbf{k},\mathbf{q}\lambda} B_{\mathbf{q}\lambda} \left(c^{\dagger}_{\mathbf{k}+\mathbf{q}} c_{\mathbf{k}+\mathbf{q}} a^{\dagger}_{\mathbf{k}} + c_{\mathbf{k}+\mathbf{q}} c^{\dagger}_{\mathbf{k}-\mathbf{q}} a_{\mathbf{k}} \right), \tag{2.7}$$

where the $B_{\mathbf{q}\lambda}$ is the electron-phonon coupling constant. For acoustic phonons, the coupling constant takes a particular simple form [131]

$$B_{\mathbf{q}\lambda} = \frac{2E_F q}{3} \sqrt{\frac{\hbar}{2MN\omega_{\mathbf{q}\lambda}}} \tag{2.8}$$

where, $q = |\mathbf{q}|$, N is the number of ions, M is the mass of the ion and E_F is the electron Fermi energy. From Eq. (2.7) the energy transfer rate between electrons and phonons, dU/dt, can be easily calculated applying the Fermi golden rule to $\mathcal{H}_{e-ph}$

$$\left[\frac{dU}{dt}\right]_{e-ph} = -\frac{2}{(2\pi)^3} \sum_{\mathbf{q}} \hbar \quad \omega_{\mathbf{q}} \quad \int d^3\mathbf{q} \|B_{\mathbf{q}}\| \delta(E_{\mathbf{k}} - E_{\mathbf{q}} + \hbar\omega_{\mathbf{q}}) \times \left[(n_{\mathbf{q}} + 1) f_{\mathbf{q}} (1 - f_{\mathbf{k}}) - n_{\mathbf{q}} f_{\mathbf{k}} (1 - f_{\mathbf{q}})\right] \tag{2.9}$$

where $f_{\mathbf{k}}$ is the electron occupation number according to the Fermi-Dirac distribution at temperature T_e and $n_{\mathbf{q}}$ is the phonon occupation number according to the Bose-Einstein distribution at temperature T_{ph}. In Eq. (2.9) the first (second) term represents the energy transfer from (to) electrons to (from) lattice by emitting (absorbing) a phonon. The phonon spectra $\omega_{\mathbf{k}}$ is taken within the Debye model. Thus, Eq. 2.9 can be written as:

$$\begin{aligned} \left[\frac{dU}{dt}\right]_{e-ph} &= H(T_e, T_{ph}) = f(T_e) - f(T_{ph}) \\ &\text{where} \quad f(T) = 4g_\infty \Theta_D \widetilde{G}_4\left(\frac{T}{\Theta_D}\right) \end{aligned} \tag{2.10}$$

and $\widetilde{G}_n(x) = x^{n+1}\int_0^{1/x} t^n dt/(e^t - 1)$. The constant g_∞ is called the **electron-phonon coupling constant**, also denoted by G_{e-ph} [6, 19]. A useful quantity is the derivative of the function $f(T)$, $g(T) \equiv df/dT$. For $T_{ph} \ll \Theta_D$ the function $g(T_{ph})$ varies as T_{ph}^4 and for $T_{ph} \gtrsim \Theta_D$ the function $g(T_{ph})$ goes to the constant value g_∞. In the limit $T_e - T_{ph} \ll T_{ph}$, see Fig. 2.4, the energy transfer function $H_{\text{e-ph}}$ may be written as

$$H(T_e, T_{ph}) = g(T_{ph})\,(T_e - T_{ph})\,. \tag{2.11}$$

Interestingly, for $T_e, T_{ph} \gtrsim \Theta_D$ the relaxation rate reduces to a linear form $H_{\text{e-ph}} = G_{e-ph}(T_e - T_{ph})$, a widely used approximation in the literature [19]. Indeed, in this limit the relaxation rate G_{e-ph} can be estimated using Eq. (2.8) for the microscopic electron-phonon coupling

$$g_\infty = G_{e-ph} = \left(\frac{2E_F}{3\hbar}\right)^2 \frac{9\pi}{8\upsilon_0}\frac{m_e}{MT_F}, \tag{2.12}$$

where m_e is the electron mass and T_F the Fermi temperature. Within these approximations the rate equations for electron and phonon temperatures read

$$\begin{aligned} C_e(T_e)\frac{dT_e}{dt} &= -H(T_e, T_{ph}) + S(z,t) + \frac{\partial}{\partial z}\left(\kappa_e \frac{\partial T_e}{\partial z}\right) \\ C_{ph}(T_{ph})\frac{dT_{ph}}{dt} &= H(T_e, T_{ph}), \end{aligned} \tag{2.13}$$

where temperature dependence of heat capacities C_e and C_{ph} are given by Eqs. (2.3) and (2.5) respectively. In Eq. (2.13) we have included an additional mechanism of energy redistribution of the hot electron bath, namely the **electron**

diffusion process. This is determined by the temperature gradient in the sample and is modeled by an additional term in the electron dynamics equation with κ_e being the electronic thermal conductivity parameter. The corresponding process for the lattice is neglected because it proceeds on timescales of several hundred picoseconds. Thermal diffusion outside the sample can be also included in Eqs. (2.13) as, for example, an exponential decaying function in time. We neglect the contribution of the probe pulse which usually carries less than a tenth of pump pulse energy.

The source term $S(z,t)$ is dependent on the optical properties of the system through the **optical penetration depth** δ_{op}. The absorption of light in metals follows an exponential spatial profile of the intensity within the material $I(d) = I_0 \exp[-z/\delta_{\text{op}}]$, where z represents the depth into the sample and $z = 0$ corresponds to the surface level. In the case of metals, the optical penetration depth for laser with wavelengths in the visible spectra range varies between 10 and 30 nm and gives the initial excitation depth profile

$$S(z,t) = (1 - R - T)\,(I_0/\delta_{\text{op}})\, e^{-z/\delta_{\text{op}}} e^{-(t/\tau_{\text{p}})^2} \tag{2.14}$$

where R and T are the reflectivity and transmission coefficients respectively and τ_{p} is the laser pulse duration.

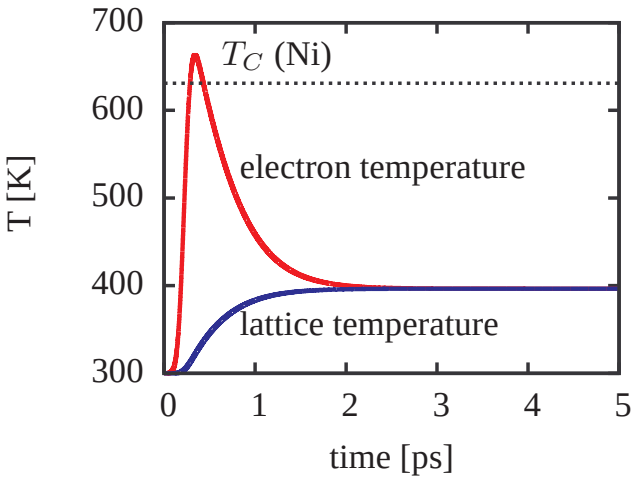

Figure 2.4: Electron and lattice temperature calculated for a Gaussian laser pulse within the two temperature model for Ni parameters. The electron temperature can increase up to and above the Curie temperature in Ni, $T_C = 631$K.

All along this thesis we will use different approximations for the general formulation of the 2TM presented above.

Fig. 2.4 shows the numerical solution of Eq. (2.13). Here the parameters are chosen so that they represent the transition metal Nickel. For the sake of simplicity, we have used a pump pulse represented by the source term in Eq. (2.14) assuming a homogeneous heating ($\delta_{\text{op}} = \infty$) and $\tau_{\text{p}} = 50$ ps. The phonon specific heat is chosen to be constant and equal to $C_{ph} = 3.1 \times 10^6 \text{Jm}^{-3}K^{-1}$ [11]. For the electronic heat capacity we use $\gamma = 3 \times 10^3 \text{Jm}^{-3}K^{-1}$ [11]. The coupling constant between electrons and phonons is $G_{e-ph} = 1 \times 10^{18} \text{Wm}^{-3}K^{-1}$ [11]. The solution of Eq. (2.13) shows that under these conditions the electron temperature reacts strongly on the laser pulse, while the lattice temperature slightly changes from equilibrium. Interestingly, the electron temperature can go up to values larger than the Curie temperature of the ferromagnetic material, in our example for Ni, $T_C = 631$K.

2.2 Magnetization dynamics: Landau-Lifshitz-Gibert equation

In most of the common ferromagnets the orbital contribution to the magnetic moment is negligibly small the magnetic moment $\boldsymbol{\mu}$ is related to the spin angular moment $\mathbf{S}$ by the simple equation $\boldsymbol{\mu} = -g\mu_B\mathbf{S}/\hbar = \gamma\mathbf{S}$. The value γ is defined as the ratio of the magnetic moment to the angular momentum, it is called **gyromagnetic ratio**, and its value is -1.76×10^7 rad s^{-}1 Oe^{-1} for $g = 2$. If a magnetic field $\mathbf{H}$ is applied, then a torque $\mathbf{T} = \boldsymbol{\mu} \times \mathbf{H}$, which is given by the rate of change of angular momentum with time, acts upon the magnetic moment so we may write

$$\frac{d\mathbf{S}}{dt} = \boldsymbol{\mu} \times \mathbf{H} \Longrightarrow \frac{d\boldsymbol{\mu}}{dt} = -\gamma\boldsymbol{\mu} \times \mathbf{H}. \tag{2.15}$$

In 1935 Landau and Lifshitz based on this idea introduced this equation of motion which was generalized for a macroscopic magnetic moment density $\mathbf{M} = \boldsymbol{\mu}/V$, where V is the total volume containing the macroscopic magnetic moment $\boldsymbol{\mu}$. The macroscopic moment precess around an effective field, $\mathbf{H}_{\text{eff}} = -\partial F/\partial\mathbf{M}$ calculated from the corresponding micromagnetic energy functional F which can contain the Zeeman, anisotropy, dipole-dipole or exchange contributions. Equation (2.15) only contains a term expressing the precession of the local moment around the effective magnetic field. This describes the conservative dynamics of an ideal spin system that does not exchange energy with its environment. Landau and Lifshitz, already in their first paper [111] on magnetization dynamics, included a term in the equation of motion (2.15) that accounted for the relaxation.

They proposed a double cross product damping term in addition to the precession term, yielding the equation known as the Landau-Lifshitz (LL) equation:

$$\frac{d\mathbf{M}}{dt} = \gamma \mathbf{M} \times \mathbf{H}_{\text{eff}} + \gamma \frac{\alpha_{\text{LL}}}{M_s} \mathbf{M} \times (\mathbf{M} \times \mathbf{H}_{\text{eff}}) \,. \tag{2.16}$$

Here $\mathbf{M}$ stands for the macroscopic magnetization and M_s is the saturation magnetization value. This new term has phenomenological origins. The damping torque is perpendicular to the precession torque. The motion of a magnetic moment exerted by an external magnetic field is a spiral motion where the vector $\mathbf{M}$ eventually aligns with the field. The constant α_{LL} reflects the rate of such relaxation. It is called the Landau-Lifshitz damping parameter.

Following classical mechanics, Gilbert used the fact that the friction force acting on a particle moving through a viscous media is to the first order approximation proportional and in opposite direction to its velocity. He introduced an analogous damping term for magnetization dynamics resulting in the Gilbert (G) equation:

$$\frac{d\mathbf{M}}{dt} = \gamma \mathbf{M} \times \mathbf{H}_{\text{eff}} - \frac{\alpha_{\text{G}}}{M_s} \mathbf{M} \times \frac{d\mathbf{M}}{dt}. \tag{2.17}$$

Just as the LL damping torque, the Gilbert damping torque is perpendicular to the precession torque. In the limit of small damping the solutions of the LL and the Gilbert equations are close to each other. For larger damping the discrepancy is substantial. It can be clearly seen if we write (2.17) in the form similar to LL equation (known as the Landau-Lifshitz-Gilbert (LLG) equation)

$$\frac{d\mathbf{M}}{dt} = \frac{\gamma}{1+\alpha_{\text{G}}^2} \mathbf{M} \times \mathbf{H}_{\text{eff}} + \frac{\gamma}{1+\alpha_{\text{G}}^2} \frac{\alpha_{\text{G}}}{M_s} \mathbf{M} \times (\mathbf{M} \times \mathbf{H}_{\text{eff}}) \,, \tag{2.18}$$

in the limit $\alpha_{\text{G}} \ll 1$ both equations coincide in the first order in α_{G}. The mechanisms for damping of the magnetic precession are manifold. Mainly, it is assumed that the spin system interacts with the phonons, electrons and impurities. The LLG equation in form of Eq. (2.18) does not depend on the temperature although one can use the macroscopic parameters, such as the anisotropy or saturation magnetization at a given temperature T.

2.2.1 LLG-Langevin equation: stochastic magnetization dynamics

A possibility for taking thermal fluctuations into account was suggested by Brown [31] by adding a stochastic field $\boldsymbol{\zeta}$ to the effective fields entering in the LLG

equation (2.18) in the sense of the Langevin equation approach [163]. Then the effective field reads

$$\mathbf{H}(t) = -\frac{\partial \mathcal{H}(t)}{\partial \mathbf{M}} + \boldsymbol{\zeta}(t,T). \tag{2.19}$$

Langevin dynamics simulations in micromagnetics were originally introduced by Lyberatos and Chantrell [116] and were further developed by many authors [39, 67, 126, 143] (for a review see Ref. [21] and references therein). This development followed the seminal work of Brown [31]. He, as mentioned above, included thermal fluctuations in the dynamics of an ensemble of noninteracting macrospins in order to describe the deviations from the average trajectory and so formally introduced random fields in the LLG for the time evolution of $\mathbf{M}(t)$ which then becomes the Langevin equation of the process. These thermal fields were supposed uncorrelated both in space and time, and so were represented by Gaussian white noise allowing one to construct a Fokker-Planck equation (FPE). The FPE and related techniques are discussed in some detail in Appendix B, see also Ref. [44]. Brown also showed how to evaluate the spectral density of the thermal fields following the Einstein method [163] by using the fluctuation-dissipation theorem or requiring the equilibrium distribution function of the orientations of the magnetization $\mathbf{M}(t)$ to coincide with the Boltzmann distribution. The concept of a fluctuating thermal field was also generalized to interacting particles [40, 67, 146], hastening the development of thermal micromagnetics. The resulting LLG-Langevin equation reads

$$\frac{(1+\alpha_{\mathrm{G}}^2)\,\mu_s}{\gamma}\frac{d\mathbf{M}}{dt} = -\mathbf{M}\times\left(\frac{\partial \mathcal{H}(t)}{\partial \mathbf{M}} - \boldsymbol{\zeta}(t,T) + \alpha_{\mathrm{G}}\boldsymbol{M}\times\left(\frac{\partial \mathcal{H}(t)}{\partial \mathbf{M}} - \boldsymbol{\zeta}(t,T)\right)\right). \tag{2.20}$$

The thermal field $\boldsymbol{\zeta}$ has the white-noise properties

$$\langle \zeta_i \rangle = 0, \quad \langle \zeta_i(0)\zeta_j(t)\rangle = 2\frac{k_B T \alpha_{\mathrm{G}}}{|\gamma| M_s}\delta_{ij}\delta(t), \quad i = x,y,z \tag{2.21}$$

meaning that the $\zeta_i(t)$ components are statistically independent and that $\zeta_i(t)$ and $\zeta_j(t)$ are uncorrelated at very short times, *i.e.* much shorter than the time of a single precession period (δ_{ij} is Kroneckers symbol). The Langevin Eq. (2.20) should be interpreted as a Stratonovitch vector stochastic differential equation. This is accomplished by a suitable choice of the numerical integration scheme, here that of Heun. The Heun scheme is stable and is in agreement with the Stratonovich stochastic calculus. We remark that several authors [**?**] have argued that even simpler integration schemes, e.g., the Runge-Kutta method, would

reproduce the correct Boltzmann equilibrium distribution, if the magnetization vector is renormalized at each time step, obeying the property $|\mathbf{M}|$ =const.

However, the simulations of the magnetization dynamics based on the micromagnetic LLG equation are not suitable for high temperatures. This is due to the fact that micromagnetic simulations do not include the high-frequency spin waves and, thus, the Curie temperature is seriously overestimated [71] and the restriction $|\mathbf{M}|$ =const.

2.2.2 Atomistic LLG Langevin simulations

An adequate approach that solves this problem is the so-called atomistic spin dynamics (ASD) [127] based on the LLG equation for each localized atomic moment.

The ASD model considers that the magnetic moment at each lattice site can be described by a classical vector $\boldsymbol{\mu}_i$ with a constant value $\mu_0 = |\boldsymbol{\mu}_i|$. The local dynamics of each normalized magnetic moment, $\mathbf{s}_i = \boldsymbol{\mu}_i/\mu_0$, follows a LLG type equation augmented by Langevin stochastic fields:

$$\frac{(1+\lambda^2)\,\mu_0}{\gamma}\frac{d\mathbf{s}_i}{dt} = -\mathbf{s}_i \times \left(\frac{\partial \mathcal{H}(t)}{\mu_0 \partial \mathbf{s}_i} - \boldsymbol{\zeta}_i(t,T) + \lambda \mathbf{s}_i \times \left(\frac{\partial \mathcal{H}(t)}{\mu_0 \partial \mathbf{s}_i} - \boldsymbol{\zeta}_i(t,T) \right) \right). \tag{2.22}$$

The thermal field $\boldsymbol{\zeta}_i$ has again the same white-noise properties

$$\langle \zeta_i \rangle = 0, \quad \langle \zeta_i(0)\zeta_j(t) \rangle = 2\frac{\lambda k_B T}{|\gamma|\mu_0}\delta_{ij}\delta(t), \quad i = x, y, z \tag{2.23}$$

Here $\mathcal{H}$ is the Heisenberg-type Hamiltonian for localized atomistic magnetic moments $\boldsymbol{\mu}_i$. The atomic coupling-to-the-bath parameter λ describes the energy transfer between the spin system and the heat bath. The macroscopic magnetization is obtained as thermal average over some volume

$$\mathbf{m} = \frac{1}{N}\sum_i \mathbf{s}_i \tag{2.24}$$

It also performes a damped motion. Due to magnon-magnon interactions the macroscopic damping constant obtained from ASD simulations is temperature dependent. Indeed, in recent ASD simulations [96] it has been demonstrated that at high temperatures several important effects occur which cannot be taken into account in the micromagnetic LLG approach. Namely, during the magnetization dynamics, (i) the magnetization vector magnitude is not conserved, (ii) longitudinal magnetization relaxation occurs with the longitudinal relaxation

time increase approaching the Curie temperature (critical slowing down), and (iii) at the same time the transverse relaxation time decreases [41]. These effects are not included in the macroscopic LLG dynamics.

Finally, we note that as the fluctuating fields are caused by a large number of weakly coupled microscopic events, they are, because of the central limit theorem, described by a Gaussian distribution. In principle the noise can be correlated both in time and space. A short, but finite, correlation time τ_c can be modeled, for example, by exponentially correlated **colored noise** (known as the Orstein-Uhlbeck process)

$$\langle \zeta_i \rangle = 0, \quad \langle \zeta_i(0)\zeta_j(t) \rangle = 2\frac{D}{\tau_c} \exp(-t/\tau_c)\delta_{ij}, \quad i = x, y, z. \tag{2.25}$$

This election, although being the most natural, regrettably does not recover the Boltzmann equilibrium distribution in the stationary state for correlation timescales of the order of the precession period. This question will be the topic of the Chapter 8 of the present thesis.

2.3 Magnetization dynamics: Landau-Lifshitz-Bloch equation

The macroscopic LLG equation can not describe many of the effects captured by atomistic simulations, especially at temperatures close to the Curie temperature T_C. However, a micromagnetic approach that correctly takes into account the thermal fluctuations and is valid at temperatures below and above T_C, also exists. This micromagnetic approach is based on the Landau-Lifshitz-Bloch (LLB) equation which was derived by D. A. Garanin for classical [64] and quantum [46] thermal average spin polarization from the Fokker-Plank equation and the density matrix equation, respectively. In this section we only present the classical version of the LLB equation and we let the quantum version of the LLB equation for the Chapter 4. In the classical derivation of the LLB equation the thermal averaging of atomistic spin directions has been performed analytically within the mean field (MFA) approximation [64]. Thus, the LLB equation for classical spins is equivalent to an ensemble of exchange-coupled atomistic spins modeled by stochastic LLG equations [41, 95] as we schematically show in Fig. 2.5. We have written down in detail the derivation of the classical LLB equation in Appendix C.

Since this equation interpolates the magnetization between the Landau-Lifshitz and the Bloch equation it is called the Landau-Lifshitz-Bloch equation. At low temperatures it coincides with the standard LLG equation but it is valid up to

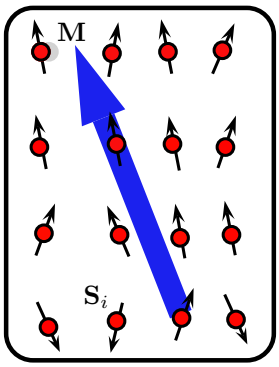

Figure 2.5: Illustration of the macro-spin model. We simulate the thermal average magnetization of a magnetic grain.

and above the Curie temperature T_C. The LLB equation was proved to describe quite well all the effects observed in the ASD simulations described above [41, 95] for example a well-known increase of damping with temperature. Also it describes well a linear domain wall, a domain wall type with non-constant magnetization length. The results are consistent with measurements of the domain wall mobility in YIG crystals close to T_C [108] and with recent atomistic simulations [98].

In ultrafast laser pump-probe experiments a femtosecond quenching of the magnetization is observed, *i.e.* the magnetization modulus decreases upon the action of the heating of the system produced by laser pulse. The change of the magnetization modulus is known as the **longitudinal relaxation**. The necessity of the longitudinal relaxation to model the pump-probe experiments via the micromagnetic approach has been already noted by Vomir *et al.* [162] who suggested to use for this purpose the Bloch equation. Very recently Koopmans' microscopic three temperature model (M3TM) [105] also introduces a macroscopic equation with longitudinal relaxation only, to describe the ultrafast magnetization dynamics.

The advantage of the LLB equation resides in the fact that it is a much more consistent approach which has a more rigorous foundation and has been tested against the predictions of atomistic modeling [41]. The purpose of the present section is to introduce a full micromagnetic approach based on the LLB equation and to show its suitability to model high temperature magnetization dynamics below and above the Curie temperature.

2.3.1 Dynamics of a macrospin

The LLB equation describes the dynamics of the magnetization of a ferromagnet at non-zero temperature. It is written for the thermal average $\mathbf{m} = \langle \mathbf{s}_i \rangle$, in the

form [64]

$$\dot{\mathbf{m}} = \gamma[\mathbf{m} \times \mathbf{H}_{\text{eff}}] - \gamma\alpha_{\parallel}\frac{[\mathbf{m} \cdot \mathbf{H}_{\text{eff}}]\,\mathbf{m}}{m^2} + \gamma\alpha_{\perp}\frac{[\mathbf{m} \times [\mathbf{m} \times \mathbf{H}_{\text{eff}}]]}{m^2}, \tag{2.26}$$

where $\mathbf{m}$ is the normalized sample average spin-polarization $\mathbf{m} = \mathbf{M}/Ms(T = 0K)$. The equation contains three terms: the first term describes the precession around the effective field, the second - the longitudinal relaxation, *i.e.* magnetization length is not conserved, and the third - the transverse relaxation of the magnetization. $\alpha_{\parallel}$ and $\alpha_{\perp}$ are dimensionless longitudinal and transverse damping parameters given by

$$\alpha_{\parallel} = \frac{2}{3}\frac{T}{T_C}\lambda \quad \text{and} \quad \alpha_{\perp} = \lambda\left(1 - \frac{T}{3T_C}\right) \tag{2.27}$$

At temperatures above Curie temperature, $T > T_C$, both damping parameters coincide

$$\alpha_{\perp} = \alpha_{\parallel} = \frac{2}{3}\frac{T}{T_C}\lambda \tag{2.28}$$

In these equations λ is a microscopic coupling constant which characterizes the coupling of the individual atomistic spins with the heat-bath. It describes the microscopic elementary processes such as electron-spin or phonon-spin scattering events. Note, that even assuming λ to be temperature independent, the macroscopic damping parameters of the LLB equation turn out to be temperature dependent via Eqs. (2.27). At zero temperature the longitudinal damping parameter, $\alpha_{\parallel}$, vanishes and the magnitude of magnetization is constant and equal to M_s (the zero temperature and field equilibrium magnetization). The LLB equation at $T = 0$K coincides with the LLG equation up to the small correction $1 + \lambda^2$.

The most important feature of the LLB equation is the presence of two relaxation terms: **longitudinal** and **transverse**, see schematic representation in Fig. 2.6. As a result of the consideration of atomic spin-spin interactions, these macroscopic parameters are temperature-dependent. In the LLB model the nature of the longitudinal and the transverse relaxation differs from the point of view of characteristic spin wave frequencies. The transverse relaxation, better known as the LLG damping, is basically the relaxation of the ferromagnetic resonance (FMR) mode ($\mathbf{k} = 0$). The contribution of other spin wave modes is reduced to the thermal averaging of the micromagnetic parameters and the main effect comes from the decrease of the magnetization at high temperature. Consequently, the transverse damping parameter increases with temperature, consistent with atomistic modeling results [41] and well-known FMR experiments [22, 113]. On the

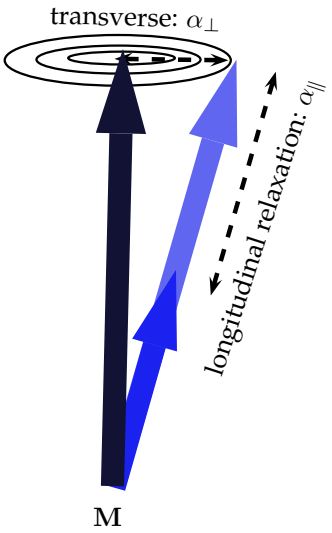

Figure 2.6: Schematic illustration of the macro-spin LLB model with two different relaxation processes: the transverse and the longitudinal ones, characterized by $\alpha_\parallel$ and $\alpha_\perp$, respectively .

contrary, the main contribution to the longitudinal relaxation comes from the high-frequency spin waves. This process occurs in a strong exchange field. As a result the longitudinal relaxation time is much faster than the transverse one but increases with temperature, known as critical slowing down.

For the comparison with the LLG dynamics, it is more convenient to make use of an equivalent form of the LLB equation as a function of the reduced magnetization, normalized to the equilibrium value $M_e = M_s(T)$ at given temperature T, $\mathbf{n} = \mathbf{M}/M_e = \mathbf{m}/m_e$, $m_e = M_e(T)/M_e(0)$. It reads

$$\dot{\mathbf{n}} = \gamma[\mathbf{n} \times \mathbf{H}_{\text{eff}}] - \gamma\widetilde{\alpha}_\parallel \frac{[\mathbf{n} \cdot \mathbf{H}_{\text{eff}}]\,\mathbf{n}}{n^2} + \gamma\widetilde{\alpha}_\perp \frac{[\mathbf{n} \times [\mathbf{n} \times \mathbf{H}_{\text{eff}}]]}{n^2}, \tag{2.29}$$

Here the damping parameters are given by $\widetilde{\alpha}_\parallel = \alpha_\parallel/m_e$ and $\widetilde{\alpha}_\perp = \alpha_\perp/m_e$. Due to the similarity of the formulation of the Eq. (2.29) with the micromagnetic LLG equation, it is the expression for $\widetilde{\alpha}_\perp$, which should be compared with the transverse relaxation parameter α_{LLG}.

Effective fields

The effective field in the LLB equation has two different forms below and above T_C [64],

$$\mathbf{H}_{\text{eff}} = \mathbf{H} + \mathbf{H}_A + \begin{cases} \frac{1}{2\widetilde{\chi}_\parallel}\left(1 - \frac{m^2}{m_e^2}\right)\mathbf{m} & T \lesssim T_C \\ -\frac{J_0}{\mu_0}\left(\frac{T}{T_C} - 1 + \frac{3}{5}m^2\right)\mathbf{m} & T \gtrsim T_C \end{cases} \tag{2.30}$$

where $\mathbf{H}$ and $\mathbf{H}_A$ are applied and anisotropy fields, $\widetilde{\chi}_{\parallel}(T) = (\partial m/\partial H)_{H\to 0}$ is the longitudinal susceptibility and μ_0 is the atomic magnetic moment. At $T = T_C$ both expressions coincide, m_e is the temperature dependent reduced zero-field equilibrium magnetization, J_0 is zero Fourier component of exchange interaction between spins in an atomistic Heisenberg model. In particular, for nearest neighbours only, $J_0 = zJ$, with exchange constant J and z nearest neighbours. This mean-field form of the effective magnetic field can be rewritten in terms of the longitudinal susceptibility and not in terms of the exchange constant. The corresponding expression for the effective magnetic field is then [95]

$$\mathbf{H}_{\text{eff}} = \mathbf{H} + \mathbf{H}_A + \begin{cases} \frac{1}{2\widetilde{\chi}_{\parallel}}\left(1 - \frac{m^2}{m_e^2}\right)\mathbf{m} & T \lesssim T_C \\ -\frac{1}{\widetilde{\chi}_{\parallel}}\left(1 - \frac{3T_C}{5(T-T_C)}m^2\right)\mathbf{m} & T \gtrsim T_C \end{cases} . \tag{2.31}$$

In this thesis we will mainly use the MFA expressions of the effective field parameters. The anisotropy field is taken through the transverse susceptibility $\chi_{\perp}$ in the following form

$$\mathbf{H}_A = -\frac{1}{\chi_{\perp}}\left(m_x \mathbf{e}_x + m_y \mathbf{e}_y\right). \tag{2.32}$$

The transverse susceptibility can be related to the micromagnetic anisotropy at low temperatures by the relation $\chi_{\perp} \sim M_s(T)/2K(T)$. We can use the MFA temperature dependence of the anisotropy constant $K \sim m^3$. The longitudinal susceptibility is defined as $\widetilde{\chi}_{\parallel} = (\partial m/\partial H)_{H=0}$ and it is also taken from MFA

$$\widetilde{\chi}_{\parallel} = \frac{\mu_0}{J_0}\frac{B'\beta J_0}{1 - B'\beta J_0} \tag{2.33}$$

$B' \equiv dB/d\xi$ is evaluated at equilibrium and $H = 0$, being $B = B(\xi)$ the Langevin function where $\xi = \beta\mu_0 H^{\text{MFA}}$ and $\beta = 1/k_B T$. (see Appendix A for a detailed description of the mean-field approximation (MFA) in Heisenberg ferromagnets).

2.3.2 Stochastic LLB equation

In the atomistic LLG approach the inclusion of the Langevin fields has been proven to give the correct thermally excited spin-wave spectrum [17]. The deterministic LLB equation describes the average magnetization trajectory. However, to describe the dispersion of different trajectories, the stochastic LLB equation is necessary. The stochastic form of the LLB equation also exists, in a similar way to the LLG Langevin equation. The stochastic fields were firstly included in the macroscopic LLB equation to take into account the fluctuations of the magnetic grain of volume V [65]. Further, they were introduced in the multi-macrospin

LLB approach in order to allow some degree of the correlation loss in the simulation of the laser induced magnetization dynamics that we will discuss in section 2.3.3. The stochastic fields can be introduced in several ways, see discussion in Ref. [58], but here we present two different ways. The first form (sLLB-I) reads

$$\dot{\mathbf{m}} = \gamma[\mathbf{m} \times \mathbf{H}_{\text{eff}}] - \frac{\gamma\alpha_{\parallel}}{m^2}\left(\mathbf{m}\cdot\mathbf{H}_{\text{eff}} + \boldsymbol{\zeta}_{\parallel}\right)\mathbf{m} + \frac{\gamma\alpha_{\perp}}{m^2}\left[\mathbf{m}\times\left[\mathbf{m}\times\mathbf{H}_{\text{eff}} + \boldsymbol{\zeta}_{\perp}\right]\right], \quad (2.34)$$

where stochastic fields $\boldsymbol{\zeta}_{\parallel}$ and $\boldsymbol{\zeta}_{\perp}$ describe the dispersion of different magnetization trajectories and have the following properties:

$$\langle\zeta_a^i\rangle = 0, \quad \langle\zeta_a^i(0)\zeta_a^j(t)\rangle = \frac{2k_BT}{|\gamma|\alpha_a M_s V}\delta_{ij}\delta(t) \quad (2.35)$$

Here a stands for one of the symbols $\parallel$ or $\perp$, i and j denote the Cartesian components x, y and z, V is the volume of the single domain magnet, and M_s is the value of the spontaneous magnetization at zero temperature. Comprehensibly, the noise decreases with increasing volume of the investigated grain. This form of the LLB equation and the noise properties have been used in several works [10, 95, 157]. Nevertheless the above presented equation does not give the Boltzmann distribution close to T_C. This disagreement has been found quite recently [58], therefore the results presented in this thesis are obtained by the use of Eq. (2.34) below. We have checked that the qualitative results remain unchanged.

The second form of the stochastic LLB equation (sLLB-II), which gives the correct Boltzmann distribution for all temperatures reads

$$\dot{\mathbf{m}} = \gamma[\mathbf{m} \times \mathbf{H}_{\text{eff}}] - \frac{\gamma\alpha_{\parallel}}{m^2}\left(\mathbf{m}\cdot\mathbf{H}_{\text{eff}}\right)\mathbf{m} + \frac{\gamma\alpha_{\perp}}{m^2}\left[\mathbf{m}\times\left[\mathbf{m}\times\mathbf{H}_{\text{eff}} + \boldsymbol{\zeta}_{\perp}\right]\right] + \boldsymbol{\zeta}_{\text{ad}}, \quad (2.36)$$

where the diffusion coefficients are given by

$$\langle\zeta_{\text{ad}}^i(0)\zeta_{\text{ad}}^j(t)\rangle = \frac{2|\gamma|k_BT\alpha_{\parallel}}{M_sV}\delta_{ij}\delta(t), \quad (2.37)$$

$$\langle\zeta_{\perp}^i(0)\zeta_{\perp}^j(t)\rangle = \frac{2|\gamma|k_BT(\alpha_{\perp}-\alpha_{\parallel})}{M_sV\alpha_{\perp}^2}\delta_{ij}\delta(t) \quad (2.38)$$

The proof and a complete numerical study can by found in work [58]. In Fig. 2.7 we show the magnetization modulus distribution function $P(m)$ for non-interacting nanoparticles without applied field and anisotropy, calculated numerically solving Eqs. (2.34) and (2.36) for two different temperature regions: far from the Curie temperature and close to T_C. Far from T_C both distributions are almost the same, whereas close to T_C a larger difference can be appreciated.

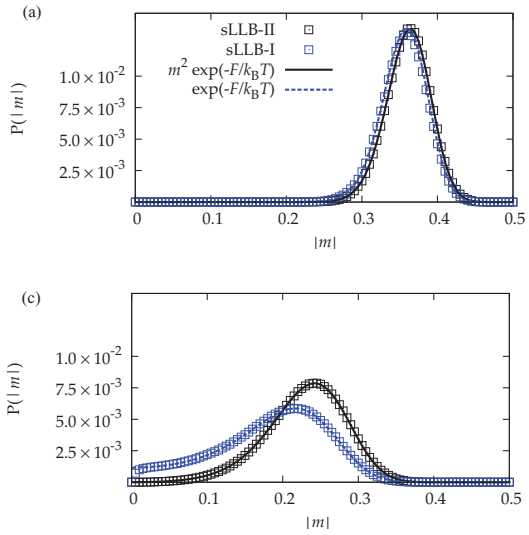

Figure 2.7: Magnetization modulus distribution function using both stochastic approaches sLLB-I and sLLB-II. (Up) At low temperatures the difference is negligible between both approaches. (Down) Only at temperatures very close to T_C appreciable differences appear.

2.3.3 Multi macro-spin micromagnetic model

As the LLB equation describes the dynamics of the mean polarization of a grain, the so called macro-spin, this approach is not strictly valid for large systems where the magnetization is not spatially homogeneous (Fig. 2.8). The micromagnetic approach based on the LLB equation and Langevin dynamics offers the possibility to simulate the magnetization dynamics of larger ferromagnetic systems at temperatures even above T_C.

Our model uses cubic discretization elements with lateral size Δ, thus, with a volume $V = \Delta^3$. For each cube, we write the stochastic LLB equation (2.34), describing its average spin polarization m_i, in the following form:

$$\dot{\mathbf{m}}_i = \gamma[\mathbf{m}_i \times \mathbf{H}^i_{\text{eff}}] - \frac{\gamma\alpha_\parallel}{m_i^2}\left(\mathbf{m}_i \cdot \left(\mathbf{H}^i_{\text{eff}} + \boldsymbol{\zeta}^i_\parallel\right)\right)\mathbf{m} + \frac{\gamma\alpha_\perp}{m_i^2}\left[\mathbf{m}_i \times \left[\mathbf{m}_i \times \left(\mathbf{H}^i_{\text{eff}} + \boldsymbol{\zeta}^i_\perp\right)\right]\right], \tag{2.39}$$

The effective magnetic fields, $\mathbf{H}^i_{\text{eff}} = \mathbf{H}_i + \mathbf{H}_{i,\text{EX}}$, are individually calculated for every macro-spin (cf. Eq. (2.31)) plus an additional term, which takes into account the exchange interaction between the macro-spins,

$$\mathbf{H}_{i,\text{EX}} = -\frac{A(T)}{m_e^2}\frac{2}{M_s\Delta^2}\sum_{\langle i,j\rangle}(\mathbf{m}_j - \mathbf{m}_i) \tag{2.40}$$

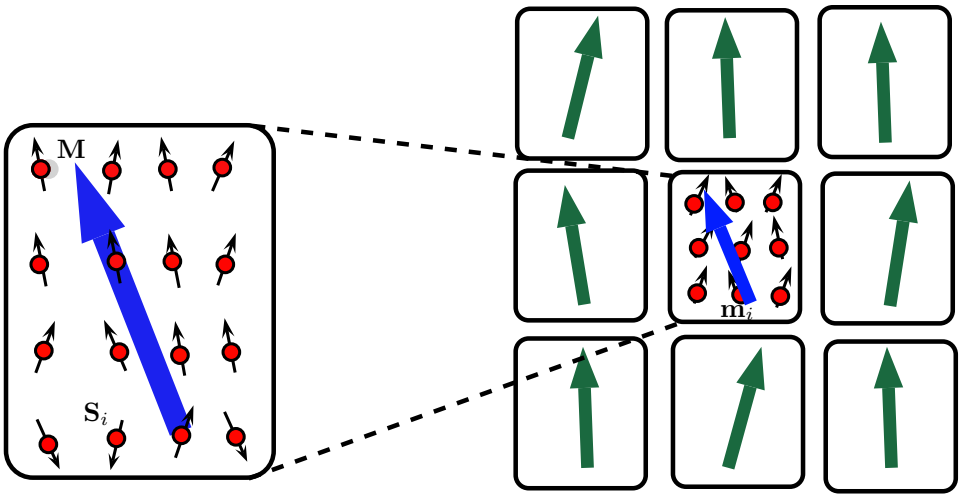

Figure 2.8: Illustration of the multi macro-spin model.

where $\langle i, j \rangle$ means a sum over nearest neighbours and $A(T)$ is the micromagnetic exchange also called exchange stiffness. The calculation of the temperature dependence of A is not straightforward as we have shown recently in Ref. [12], see also appendix D. Nevertheless, for practical simulations in several cases we will use the MFA scaling with the magnetization, $A \sim m_e^2$.

2.4 Multiscale modeling of magnetic materials

Although in the present thesis we will mostly make use of the mean-field approximation (MFA) for the temperature dependence of the micromagnetic parameters such as anisotropy constant K, micromagnetic exchange A, equilibrium magnetization m_e or longitudinal susceptibility $\widetilde{\chi}_{\parallel}$, a more robust multiscale modeling can be done. *Ab-initio* techniques can provide insight into the local atomic scale values such as the local magnetic moment μ_0, the local anisotropy d, or a pairwise exchange parameters J_{ij}. Firstly, the *ab-initio* local parameters have to be mapped onto a Heisenberg type Hamiltonian, however, this step is not always possible and effective parameters are introduced, as for example in the FePt case [124]. Then, the challenge is to pass this atomic information to micromagnetic length scale at finite temperatures. Most of the *ab-initio* calculations are zero temperature, then, for the temperature dependence of the micromagnetic parameters statistical techniques are required.

Once the Heisenberg Hamiltonian is defined several techniques can be used. For example, constrained Monte Carlo technique [9], which has been used to calculate the temperature dependence of the anisotropy in nanoparticles and thin

films as a function of the equilibrium magnetization. This technique has been tested in simple cubic (sc) as well in face center cubic (fcc) structured thin films. The Callen theoretical prediction for low temperatures was well described; for uniaxial anisotropy it was found that $K \sim m^3$ and for cubic anisotropy $K \sim m^{10}$ [34]. This technique is useful for more complex situations where the analytical solutions are almost impossible and for artbitrary temperatures.

A successful technique giving access to the temperature dependent magnetic parameters (such as $M_s(T)$) is the Langevin dynamics based on the Landau-Lisfhitz-Gilbert (LLG) equation of motion for the atomic spins. The LLG Langevin technique has been tested against the analytical Green function technique giving the same temperature dependence of the spin wave spectrum [17] and consequently the same equilibrium magnetization. The main issue using the LLG Langevin simulations is how to extract the correct micromagnetic parameters. It is sometimes not simple neither straightforward. The equilibrium magnetization is quite simple, it can be calculated as

$$\mathbf{m}_e = \langle \mathbf{s} \rangle = \frac{1}{N} \sum_i \int_0^\infty \mathbf{s}_i(t) dt \tag{2.41}$$

where N is the number of spins and $\mathbf{s}_i$ is the normalized atomic magnetic moment for the lattice site i. Computationally speaking, the upper integration time (∞) can not be achieved and therefore the calculation has to be stopped at a given finite time T_f. For temperatures far from the critical one, the value of $\mathbf{m}_e$ quickly converges, thus, the total needed integration time t_f is quite short. However, for T close to T_C the task becomes more difficult due to the finite size effects and critical fluctuations has to be taken into account and thereby the calculations can be quite long.

The longitudinal and transverse susceptibilities are also easy to compute, though computationally expensive, from the fluctuations of the magnetization [80] in the corresponding direction via the following expressions:

$$\widetilde{\chi}_\parallel = \frac{\mu_0 N}{k_B T} \left(\langle s_z^2 \rangle - \langle s_z \rangle^2 \right) \tag{2.42}$$

$$\widetilde{\chi}_\perp = \frac{\mu_0 N}{2 k_B T} \left(\langle s_x^2 \rangle + \langle s_y^2 \rangle - \langle s_x \rangle^2 - \langle s_y \rangle^2 \right) \tag{2.43}$$

where N is the number of spins and

$$\langle \mathbf{s}^2 \rangle = \frac{1}{N} \sum_i \int_0^\infty \mathbf{s}_i^2(t) dt. \tag{2.44}$$

The same problem close to T_C as in the calculation of $\mathbf{m}_e$ arises in the susceptibility calculations [80, 95].

The most difficult calculations are those of temperature dependent exchange stiffness. In Ref. [12] we suggested two methods: via domain wall width and via spin wave stiffness, which are outlined in appendix D.

2.5 Ultrafast laser-induced demagnetization within the LLB model

In this section we show the utility of the LLB model to study the heat induced magnetization dynamics induced by a powerful femtosecond laser pulse. Following [10], we assume that the magnetization is directly coupled to the electron temperature T_e which is calculated within the simplified two-temperature model

$$\begin{aligned} C_{\mathrm{e}}(T_{\mathrm{e}})\frac{dT_{\mathrm{e}}}{dt} &= -G_{\text{e-ph}}(T_{\mathrm{e}} - T_{ph}) + S(t) \\ C_{\mathrm{ph}}(T_{\mathrm{ph}})\frac{dT_{\mathrm{ph}}}{dt} &= G_{\text{e-ph}}(T_{\mathrm{e}} - T_{ph}) \end{aligned} \tag{2.45}$$

where C_e and C_{ph} are the electron and lattice specific heat constants, G_{e-ph} is the electron-phonon coupling constant, and $S(t)$ is the absorbed laser fluence.

As the present section is focused on the study of the ultrafast demagnetization and the subsequent magnetization recovery we calculate the magnetization dynamics up to the first 5 ps. We use the stochastic LLB multi-macrospin approach presented in Eq. (2.34) and system parameters in Table 2.1. The considered paramaters correspond to Ni thin films and the anisotropy is taken in-plane, thus, the magnetization lies in the film plane and we assume that $z-$axis corresponds to the equilibrium magnetization direction. The inital temperature is taken as $T = 300K$. The temperature-dependent parameters are evaluated via MFA.

The results of our simulations are presented in Fig. 2.9. We note here that laser pulses, producing maximum electron temperatures far above the Curie temperature are required for demagnetization. This is consistent with atomistic simulations [96], and is because the rate of energy transfer from the conduction electrons takes place with a characteristic relaxation time determined by the coupling between the conduction electrons and the spins. The response of the spins is slow (due to the finite longitudinal relaxation). Essentially the magnetization lags the electron temperature. This is an important effect which is well-described by the LLB approach. Our model reproduces all essential features of the heat-assisted

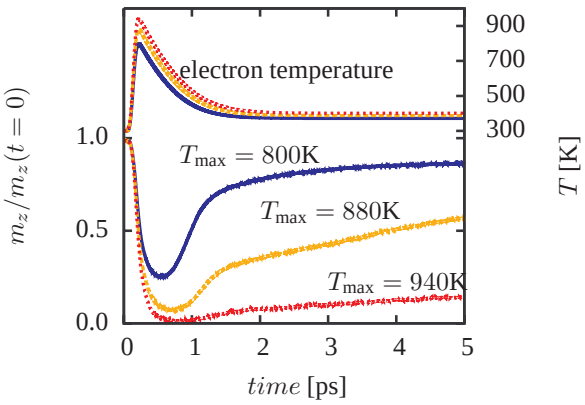

Figure 2.9: Magnetization dynamics calculated via the integration of the multi-macrospin LLB model for three maximum electron temperatures $T_{\max} = 800, 880$ and 940K. The femtosecond demagnetization and the subsequent recovery of the magnetization in picosecond timescale are well described by the model.

demagnetization. Namely, we observe a very fast demagnetization, occurring at femtosecond scale, followed by a more slow *picosecond* recovery. The rate of the recovery is different depending on the minimum magnetization value achieved during the demagnetization. A similar effect has been observed in atomistic simulations [96] as well as in experiments [97]. The observed slow recovery rate is due to the loss of correlations at high temperature since the micromagnetic exchange vanishes. Consequently, additional time is necessary to recover the correlations.

2.6 Ultrafast laser-induced magnetization precession

Finally, we show that the three characteristic time scales present in ultrafast magnetization dynamics can be correctly described within our approach. We will use this model to simulate the laser induced magnetization precession. The idea behind the generation of coherent precession is sketched in Fig. 2.10. Before the pulse arrival the magnetization is aligned with the effective field $\mathbf{H}_{\text{eff}} = \mathbf{H}_a + \mathbf{H}_{\text{ext}}$. The different anisotropy contributions to $\mathbf{H}_a$, crystalline and shape anisotropies, strongly depend on the instantaneous magnetic state. Here we consider that the micromagnetic crystalline anisotropy constant follows the well-known Callen-Callen [34] law, for uniaxial anisotropy $K \sim m^3$, while the shape anisotropy, $H_{\text{d}} = -4\pi M_{\perp}$, depends linearly on the magnetization value. Thus, during the ultrafast demagnetization process the anisotropy field is time dependent, $\mathbf{H}_a(t)$,

Table 2.1: Parameters in the 2TM and the LLB equation (Ni) used in the simulations. The Ni parameters are taken from Ref. [11].

2TM		LLB	
Parameter	Value	Parameter	Value
γ_e	2.25×10^2 J/m^{3}K^2	$M_s(T=0K)$	500 emu/cm^3
G_{e-ph}	2.5×10^{17} W/m^{3}K	$K(T=0K)$	5.3×10^4 erg/cm^3
C_{ph}	40 Jmol^{-1}K^{-1}	T_C	631 K
t_p	50 fs	a	0.35 nm
		Δ	2.5 nm
		λ	0.1

through the time dependence of the magnetization. At the same time the external magnetic applied field, being temperature independent, rests with the same value during the process. This different temperature dependence leads to a change in the direction of the effective field, if both contributions to the effective field are non-collinear. If this change is faster than the transverse relaxation time, the magnetization is not able to follow the new effective field and will be taken out of equilibrium.

After a few picoseconds the sample cools down to a quasi-equilibrium electron temperature which can be taken as a constant, and the anisotropy direction and value stabilize, therefore a new equilibrium direction is created around which the magnetization coherently precesses towards the equilibrium in a timescale of nanoseconds. The laser induced coherent magnetic precession experiments provide a useful tool to study the magnetic precession properties as, for example the Gilbert damping parameter [147, 165].

From the modeling point of view, the correct description of the coherent laser induced precession can be achieved by an adequate description of the ultrafast demagnetization and the subsequent magnetization recovery as the LLB model does (see previous section). It is also necessary to achieve a correct description of the effective field dynamics during all stages of the process. The LLB model correctly describes all these effects. We use again the multispin micromagnetic LLB model with the same parameters as in the previous section (see Table 2.1) but now with a different initial configuration in order to cause magnetization precession. An out of plane external magnetic field $\mathbf{H}_{ap} = 1$T is applied, which is strong enough to tilt up the initial magnetization to an out of plane configuration. We use in-plane magnetic anisotropy and the magnetostatic fields are evaluated in the MFA approach for thin films. Fig. 2.10 shows that after the first picosecond

demagnetization follows a slower magnetization recovery and it finishes with a coherent nanosecond magnetization precession. All three magnetization rates are then described by the same LLB model presented in the present Chapter.

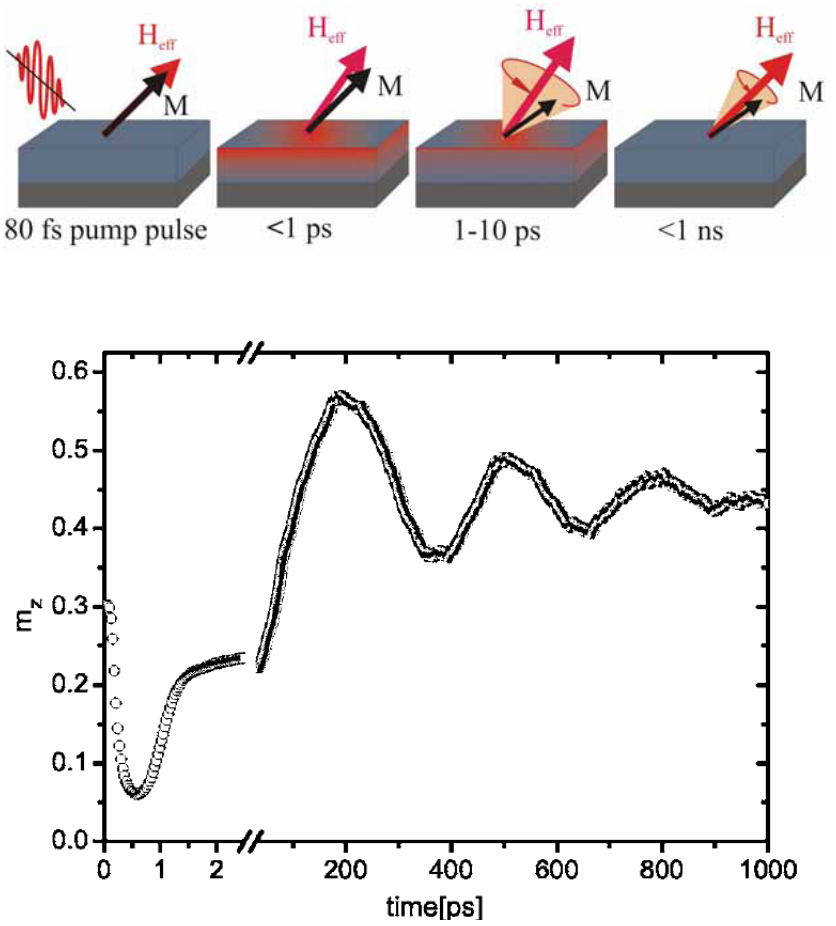

Figure 2.10: Laser-induced coherent magnetic precession. (Up) A schematic representation of the process leading to magnetization precession. Figure taken from Ref. [164]. (Down) Laser-induced coherent magnetic precession simulated in the stochastic LLB multi macrospin approach.

3

Modeling of ultrafast magnetization dynamics in Nickel

3.1 Introduction and Motivation

In the previous Chapter we have only presented novel theoretical approaches for modeling of the ultrafast laser induced magnetization dynamics. However, we have somehow, let the experimental results out of discussion in comparison with our model. In that sense and motivated by the experimental results in Nickel of our partners in University of Göttingen (Germany) lead by Prof. M. Münzenberg, we have modeled their experimental results in laser induced ultrafast magnetization dynamics using our model.

Ni was the first ferromagnetic metal where femtosecond demagnetization was observed [19], thereafter many experimental as well as theoretical effort has been done in Nickel [23, 105, 166] with the aim of understanding both the fundamental mechanisms and control of the magnetic properties. From theoretical point of view several possible underlying quantum mechanisms have been proposed to explain the loss of magnetic order: the Elliott-Yafet (EY) electron scattering mediated by phonons or impurities [105, 152] or other electrons [109], electron-electron inelastic exchange scattering [85], superdiffusive spin-polarized electrontransport [18], or coherent light-spin coupling [23].

Here we use the "*thermal*" description of the femtosecond magnetization dynamics described in Chapter 2. The electron and phonon energy flow is modeled within the two temperature model (2TM), see Chapter 2 for details. The thermal model assumes that stochastic spin-flip processes are driven by the increased electron temperature and the magnetization dynamics is described by the LLB equation which includes the magnetic critical fluctuations near the critical temperature T_C. A similar model allowing one of the first quantitative comparisons

has been published recently [105]. In this model the spin fluctuations have been introduced by a mean field Weiss model and incorporating thermal statistics with spin $S = 1/2$. In Chapter 4 we will discuss the relation between this model, the so-called microscopic three temperature model (M3TM), and ours.

In our LLB macrospin approach for Ni, the microscopic spin-flip process is parameterized by the coupling parameter λ between the spin and the electron system. Here we use the fact that spin-orbit interaction intermixes the spin channels and allows spin-flip processes in principle. The thermal macrospin is also advantageous because of a reduced computational expense compared to the atomistic calculations. At the same time this approach is more general, since the restriction of the classical spin is removed and characteristics of itinerant ferromagnets, their quantum character (see Chapter 4) and scattering mechanisms can be implemented in extension of the model (see Chapter 5). In this chapter, we present a quantitative comparison between the described experiment and our LLB model for the ultrafast magnetization dynamics in Ni for a set of different excitation powers and thin film thicknesses. The excellent agreement between experiment and model proves that the ultrafast demagnetization in Ni can be modeled assuming a purely thermal origin.

3.2 Absorbed power as a function of film thickness

We briefly describe the experiments carried out by Prof. Münzenberg's group in Nickel thin films.

The experiment was performed on 10 nm to 40 nm thick ferromagnetic Ni films deposited on a Si(100) substrate using electron-beam evaporation in ultra-high vacuum. A femtosecond pump-probe experiment was used to determine the reflectivity $R(\tau)$ and the Kerr rotation $\theta_K(\tau)$ as a function of the probe pulse delay τ [104**?**]. The exciting pump-pulse fluence was varied from 10 to 50 mJ/cm^2 per pulse (80 fs, $\lambda = 800$ nm). A static field was applied in-plane to saturate the sample.

The optical penetration depth, λ_{opt}, for Ni is approximately 14 nm, thus in the same range as the thicknesses of the measured thin films, $t_{\mathrm{Ni}} = 10 - 40$ nm. The absorbed laser power decays as a function of the distance from the surface (see Fig. 3.1). We will assume that the absorption is faster than the energy diffusion to the substrate, therefore for film thickness smaller than optical penetration depth we will consider that all the absorbed energy rests inside the optical region. For film thickness larger than λ_{opt} we will assume that some of

the laser energy is absorbed by thin film layers beyond the optical region. Within this assumption for each thin film thickness different mean absorbed energy by layer has to be considered in the data analysis. By doing so, we will show that the maximum observed demagnetization in the experimental data depends on the mean absorbed power more than on the absolute value of the pulse laser fluence. In order to describe the incident laser intensity more accurately we adopt the

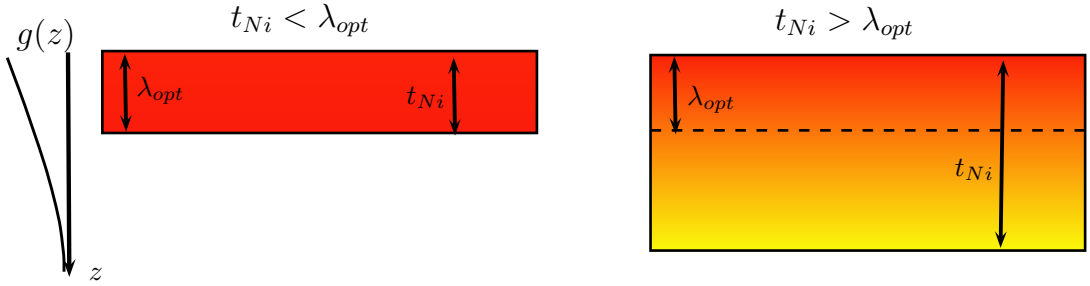

Figure 3.1: Schematic representation of absorption in thin films with different thicknesses. (Left) The thin film thickness, t_{Ni}, is smaller than the optical penetration depth, λ_{opt}, which defines the optical region. (Right) For films with thickness larger than λ_{opt} the incident laser energy has to be shared by all film layers, included those beyond the optical region.

laser incident intensity expressed by a Gauss function:

$$I(t) = I_0 \exp\left[-\left(\frac{t}{\sqrt{2}\sigma}\right)^2\right] \frac{\exp\left[-\alpha z\right]}{1-\exp\left[-t_{\mathrm{Ni}}\alpha\right]} \tag{3.1}$$

where I_0 is the maximal laser power intensity, $\alpha = \lambda_{opt}^{-1}$, $s = \sqrt{2}\sigma$ is the laser pulse width and z is the distance to the surface of the thin film. The full width at half maximum (FWHM) is defined as $\tau_L = s\sqrt{2\ln 2}$. The fluence F, I_0 and τ_L are related by the following relation $F = \sqrt{(\pi/4)\ln 2} I_0 \tau_L \approx 1.0645 I_0 \tau_L$. In order to calculate the absorbed power we have to include the effect of the reflected and transmitted energy. The reflectivity and transmission coefficients, R and T respectively, are then included in the laser power density absorbed in the material $S(t)$:

$$S(t) = (1-R-T)\alpha \frac{F}{1.0645 s\sqrt{2\ln 2}} \exp\left[-\left(\frac{t}{\sqrt{2}\sigma}\right)^2\right] \frac{\exp\left[-\alpha z\right]}{1-\exp\left[-t_{\mathrm{Ni}}\alpha\right]} \tag{3.2}$$

We simplify the notation by the definition of the following variables

$$\widetilde{I}_0 = \frac{(1-R-T)}{1.0645 s\sqrt{2\ln 2}}, \quad \text{includes intrinsic parameters contribution}$$

$$G(s) = \exp\left[-\left(\frac{t}{\sqrt{2}\sigma}\right)^2\right], \quad \text{Gaussian distribution with width } s = \sqrt{2}\sigma$$

$$g(z, t_{\mathrm{Ni}}) = \alpha \frac{\exp\left[-\alpha z\right]}{1-\exp\left[-t_{\mathrm{Ni}}\alpha\right]}, \quad \text{distribution function of the absorbed energy.}$$

Thus, $S(z, t_{\mathrm{Ni}})$ can be written as a function of the above defined parameters,

$$S(z, t_{\mathrm{Ni}}) = \widetilde{I}_0 F G(s) g(z, t_{\mathrm{Ni}}) = S_0 g(z, t_{\mathrm{Ni}}). \tag{3.3}$$

The function $g(z, t_{\mathrm{Ni}})$ depends on the thin film thickness t_{Ni} and the depth z (surface corresponds to $z = 0$). We compare different thicknesses by taking the average value of $g(z, t_{\mathrm{Ni}})$ over the layers defined as

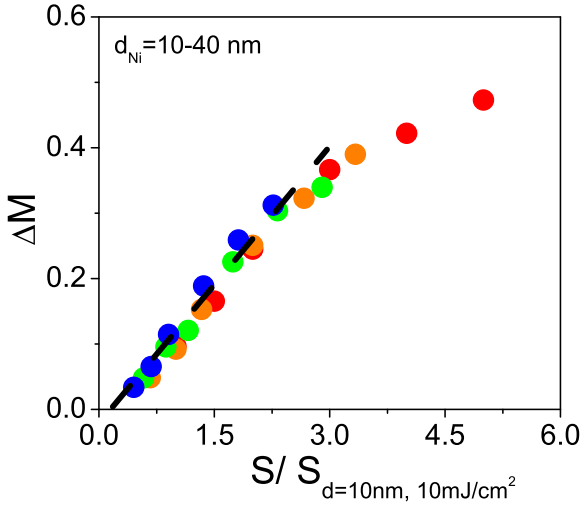

Figure 3.2: The experimental results of the femtosecond demagnetization for pump fluence $F = 50\mathrm{mJ/cm}^2$ and for Ni thicknesses of $10, 15, 20$ and $40\,\mathrm{nm}$ rescaled to the absorbed fluence per Ni layer S/S_{10}.

$$\langle g(z)\rangle = \frac{1}{t_{\mathrm{Ni}}}\int_0^{t_{\mathrm{Ni}}} g(z)dz = \begin{cases} \frac{1}{t_{\mathrm{Ni}}} & , \; t_{\mathrm{Ni}} < \lambda_{\mathrm{opt}} \\ \frac{1}{\lambda_{\mathrm{Ni}}}\frac{1-\exp(-1)}{1-\exp(-t_{\mathrm{Ni}}\alpha)} & , \; t_{\mathrm{Ni}} > \lambda_{\mathrm{opt}} \end{cases} \tag{3.4}$$

We normalized $S(t)$ to the mean absorbed power of the thinnest film (10 nm) and at the lowest fluence 10mJ/cm^2,

$$S_{10}(z, t_{\text{Ni}} = 10\text{nm}) = I_0 F_{10} G(s, t_0) \langle g(z, t_{\text{Ni}} = 10\text{nm}) \rangle \tag{3.5}$$

thereby

$$\frac{S}{S_{10}} = \begin{cases} \frac{F}{F_0} \frac{10\text{nm}}{t_{\text{Ni}}} & , t_{\text{Ni}} < \lambda_{\text{opt}} \\ \frac{2}{3} \frac{F}{F_0} \frac{1-\exp(-1)}{1-\exp(-t_{\text{Ni}}\alpha)} & , t_{\text{Ni}} > \lambda_{\text{opt}} \end{cases} \tag{3.6}$$

Fig. 3.1 shows the resulting demagnetization ΔM for various pump fluences F for Ni thicknesses from $10, 15, 20$ and 40 nm rescaled to the normalized absorbed fluence per Ni layer S/S_{10}. From Fig. 3.1 it can be appreciated that ΔM scales with this quantity and linearly depends on S/S_{10} (with the exception of strong pulses) regardeless the thin film thicknesses. Therefore in the following we will restrict our modeling to the 15 nm Ni film without losing generality.

3.3 Magnetization dynamics model

The main assumption of the thermal model is that the hot electrons provide a heat bath for the spin dynamics [96]. This is a reasonable assumption: in a good approximation for a ferromagnetic transition metal microscopically the spin system is dominantly coupled to the electronic temperature [125]. Thus, in the following the heat bath temperature T is set to $T = T_e(t)$, the electronic temperature, driving the magnetic fluctuations and the weaker spin-lattice interaction will be neglected on the ultrafast timescale. It will be shown in the following in how far a quantitative description of the magnetization dynamics using the LLB equation is possible. In the experimental timescales of the demagnetization and remagnetization processes the precession terms are negligible and the magnetization dynamics can be described using the longitudinal term of the LLB dynamical equation (2.26). It reads as follows:

$$\frac{\dot{m}}{\gamma} = -\lambda \frac{2T_e}{3T_C} \begin{cases} \frac{1}{2\tilde{\chi}_{||}} \left(1 - \frac{m^2}{m_e^2}\right) m & T_e \leq T_{\text{C}} \\ \frac{1}{\tilde{\chi}_{||}} \left(1 + \frac{3m^2 T_{\text{C}}}{5(T_e - T_{\text{C}})}\right) m & T_e \geq T_{\text{C}} \end{cases} \tag{3.7}$$

The coupling parameter λ is proportional to the spin-flip rate due to the interaction with the environment. Fig. 3.3 shows the temperature-dependent equilibrium magnetization m_e and longitudinal susceptibility $\tilde{\chi}_{||}$ as determined from the MFA, see Appendix A, by adjusting the Curie temperature value to the experimental one $T_C = 631\,\text{K}$.

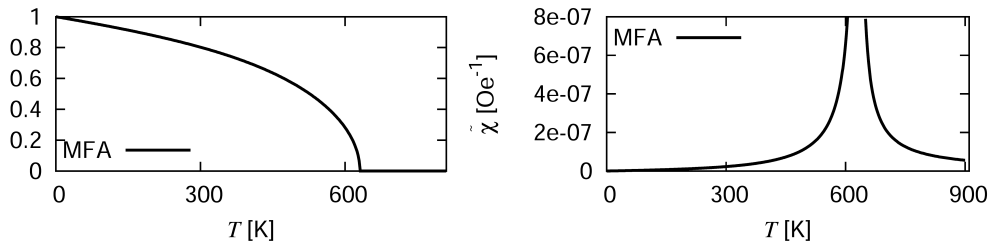

Figure 3.3: (Left) Equilibrium magnetization m_e *vs.* temperature calculated for Ni from MFA approach, (Right) Parallel equilibrium susceptibility *vs.* temperature for Ni.

We use the following parameters for Ni as measured from previous experiments in the same samples [**?**]: the saturation magnetization $M_s = 500\text{emu/cm}^3$ (at $T = 0\,\text{K}$), the applied field was $\mathbf{H} = 1500\,\mathbf{e}_x\,\text{Oe}$. The easy plane anisotropy, defined by magnetostatic interactions for the thin film geometry, is given by $\mathbf{H}_A = 4\pi M_s(T)\,(m_x\mathbf{e}_x + m_y\mathbf{e}_y)$. The magneto-crystalline anisotropy is neglected. Finally the damping parameter for the Ni films is $\alpha_\perp = 0.04$ at $T = 300\,\text{K}$ as experimentally determined [**?**] for the same samples. The intrinsic coupling parameter $\lambda = 0.045$ directly follows from the transverse relaxation damping $\alpha_\perp$ using the formula (2.27). Fig. 3.4 (b) shows a sketch of both relaxation processes, longitudinal and transverse relaxation, after the laser pulse excitation represented in Fig. 3.4 (a). Therefore all parameters that enter into the equation of motion (3.7), besides the electron temperature T_e, have been determined independently from the experiment.

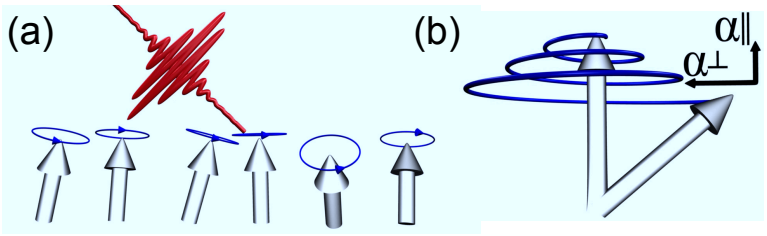

Figure 3.4: Schematics of the thermal model. (a) The laser deposits energy on the spin system leading to the excitation of THz spin waves. (b) The resulting "*macrospin*" experiences two relaxations: longitudinal and transverse damping $\alpha_{||}$ and $\alpha_\perp$.

3.4 Two temperature model parametrization from experimental reflectivity

The data of the delayed reflectivity $R(\tau)$ for various pump fluences are presented in Fig. 3.5 and show a contribution mirroring the electron dynamics with a steep peak like increase that equilibrates on a constant slope plus oscillations with a main period of about 7 ps. They originate from the coherent excitation of a shockwave (sound velocity $\nu_{Ni} = 5400\,\mathrm{m/s}$). In the case of a film thickness in the range of $t_{\mathrm{Ni}} \sim t_{\mathrm{opt,800\,nm}}$ a standing shock wave forms with the wave vector $k = \pi/t_{\mathrm{Ni}}$ [52]. For a threshold fluence above $30\,\mathrm{mJ/cm^2}$ the strong coherent stress wave excitations appear to have an incoherent counterpart (lattice heating and thermal expansion) owing to an effect on the reflectivity. The transient reflectivity $R(\tau)$ will be taken as an independent input to extract the relevant parameters for the modeling of the electron temperature $T_e(t)$. To calculate the electronic temperature $T_e(t)$ within a two-temperature ($2T$) model (symbols), the relevant parameters are extracted from the decay rates of the measured reflectivity (solid lines). The assumption needed here that in first approximation the reflectivity change is defined by the electron temperature change $\Delta R(t) \propto \Delta T_e(t)$, which is only valid on a small range with limitations [141]. The electron temperature $T_e(t)$ is coupled to the lattice temperature T_{ph} within the $2T$ model [92] in the form of two differential equations:

$$\begin{aligned} C_e \frac{dT_e}{dt} &= -G_{e-ph}(T_e - T_{ph}) + S(t) - C_e \frac{(T_e - T_{\mathrm{room}})}{\tau_{th}} \\ C_{ph} \frac{dT_{ph}}{dt} &= G_{e-ph}(T_e - T_{ph}), \end{aligned} \tag{3.8}$$

Here C_e and C_{ph} are the specific heats of the electrons and the lattice, G_{e-ph} is an electron-phonon coupling constant which determines the rate of the energy exchange between the electrons and the lattice [6], and τ_{th} is the heat diffusion time to the outer space. The electronic specific heat is calculated in the free electron approximation as described in the previous Chapter, $C_e = \gamma_e T_e$, $\gamma_e = 3 \times 10^3\,\mathrm{Jm^{-3}K^{-2}}$. The lattice specific heat at low pump fluences is taken constant and equal to $C_{ph} = C(300\ \mathrm{K}) - C_e(300\ \mathrm{K}) = 3.1 \times 10^6\,\mathrm{Jm^{-3}K^{-1}}$, where $C(300\ \mathrm{K}) = 4 \times 10^6\,\mathrm{Jm^{-3}K^{-1}}$ is the experimental total specific heat of Ni [28]. The remaining parameters of the model were obtained by the fitting of the transient reflectivity as sketched in Fig. 3.6 for all data from Fig. 3.5 using the following procedure [84]:

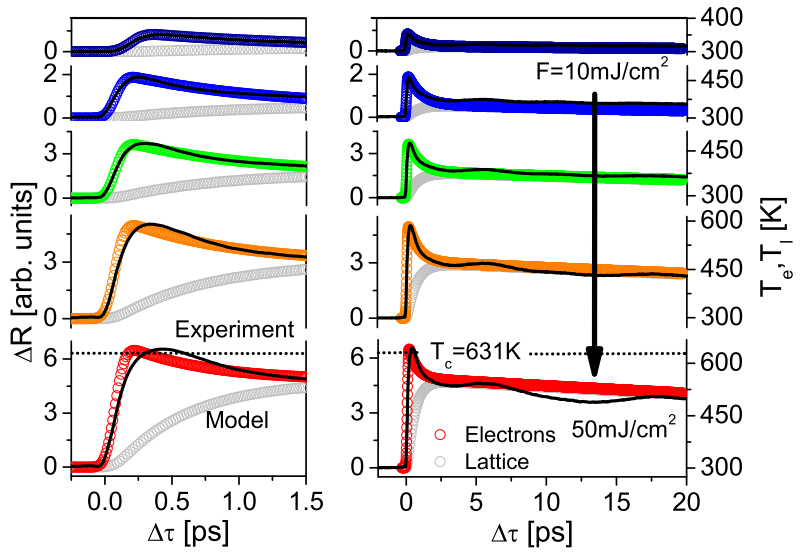

Figure 3.5: Response after femtosecond laser excitation revealing the dynamics of the heated electrons, coherent stress waves and incoherent lattice excitations at various pump fluences F contributing to the transient reflectivity for a 15 nm Ni thin film (solid lines). The relaxation rates allow to extract the parameters for the integration of the $2T$ model from the normalized curves. Therefrom the electron temperatures T_e (colored symbols) and lattice temperature T_{ph} (gray symbols) are derived as described in the text. Note that a different linear scale relating ΔR and T_e was used to present the data for different fluences F. The same data is plotted on the long time scale (right) and sub-picosecond time scale for details (left).

- From the low-fluence reflectivity curve the scattering rate G_{e-ph} was determined by the first decay rate, *i.e.* the electron-phonon equilibration time τ_E. They are related by the linear expression $\tau_E = C_e/G_{e-ph}$. This procedure gives $G_{e-ph} \approx 10 \times 10^{17}\,\mathrm{Wm^{-3}K^{-1}}$, consistent with similar values reported for Ni earlier [33].

- The heat diffusion time of $\tau_{th} \approx 50\,\mathrm{ps}$ was determined by the slow decay on the long term behavior, related to the time needed to equilibrate the heated film with the ambient temperature.

- Next both the reflectivity and the electron temperature curves were normalized to ΔR^{max} and T_e^{max}, respectively. At high pump fluency, the fitting of the $2T$ model to the reflectivity data shows that as the energy deposited increases, a decrease of the ratio T_e^{max}/T_{ph}^{max} is observed, see Fig. 3.6 (a),

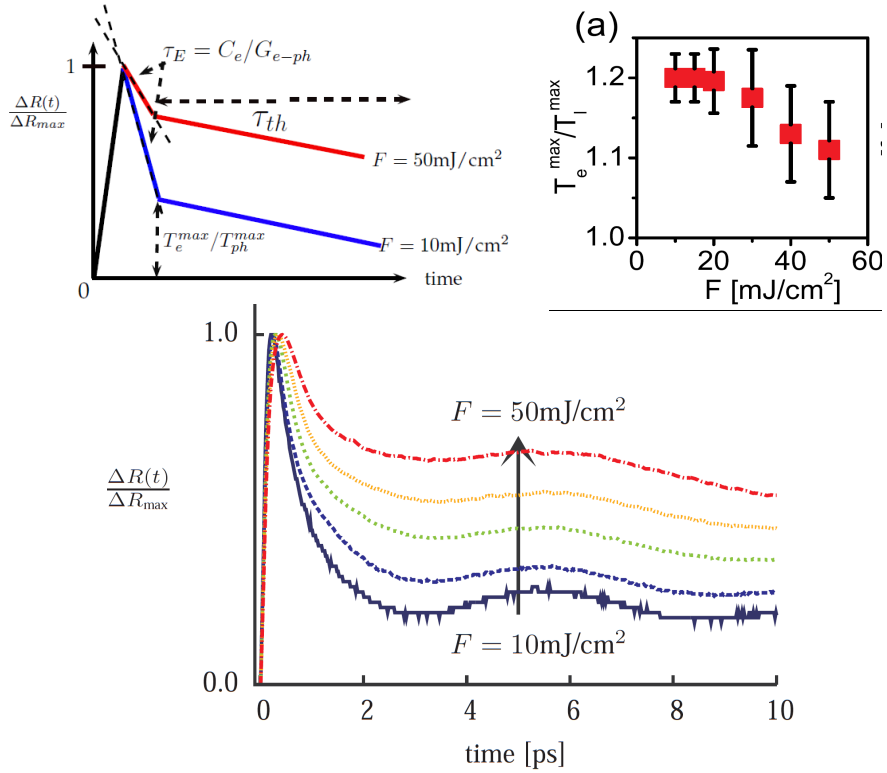

Figure 3.6: (Up) Schematic representation of the fitting procedure of the experimental reflectivity data. (Down) Experimental normalized reflectivity change data for different laser fluences from $F = 10\text{mJ/cm}^2$ to $F = 50\text{mJ/cm}^2$.

related to the ratio of C_{ph}/γ_e. This decrease may contain different contributions not included in our simplistic model, such as (i) nonlinear temperature dependence of the specific heat C_e, (ii) fluence dependence of the energy dissipation mechanisms, such as electron diffusion or elecron-phonon coupling, or (iii) dependence of the reflectivity data on T_{ph} at high pump fluencies [52]. The behavior was taken into account by considering that the lattice specific heat is a function of the pump fluency decreasing from the value above (at the lowest pump fluence) down to $C_{ph} = 1.0 \times 10^6\ \text{Jm}^{-3}\text{K}^{-1}$ at the highest pump fluence. This choice remains at this point arbitrary, but will have no impact on our final analysis since the numerical model is adapted to the experimental electron temperature. Alternatively, we could have used the adjustment of the γ_e value, as in Ref. [105], which would produce a similar effect.

- Finally, the absolute temperature variation has to be calculated, determined by the Gaussian source term $S(t)$ which describes the laser power

density absorbed in the material. It is proportional to the fluence $F(t)$. The proportionality factor is difficult to determine in praxis because the absorption of substrate and interfaces is typically found too large. It is determined from the boundary condition of the numerical calculation: the temperature of the electron system T_e is set to the temperature of the spin system T_s for long time scales (determined from the demagnetization via $m_e(T_s) = (M_{0,300\mathrm{K}} - \Delta M_{20\mathrm{ps}})/M_{0,0\mathrm{K}}$). The resulting proportionality factor is independent on the laser pump fluence.

The parameterization of the $2T$ model allows now its integration for all fluences to determine the absolute temperature T_e. The results are given in Fig. 3.5, overlayed to the reflectivity data. The scaling factor, calculated to scale the normalized data to the model, is different for all fluences and systematically increasing by a factor of two. Here it is used to present the data only for direct comparison, however it points to a more complex dependence in between ΔR and ΔT_e and limits the application of a simple linear scaling. We want to note that reducing the parameters to a minimum number and keeping as many parameters the same for the fit for all fluence data, a reasonable agreement is found. However more advanced models that include further parameters, as the electron-electron equilibration time τ_{ee} [52] related to the steepness of the rising edge, can achieve a better description of the data. For the highest pump fluence the electron temperature exceeds the Curie temperature T_C while the lattice temperature stays well below that value.

3.5 Comparison between experiment and modelling

As a central result, we directly calculate the femtosecond magnetization dynamics in the LLB model by coupling Eq. (3.7) and the integration of the rate equations (3.8), taking the input temperature $T = T_e(t)$ for the heat bath. The results are presented in Fig. 3.7 (symbols) in direct comparison with the experimental data from the time-resolved Kerr effect $\Delta\theta_K$ normalized to the saturation value $\Delta\theta_{K,0}$ for negative delay (solid lines), equal to the normalized magnetization $M_x/M_{x,0}$ for timescales > 100 fs ($M_{x,0}$ is the room temperature value $M_{0,300\mathrm{K}}$). Characteristic effects as the double exponential remagnetization described in earlier work are reproduced in detail [**?**]. Moreover the modeled data describes the experimental data in their absolute value, in their detailed slope and predicts the correct time scales.

Let us focus on a very prominent feature: as the pump fluence is raised, the restoration to the original value of the magnetization slows down dramatically. It takes more than > 20ps for a demagnetization value of $0.6M_\mathrm{s}$. For a quantitative comparison, the results of the integration (modeled data) and experimental data of Fig. 3.7 are analyzed using the analytic solution for the three-temperature-model (including the spin temperature) given by Dalla Longa *et al.* [48, 166].

$$-\frac{\Delta M_x(t)}{M_{0,x}} = \Big[A_1 F(\tau_0, t) - \frac{(A_2\tau_E - A_1\tau_M)}{\tau_E - \tau_M} e^{-t/\tau_M} - \frac{\tau_E(A_1 - A_2)}{\tau_E - \tau_M} e^{-t/\tau_E}\Big]\Theta(t) * G(t) \quad (3.9)$$

Here $*G(t)$ represents the convolution product with the Gaussian laser pulse profile, $\Theta(t)$ is the step function, A_i are the fitting constants. Fig. 3.7 (b) shows the demagnetization time τ_M, and (c) the magnetization recovery time τ_E as fitted to Eq. (3.9) for both modeled and experimental data showed in Fig. 3.7.

We extended Eq. 3.9 by a second remagnetization time $\tau_{M,re}$.

$$\begin{aligned} -\frac{\Delta M_x(t)}{M_{0,x}} = \Big\{\Big[&A_1 F(\tau_0, t) - \frac{(A_2\tau_E - A_1\tau_M)}{\tau_E - \tau_M} e^{-t/\tau_M} \\ &- \frac{\tau_E(A_1 - A_2)}{\tau_E - \tau_M} e^{-t/\tau_E} - A_3 e^{-t/\tau_{M,re}}\Big]\Theta(t)\Big\} * G(t) \end{aligned} \quad (3.10)$$

Three time scales characterize the magnetization dynamics: the demagnetization time τ_M and the remagnetization times τ_E, $\tau_{M,re}$. The results are presented in Table 3.1 for direct comparison.

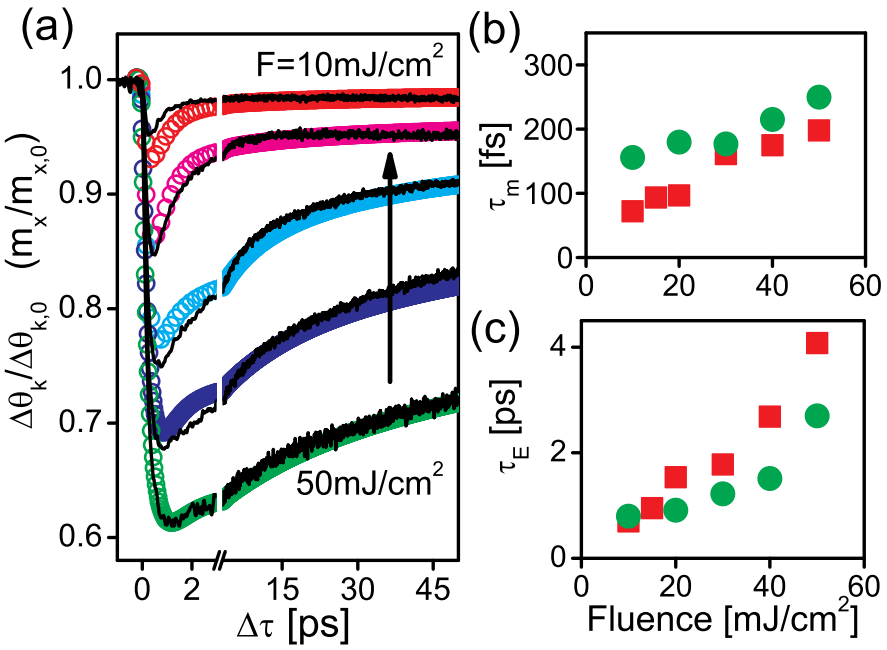

Figure 3.7: (a) Absolute values of the measured dynamics of the Kerr angle rotation (solid lines) and the modeled magnetization dynamics (symbols) for various laser pump fluences F. (Right) The magnetization dynamics rates as a function of pump fluence: (b) demagnetization time τ_M and (c) magnetization recovery time τ_E as function of the pump fluence are plotted. Experimental (circles) and modeling (squares) values are given for a direct comparison. Note that τ_E differs from the electron-phonon equilibration τ_{ep} by its magnetic contribution.

	time-resolved MOKE			LLB Model		
Fluence [mJ/cm^2]	τ_M [fs]	τ_E [ps]	$\tau_{M_{re}}$ [ps]	τ_M [fs]	τ_E [ps]	$\tau_{M_{re}}$ [ps]
10	70(10)	0.70(2)	-	160(15)	1.18(2)	–
20	101(10)	1.85(2)	-	175(15)	1.48(3)	–
30	160(10)	2.23(4)	18.4(3)	185(15)	1.45(2)	18.55(7)
40	178(10)	3.2(1)	39(1)	215(15)	1.03(1)	26.99(6)
50	193(15)	3.7(4)	58(5)	250(10)	1.15(1)	38.51(6)

Table 3.1: Direct comparison of the demagnetization time τ_M and magnetization recovery times from a two exponential fit τ_E and $\tau_{M,re}$. Note that τ_E can differ from the electron-phonon equilibration τ_{ep} by its magnetic contribution.

3.6 Discussion

We observe a slowing down of all magnetization times τ_M, τ_E and $\tau_{M,re}$ as a function of laser pump fluence. The demagnetization time τ_M is increased by about a factor of two. More dramatic is the effect on τ_E and $\tau_{M,re}$. A strong increase is observed. As a result, the recovery time of the magnetization τ_E, and the reflectivity (electron-phonon equilibration time), $\tau_{ep} \simeq 0.4$ to 0.5 ps, have different magnitudes.

The appearance of a slowing down for high fluences is a very general phenomena. It was observed in the recovery time for Ni previously [**?**], and also reported for the demagnetization time for Fe and Co [36, 42]. It is one of the immediate consequence of the longitudinal term in the LLB equation: it determines the rate at which the spin system disorders at a given temperature and mirrors the appearance of short wavelength spin excitations at THz frequency, the critical slowing down [38]. Fluctuations at all length scales appear at high temperatures and result in a large dynamic parallel susceptibility, inversely proportional to the strength of exchange interactions ($\chi_{||} \propto J^{-1}$) and diverging at T_C [41, 47]. Thus at given pump fluency different demagnetization rates are achieved for materials with different strength of exchange interactions J. Additionally, the magnetization relaxation rate $\tau_{||}$, see Fig. 3.8, is inversely proportional to the intrinsic coupling-to-the-bath parameter λ, *i.e.* to the scattering rate [106, 125]. Both directly leads to the classification of fast and slow materials introduced recently by Koopmans [105]. Therefore one concludes that during the laser-induced demagnetization the electron temperature is changed on the timescale faster than the longitudinal relaxation time of $\approx 1\,\mathrm{ps}$. Consequently, the spin system cannot follow the electron temperature. The magnetic response is delayed by the slowing down of the longitudinal relaxation, evident in a slower demagnetization (τ_M) and magnetization recovery times (τ_E, $\tau_{M,re}$).

The first experimental and theoretical approaches for FePt and CoPt attributed the slowing down of the magnetization recovery τ_E to a total magnetic correlation loss at high pump fluences [95]. In contrast to this, here even for the highest pump fluence of $50\,\mathrm{mJ/cm^2}$ per pulse, the absolute measurements of the dynamic Kerr effect reveal a reduction of the magnetization of $0.6 M_{0,300\,K}$ within the film depth probed. This is not sufficient to produce a magnetization correlation loss. Our analysis of the reflectivity data reveals that the relative balance between the energy put into the lattice and electron system is different for high fluency compared to low fluency, mirrored by the ratio between maximum electron and lattice temperatures (see Fig. 3.6 (a)). We capture as an important result that only the full description of the longitudinal relaxation, mirroring the

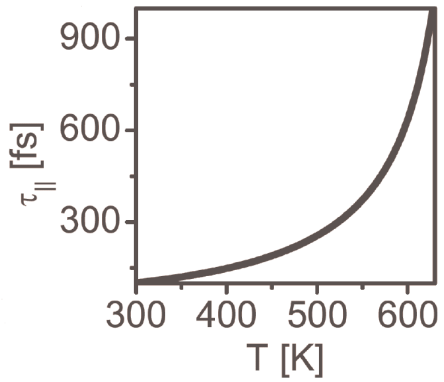

Figure 3.8: The longitudinal relaxation time for Ni as a function of temperature evaluated from the MFA.

magnetic correlations of the spin system, and the cooling dynamics of the lattice and electrons together leads to the correct description of the characteristic slowing down of the magnetization recovery. In the last part we want to discuss possible limitations. They can appear at very short time scales, where the electronic nature of the Stoner excitation may dominate the dynamics (< 100fs) and our value of the demagnetization time τ_M is consistently found too large. On the other hand also the approximation used for the thermal averaged spin distribution function, given by the Langevin function for the infinite spin $S \to \infty$, may have some limited validity. However in principle the LLB equation has no limitations and more general formulation of the LLB equation can be used to improve this imprecise description in the future.

3.7 Conclusions

In conclusion, the full simulation using the thermal macrospin model reveals the thermal demagnetization mechanism in Ni mediated by thermalized hot electrons. The theoretical model allows us to identify the longitudinal relaxation as a limiting factor for the demagnetization rates, a general phenomenon which is present in all ferromagnetic materials. Therefore it is suitable for all other ferromagnets where the high temperature dynamics of the itinerant electrons can

similarly be described by a heat bath description. The longitudinal relaxation depends thereby also on the coupling strength between electron and spin system given by the coupling parameter λ. The latter means that the magnitude of the demagnetization rate strongly depends on the microscopic coupling mechanisms. λ contains the information of the microscopic spin-flip mechanism acting on femtosecond timescale, either the Elliott-Yafet scattering or the exchange scattering. Probably both mechanisms play an important role and their contribution on different time scales needs to be determined by future experiments and theory. The agreement between the experimental data and our modeled theoretical data relies very sensitively on the strength of the coupling parameter, taken as temperature independent $\lambda = 0.045$ throughout the chapter and equal to the room temperature value. The most successful recent calculations of damping rates in transition metals within the first-principle approach are based on the spin-orbit torque correlation functions and thus, the results depend strongly on the spin-orbit coupling and have a complicated temperature dependence [69, 110]. The fact that the experimental τ_M deviates and is slightly faster than the modeling results, could suggest the possibility of an increase of λ with electron temperature for the excited ferromagnet.

On the other hand the nevertheless remarkable good agreement between measured and modeling data has been obtained using the intrinsic coupling parameter $\lambda = 0.045$ determined from the experimental value of damping parameter $\alpha_\perp$. Therefore we can conclude that for Ni, in contrast to earlier findings for rare earth doped Permalloy films [166], the same spin scattering mechanism dominates the spin relaxation on long (100 ps) and femtosecond timescales. For future experiments on different ferromagnets we suggest using a multi-experimental approach as demonstrated: with varied pump fluence and film thickness, and measuring the reflectivity at the same time. This will reduce unknown parameters in the analysis to determine the electron temperature as input independent from the magnetization dynamics and come closer to the nature of the elementary spin-scattering mechanism.

Conclusiones en español

En este capítulo hemos utilizado el modelo térmico de macro espín, presentado en el capítulo anterior, en el estudio de la velocidad de desimanación del Nickel. Los cálculos nos han permitido evidenciar el mecánismo de desimanación térmica mediado por los electrones "calientes" termalizados. El modelo teórico nos ha permitido identificar la susceptibilidad longitudinal como el factor limitante de

la velocidad de desimanación. Un fenómeno que se encuentra presente en todos los materiales ferromagnéticos. Por tanto, este modelo es conveniente para otros materiales ferromagnéticos en lo cuales la dinámica de los electrones a alta temperatura pueda ser descrita como un baño térmico.

La relajación longitudinal también depende de la fuerza de acoplo entre electrones y espines, definida por el parámetro λ. Esto significa que la velocidad de desimanación depende fuertemente del mecanismo de acoplo. El parámetro λ contiene información de los mecanismos de spin-flip que actúan en escalas de tiempo de femtosegundos, tanto scattering tipo Elliot-Yafet como de tipo intercambio.

Probablemente, ambos mecanismos desempeñan un rol importante en el proceso de desimanación, por tanto el conocimiento de la contribución de cada uno de ellos en diferentes escalas de tiempo sería deseable. En ese sentido, aún los más exitosos cálculos de los parámetros de relajación en metales de transición mediante el uso de métodos de "*primeros principios*" están basados en funciones de correlación de espín-torque y por tanto, los resultados dependen fuertemente del acoplo espín-órbita y tienen una complicada dependencia con la temperatura [69, 110].

El hecho de que los valores experimentales de τ_M sean un poco más rápidos que el módelo sugiere un incremento del parámetro λ con la temperatura electrónica del material ferromagnético excitado. Por otro lado, hemos usado como parámetro de acoplo $\lambda = 0.045$, determinado experimentalmente a través del parámetro de relajación $\alpha_\perp$, con el cúal hemos obtenido un buen acuerdo entre los datos experimentales y el modelo. Podemos concluir que para Ni, a diferencia del caso del Permalloy dopado con tierras raras [166], el mismo mecanismo de scattering domina la relajación en escalas de tiempo largas (100 ps) y ultracortas (femtosegundos).

4

Ultrafast magnetization dynamics using the quantum version of LLB equation

The first attempt to relate the sub-picosecond demagnetization time τ_M with the macroscopic damping α_{LLG} was given by Koopmans *et al.* [106] who suggested the relation $\tau_M \sim 1/\alpha_{LLG}$. Subsequently and with the aim to check this relation several experiments in doped Permalloy were performed [133, 166, 170]. The Permalloy thin films were doped with rare earth impurities, allowing to increase in a controlled way the damping parameter α_{LLG}. The effect on the demagnetization time τ_M was shown to be opposite [133] or null [166], in contrast to the above relation. However, it should be noted that the analysis leading to this expression was performed in terms of the Landau-Lifshitz-Gilbert (LLG) equation, relating the ultra-fast demagnetization time τ_M to the transverse damping without taking into account their temperature dependence. Moreover, one should take into account that the rare-earth impurities may introduce a different spin-flip mechanism with a slower timescale [170].

Partially basing on the above mentioned experimental results and from a general point of view, the ultra-fast demagnetization rate τ_M and the transverse relaxation may be thought to be independent quantities. Indeed, different intrinsic and extrinsic mechanisms can contribute to the demagnetization rates at different timescales. One can, for example, mention that during the femtosecond demagnetization the electron temperature is often raised up to the Curie temperature [11, 157]. At this moment, the high frequency THz spinwaves [54**?**] including the Stoner excitations [15] contribute. At the same time, the transverse relaxation is related to the homogeneous magnetization precession mode at lower temperatures.

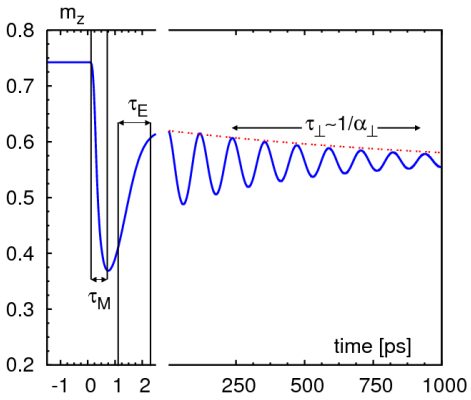

Figure 4.1: Characteristic time scales in ultrafast laser-induced magnetisation dynamics experiments. The curve is obtained by the integration of the Landau-Lifshitz-Bloch equation coupled to the two-temperature model with the parameters from Ref. [10]. For the modelling of precession the applied field $H_{ap} = 1$T at 30 degrees was used.

In the Landau-Lifshitz-Bloch (LLB) model the intrinsic quantum mechanical mechanisms are parametrized by λ which defines the coupling-to-the-bath strength. It should be distinguished from that of the macroscopic damping α_{LLG} ($\alpha_\perp$ in the LLB model), a more complicated quantity which includes the magnon-magnon processes. Fig. 4.1 shows the laser induced magnetization precession modeled by the LLB equation using a unique coupling-to-the-bath parameter λ. It describes the sub-ps demagnetization time scale τ_M as well sub-ns magnetization precession characterized by $\tau_\perp \sim 1/\alpha_\perp$. Thus, the LLB equation takes care of the different natures of longitudinal and transverse relaxation, arising from the spin disordering. Consequently, the relation between the ultrafast demagnetization and precession remains valid but with a temperature-dependent correction. If this relation is confirmed experimentally, a unique intrinsic coupling parameter means that the same main microscopic mechanism is acting on both timescales.

The LLB equation for classical spins ($S \to \infty$) describes quite well the dynamics of the thermal averaged spin polarization of an ensemble of exchange-coupled atomistic spins modeled by stochastic Landau-Lifshitz-Gilbert (LLG) equations [41, 95]. At the same time, in some cases the LLB equation may be preferable with respect to the atomistic Heisenberg model, since being micromagnetic it can incorporate quantum nature of magnetism and the quantum derivation of LLB also exists [46]. In particular the limits of validity for the statistical mechanics based on the classical Heisenberg model for the description of materials with delocalized magnetism of d-electrons in transition metals or magnetism of f-electrons in rare earths are not clear. An alternative statistical simplified description of

d-metals consists of a two level system with spin-up and spin-down bands (*i.e.* $S_z = \pm 1/2$), as has been done by B. Koopmans *et al.* [105]. Their model, as we show in the present chapter, can be connected to the quantum ($S = 1/2$) LLB equation.

4.1 The Landau-Lifshitz-Bloch model with quantum spin number S.

The derivation of the quantum Landau-Lifshitz-Bloch (LLB) equation starts from the density matrix equation for a quantum spin interacting with the environment [46]. In strongly exchange coupled systems, as in ferromagnets, the spin-spin interactions were taken into account in the spirit of the mean field approximation (MFA), replacing the applied field by the MFA one containing the exchange field acting on a given magnetic moment. The resulting dynamical equation interpolates between the standard micromagnetics; the macroscopic Landau-Lifshitz-Gilbert equation ($S \gg 1$) and low temperatures, and the Bloch equation ($S = 1/2$) or high temperatures.

The micromagnetic equation for the magnetization dynamics, valid at all temperatures, is written in the following form [65]:

$$\dot{\mathbf{n}} = \gamma[\mathbf{n} \times \mathbf{H}_{\text{eff}}] + \frac{\gamma\alpha_{\parallel}}{n^2}\left[\mathbf{n} \cdot \mathbf{H}_{\text{eff}}\right]\mathbf{n} - \frac{\gamma\alpha_{\perp}}{n^2}\left[\mathbf{n} \times [\mathbf{n} \times \mathbf{H}_{\text{eff}}]\right], \tag{4.1}$$

where T is the bath temperature, $n = M/M_e(T) = m/m_e$ is the reduced magnetization, normalized to the equilibrium value M_e at given temperature T and $m = M/M_e(T = 0K)$. The internal field $\mathbf{H}_{\text{int}}$ contains all usual micromagnetic contributions (Zeeman, anisotropy, exchange and magnetostatic) and is augmented by the contribution coming from the temperature

$$\mathbf{H}_{\text{eff}} = \mathbf{H}_{\text{int}} + \frac{m_e}{2\widetilde{\chi}_{\parallel}}\left(1 - n^2\right)\mathbf{n}, \tag{4.2}$$

where $\widetilde{\chi}_{\parallel}(T)$ is the longitudinal susceptibility which in the MFA reads

$$\widetilde{\chi}_{\parallel} = \frac{\mu_0}{S^2 J_0}\frac{\beta S^2 J_0 B'_S}{1 - \beta S^2 J_0 B'_S} \tag{4.3}$$

where $\beta = 1/k_B T$, $J_0 = zJ$ is the exchange constant multiplied by the number of nearest neighbours z and $B'_S \equiv dB_S/d\xi$ is evaluated at the equilibrium ξ_e, where $\xi = mS^2 J_0 \beta$ and B_S is the Brillouin function for the spin value S. Finally, μ_0 is the atomic magnetic moment.

4. ULTRAFAST MAGNETIZATION DYNAMICS USING THE QUANTUM VERSION OF LLB EQUATION

The LLB equation contains two relaxation parameters: transverse $\alpha_\perp$ and longitudinal $\alpha_\parallel$, related to the intrinsic coupling-to-the-bath parameter λ. In the quantum case the temperature dependence of the LLB damping parameters is given by the following expressions [65]:

$$\alpha_\parallel = \frac{\lambda}{m_e}\frac{2T}{3T_C}\frac{2q_S}{\sinh(2q_S)} \underset{S\to\infty}{\Longrightarrow} \frac{\lambda}{m_e}\frac{2T}{3T_C}, \tag{4.4}$$

$$\alpha_\perp = \frac{\lambda}{m_e}\left[\frac{\tanh(q_S)}{q_S} - \frac{T}{3T_C}\right] \underset{S\to\infty}{\Longrightarrow} \frac{\lambda}{m_e}\left[1 - \frac{T}{3T_C}\right], \tag{4.5}$$

with $q_S = 3T_C m_e/[2(S+1)T]$, where S is the quantum spin number and T_C is the Curie temperature. In the quantum description the coupling parameter λ contains the matrix elements representing the scattering events and, thus, is proportional to the spin-flip rate due to the interaction with the environment. This parameter, in turn, could be temperature dependent and, in our opinion, it is this microscopic parameter which should be related to the Gilbert parameter calculated through *ab-initio* calculations as in Refs. [69, 110], since the contribution coming from the spin disordering is not properly taken into account in these models. In the case $S \to \infty$ the damping coefficients have the forms presented in Chapter 2 and used in several previously published works [10, 41, 95], suitable for the comparison with the Langevin dynamics simulations based on the classical Heisenberg Hamiltonian and in agreement with them [41, 95].

Eq. (4.1) is singular for $T > T_C$, in this case it is more convenient to use the LLB equation in terms of the variable $m = M/M_e(T = 0K)$ [41]:

$$\dot{\mathbf{m}} = \gamma[\mathbf{m}\times\mathbf{H}_{\text{eff}}] + \gamma\widetilde{\alpha}_\parallel\frac{[\mathbf{m}\cdot\mathbf{H}_{\text{eff}}]\,\mathbf{m}}{m^2} - \gamma\widetilde{\alpha}_\perp\frac{[\mathbf{m}\times[\mathbf{m}\times\mathbf{H}_{\text{eff}}]]}{m^2}. \tag{4.6}$$

The corresponding LLB equation is indistinguishable from Eq. (4.1) but with different relaxation parameters $\widetilde{\alpha}_\parallel = m_e\alpha_\parallel$, $\widetilde{\alpha}_\perp = m_e\alpha_\perp$ and $\widetilde{\alpha}_\perp = \widetilde{\alpha}_\parallel$ for $T > T_C$, in this case the effective fields reads

$$\mathbf{H}_{\text{eff}} = \mathbf{H} + \mathbf{H}_A + \begin{cases} \frac{1}{2\widetilde{\chi}_\parallel}\left(1 - \frac{m^2}{m_e^2}\right)\mathbf{m} & T \lesssim T_C \\ -\frac{J_0}{\mu_0}\left(\frac{T}{T_C} - 1 + \frac{3}{5}m^2\right)\mathbf{m} & T \gtrsim T_C \end{cases} \tag{4.7}$$

as we have already introduced in Chapter 2. Although this formulation is more suitable for the modeling of the laser-induced demagnetization process, during which the electronic temperature is usually raised higher than T_C, it is the expression (4.5) which should be compared with the transverse relaxation parameter α_{LLG} due to the similarity of the formulation of the Eq. (4.1) with the micromagnetic LLG equation. In the classical case and far from the Curie temperature $T \ll T_C$, $\lambda \approx \alpha_\perp \approx \widetilde{\alpha}_\perp$ (α_{LLG}).

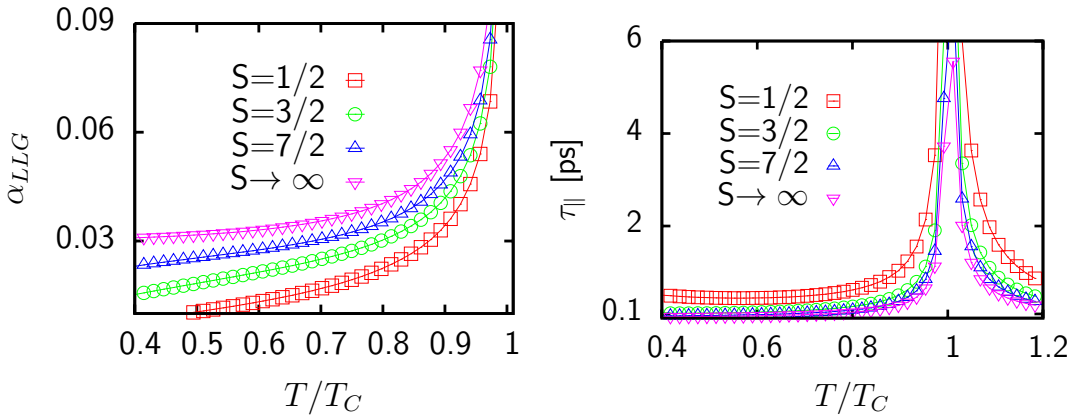

Figure 4.2: (Up) The transverse damping parameter $\alpha_{\perp}$ (α_{LLG}) as a function of temperature within the LLB model for different spin values S. The intrinsic coupling parameter was set to $\lambda = 0.03$. (Down) The longitudinal relaxation time $\tau_{\parallel}$ as a function of temperature within the LLB model for different spin values S. The temperature-dependent magnetization and the longitudinal susceptibility $\widetilde{\chi}_{\parallel}$ were evaluated in both cases in the MFA approach using the Brillouin function.

Within the LLB model the characteristic longitudinal timescale is not only defined by the longitudinal damping parameter (4.4) but also by the temperature-dependent longitudinal susceptibility $\widetilde{\chi}_{\parallel}(T)$ [41], according to the following equation:

$$\tau_{\parallel}(T) = \frac{\widetilde{\chi}_{\parallel}(T)}{\gamma \widetilde{\alpha}_{\parallel}(T)}. \tag{4.8}$$

As it can be observed in Fig. 4.2 the transverse relaxation parameter $\alpha_{\perp}(\alpha_{LLG})$ and the longitudinal relaxation time $\tau_{\parallel}$ have a strong dependence on the quantum spin number S. We conclude here about the occurrence of quite different relaxation rates for the two extreme cases $S = 1/2$ and $S = \infty$.

4.2 Modeling of the laser-induced ultrafast demagnetization within the quantum LLB

For the modeling of the ultrafast demagnetization we have to specify the origin of the external bath whose role is to produce an energy input. As we have discussed in Chapter 2 the modeling of ultrafast magnetization dynamics is based on some reasonable assumptions about the energy transfer taking place between different subsystems; electrons, phonons and magnetic excitations. We remember here that the 2T model assumes that the absorbed energy from the laser pump pulse

goes to the electron system which thermalizes ($\gtrsim$ 10 fs) to an internal quasi-equilibrium distribution at a well-defined temperature T_e, whereas there is still a non-equilibrium energy transfer between electrons and lattice, also assumed to be in a local thermal equilibrium with temperature T_{ph}. Finally, the electron-phonon coupling, G_{e-ph}, drives both systems to a final common temperature.

In all previous works on the modeling of ultrafast processes within the LLB model as well as within atomistic LLG approach [10, 11, 94, 95, 96, 97, 157], it has been assumed that the bath is produced by the electron systems and thus $T = T_e$. This idea goes in the line of a pure electronic spin-flip mechanism and has been shown to adequately describe the ultrafast dynamics in relation to experiments. The possibility of the intrinsic temperature dependence of the spin-flip probability is normally disregarded, assuming λ = const. Therefore, in this approach the longitudinal relaxation time $\tau_{\parallel} \sim \widetilde{\chi}_{\parallel}/\lambda T_e$ (see Eq. 4.8) is defined by the dynamics of the electron temperature T_e, until the temperatures, close to the Curie temperatures, where the critical slowing down, provided by the longitudinal susceptibility $\widetilde{\chi}_{\parallel}$, starts to play a role.

4.2.1 M3TM versus LLB model

Recently, B. Koopmans *et al.* have used a similar approach to describe the ultrafast demagnetization dynamics [105], called M3TM model, obtained through the general Master equation for the dynamics of the populations of a two level system (spin $S = 1/2$ was used) with the spin-flip probability of the phonon-mediated EY scattering events a_{sf}. The M3TM model reads

$$\frac{dm}{dt} = Rm\frac{T_{ph}}{T_C}\left(1 - m\coth\left(\frac{mT_C}{T_e}\right)\right). \tag{4.9}$$

R is a material specific parameter linearly proportional to the spin-flip probability $R \sim a_{\mathrm{sf}}$. Eq. (4.9) is coupled to the 2T model. The authors fitted experimental demagnetization rates in Ni, Co, Gd to the M3TM model which allowed to extract the values of R and relate them to a_{sf}. These values were consistent with the values estimated on the basis of *ab-initio* theory [152]. Nevertheless, recently more accurate *ab-initio* calculations [**?**] have showed that EY spin-flip probabilities were overstimated in that work [152], therefore making the M3TM a less consistent approach.

To show the equivalence between the LLB model with $S = 1/2$ and the M3TM model [105], we compare the relaxation rates resulting from both equations. We start with the M3TM equation

$$\frac{dm}{dt} = -R\frac{T_{ph}}{T_C}\left(1 - m\coth\left[\left(\frac{T_C}{T_e}\right)m\right]\right)m \tag{4.10}$$

where we identify the Brillouin function for the case $S = 1/2$, $B_{1/2} = \tanh(q)$ with $q = q_{1/2} = (T_C/T_e)\,m$. Now, we use the identity $B_{1/2} = 2/B'_{1/2}\sinh(2q)$ to write

$$\frac{dm}{dt} = -R\frac{T_{ph}}{T_C}\left[\frac{2}{\sinh(2q)}\right]\left(\frac{1-\frac{B_{1/2}}{m}}{B'_{1/2}}\right)m^2 \tag{4.11}$$

we multiply and divide by $q\mu_0\beta$ to obtain

$$\frac{dm}{dt} = -R\frac{T_{ph}}{T_C}\frac{\mu_0}{k_B T_C}\left[\frac{2q}{\sinh(2q)}\right]\left(\frac{1-\frac{B_{1/2}}{m}}{\mu_0\beta B'_{1/2}}\right)m \tag{4.12}$$

We expand around equilibrium $m_e = B_{1/2}(q_e)$ the small quantity $1 - B_{1/2}/m$

$$1 - \frac{B_{1/2}(q)}{m} \cong \frac{\delta m}{m_e}\left(1 - \left(\frac{T_C}{T_e}\right)B'_{1/2}(q_e)\right) \tag{4.13}$$

where $\delta m = m - m_e$. Next, we expand m around m_e^2

$$m = m_e + \frac{1}{2}\frac{(m^2 - m_e^2)}{m_e} \Longrightarrow \frac{\delta m}{m_e} = \frac{(m^2 - m_e^2)}{2m_e^2} \tag{4.14}$$

and,

$$\frac{1 - B_{1/2}/m}{\beta\mu_0 B'_{1/2}} \approx \frac{1}{2\widetilde{\chi}_\parallel}\frac{(m^2 - m_e^2)}{m_e^2} \tag{4.15}$$

Finally, collecting the equations (4.12) and (4.15) altogether:

$$\frac{dm}{dt} = \left(\frac{3R}{2}\frac{\mu_0}{k_B T_C}\right)\frac{2T_{ph}}{3T_C}\frac{2q}{\sinh(2q)}\left(\frac{1}{2\widetilde{\chi}_\parallel}(1 - \frac{m^2}{m_e^2})m\right) \tag{4.16}$$

Comparing this to the LLB equation with longitudinal relaxation only and without anisotropy and external fields, we can write Eq. (4.16) in terms of $\mathbf{n}$:

$$\frac{dn}{dt} = \gamma\frac{\lambda}{m_e}\frac{2T_e}{3T_C}\frac{2q}{\sinh(2q)}H_{\text{eff}} = \gamma\alpha_\parallel H_{\text{eff}} \tag{4.17}$$

where $H_{\text{eff}} = \frac{m_e}{2\widetilde{\chi}_\parallel}(1 - n^2)n$, and

$$\alpha_\parallel = \left[\frac{3R}{2\gamma}\frac{\mu_0}{k_B T_C}\frac{T_{ph}}{T_e}\right]\frac{2T_e}{3T_C}\frac{2q}{\sinh(2q)} \tag{4.18}$$

Thus the Koopmans' M3TM equation is equivalent to the LLB equation with $S = 1/2$ and where the transverse terms are not considered. The link between both of them is the identification

$$\lambda = \frac{3R}{2\gamma}\frac{\mu_0}{k_B T_C}\frac{T_{ph}}{T_e} = \lambda_0 \frac{T_{ph}}{T_e}. \tag{4.19}$$

Thus, the Koopmans' model coincides with the LLB equation with $S = 1/2$ where the Elliott-Yafet scattering mechanism is incorporated from the beginning in its functional form. Consequently, if a phonon-mediated EY process was acting, this would correspond to the use of a temperature-dependent coupling rate (4.19) in the LLB equation.

Oppositely to the pure electronic process, in the case of a phonon-mediated EY process, the longitudinal relaxation timescale should be defined by the dynamics of the phonon temperature leading to $\tau_\parallel \sim \widetilde{\chi}_\parallel(T_e)/RT_{ph}$, again at temperatures not close to T_C where the critical slowing down starts to play an important role. The linear dependence of demagnetization rate in T_{ph} originates from the linear increase of the phonon occupation number n_E with temperature $n_E \sim T$ within the Einstein model, since $\hbar\omega_E \ll k_B T$ is assumed in the M3TM model. Differently to that, at low temperatures, not considered in Eq. (4.9) we would get $\tau_\parallel \sim 1/T_{ph}^3$.

4.2.2 Diversity of magnetization dynamics within the LLB model

We now present modeling of the ultrafast magnetization dynamics following the laser pulse excitation using the LLB model coupled to the electron temperature T_e. We perform simultaneous integration of Eqs. (4.1) and 2T model with the material specific parameters taken from our previous modeling in Nickel. The Ni parameters, such as magnetization as a function of temperature were taken assuming the Brillouin (Langevin for $S \to \infty$) function.

The most important parameter defining the diversity of the ultrafast demagnetization in different materials is the coupling to the bath parameter λ. Thus, it is natural first to investigate qualitatively its influence. In Fig. 4.3 we show the diversity of magnetization dynamics for various values of the coupling parameter λ, chosen to be independent on temperature. The largest value of λ approximately corresponds to that of the transition metals while the smallest one - to rare earths and half metals. As it can be clearly observed, for relatively large value of the spin-flip rate, corresponding to the transition metal, the magnetization dynamics can follow the electronic temperature, showing a ps timescale

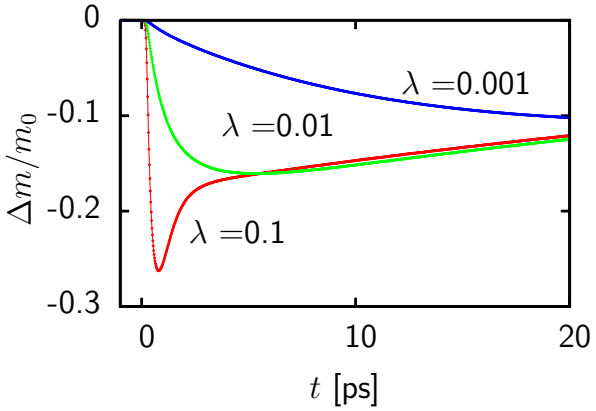

Figure 4.3: The result of integration of the LLB model ($S \to \infty$) with different parameters λ (increasing from top to the bottom).

magnetization recovery. This does not happen for small values of λ and these materials does not recover their magnetization even at 100 ps timescale. Thus this parameter defines the diversity of the demagnetization rates in larger extend than the ratio μ_0/T_C, suggested in Ref. [105].

The sub-ps demagnetization generally speaking is not exponential and cannot be described in terms of one relaxation time τ_M. Simple analytical expression is possible to obtain with the supposition of a square-shaped temperature pulse [94]. To comply with the existing approaches, we still discuss the demagnetization rate in terms of a unique parameter τ_M.

The magnetization dynamics is determined by a large extend by the dynamics of the bath. However, it is clear that it can only follow the dynamics of the bath temperature if $\tau_{||} \gtrsim 100$ fs is faster than the characteristic timescale of the electron dynamics. Thus at fs timescale the magnetization dynamics is always delayed with respect to the electrons/phonons. At temperatures close to the Curie temperature, the magnitude $\tau_{||}$ experiences a critical slowing down, and thus the characteristic timescale τ_M is also slowed.

It is clear that independently of the nature of the spin-flip mechanism, the most important parameter, determining the value of $\tau_{||}$ remains the material-specific intrinsic scattering rate parameter λ. This parameter substitutes for the ultrafast dynamics the Landau-Lifshitz-Gilbert parameter α_{LLG}, which is normally extracted from the experiment. Similarly, λ at the present state of art should be extracted from the experimental measurements although, in theory, it can be also calculated from the *ab-initio* approach, similar to how it was done for the Elliott-Yafet process [152]. The available values of λ are presented in Table 4.1. The value of λ for Gd was found to be 60 times smaller than for Ni (see Table 4.1), such a small value of the spin-flip rate in Gd can be qualitatively understood if we recall that magnetism in Gd is defined by the half-filled $4f$ shell

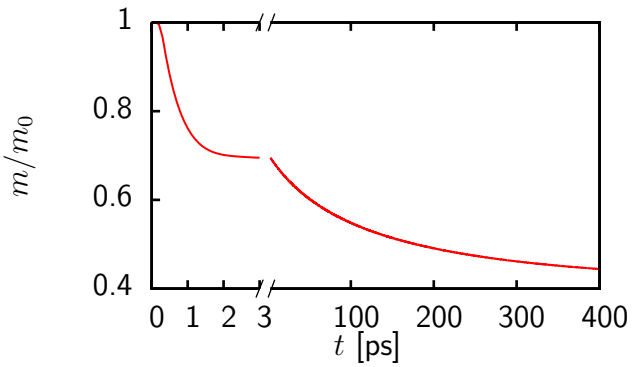

Figure 4.4: The result of integration of the LLB model ($S \to \infty$) with constant $\lambda = 0.0015$ (see Table 4.1). In this case the 2T model parameters were taken from Ref. [105] corresponding to Gd. The laser fluence was taken to be $F = 30$ mJ/cm^2

electrons while the laser primarily excites $5s6d$ electrons. In the next chapter we will carefully study the case of Gd.

Another parameter strongly influencing the demagnetization rates is the phonon-electron coupling G_{e-ph} defining the rate of the electron-phonon temperatures equilibration time τ_E. Indeed, in Ref. [105] the value of G_{e-ph} was reported to be 20 times smaller for Gd than for Ni. The small values of the two parameters ensure the correct modeling of the experimentally observed slow demagnetization rates in TbFe alloy [99], Gd [169] and in half-metals [63] as well as the two time-scales demagnetization [105, 169] are also well-reproduced (see, as an example, Fig. 4.4). Within this model the two-time scale process consists of a relatively fast demagnetization in the order of ~ 1 ps (however much slower than ~ 100 fs in Ni), defined by the electron temperature and small value of λ, followed by a much slower process due to a slow energy transfer from the electron to the lattice system.

As it was mentioned in the previous section, the phonon-mediated EY mechanism predicts the coupling to the bath parameter λ to be dependent on the ratio between the phonon and electron temperature through the relation (4.19). In Fig. 4.5 we present the magnetization dynamics for Ni evaluated for two laser pulse fluencies, assuming various values of the spin S and temperature-dependent and independent λ values. Note quite different demagnetization rates at high fluency for two limiting cases $S = 1/2$, used in Ref. [105] and $S = \infty$, used in Ref. [11]. The differences in the choice of the mechanism are pronounced at high pump fluency but are not seen at low fluency. One can also hope that in the experiment it would be possible to distinguish the two situations. Considering the experimental data from Ref. [105] for Ni for high fluence, we have found that the

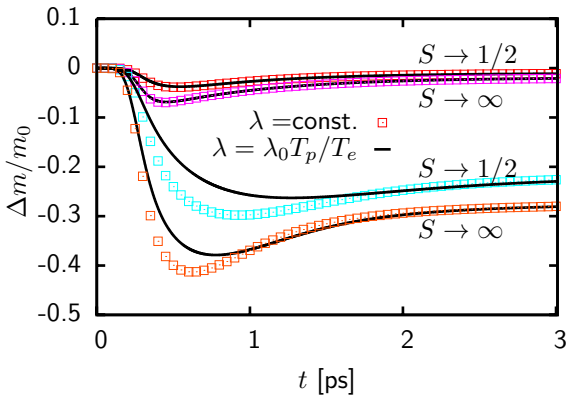

Figure 4.5: Magnetization dynamics during laser-induced demagnetization process calculated within the LLB model with different spin numbers and for two laser-fluencies $F = 10$ mJ/cm^2 (upper curves) and $F = 40$ mJ/cm^2 (bottom curves). Ni parameters from Ref. [11] were used. The symbols are calculated with the LLB equation with the intrinsic damping parameter using a constant $\lambda_0 = 0.003$ value, and the solid lines with the LLB equation and the intrinsic coupling with the temperature dependent $\lambda = \lambda_0 (T_{ph}/T_e)$.

case of the temperature-dependent $\lambda = \lambda_0(T_{ph}/T_e)$ can be equally fitted with the temperature-independent $\lambda \approx \lambda_0/2$. Since this is within the discrepancy between the theoretical and experimental values, it does not allow to answer definitely which mechanism is acting. We conclude that more experimental data promoting one or another intrinsic mechanism and varying laser fluency is necessary.

4.3 Linking different timescales

Since the longitudinal relaxation occurs under strong exchange field and the transverse relaxation - under external applied and/or anisotropy field, their characteristic timescales are quite different. However, the LLB equation provides a relation between the ultrafast demagnetization (longitudinal relaxation) and the transverse relaxation (ordinary LLG damping parameter) via the parameter λ_0 ($\lambda = \lambda_0$ or $\lambda = \lambda_0(T_{ph}/T_e)$ for $T_{ph} = T_e$). By separate measurements of the two magnetization rates, the relations (4.5) and (4.8) given by the LLB theory could be checked. This can provide the validation of the LLB model, as well as the answer to the question if the same microscopic mechanism is acting on femtosecond and picosecond timescales. Unfortunately, the damping problem in ferromagnetic materials is very complicated and the literature reveals the diversity of measured values in the same material, depending on the preparation conditions. It has

been recently demonstrated [147] that the damping of the laser-induced precession coincides with the measured by FMR in transition metals. Thus the two demagnetization rates could be measured independently by means of the ultrafast laser pump-probe technique [165].

To have a definite answer the measurement on the same sample is highly desired. The measurements of both $\alpha_\perp$ and τ_M are available for Ni [11] where an excellent agreement between ultrafast magnetization rates via a unique temperature-independent parameter $\lambda = 0.04$ has been reported [11] (see also Chapter 3). The results of the systematic measurements of τ_M are also available for Ni, Co, Gd in Ref. [105], as well as for Fe [36]. The next problem which we encounter here is that the demagnetization rates strongly depend on the spin value S, as is indicated in Figs. 4.2 and 4.5. The use of $S = 1/2$ value [105] or $S = \infty$ value [11] is quite arbitrary and these values do not coincide with the atomic spin numbers of Ni, Co and Gd. Generally speaking, for metals the spin value is not a good quantum number. The measured temperature dependence of magnetization, however, is well fitted by the Brillouin function with $S = 1/2$ for Ni and Co and $S = 7/2$ for Gd [43]. These are the values of S which we use in Table 4.1.

In Table 4.1 we present data for the coupling parameter λ_0 extracted from Ref. [105] basing on the M3TM model and within the EY mechanism. Differently to that article, for Gd we corrected the value of the parameter R to account for a different spin value by the ratio of the factors,*i.e.* $R^{S_1} = (f_{S_2}/f_{S_1})\, R^{S_2}$ with

$$f_S = \frac{2q_S}{\sinh(2q_S)} \frac{1}{m_{e,S}^2 \chi_\parallel^S}, \tag{4.20}$$

where the parameters are evaluated at $120K$ using the MFA expressions for each spin value S. Using the data presented in Table 4.1, we estimated the value of the Gilbert damping parameter $\alpha_\perp$ through formula (4.5) at $300K$ (for Ni and Co) and at $120K$ for Gd. Note that for temperature-independent $\lambda = \lambda_0$ the resulting λ_0 and $\alpha_\perp$ values are approximately two times smaller for Ni and Co. The last column presents experimental values for the same parameter found in literature for comparison with the ones in the fifth column, estimated through measurements of the ultrafast demagnetization times τ_M and the relation provided by the LLB equation.

The results presented in Table 4.1 demonstrate quite a satisfactory agreement between the values, extracted from the ultrafast demagnetization time τ_M and the Gilbert damping parameter $\alpha_\perp$ via one unique coupling-to-the-bath parameter λ. The agreement is particularly good for Ni, indicating that the same spin flip mechanism is acting on both timescales. This is true for both experiments in

Table 4.1: The data for ultrafast demagnetization rate parameters for three different metals from ultrafast demagnetization rates and from FMR measurements. The third column presents the demagnetization parameter R from Ref. [105], corrected in the case of Gd for spin $S = 7/2$. The fourth column presents the value of the λ_0 parameter, as estimated from the M3TM model [105] and the formula Eq. (4.19). The fifth column presents the data for $\alpha_\perp$ estimated via the LLB model Eq. (4.5) and the λ_0 value from the third column, at room temperature $T = 300K$ for Co and Ni and at $T = 120K$ for Gd . The last column presents the experimentally measured Gilbert damping collected from different references.

Material	S	R[105]	λ_0	$\alpha_\perp$	α_{LLG}
Ni	1/2	17.2	0.0974	0.032	0.019[50]-0.028 [22]
Co	1/2	25.3	0.179	0.025	0.0036[22]-0.006[114]-0.011 [76]
Gd	7/2	0.009	0.0015	0.00036	0.0005 [170]

Refs. [11] and [105]. For Co the value is some larger. However, if the temperature-independent $\lambda = \lambda_0/2$ was used, the resulting value would be two times smaller and the agreement would be again satisfactory. For Ni this would also be within the expected discrepancy between measured FMR values. We would like to note that no good agreement was obtained for Fe. The reported damping values [22] are 5-10 times smaller as estimated from the demagnetization rates measured in Ref. [36].

4.4 Discussion

The Landau-Lifshitz-Bloch (LLB) equation provides a micromagnetic tool for the phenomenological modeling of the ultra-fast demagnetization processes. Within this model one can describe the temperature-dependent magnetization dynamics at arbitrary temperature, including close and above the Curie temperature.

The macroscopic damping parameters (longitudinal and transverse) have different natures in terms of the involved spin waves and in terms of the timescales. Their temperature dependence is different, however, they are related by the spin-flip rate. We have tried to check this relation in several transition metals such as Ni, Co, Fe and the rare-earth metal Gd. A good agreement is obtained in Co and Gd and an excellent agreement in Ni. This indicates that on both timescales the same main microscopic mechanism is acting. In Ni the agreement is good both within the assumptions $\lambda = \lambda_0$ and $\lambda = \lambda_0 T_{ph}/T_e$. In Co the agreement seems to be better with the temperature-independent parameter $\lambda = \lambda_0$ which does not indicate towards the phonon-mediated EY mechanism. However, given a small discrepancy and the complexity of the damping problem, this conclusion

cannot be considered definite. We can neither exclude an additional temperature dependence of the intrinsic scattering probability (*i.e.* the parameter λ_0) for both phonon-mediated EY and exchange scattering mechanisms which was not taken into account. The observed agreement of the perpendicular and transverse relaxation rates, generally speaking, validates the LLB theory but cannot answer the question which of the mechanisms is acting.

Recently, Fähnle *et al.* [61] have used the Fermi-surface breathing model to link the conductivity contribution to LLG damping and τ_M. Such a contribution dominates at low temperatures and it gives a linear relation $\tau_M \sim \alpha_{LLG}$, in contrast to our and previous approaches, where $\tau_{\parallel} \sim 1/\alpha_{LLG}$. At room temperature both contributions seems to be relevant. In their model the electronic properties are taken into account in a more material specific way, but leaving the spin fluctuations untreated. At the present state of art our model does not include the conductivity contribution. In that direction we conclude that both models are complementary and could be combined to produce a better understanding of the present problem.

An open question is the problem of doped permalloy where an attempt to systematically change the damping parameter by doping with rare-earth impurities was undertaken [170] in order to clarify the relation between the LLG damping and the ultrafast demagnetization rate [133, 166]. The results are not in agreement with the LLB model. However in this case we think that the hypothesis of the slow relaxing impurities presented in Ref. [133] might be a plausible explanation. Indeed, if the relaxation time of the rare earth impurities is high, the standard LLB model is not valid since it assumes an uncorrelated thermal bath. The correlation time will be introduced in the classical spin dynamics via the Landau-Lifshitz-Miyasaki-Seki approach in Chapter 8.

4.5 Conclusions

We have shown that the micromagnetic LLB equation for modeling of ultrafast laser induced magnetization dynamics can take into account the quantum spin number. The LLB model includes the dynamics governed by both the atomistic LLG model and the M3TM model by Koopmans *et al.* [105]. In the future it represents a real possibility for the multiscale modeling [95].

Within this model the ultrafast demagnetization rates could be parameterized through a unique temperature dependent or independent parameter λ, defined by the intrinsic spin-flip rate. We have shown that for the phonon-mediated EY mechanism the intrinsic parameter λ is dependent on the ratio between phonon

and electron temperatures and therefore is temperature dependent on the femtosecond - several picosecond timescale. The magnetization dynamics is coupled to the electron temperature through this parameter and on the ultrafast timescale is always delayed in time. The observed delay is higher for higher electron temperature. This is in agreement with the experimental observation that different materials demagnetize at different rates [63, 105] and that the process is slowed down with the increase of laser fluency. The LLB equation can reproduce slow demagnetizing rates observed in several materials such as Gd, TbFe and half metals. This is in agreement with both phonon-mediated EY picture since in Gd a lower spin-flip probability was predicted and also with the inelastic electron scattering picture, since the electron diffusive processes are suppressed in insulators and half-metals [18, 63]. However, we also stress the importance of other parameters determining the ultrafast demagnetization rates, such as the electron-lattice coupling.

Conclusiones en español

En este capitulo hemos demostrado que nuestro modelo LLB micromagnetico para la descripcion de la dinamica de la imanacion inducida por laser de femtosegundos puede tener en cuenta el numero cuantico de espin. El modelo LLB incluye tanto la dinamica descrita por el modelo atomistico LLG como el modelo M3TM de Koopmans *et al.* [105]. Ademas este modelo es un buen candidato para la modelizacion multi-escala [95].

En este modelo las velocidades de desimanacion puede ser parametrizada a traves de un unico parametro que puede ser dependiente o independiente de la temperatura que representa la tasa intrinseca de proceso de spin-flip. Asimismo, hemos demostrado que en el mecanismo EY mediado por fonones el parametro intrinseco λ depende del cociente entre las temperaturas de los fonones y electrones. Por tanto, es un parametro que depende de la temperatura en las escalas de tiempo donde ambas temperaturas son distintas, es decir, hasta varios picosegundos. La dinamica de la imanacion esta acoplada a la temperatura electronica a traves de este parametro, en la escala de tiempo ultrarrapida siempre retrasada con respecto a esta. El retraso observado es mayor cuanto mayor es la temperatura electronica. Este hecho esta en acuerdo con las observaciones experimentales que sugieren que el ritmo de desimanacion es distinto para diferentes materiales y que el proceso de desimanacion se desacelera al incrementar la potencia del laser. La ecuacion de LLB is capaz de reproducir la lenta desimanacion observada en varios materiales como el Gd, TbFe o los medio metales. Esto esta en acuerdo con el modelo de procesos EY mediados por fonones ya que en Gd

una menor probabilidad de spin-fip es predicha y tambien con el mecanismo de scatering inelastico, dado que los procesos difusivos de electrones en aislantes y medio metales esta suprimido. Sin embargo, queremos hacer notar la importancia de otros parametros que determinan los ritmos de desimanacion, tales como el acoplo electron-fonon.

Los parametros macroscopicos de relajacion, tanto la relajacion longitudinal como la transversal, tiene diferentes naturalezas en terminos de las ondas de espin involucradas como en terminos de escalas de tiempo. Aunque su dependencia con la temperatura es diferente estan relacionados con el ritmo de spin-flip. En este capitulo hemos comprobado esta relacion en varios metales de transicion tales como el Ni, Co, Fe y la tierra rara Gd, obteniendo un buen acuerdo en Co y Gd, uno excellente en Ni. Esto nos indica que en ambas escalas de tiempo el mismo proceso microscopico elemental esta actuando.

El acuerdo en Ni es bueno bajo las dos presunciones, para $\lambda = \lambda_0$ y $\lambda = \lambda_0 T_p/T_e$. En Co el acuerdo parece ser mejor con un parametro independiente de la temperatura $\lambda = \lambda_0$ lo que nos indica que el mecanismo mediado por fonones no es el principal mecanismo. Sin embargo, dada la pequea discrepancia y la complejidad de el problema de la relajacion esta conclusion no puede ser considerada como definitiva. No podemos excluir un dependecia adicional con la temperatura de la probabilidad de scattering para ambos mecanismos que no ha sido tenido en cuenta. El acuerdo observado en los ritmos de relajacion longitudinal y transversal valida el modelo LLB pero no puede responder la cuestion de cual es el mecanismo que actua.

5

Modeling of laser-induced demagnetization in Gd

The rare-earth metal Gd is an important example of the diversity of different materials since its response to fs laser excitation has been experimentally reported to be slower than in transition metals [160, 169]. Several mechanisms for ultrafast demagnetization in Gd have been discussed on theoretical background: the EY phonon-mediated scattering [105]; the diffusion mechanism [18] and the direct spin-phonon interaction caused by the spin-orbit coupling such as the Raman processes [86]. As discussed in Chapters 3 and 4, the spin system also contributes to the observed demagnetization rates, slowing them down at elevated temperatures $T \to T_C$ (T_C is the Curie temperature) via the spin-spin interaction and critical slowing down effects [11, 94]. In recent experimental findings [169] two well defined demagnetization timescales have been observed in Gd, a ultrafast subpicosecond one followed by a slower tens of picoseconds demagnetization. The first ultrafast demagnetization suggest that the scattering of conduction band electrons is also relevant [169]. The predicted timescale associated with the Raman processes of the order of 100 ps does not account for all observed demagnetization at the femto- and picosecond range. The main objective of this chapter is to elucidate the role of the different processes leading to the observed demagnetization rates.

We proceed as follows, we introduce a general microscopic Hamiltonian for the electron, phonon and spin systems in Gd from where we get a particular form of the two-temperature model (2TM). The magnetization dynamics will be treated using the quantum version of the Landau-Lisfhitz-Bloch (LLB) equation described in the previous Chapter. The localized spin system dynamics is driven by the spin-electron (conduction band) and spin-phonon interaction included in the Hamiltonian. Finally, the comparison with the experimental data allows a

quantification of phonon- and electron-mediated contributions to the fs laser-induced demagnetization. The key to this result is a variation of the initial equilibrium temperature T_0 and its quantitative effect on the demagnetization dynamics probed by the time-resolved magneto-optical Kerr effect (tr-MOKE). We find that at temperatures well below the Debye temperature Θ_D, electronic scattering can explain the observed demagnetization times. Above Θ_D phonon mediated processes have to be taken into account in addition.

Electronic structure and magnetism of Gd

We briefly describe the ferromagnetic Gd metal and the relationship between magnetism and electronic structure specific to this material, an excellent review can be found in Ref. [26]. Gadolinium (Gd) belongs to the rare-earth elements that comprise the group of lanthanides metals. In lanthanides the magnetic moment μ is dominated by the spins of $4f$ electrons. These are localized at the ion core, polarize the valence band, and generate an itinerant contribution to μ. The magnetic moment of Gd consists $7\mu_{\mathrm{B}}$ originating from the highly localized half filled $4f$ shell occupied by seven electrons and $0.58\mu_B$ from the $5d$ conduction band, see Fig. 5.1. Polarization of the conduction band leads to: (i) indirect exchange interaction (RKKY interaction), which is responsible for the ferromagnetic order in the material ($T_C = 293$ K for bulk) , and (ii) an itinerant contribution to magnetic moment of $\mu_{5d6s} = 0.58\mu_{\mathrm{B}}$. Gadolinium is regarded as the prototype of the Heisenberg ferromagnet since the $4f$ wave functions are strongly localized at the core level having a small overlap with the corresponding wave functions in neighboring atoms, there is a weak direct interaction among the $4f$ moments. As a remark, in general for the rare earth metals, the $4f$ magnetic moments retain their atomic value also in the solid state phase because the orbital momentum contribution to the total magnetic moment is not quenched by the crystal field as for $3d$ ferromagnets, due to the screening realized by the closed shells electrons $5s^2 5p^6$.

Albeit the total magnetization of Gd in equilibrium M is the sum of these $5d$ and $4f$ contributions, a dynamics picture might require a separate treatment of the localized and the conduction electrons. The conduction electrons are responsible for the optical properties, mediate the exchange interaction among localized magnetic moments, and facilitate their coupling to the lattice by means of the spin-orbit coupling. Absorption of optical photons by $5d$ electrons leads to $e-h$ pair excitation in the conduction band. Excitation of $4f$ electrons can be considered like in an atom, they follow selection rules and require ultraviolet or x-ray photons. Due to half-filled $4f$ shell (orbital quantum number $L = 0$, following

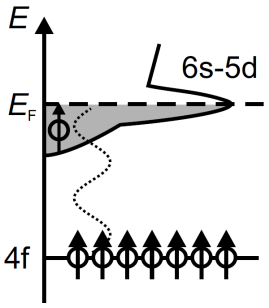

Figure 5.1: Electronic structure of Gd: A $4f$ shell, which is occupied by seven electrons that generate a magnetic moment $\mu_{4f} = 7\mu_{\mathrm{B}}$. An itinerant contribution to magnetic moment of $\mu_{5d6s} = 0.58\mu_{\mathrm{B}}$ of $5d6s$ valence band. Figure taken from Ref. [26].

Hund's rules) and hence absence of direct spin-lattice excitation which occurs through their interaction with the conduction band electrons only. This fact is responsible of the small damping parameter observed in Gd

In principle two well separated time regimes has been observed in Gd magnetization dynamics after the application of a strong ultrafast laser pulse: (i) an ultrafast one, of the order of 1 ps, and (ii) a slower quasi-equilibrium one, of the order of several tens of picoseconds. For the former timescale several mechanism has been discussed: the EY phonon-mediated scattering [105]. the diffusion mechanism [18] and the scattering of conduction band electrons [169]. While for the latter the spin-orbit mediated spin-lattice interaction is considered as the principal source of magnetization relaxation and which is in good agreement with theoretical predictions [].

5.1 Experiment

The experimental part has been done by the group of Prof. Bovensiepen in the University of Duisburg-Essen (Germany).

We briefly describe the experimental sample preparation and set up. The experimental set-up combined epitaxial film growth of Gd(0001) with 20 nm thickness on W(110) [8, 26]. The MOKE polarization rotation θ and ellipticity

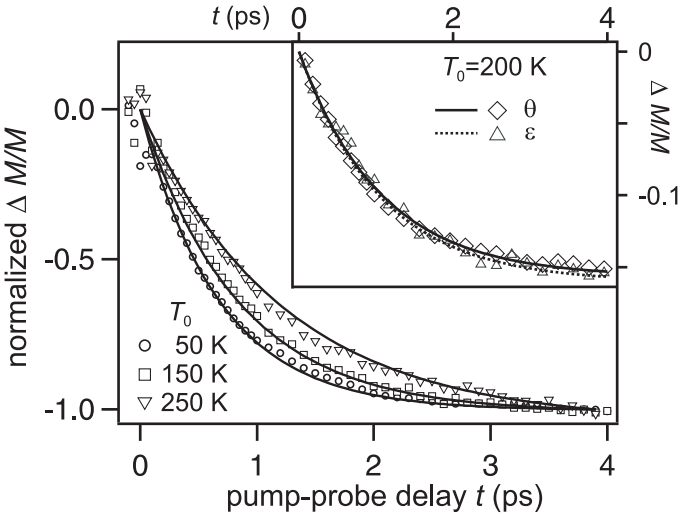

Figure 5.2: The main panel depicts $\Delta M/M$ extracted from $\Delta\theta/\theta$ for selected equilibrium temperatures. The curves have been normalized to -1 at $t = 4$ ps. The inset compares the transient changes in the magnetization $\Delta M/M$ at $T_0 = 200$ K which were determined from the MOKE rotation and the ellipticity measurements. Lines represent single exponential fits. Data from M. Sultan and U. Bovensiepen from the University of Duisburg-Essen (Germany).

ε, which are proportional to the magnetization M, were measured as a function of pump-probe delay t as detailed in [155]. In brief, in the longitudinal MOKE geometry the pump-induced change in the rotation $\Delta\theta(t)$ was recorded with an absorbed pump fluence of 1 mJ/cm^2. The equilibrium temperature T_0 was varied from 50 K to 280 K by cooling the sample by liquid He and then stabilizing T_0.

We focus on the demagnetization process during $t < 4$ ps, where the contributions of $4f$ and $5d$ electrons to M exhibit a concomitant change [155, 169]. To illustrate the dependence on T_0, data for $\Delta M(t)/M$ are shown in Fig. 5.2 after normalization to -1 at $t = 4$ ps. It is evident that the demagnetization develops slower for higher T_0. We determined the demagnetization time τ_m by fitting $\Delta M/M$ for different T_0 by a single exponential in the time interval from 0.2 to 4 ps. Fig. 5.3 depicts the temperature dependent τ_m. We observe a substantial increase in τ_m with rising T_0. In more detail, τ_m exhibits a five time increase in $\partial\tau_m/\partial T_0$ at temperatures above 170 K compared to lower T_0.

In the following we describe the laser-induced dynamics in Gd by considering that the localized $4f$ part of its magnetic moment is affected by two contributions: (i) coupling to the $5d$ fraction through electronic scattering processes, and (ii) scattering with phonons.

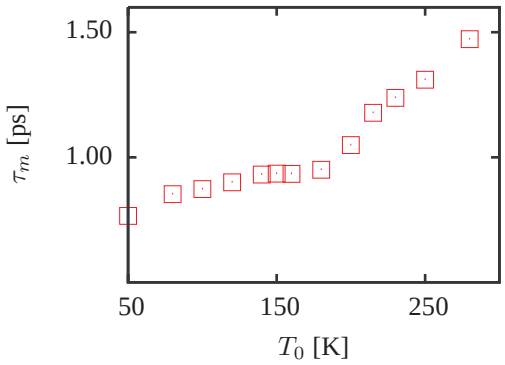

Figure 5.3: Fitted demagnetization times τ_m from experimentally measured data showed in Fig. 5.2, τ_m exhibits a five time increase in $\partial\tau_m/\partial T_0$ at temperatures above 170 K compared to lower T_0. Data from M. Sultan and U. Bovensiepen. University of Duisburg (Germany).

5.2 Model Hamiltonian

We present a microscopic model for the interaction of the different subsystems interacting in Gd; electrons, phonons and spins. The considered Hamiltonian is composed of the following terms:

$$\mathcal{H} = \mathcal{H}_e + \mathcal{H}_{ee} + \mathcal{H}_{ph} + \mathcal{H}_{e-ph} + \mathcal{H}_{s-e} + \mathcal{H}_{s-ph} \tag{5.1}$$

The first 4 terms correspond to the electron and phonon subsystems an their mutual interactions. As we have already seen in Chapter 2 they can be modeled via the two temperature model (2TM). The last 2 terms correspond to the interaction with the spin system. These terms are responsible for the magnetization dynamics. The interaction with the electron and phonon system is treated using standard interaction Hamiltonian, $sd-f$ interaction for electron-spin and Debye model for spin-phonon interaction. The spin-spin interaction is treated in the mean field approximation (MFA) using the quantum LLB equation to model the magnetization dynamics.

5.2.1 Two temperature model: electron and phonon temperature dynamics

We first treat the Hamiltonian components related to the electron and phonon subsystem which leads to a particular form of the 2TM. The basic assumption in the 2TM is that the electron and phonon subsystems are each maintained in a thermalized state by (Coulombic) $e-e$, $\mathcal{H}_{e-e}$ and (anharmonic) $ph-ph$, $\mathcal{H}_{ph-ph}$,

interactions, respectively. As we have already seen in Chapter 2 the electronic Hamiltonian, $\mathcal{H}_e$ is considered in the free electron approximation. This consideration gives the well-known linear expression for the electronic specific heat $C_e = \gamma T_e$. The phonon Hamiltonian, $\mathcal{H}_{ph}$ is taken from the Debye model, this yields $C_{ph}(T_{ph}) = 9N_A k_B \left(T_{ph}/\Theta_D\right)^3 G_4\left(\Theta_D T_{ph}\right)$ with $G_4(y) \equiv \int_0^y dx x^4 e^x/\left(e^x-1\right)^2$, see Chapter 2 for details. For $T \gg \Theta_D$ we get $C_{ph} \to C_{ph,\infty} = 25\text{Jmol}^{-1}\text{K}^{-1}$. In Gd we use the effective value $C_{ph,\infty} = 40\text{Jmol}^{-1}\text{K}^{-1}$, see Ref. [26], and we keep the shape with temperature. The electron-phonon interaction defined by $\mathcal{H}_{e-ph}$ gives a energy transfer term between electrons and phonons in the 2TM, defined by the constant G_{e-ph}. Therewith, the time evolution of the temperature of the electron and phonon system is given by two coupled heat equations

$$\begin{aligned} C_e(T_e)\frac{dT_e}{dt} &= G_{e-ph}(T_{ph}-T_e) + S(z,t) + \frac{\partial}{\partial z}\left(\kappa_e \frac{\partial T_e}{\partial z}\right) \\ C_{ph}(T_{ph})\frac{dT_{ph}}{dt} &= -G_{e-ph}(T_{ph}-T_e) \end{aligned} \tag{5.2}$$

where the thermal diffusion within the sample is described by the additional term, $\partial_z \kappa_e \partial_z T_e(z)$, in the electron dynamics with $\kappa_e = \kappa_0 T_e/T_{ph}$ and $\kappa_0 = 11$ W $\text{m}^{-1}\text{K}^{-1}$. After the pump pulse excitation, represented by $S(z,t)$ in 2TM and taken with a Gaussian shape with duration $t_\text{p} = 35$fs, a temperature gradient $\nabla_z T_e$ is created due to optical penetration depth $\lambda_{op} = 20$ nm and the electron thermal conductivity, leading to different quasi-equilibrium temperatures $T_e^i(t)$ and $T_{ph}^i(t)$ for each layer, obtained from the integration of the 2TM model.

In Fig. 5.4 we present the differential electron temperature transients, $\Delta T_e(t) = T_e(t) - T_0$, of the surface layer for three different initial equilibrium temperatures $T_0 = 50, 150$ and 250 K. We have integrated Eqs. (5.2) using the parameters in Table 5.1 with the thermal diffusion term and without it. Fig. 5.4 shows that the electron temperature variation is fasten under the consideration of the thermal diffusion term. From Fig. 5.4 it can also be seen that the electron-phonon equilibration time given by the slope of the first decay of ΔT_e slows down as T_0 increases.

5.2.2 Many LLB-macrospin model

In our model for laser-induced demagnetization the laser excites the conduction $5d$ electron system which forms a bath for the localized $4f$-electron spin system. We neglect the contribution to the total magnetization of the conduction electrons and let them to act only as a heat bath interacting with the localized spins and responsible of the heat diffusion within the sample. In this section we introduce

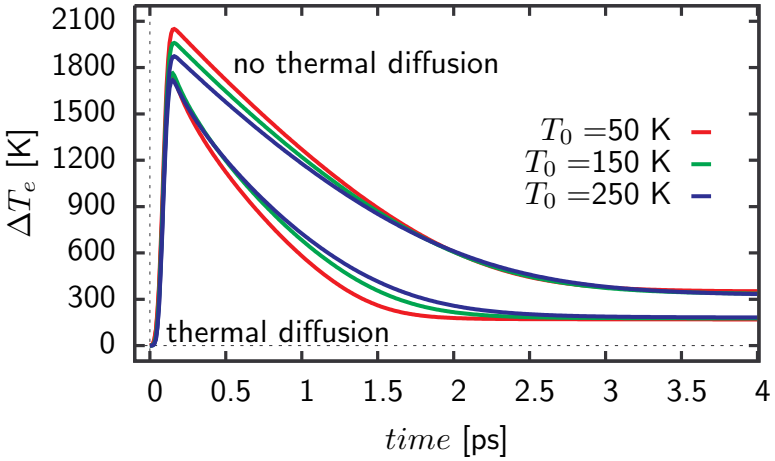

Figure 5.4: Differential electron temperature $\Delta T_e = T_e(t) - T_0$ obtained from the integration of the 2TM for Gd parameters for three initial temperatures $T_0 = 50, 150$ and 250K. We also show the effect of the thermal diffusion on $\Delta T_e(t)$.

Table 5.1: Parameters used in the 2TM.

Parameters	Value	Units
electron heat capacity, γ_e	2.25×10^2	$\mathrm{J/m^3K^2}$
electron-phonon coupling, G_{e-ph}	2.5×10^{17}	$\mathrm{W/m^3K}$
thermal diffusion coefficient, κ_0	11	W/m K
phonon heat capacity, $C_{ph,\infty}$	40	$\mathrm{Jmol^{-1}K^{-1}}$
optical penetration depth, λ_{op}	20	nm
pulse duration t_p	35	fs

the equation that describes the magnetization dynamics. We use the quantum version of the LLB equation introduced in the Chapter 4. In order to include the effect of the gradient of temperature in the sample due to the optical penetration depth and the thermal diffusion we use the LLB multispin approach already presented in Chapter 2. Within this approach each Gd layer in the thin film can be represented by one LLB macrospin micromagnetically coupled with the others layers as presented in Fig. 5.5.

Thus, the dynamical equation for each layer magnetization that should be numerically solved reads

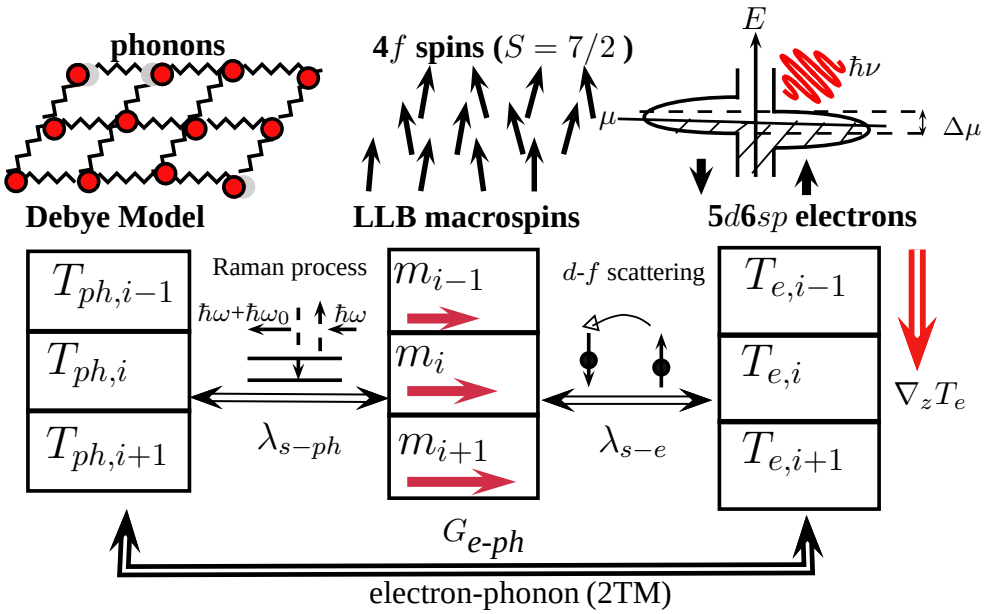

Figure 5.5: Schematic diagram of the model. The multispin LLB model (center) is coupled to the 2T model via two coupling mechanisms: phonon contribution via Raman processes (left) and electron contribution via dynamical spin polarization of carriers which produces a change of chemical potential $\Delta\mu$ [45] (right). The 2T model and the LLB model are time and layer resolved and the electron temperature diffusion is considered. The change in the phonon population with temperature is taken into account within the Debye model. The parameters of the 2T model were taken from Refs. [26, 115].

$$\frac{\dot{m}_i}{\gamma} = -\sum_{\mathrm{b}} \Lambda^i_{\mathrm{b}}(T^i_{\mathrm{b}}) \begin{cases} \frac{1}{2\widetilde{\chi}_{||,\mathrm{b}}} \left(1 - \frac{m_i^2}{m^2_{\mathrm{e,b,i}}}\right) m_i & T^i_{\mathrm{b}} \leq T_{\mathrm{C}} \\ \frac{1}{\widetilde{\chi}_{||,\mathrm{b}}} \left(1 + \frac{3m_i^2 T_{\mathrm{C}}}{5(T^i_{\mathrm{b}} - T_{\mathrm{C}})}\right) m_i & T^i_{\mathrm{b}} \geq T_{\mathrm{C}} \end{cases} \tag{5.3}$$

where the sum is over the heat baths b. Here, $m^i_{e,\mathrm{b}}(T^i_{\mathrm{b}})$ is the quasi-equilibrium magnetization corresponding to T^i_{b}. In the next section we will present the different possibilities that we have considered for such a bath. The longitudinal damping parameter

$$\Lambda^i_{\mathrm{b}}(T^i_{\mathrm{b}}) = \lambda^i_{\mathrm{b}} \frac{2T^i_{\mathrm{b}}}{3T_C} \left[\frac{2q^i_{\mathrm{b}}}{\sinh 2q^i_{\mathrm{b}}}\right], \tag{5.4}$$

includes an intrinsic coupling-to-the-bath parameter λ^i_{b} (defined by the square of the scattering matrix elements) and the spin part coming from the disordering at the quasi-equilibrium heat bath temperature T^i_{b}. Note that, up to now, the LLB equation was only used coupled to one heat bath. In this work for the first

time we use the coupling to more than one heat bath to the LLB equation. The main assumption to do that is to consider that the two contributions, electron and phonon interaction, sum up linearly.

The LLB equations are exchange coupled by the micromagnetic exchange field given by Eq. (2.40) in Chapter 2 and it can be written in the one dimensional case as

$$H_{\mathrm{EX},i} = \frac{2A}{m_{e,b,i}^2 M_s^0 \Delta^2} \sum_j (m_j - m_i) \tag{5.5}$$

where $A(m)$ is the micromagnetic exchange constant and Δ is the distance between layers, in this work we have used $\Delta = 0.5$ nm and 40 macromagnetic LLB layers to describe the experimental 20nm Gd thin film. The temperature dependence of the micromagnetic coupling, A has been considered in the MFA defined as $A/m_{e,b,i}^2 = A(T = 0\mathrm{K})$, *i.e.* coupled to the dynamics of the equilibrium magnetization of the own layer via $m_{e,b,i}(t)$. A similar modeling using the unidimensional LLB equation have been performed by U. Nowak's group in two different systems, spin-torque [138] and magnonic spin Seebeck effect [79] driven domain wall motion, in the latter work a temperature gradient was considered as in our present case.

5.2.3 Spin-phonon interaction Hamiltonian

Now, we look at the possible dissipation mechanisms leading to a reduction of magnetization present in Gadolinium. Up to now, it was assumed that the spin-lattice relaxation due to spin-orbit coupling [120, 159] was the main source of magnetization relaxation in Gd. The energy and the angular momentum conservations require $\mathcal{H}_{s-ph}$ two-magnon and two phonon operators. Since the spin-orbit coupling is already treated as a perturbation, in the second order in the spin-orbit coupling parameter and it is expected to be rather small. This mechanism leads to a characteristic spin-lattice relaxation time of the order of several tens of picoseconds [86]. In this section we resort the spin-phonon model Hamiltonian as used in the derivation of the quantum version of the Landau-Lifhsitz-Bloch equation [46]. It is of the form

$$\mathcal{H}_{\text{s-ph}} = -\mathbf{H} \cdot \mathbf{S} - \sum_{\mathbf{q}} V_{\mathbf{q}} \left(a_{\mathbf{q}}^{\dagger} + a_{\mathbf{q}} \right) - \sum_{\mathbf{p},\mathbf{q}} V_{\mathbf{p},\mathbf{q}} a_{\mathbf{p}}^{\dagger} a_{\mathbf{q}} \tag{5.6}$$

where second term is linear in phonon operators and describes direct phonon processes with amplitude $|V_{\mathbf{q}}|^2$ and third one is quadratic and describes Raman processes with amplitude $|V_{\mathbf{p},\mathbf{q}}|^2$. The Hamiltonian also includes the Zeeman energy due to the external field $\mathbf{H}$. The inclusion of the spin-spin interactions in

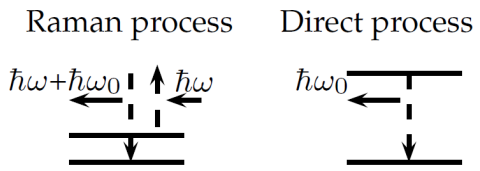

Figure 5.6: Sketch of Raman and direct process. The Raman process is a second order process. It involves a spin-flip, the absorption of a phonon of frequency ω and of the emission of a phonon of frequency $\omega + \omega_0$. In the direct process, instead, one phonon is absorbed (emitted) in conjunction with a spin-flip

the quantum LLB equation is performed by the substitution of the external field by the MFA field $\mathbf{H} \to \mathbf{H}^{\mathrm{MFA}}$ [46].

The direct processes are of the first order, one phonon is absorbed (emitted) in conjunction with a spin-flip process, and generally more efficients than that due to the Raman processes, consisting of a spin-flip, the absorption of a phonon of frequency ω and of the emission of a phonon of frequency $\omega+\omega_0$ and vice versa, since they are the next order in the spin-phonon interaction, see Fig. 5.6 for a schematic representation of direct and Raman processes. Relaxation rates due to Raman processes are generally much smaller than that due to the direct processes. However, the rates of direct processes can be small at elevated temperatures, then Raman processes become important. Processes of orders higher than Raman can be always neglected. Thus, we neglect the contribution of direct processes and focus in the Raman processes in this work as dissipation mechanism dominating the magnetization dynamics in Gd at temperatures we are working on (up to 2000 K in the first ps). We use a spin value of $S = 7/2$ to describe the $4f$ electrons' spin within the quantum LLB equation. It reads

$$\frac{1}{\gamma}\frac{dm}{dt} \cong -\overbrace{2K_2}^{\text{Raman}} \underbrace{\left(\frac{2T_{ph}}{3T_C}\right)\left[\frac{\xi}{\sinh(\xi)}\right]}_{\text{spin-spin}} \overbrace{\frac{1}{\widetilde{\chi}_{||}(T_{ph})}}^{\text{critical slowing down}} \left(1-\frac{m^2}{m_e^2}\right) m \tag{5.7}$$

where the effective field is defined as $\xi = mS^2 J_0 \beta$, equilibrium magnetization $m_e = B_S(\xi_e)$ with $B_S(\xi)$ the Brillouin function for spin value S. We use the MFA expression for the longitudinal susceptibility

$$\widetilde{\chi}_{\parallel} = \frac{\mu_{4f}}{S^2 J_0}\frac{\beta S^2 J_0 B_S'}{1-\beta S^2 J_0 B_S'} \tag{5.8}$$

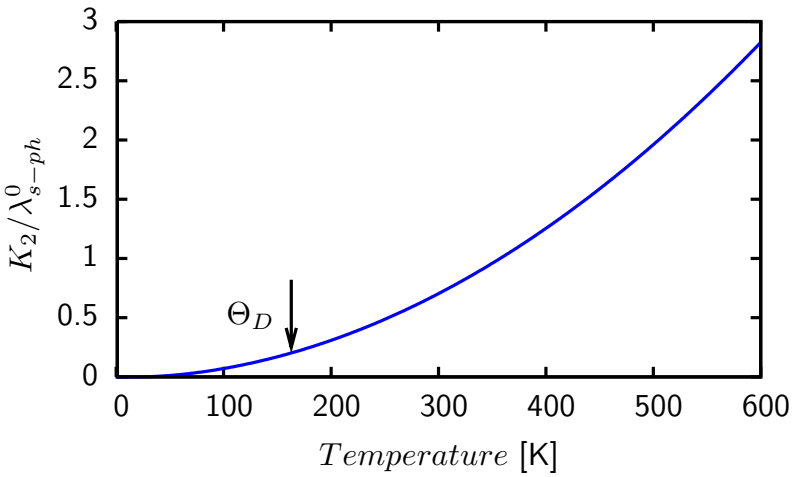

Figure 5.7: Spin-phonon interaction amplitude as a function of temperature. The Gd Debye temperature is Θ_D=163K.

where $\beta = 1/k_B T_{ph}$, $J_0 = zJ$ is the exchange constant multiplied by the number of nearest neighbours z and $B'_S \equiv dB_S/d\xi$ is evaluated at the equilibrium ξ_e. K_2 is defined by the Raman spin-phonon processes and correspond to the spin flip probability at phonon temperature T_{ph}. In the density matrix formalism used by D. Garanin in Ref. [46] to derive the quantum version of the LLB equation the relaxation constant K_2 for Raman process has the form

$$K_2 \;=\; \frac{\pi}{2}\sum_{\mathbf{p},\mathbf{q}} |V_{\mathbf{p},\mathbf{q}}|^2\, n_{\mathbf{p}}\,(n_{\mathbf{q}}+1)\,\delta\left(\omega_{\mathbf{p}}-\omega_{\mathbf{q}}-H\right). \tag{5.9}$$

We work out the term K_2 to find its temperature dependence. Since Raman processes can become important only at high temperatures, one can drop spin transition frequencies in the energy δ-functions. Next, one can replace summation by integration and introduce the characteristic Raman rate, following Ref. [86] K_2 can be written as follows

$$K_2 \sim \frac{D^2}{\Omega_t^8}\int d\omega_{\mathbf{k}}\omega_{\mathbf{k}}^6 n_{\mathbf{k}}\,(n_{\mathbf{k}}+1) \underbrace{\sim}_{\text{Debye}} \lambda^0_{\text{s-ph}}\left(\frac{T_{ph}}{\Theta_D}\right)^7 G_6\left(\frac{\Theta_D}{T_{ph}}\right) \tag{5.10}$$

where we have used the Debye model for the phonon frequencies $\omega_{\mathbf{k}}$ and we have left a free parameter $\lambda^0_{\text{s-ph}}$ as a phenomenological parameter which can be estimated from the magnetocrystalline anisotropy D and the Ω_t acoustic phonon speed. In Fig. 5.7 we can see the temperature dependence of the spin-phonon interaction rate K_2/λ^0_{s-ph}. For $T \ll \Theta_D$ the rate grows as T^7_{ph}, whereas for

$T \gg \Theta_D$ it does as T_{ph}^2 with transition between two regimes at $T_{ph} > 0.2\Theta_D$. We observe a substantial increase of the rate for temperature above the Debye temperature, as expected, due to the increase of the phonon population and therefore the increase of the spin-phonon scattering events.

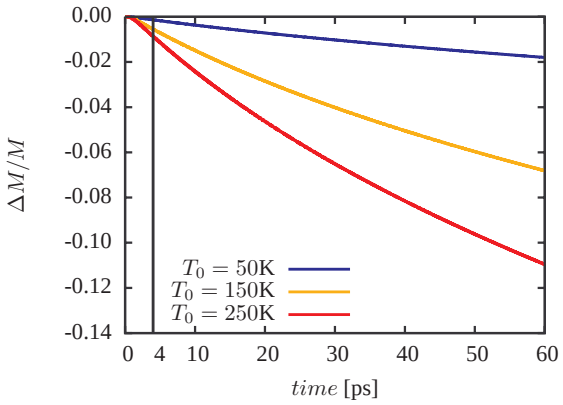

Figure 5.8: Phonon mediated magnetization relaxation calculated by the integration of the 2TM and the LLB equation for three initial temperatures $T_0 = 50, 150$ and 250K are showed. Note that the experimentally observed relative demagnetization at $t = 4$ps can not be explained by spin-phonon interaction.

Fig. 5.8 shows magnetization dynamics after laser pulse excitation for different initial temperatures T_0. For the description of phonon temperature we have used the 2TM described by Eqs. (5.2). Fig. 5.8 shows that in the first 4 picoseconds, the demagnetization due to spin-phonon interaction is not relevant in comparison with the experimentally observed values, see inset of Fig. 5.2. Fig. 5.7 shows that for high temperature the maximum relative demagnetization $\Delta M/M$ is larger as initial temperature T_0 increases, in good agreement with the fact that the number of spin-phonon scattering events increase with temperature due to the increment of phonon population.

5.2.4 Spin-carriers interaction Hamiltonian

In this section we consider the electron-spin interaction where the spin system is represented by $4f$ electron system spin and the electron heat bath by the $6s5d$ conduction band electrons. The localized $4f$ spins are coupled to carriers spins by $sd-f$ exchange interaction as in Ref. [45] where the ultrafast spin dynamics were studied within the $s-pd$ model in ferromagnetic semiconductors. The electron-spin interaction $\mathcal{H}_{CS}$ is then modeled by the conventional exchange interaction Hamiltonian

$$\mathcal{H}_{CS} = -\frac{J_{CS}}{V}\sum_{l}\sum_{\mathbf{k},\mathbf{k}'}(\hat{\mathbf{s}}\cdot\hat{\mathbf{S}}_l)e^{i(\mathbf{k}'-\mathbf{k})\mathbf{R}_l}a^{\dagger}_{\mathbf{k}}a_{\mathbf{k}'} \tag{5.11}$$

where $\hat{\mathbf{S}}_l$ is the spin operator of localized spins at $\mathbf{R}_l$, $\hat{\mathbf{s}}$ is the carrier spin operator. J_{CS} is the exchange interaction. When one replaces $\hat{\mathbf{s}}\cdot\hat{\mathbf{S}}_l$ by $\hat{s}_z\hat{S}^z_j+\frac{1}{2}(\hat{s}_-\hat{S}^+_j+\hat{s}_+\hat{S}^-_j)$, the above $\mathcal{H}_{CS}$ contains two effects: the first term is responsible for the spin-splitting of the conduction bands and the second term leads to a transfer of angular momentum between the spins of the hot electrons and the spins of the ground state. While the interaction conserves the total spin angular momentum, the thermalization process of each bath is not spin conserving. Therefore, this interaction transfers energy between the electron and the spin baths, which results in the effective demagnetization of the localized spins.

Now, we use the quantum LLB equation with relaxation rate, Γ_{CS} derived from Hamiltonian $\mathcal{H}_{CS}$. It reads

$$\frac{1}{\gamma}\frac{dm}{dt} \cong -\lambda^0_{e-s}\left(\frac{2T_e}{3T_C}\right)\left[\frac{\xi}{\sinh(\xi)}\right]\frac{1}{\widetilde{\chi}_{||}(T_e)}\left(1-\frac{m^2}{m_e^2}\right)m \tag{5.12}$$

here the equilibrium magnetization m_e is still defined by the Brillouin function but now calculated for electron temperature T_e, as well as the effective field $\xi = mJ_0S^2/(k_BT_e)$ and the longitudinal susceptibility $\widetilde{\chi}_{||}(T_e)$. Eq. (5.12) tends to push the transient magnetization $m(t)$ to the equilibrium magnetization given by the electron heat bath temperature. The phenomenological coupling parameter λ^0_{e-s} is related to the transition probability rate given by [45]

$$\Gamma^{+-}_{CS} = \frac{2\pi}{\hbar}\frac{J_{CS}}{4}\int dE f_{\text{up}}(E)\left[1-f_{\text{down}}(E-\delta)\right]D_{\text{up}}(E)D_{\text{down}}(E-\delta) \tag{5.13}$$

here $f_{\text{up(down)}}$ distribution function for spin s =up (down), characterized by two different chemical potentials μ_s and a common temperature T_e, $D_s(E)$ are the spin-resolved density of states.

We first analyze the case in which the carrier-spin relaxation is so fast that the carriers are a good sink of polarization, so that $\Delta\mu = 0$ at each moment of time. The occupation factors $f_{\mathbf{k}}$ are the same for both spins and are characterized by the time varying temperature $T_e(t)$ and chemical potential μ. The relaxation rate is then $\Gamma^{+-}_{CS} \sim J^2_{ex}D_{\text{up}}(\mu)D_{\text{down}}(\mu)$. In this situation we can assume a constant intrinsic damping parameter $\lambda_{e-s} = \lambda^0_{e-s}$

The interaction between the carriers and the localized spins produces a mean-field term and a secondary term corresponding to simultaneous flips of the itinerant and localized spins. The latter causes exchange of angular momentum

Table 5.2: Gadolinium magnetic system parameters.

Parameter	Value	Units
atomic magnetic moment, μ_0	7	μ_B
spin number, S	7/2	
exchange constant, J_0	1.21×10^{-20}	J
Curie temperature, T_C	273	K

between the excited carriers and the localized spin system. Due to the spherical symmetry of the $sd-f$ Hamiltonian, the $sd-f$ interaction alone conserves the total spin, and it can only move the spin polarization from one system to another.

The spin transferred into the carrier system is not conserved due to the spin-orbit interaction. In its presence, the scattering within the electronic system is accompanied by spin relaxation ultimately into the lattice (spin-phonon interaction). However, the spin relaxation occurs on a finite time scale τ_{sr}. If the rate at which the carriers relax their spins is smaller than the rate at which angular momentum is injected into the carrier population, there is a dynamic spin polarization of the carriers. In this case the relaxation rate can be estimated as $\lambda_{s-e} \sim \lambda^0_{s-e}\,(1 + \Delta\mu/k_B T_e)$. We assume that the time evolution of non-equilibrium spin polarization $\Delta\mu$ can be expanded at the first order around the transient electron temperature difference ΔT_e, then an electron temperature (time) dependent damping parameter is obtained in the linear approximation as

$$\lambda_{e-s} = \lambda^0_{e-s}\left(1 - \frac{\Delta T_e}{T_e}\right) \tag{5.14}$$

It phenomenologically describes the magnetization relaxation via coupling between carriers and localized electrons. It also describes the ultrafast dynamical spin-polarization which acts as a bottleneck for angular momenta exchange between electrons and spins.

5.2.5 Demagnetization via electron scattering in Gd: phenomenological model

Because we are interested in the first 4 ps and as we have seen that it seems that the spin-lattice relaxation does not start to contribute until several tens of picoseconds, see Fig. 5.8, we initially focus our modeling efforts in the electron mediated demagnetization process. First of all we model the electron contribution

as we did in the Nickel thin films in Chapter 3, *i.e.* we use a constant coupling parameter $\lambda =$. Through this thesis we have mainly used such a kind of coupling in all our models, although the above consideration show that it can depend on the electron population or alternatively on the available phase-space. In any case, we start studying the magnetization dynamics in Gd using a constant coupling parameter. In Fig. 5.9 we show the results from the integration of the LLB equation within this model. We show the demagnetization characteristic timescales and the relative demagnetization $\Delta M/M$ obtained from the calculation of the demagnetization dynamics. The coupling parameter λ_{s-e} has been chosen in such a way that the total relative demagnetization at $T = 50$K coincides with experimental results, in this case $\Delta M/M = 15\%$. We can see in the inset of Fig. 5.9 that the LLB model demagnetization times τ_m are around two times faster in comparison with experimental findings. We conclude that this coupling mechanism can not explain the observed change in the slope of demagnetization timescales as a function of T_0, see Fig. 5.3.

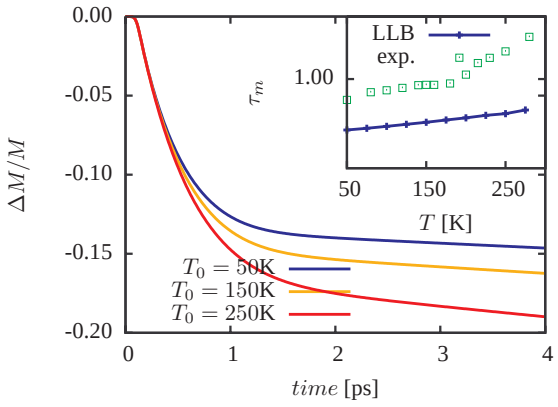

Figure 5.9: Electron mediated magnetization relaxation calculated by the integration of the 2TM and the LLB equation for three initial temperatures, $T_0 = 50, 150$ and 250K. (Inset) The demagnetization times calculated from the magnetization transients in comparison with the experimental observations (squares).

After that we look at the effect on the demagnetization dynamics with a (time) temperature dependent coupling. As we have seen in section 5.2.4, when the photo excitation of the delocalized electrons is strong enough and the electron temperature increases to values where $k_B T_e \gg \Delta\mu$, then the finite relaxation time of the electron-hole pairs reduces the phase-space available for the scattering events between spin and electrons. This effect is known as **dynamical spin polarization**. It can be phenomenologically modeled within the LLB equation by using a time or temperature dependent coupling parameter as given by Eq.

(5.14). Alternatively, in Ref. [45] this behaviour was modeled using another phenomenological equation for the dynamics of the carrier system spin polarization. In the latter model [45] the finite relaxation time of the electron-hole pairs is characterized by an had-oc "relaxation time".

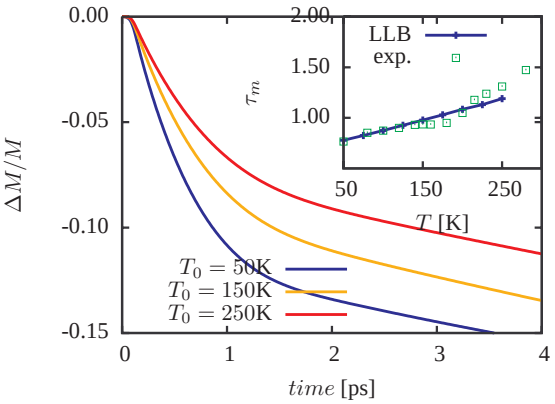

Figure 5.10: Electron mediated magnetization relaxation calculated by the integration of the 2TM and the LLB equation for three initial temperatures, $T_0 = 50, 150$ and 250K. (Inset) The demagnetization times calculated from the magnetization transients in comparison with the experimental observations (squares).

Fig. 5.10 shows the results from the integration of the LLB equation within this model. We show the demagnetization characteristic timescales and the relative demagnetization $\Delta M/M$ obtained from the calculation of the demagnetization dynamics for three characteristic initial temperatures $T_0 = 50, 150, 250$K. As for the previous modeling the coupling parameter λ^0_{s-e} is chosen in such a way that the total relative demagnetization at $T = 50$K coincides with experimental results, in this case $\Delta M/M[4\text{ps}] = 15\%$. Contrary to the model where the coupling parameter was considered constant and represented in Fig. 5.9, now, as it is shown in the inset of Fig. 5.9, under the consideration of a temperature dependent coupling parameter the demagnetization times closely follows the experimental observations for temperatures $T_0 < 170$K. As we can see from Fig. 5.10 the demagnetization time calculated from the previous modeling does not show any change in the slope $\partial\tau_m/\partial T_0$ as a function of the initial temperature T_0.

5.2.6 Inclusion of spin-phonon interaction

Since the phonon population is well characterized as a function of T_0 the pronounced change in $\tau_m(T_0)$ in the vicinity of the Debye temperature Θ_D should provide a key to separate electron- and phonon-mediated spin-flip processes.

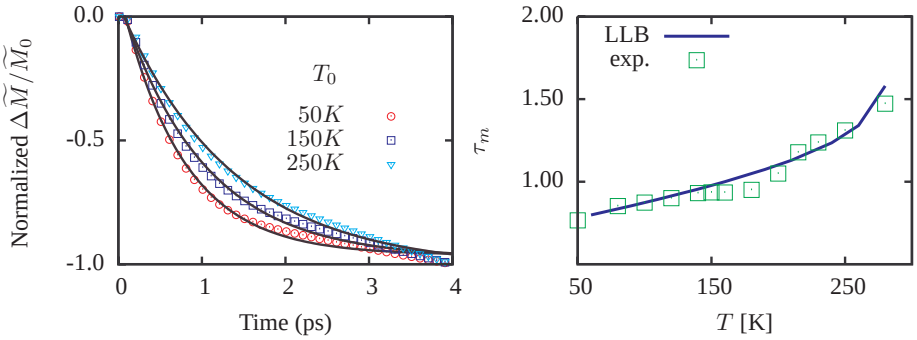

Figure 5.11: (Left) Normalized demagnetization for three different intial temperatures $T_0 = 50, 150$ and 250K. (Right) The slow demagetization time at long time scale.

Thus, we include the spin-lattice mechanism in addition to the electron-spin. In principle the inclusion of another dissipation mechanism should fasten up the magnetization dynamics. It is true only for linear process where the rate sums up. In our case, as we have already seen, the rate parameters are time dependent and strongly non-linear. In Fig. 5.11 (Left) we can see the effect of the inclusion of the spin-lattice coupling in the normalized demagnetization curves, we note that a single exponential fitting of the demagnetization curves still is allowed. We have observed that if the coupling parameter λ_{s-ph} is small enough negligible contributions to total demagnetization are present. As a consequence, the characteristic times are not modified. As the spin-phonon coupling parameter increases we have observed that the timescales at the high temperature region $T_0 > \Theta_D$ slows down. We have found that a value of $\lambda^0_{s\text{-}ph} = 0.0002$ fits very well the experimental results. In Fig. 5.11 (Right) we show both the experimental and theoretical demagnetization times.

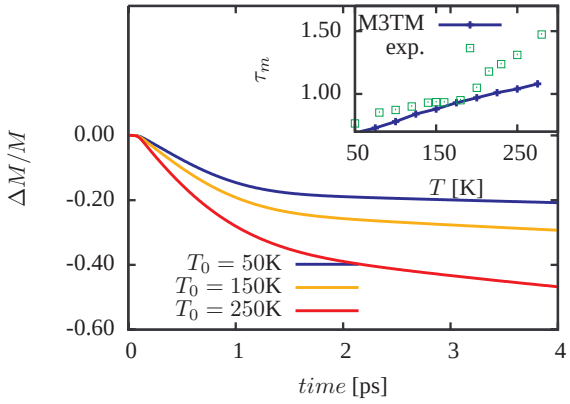

Figure 5.12: Magnetization dynamics calculated by the integration of the M3TM model for three initial temperatures, $T_0 = 50, 150$ and 250K. (Inset) The demagnetization times calculated from the magnetization transients in comparison with the experimental observations (squares).

5.2.7 Comparison with M3TM model

For comparison, we present in Fig. 5.12 the results of the integration of the M3TM model, recently proposed in Ref. [105], which is based on phonon-mediated EY scattering. The M3TM model has been implemented using the same 2T model as in the LLB model. As we have seen in detail in Chapter 4 it is equivalent to the LLB model with $S = 1/2$ and $\lambda_{EY} \sim (T_{ph}/T_e)$. The results are presented in Fig. 5.12. Although τ_m shows a similar behavior as our LLB results for $T_0 < 170$ K, it does not account for the slower demagnetization at $T_0 > 170$ K. Furthermore, $|\Delta M/M|$ at 4 ps increases with temperature, contrary to the experimental observation.

5.2.8 Long timescale demangetization

We complete the picture of the magnetization dynamics in Gd after the action of a strong femtosecond laser pulse calculating the long time (several tens of picoseconds) magnetization dynamics within our model. At such timescales the electron and phonon temperatures are the same and at high T_0 the coupling to phonon system starts to dominate. As a result $\Delta M/M$, measured at 60 ps, increases with temperature, contrarily to the behavior at 4 ps and in agreement with the experimental observation [57]. In Fig. 5.13 we show the initial equilibrium temperature T_0 dependence of the long time characteristic times $\tau_{m,\text{long}}$ for the same parameters used in the calculation corresponding to timescales up to 4 ps. The relative demagnetization at $t_0 = 4$ ps decreases as equilibrium temperature increases, this is due to the lost of efficiency in the electron channel, dominating the first picoseconds. However, when the timescale is dominated by spin-phonon coupling, $t_0 = 60$ ps, it increases, in this case related to the increase of K_2 (see Fig. 5.7) with temperature

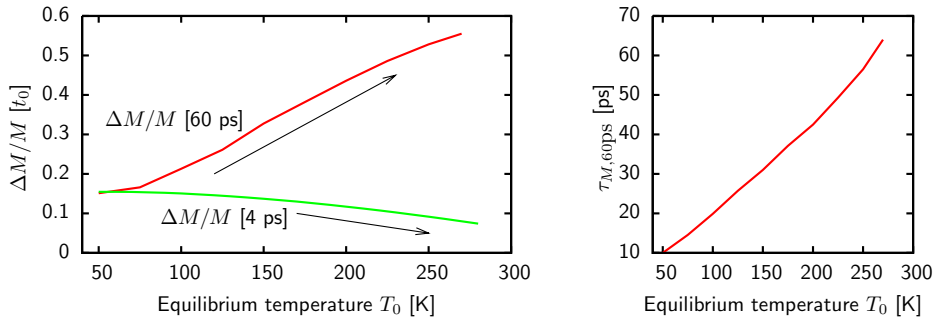

Figure 5.13: (Left) Relative demagnetization at fast $t_0 = 4$ ps and slow $t_0 = 60$ ps (quasi-equilibrium) regimes. (Right) The slow demagetization time at long time scale.

5.3 Discussion and outlook

The results of the LLB modeling shows a good agreement with the experimental data. We have summarized all the modeling results in comparison with experimental data in Fig. 5.14. We note that the phonon-mediated demagnetization is intrinsically slower than the electronic one. Thus the observed behavior is different at different timescales. At $t < 4$ ps the dynamics is dominated by T_e.

In agreement with the slowing down of $\Lambda_{\mathrm{e}}(T_e)$, the value τ_m increases and the demagnetization value $|\Delta M/M_0|$(4ps) changes weakly as a function of T_0 (see Fig. 5.14). At longer timescales > 10 ps, the electron and phonon temperatures have equilibrated and the coupling to the phonon system starts to dominate, increasing with temperature. As a result $\Delta M/M_0$, at 60 ps, increases with T_0 , contrarily to the behavior at 4 ps. These contributions were already discussed in Ref. [169], where electronic and phononic processes were associated with the non-equilibrium and quasi-equilibrium demagnetization, respectively. The analysis of experimental and theoretical data also show that there is a contribution of phonons to τ_m at $T_0 > \Theta_D$ when the coupling to the phonon system increases considerably. The contribution of both relaxation mechanisms increases $m(t)$ in this timescale and thus additionally slows down the demagnetization via the nonlinearity of the response in Eq. (5.12).

As the LLB equations correctly take magnetic fluctuations at temperatures close to T_C into account [41] and explicitly includes the critical slowing down effect, we also discard the latter mechanism [94], as responsible for the observed increase in $\partial\tau_m/\partial T_0$ for $T_0 \gtrsim 170$ K. Finally, in contrast to the widely used Matthiessen's rule, the scattering rates $\Gamma = 1/\tau_M$ of different processes do not add up $\Gamma \neq \Gamma_{s\text{-}ph} + \Gamma_{s\text{-}e}$ due to the nonlinear dependence on m of the relaxation rates in Eq. (5.12).

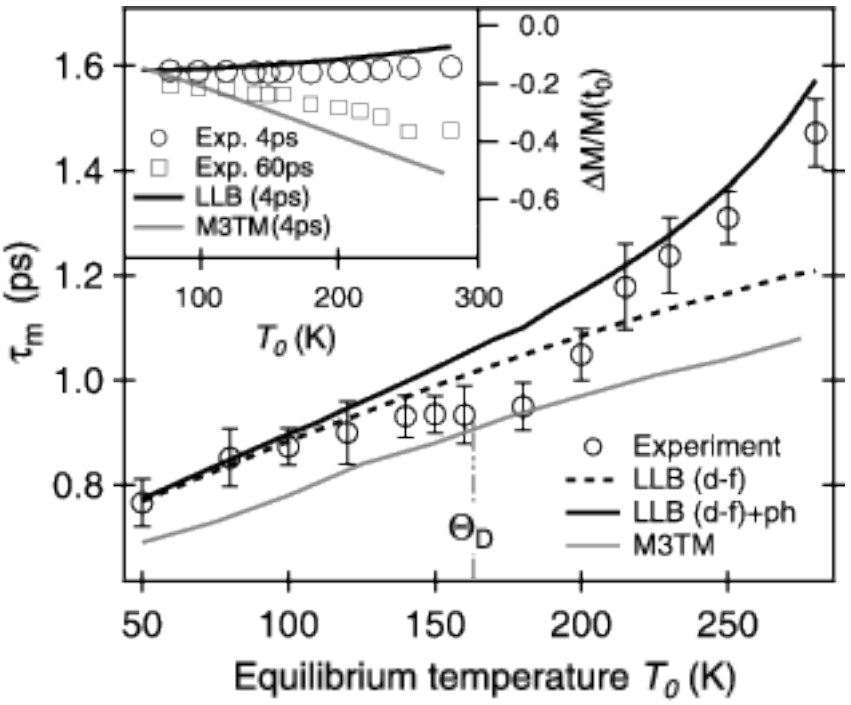

Figure 5.14: The demagnetization time τ_m as a function of T_0. Symbols represent the experimental data points while lines represent the modelling results considering only electron-spin flip coupling (dashed) and combined electron- / phonon-mediated spin-flips (solid line) with $\lambda^0_{s\text{-}ph} = 0.0002$. The gray line represent the results obtained within the M3TM model assuming EY scattering mechanism.

We would like to mention that in principle a separate equation of motion for the spin polarization of d electrons can be written, similar to Ref. [144]. In this case we would have to consider that $4f$ electrons are interacting with the laser pulse and the environment via $5d$ electrons only. For a macroscopic description of such processes, the derivation of a two-component LLB equation with a correct treatment of $sd-f$ exchange interaction within the mean-field approach is necessary. This work is now in progress.

5.4 Conclusions

We performed a temperature-dependent analysis of fs laser induced demagnetization of Gd(0001) by the Landau-Lifshitz-Bloch model. Oue experimental partners observe a two time increase in the characteristic demagnetization time from 0.8 ps at 50 K to 1.5 ps at 280 K which we explain on the basis of the results from the Landau-Lifshitz-Bloch model by microscopic electron- and phonon-mediated demagnetization processes quantitatively. In general a temperature increase results in a slower demagnetization. At low temperature the demagnetization times observed in experiment can be modeled by considering electronic processes only. At temperatures above the Debye temperature phonon-mediated processes have to be taken into account in addition.

The consideration of both electron and phonon processes shows a good agreement with experiment, see Fig. 5.14. We observe a change in the slope of the demagnetization times for $\lambda^0_{s\text{-}ph} \gtrsim 0.0001$. To understand the observed behavior we note that (i) the phonon-mediated demagnetization is intrinsically slower than the electronic one, (ii) the LLB equation has a nonlinear demagnetization rate (depending on the instantaneous $m(t)$) originating from spin fluctuations. Thus the observed behavior is different at different timescales. At $t < 4$ ps, see Fig. 5.14, the dynamics is dominated by T_e which is in this time interval much larger than the phonon one. At low equilibrium temperatures $T_0 < \Theta_D$ the coupling to the phonon system is negligible and the electronic mechanism is dominating. The nonlinearity can be neglected and τ_m increases with T_0 in agreement with the decrease of the electronic coupling. At $T_0 > \Theta_D$, however, the coupling to the phonon system increases dramatically. The contribution of both relaxation mechanisms increases the value of $m(t)$ and thus produces a slowing down of the demagnetization rate via the nonlinearity of the magnetization response. The resulting demagnetization value $\Delta M/M$ at 4 ps, decreases as a function of T_0 as observed experimentally and in modeling, see Fig. 5.14.

Conclusiones en español

En este capítulo hemos realizado un análisis de la desimanación inducida por láser de femtosegundos de la tierra rara Gd(100) en función de la temperatura inicial usando el módelo de Landau-Lifshitz-Bloch. Nuestros colegas experimentales observaron que el tiempo característico de desimación aumentaba en un factor dos con la temperatura inicial, de 0.8 ps a 50K hasta 1.5 ps a 280K. En base a los resultados de nuestro módelo podemos explicar cuantitativamente el comportamiento observado mediante procesos microscópicos mediados por electrones y fonones. En general, un aumento de la temperatura resulta en una desimanación más lenta. Aunque a bajas temperaturas los tiempos de desimanación observados en el experimento pueden ser modelizados considerando sólamente procesos electrónicos, a temperaturas por encima de la temperatura de Debye, los procesos mediados por fonones tienen que ser tenidos en cuenta.

Cuando en nuestro modelo consideramos ambos procesos, mediados por electrones y fonones, obtenemos un buen acuerdo con los resultados experimentales. Observamos un cambio en la pendiente de la curva de tiempos de desimanación. Para entender este comportamiento, hacemos notar que primero, la desimanación mediada por fonones es intrínsecamente más lenta que la electrónica, y segundo, el término de relajación longitudinal en la ecuación LLB es no lineal.

A tiempos $t < 4$ ps, ver figura 5.14, la dinámica esta dominada por T_e que en ese intervalo temporal es mucho mayor que la de los fonones. Para temperaturas de equilibrio $T_0 < \Theta_D$ el acoplo al sistema de fonones es despreciable y los mecanismos electronicos son los dominantes. Sin embargo, para $T_0 > \Theta_D$, el acoplo al sistema de fonones incrementa dramaticamente. La contribución de ambos mecanismos de relajación aumenta el valor de $m(t)$ y por tanto produce una desaceleración de la velocidad de desimanación a través del termino no lineal de la respuesta magnética. La desimanación resultante $\Delta M/M$ a 4 ps, disminuye como función de T_0 como en los resultados experimentales y en el modelo, ver figura 5.14.

6

The Landau-Lifshitz-Bloch equation for ferrimagnet

6.1 Introduction

Up to now, the fastest precessional reversal time demonstrated experimentally using an external magnetic field [13, 156] was of the order of 100 ps, with similar reversal times achieved using a spin-polarized current [2, 49, 145]. Magnetization precession at picosecond timescale [13, 156] was considered to be the limiting factor for the speed of the magnetization switching, until using optical excitation with femtosecond (fs) pulsed lasers the possibility to influence the magnetization on fs timescale was demonstrated [19, 82, 142]. However, controllable magnetization switching has only been observed in GdFeCo alloys, and this has stimulated a great deal of effort to attempt on many levels to explain this process, see review in Ref. [102]. The ferrimagnetic materials consist of at least two magnetic sublattices antiferromagnetically coupled. Differently to antiferromagnets, in ferrimagnets the magnetic moments of each sublattice are different, leading to a net macroscopic magnetization $M(T)$. The main characteristics of the ferrimagnetic materials is that for some temperature , called magnetization compensation temperature T_M, the net macroscopic magnetization can be zero $M(T_M) = 0$, although the net magnetization of each sublattice is not. The angular momentum compensation temperature, T_A is also of interest. At this temperature the total angular moment, $A(T) = M(T)/\gamma$, is zero.

Recently, Vahaplar *et al.* [157], demonstrated that the switching in GdFeCo involves a novel "linear" reversal mechanism, proposed theoretically in Ref. [94] using a macroscopic description based on the ferromagnetic LLB equation [64]. This is an especially fast mechanism since it is governed by the longitudinal relaxation time, which can be two orders of magnitude faster than the transverse

relaxation time governing precessional switching. The main criticism we can do to this approach is that GdFeCo is treated theoretically as a ferromagnet, therefore, losing the possibility to include different dynamics of each sublattice. The use of that kind of simplifications could be crucial in the description of the magnetization switching mechanisms and it could lead to a misunderstanding of the process. In that sense Radu *et al.* [134] used an atomistic model of the magnetization dynamics to simulate such a material. In these models the complexity of two-sublattice materials can be easily included. They compared the simulation results to experimental data measured using the element-specific technique X-ray magnetic circular dichroism (XMCD) to study magnetization reversal in GdFeCo. They unexpectedly found that the ultrafast magnetization reversal in this material, where spins are coupled antiferromagnetically, occurs by way of a transient ferromagnetic-like state. More recently, it has been demonstrated [**?**] that such reversal occurs also in the absence of external applied magnetic field and energy input from the laser pulse acts as the only external stimulus.

Atomistic models are convenient to model ferrimagnetic materials but for a better understanding of the mechanisms leading to these new phenomena a macroscopic equation similar to ferromagnetic LLB equation is desirable.

In this chapter we deal with this problem, we derive a macroscopic equation for the magnetization dynamics of a ferrimagnetic system valid at elevated temperatures. Fig. 6.1 shows a sketch of an atomistic model for a ferrimagnetic material and the corresponding micromagnetic approximation. Firstly, we present an atomistic classical Heisenberg model for a crystallographically amorphous ferrimagnetic alloy [128]. The model is based on the Langevin dynamics simulations of the Landau-Lifshitz-Gilbert (LLG) equations for localized atomistic spins. We also present the corresponding mean-field approximation (MFA) for this system from where we obtain static properties like equilibrium magnetization and critical temperatures, such as angular and magnetization compensation temperatures, T_A and T_M, and the Curie temperature, T_C.

We use MFA to derive a macroscopic equation of motion for the magnetization of each sublattice. It contains both transverse and longitudinal relaxation terms and interpolates between the Landau-Lifshitz equation at low temperatures and the Bloch equation at high temperatures. We preview the possibility to explain the thermally driven magnetization switching via momenta transfer between sublattices. We conclude that it is a good starting point for performing large scale simulations in multi-lattice magnetic systems as the LLB equation is for ferromagnetic materials [10, 95].

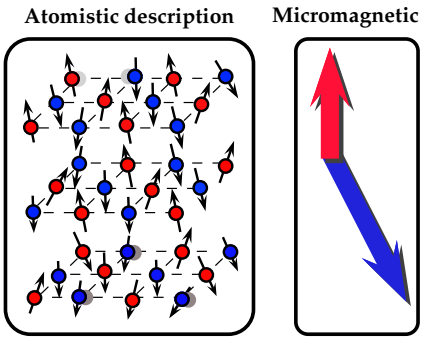

Figure 6.1: (Left) Sketch of atomistic regular ferrimagnetic lattice. Each point represents a magnetic moment associated with an atomic site. Magnetic moment of blue points are pointing downwards and red ones upwards. (Right) A macroscopic view of partial average magnetization $m_A = \langle S_A \rangle$ and $m_B = \langle S_B \rangle$ by two macrospins. We will derive the equation of motion of each sublattice based on the Landau-Lifshitz-Bloch equation.

6.2 Atomistic model

The models for a binary ferrimagnetic alloy of the type A_xB_{1-x}, randomly occupied by two different species (A and B) of magnetic ions have been previously extensively investigated theoretically [93, 118, 119]. In such models A and B ions have different atomic quantum spin values S_A and S_B ($S_A \neq S_B$).

In contrast, in the present section we investigate the classical counterpart of these models by considering the classical spins with $\mu_A \neq \mu_B$. A further but non essential simplification is to assume that the interactions between spins in the disordered binary alloy are of the Heisenberg form with the exchange interactions different for different pairs of spins (AA, BB or AB).

Let us start with the model for a ferrimagnet described by the classical Hamiltonian of the type

$$\mathcal{H} = -\sum_{i}^{\mathcal{N}} \mu_i \mathbf{H} \cdot \mathbf{s}_i - \sum_{i}^{\mathcal{N}} D_i (s_i^z)^2 - \sum_{\langle ij \rangle} J_{ij} \mathbf{s}_i \cdot \mathbf{s}_j, \tag{6.1}$$

where $\mathcal{N}$ is the total number of spins, (i, j) are lattice sites, μ_i is the magnetic moment located at lattice site i. The external applied field is expressed by $\mathbf{H}$. The anisotropy is considered as uniaxial with D_i being the anisotropy constant of site i. The third sum is over all nearest-neighbour pairs and we have considered unit length classical vectors for all lattice sites $|\mathbf{s}_i| = 1$. Heisenberg exchange interaction parameter between adjacent sites is $J_{ij} = J_{AA(BB)} > 0$ if both sites

(i, j) are occupied by $A(B)$ type magnetic moments and $J_{ij} = J_{AB} < 0$ if the sites (i, j) are occupied by A and B respectively.

The magnetization dynamics of this model interacting with the bath is described by the stochastic Landau-Lifshitz-Gilbert (LLG) equation

$$\dot{\mathbf{s}}_i = \gamma_i[\mathbf{s}_i \times \mathbf{H}_{i,\text{tot}} + \boldsymbol{\zeta}_i] - \gamma_i\lambda_i[\mathbf{s}_i \times [\mathbf{s}_i \times \mathbf{H}_{i,\text{tot}}]] \tag{6.2}$$

where λ_i is the coupling to the heat bath parameter. The stochastic thermal fields $\boldsymbol{\zeta}_i$ are uncorrelated in time and on different lattice sites. They can be coupled to different heat baths (via temperature, e.g. phonon or electron) and could have different strength of coupling (via λ_i and μ_i) for each atom type (A or B). The correlator of different components of thermal field can be written as:

$$\langle \zeta_{i,\alpha}(t)\zeta_{j,\beta}(t')\rangle = \frac{2\lambda_i k_\text{B} T}{\mu_i\gamma_i}\delta_{ij}\delta_{\alpha\beta}\delta(t - t') \tag{6.3}$$

where α, β are Cartesian components and T is the temperature of the heat bath to which the spins are coupled. The effective fields are given by

$$\mathbf{H}_{i,\text{tot}} \equiv -\frac{1}{\mu_i}\frac{\partial\mathcal{H}}{\partial\mathbf{s}_i} = \mathbf{H} + \frac{2D_i}{\mu_i}s_i^z\mathbf{e}_z + \frac{1}{\mu_i}\sum_{j\in\text{neig}(i)} J_{ij}\mathbf{s}_{ij}$$

In the next section we test the static properties of this atomistic model against the corresponding mean field approximation (MFA)(in collaboration with Thomas Ostler a PhD. student from R. W. Chantrell's group at the University of York (UK)).

6.3 Mean Field Approximation for Ferrimagnet

In this section we present an adapted mean field approximation (MFA) to calculate the free energy, $\mathcal{F}$, of a disordered ferrimagnetic compound consisted of a transition metal (TM) doped with a rare-earth (RE) metal. From $\mathcal{F}$ we calculate the equilibrium magnetization of each sublattice as a function of temperature and we derive the effective fields acting on each sublattice. The standard MFA model (see, e.g. Refs. [32, 118, 119]) has been generalized to a disordered case with the aim to parameterize the atomistic model in relation to static measurements in FeCoGd compound [128]. We use the MFA to verify the atomistic model by comparing the corresponding values of the Curie and magnetization compensation temperatures. We extract the equilibrium magnetization of each sublattice and compare the results with those obtained from the numerical model.

The free energy: $\mathcal{F} = -k_{\rm B}T \ln \mathcal{Z}$ of the spin system ($\mathcal{Z}$ is the partition function) described by the Hamiltonian (6.1) can be calculated in the MFA by considering each spin on a site i as an isolated spin with the effective field containing contributions determined by the mean values of the neighboring ones [91]. Here we are dealing with a disordered case of the two-sublattice model. We can subdivide the lattice into two non-equal sublattices, the impurity sublattice with B =RE spins and the bulk one with A =TM spins. Namely,

$$\mathcal{H} \Rightarrow \mathcal{H}^{\rm MFA} = \mathcal{H}_{00} - \mu_{\rm TM} \sum_{\rm TM} \mathbf{H}^{\rm MFA}_{\rm TM} \cdot \mathbf{s}_{\rm TM} - \mu_{\rm RE} \sum_{\rm RE} \mathbf{H}^{\rm MFA}_{\rm RE} \cdot \mathbf{s}_{\rm RE}, \tag{6.4}$$

where $\mathcal{H}_{00} = \sum_{ij} J_{ij} \mathbf{m}_i \cdot \mathbf{m}_j + \sum_i D_i m_{zi}^2$, with $\mathbf{m}_i \equiv \langle \mathbf{s}_i \rangle$ standing for thermally averaged spin polarization of the site i, and the molecular field $\mathbf{H}^{\rm MFA}_i$ is given by

$$\mu_i \mathbf{H}^{\rm MFA}_i = \mu_i \mathbf{H} + 2D_i m_{zi} \mathbf{e}_z + \sum_j J_{ij} \mathbf{m}_j. \tag{6.5}$$

Eq. (6.5) is an expression for a particular configuration of structural disorder, and hence it is necessary to take the random average $\langle\ \rangle^{\rm conf}$ over all possible alloy configurations. After that, the exchange part is treated by firstly dividing the sum over the neighbours in two, *i.e.* $\sum_j \longrightarrow \sum_{\rm TM} + \sum_{\rm RE}$, where, for instance, $\sum_{\rm TM}$ means that we only sum up neighbours of type TM. In each sublattice separately we pass to the continuous limit $\mathbf{m}_{i=\rm TM(RE)} \Rightarrow \mathbf{m}_{\rm TM(RE)}(\mathbf{r})$, assuming $\triangle \mathbf{m}_i(\mathbf{r}) = 0$, where Δ is the Laplace operator. Thus, in each sublattice on average almost homogeneous magnetization is assumed ($k = 0$ mode, but with averaging of internal degrees of freedom over thermal fluctuations and disorder). Then the molecular field reads

$$\mu_{\rm TM(RE)} \mathbf{H}^{\rm MFA}_{\rm TM(RE)} = \mu_{\rm TM(RE)} \left(\mathbf{H} + \mathbf{H}_{A,\rm TM(RE)} \right) + \sum_{\rm TM} J^{\rm TM}_i \mathbf{m}_{\rm TM} + \sum_{\rm RE} J^{\rm RE}_i \mathbf{m}_{\rm RE}, \tag{6.6}$$

where the anisotropy field is defined as $\mathbf{H}_{A,\rm TM(RE)} = \left(2D_{\rm TM(RE)}/\mu_{\rm TM(RE)}\right) m_{\rm TM(RE),z} \mathbf{e}_z$. If z is the number of nearest neighbours and x is the RE concentration, then a TM moment will have on average zx neighbouring RE moments and $z(1-x) = zq$ neighbouring TM moments and accordingly for the RE moments. Averaging over the system configurations [93] and defining $\mathbf{H}'_{\rm eff,TM(RE)} = \mathbf{H} + \mathbf{H}_{A,\rm TM(RE)}$ we can write the average molecular field acting on each sublattice spin as

$$\mu_{\rm RE} \langle \mathbf{H}^{\rm MFA}_{\rm RE} \rangle^{\rm conf} = \mu_{\rm RE} \mathbf{H}'_{\rm eff,RE} + x \widetilde{J}_{0,\text{RE-RE}} \mathbf{m}_{\rm RE} + q \widetilde{J}_{0,\text{TM-RE}} \mathbf{m}_{\rm TM}, \tag{6.7}$$

$$\mu_{\rm TM} \langle \mathbf{H}^{\rm MFA}_{\rm TM} \rangle^{\rm conf} = \mu_{\rm TM} \mathbf{H}'_{\rm eff,TM} + q \widetilde{J}_{0,\text{TM-TM}} \mathbf{m}_{\rm TM} + x \widetilde{J}_{0,\text{TM-RE}} \mathbf{m}_{\rm RE}, \tag{6.8}$$

where $\widetilde{J}_{0,\text{TM-TM}} = zJ_{\text{TM-TM}}$, and so on. Note that to recover the MFA field for the pure ferromagnet in Eqs. (6.7) and (6.8) we must set $q = 0$ ($x = 0$) and $J_{\text{RE-TM}} = 0$. Or we can consider the same magnetic moment for both lattices $\mu_A = \mu_B$ and the same exchange parameters between all pairs (i, j).

The free energy takes the form [91]:

$$\mathcal{F} = \mathcal{H}_{00} - \mathcal{N}k_{\text{B}}T \ln(4\pi) - k_{\text{B}}T \sum_i \Lambda(\xi_i), \tag{6.9}$$

where $\Lambda(\xi) \equiv \ln(\sinh(\xi)/\xi)$, $\xi_i \equiv |\boldsymbol{\xi}_i|$, and $\boldsymbol{\xi}_i \equiv \mu_i \mathbf{H}_i^{\text{MFA}}/k_{\text{B}}T$, where i stands for a lattice site and the sum runs over all lattices sites i. The MFA free energy determined by Eqs. (6.7) (6.8) and (6.9) can be minimized with respect to the spin averages $\mathbf{m}_{\text{RE}}$ and $\mathbf{m}_{\text{TM}}$ to find the equilibrium solution. The minimum condition for the free energy, $\partial\mathcal{F}/\partial\mathbf{m}_{\text{RE}} = 0$ and $\partial\mathcal{F}/\partial\mathbf{m}_{\text{TM}} = 0$, leads to the system of coupled Curie-Weiss equations

$$\mathbf{m}_{\text{RE}} = B(\xi_{\text{RE}}) \frac{\boldsymbol{\xi}_{\text{RE}}}{\xi_{\text{RE}}}; \quad \mathbf{m}_{\text{TM}} = B(\xi_{\text{TM}}) \frac{\boldsymbol{\xi}_{\text{TM}}}{\xi_{\text{TM}}}, \tag{6.10}$$

where $B(\xi) = \coth(\xi) - 1/\xi$ is the Langevin function. Then the equilibrium magnetization of each sublattice, $\mathbf{m}_{e,\text{TM(RE)}}$, can be obtained via the self-consistent solution of equations (6.10). The total equilibrium magnetization per atom is evaluated as:

	μ/μ_B	D [Joule]	J [Joule]
Transition Metal (TM)	2.217	8.0725×10^{-24}	4.5×10^{-21}
Rare-Earth (RE)	7.63	8.0725×10^{-24}	1.26×10^{-21}
TM-RE	–	–	-1.09×10^{-21}

Table 6.1: Table with parameters of transition metal (TM) and rare-earth (RE) compounds used along this chapter. Magnetic moments are taken from literature [27] and [88], respectively. Anisotropy constant $D_{\text{TM(RE)}}$ is taken equal for both lattices. Exchange parameters $J_{\text{TM(RE)}}$/per link are taken in order to give correct Curie temperature of pure compounds ($x = 0$ pure TM or $x = 1$ pure RE). Antiferromagnetic exchange parameter $J_{\text{RE-TM}}$ is chosen so that the temperature dependence of the TM and RE sublattices agrees qualitatively with results of XMCD measurements of static magnetization [128], shown in Fig. 6.2.

$$\mathbf{M} = \mu_{\text{TM}}\, q\, \mathbf{m}_{e,\text{TM}} + \mu_{\text{RE}}\, x\, \mathbf{m}_{e,\text{RE}}. \tag{6.11}$$

Close to T_{C} we may expand $B(\xi) \cong \xi/3$, and calculate $T_{\text{C}}^{\text{MFA}}$ of the ferrimagnet. We obtain the equation:

$$T_{\rm C}(x)^{\rm MFA} = \frac{b}{6k_{\rm B}b}\left(\sqrt{1+4a/b^2}+1\right), \tag{6.12}$$

where

$$\begin{aligned} a &= qx\left(\widetilde{J}^2_{0,\text{TM-RE}} - \widetilde{J}_{0,\text{RE-RE}}\widetilde{J}_{0,\text{TM-TM}}\right) = J^2_{0,\text{TM-RE}} - J_{0,\text{RE-RE}}J_{0,\text{TM-TM}}, \\ b &= q\widetilde{J}_{0,\text{TM-TM}} + x\widetilde{J}_{0,\text{RE-RE}} = J_{0,\text{TM-TM}} + J_{0,\text{RE-RE}}, \end{aligned}$$

where we have defined the configuration averaged exchange parameters $J_{0,\text{TM-TM}} = q\widetilde{J}_{0,\text{TM-TM}}$, $J_{0,\text{RE-RE}} = x\widetilde{J}_{0,\text{RE-RE}}$, $J_{0,\text{TM-RE}} = x\widetilde{J}_{0,\text{TM-RE}}$ and $J_{0,\text{RE-TM}} = q\widetilde{J}_{0,\text{RE-TM}}$. In the low concentration limit we obtain a linear decrease of the Curie point $k_B T_{\rm C}^{\rm MFA} = q\widetilde{J}_{0,\text{TM-TM}}/3$, with the correct expression for pure ferromagnet in MFA, $k_B T_{\rm C}^{\rm MFA} = J_{0,\text{TM-TM}}/3$. In the particular case $J_{0,\text{TM-TM}} \gg J_{0,\text{RE-RE}}$, we obtain $k_B T_{\rm C}^{\rm MFA} = (J_{0,\text{TM-TM}} + J_{0,\text{RE-RE}})$. The boundary for the existence of magnetic order: $J^2_{0,\text{TM-RE}} = J_{0,\text{RE-RE}}J_{0,\text{TM-TM}}$ is also obtained.

Fig. 6.2 presents a comparison between the MFA and the atomistic LLG-Langevin stochastic modeling for the total magnetization as a function of temperature for different TM-RE concentrations. The typical parameters corresponding to GdFeCo, parameterized through experimental measurements using static XMCD in Ref. [128] are presented in Table 6.1. The MFA as always overestimates the Curie temperature value. Following the conventional comparison, the data are normalized to the corresponding Curie temperature for each composition.

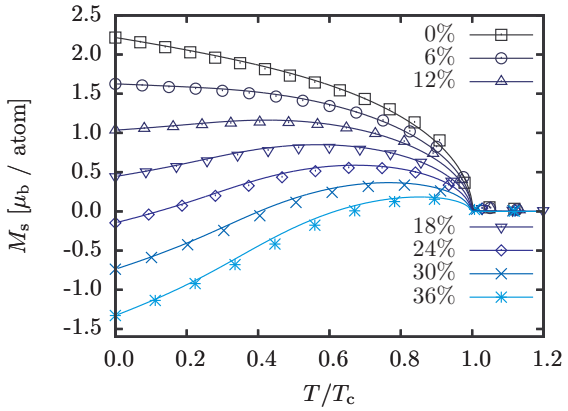

Figure 6.2: Magnetization as a function of temperature (normalized to the Curie temperature $T_{\rm C}$ for each composition and model) for different concentrations of RE. The data is calculated via the MFA approach (solid lines) and direct integration of the Langevin dynamics equation (6.2) (symbols).

To compare the MFA results with the predictions of atomistic model, Fig. 6.3 includes the Curie temperature calculated using Eq. (6.12) with rescaled interactions J_{ij} to fit the exact values in the pure ferromagnetic (antiferromagnetic) limits, (3.18$J = k_{\mathrm{B}}T_{\mathrm{C}}$ for a face centered cubic structure [136]). For the atomistic-LLG model in order to calculate the Curie temperature in a consistent way and to overcome the problem of finite size effects, we performed a fit of the numerical data using the same method as in Ref. [95], whereby the data were interpolated to $M = 0$ to get the point representing the phase transition. We have also compared the calculated compensation temperature (where it exists) as a function of composition. The results are shown in Figure 6.3.

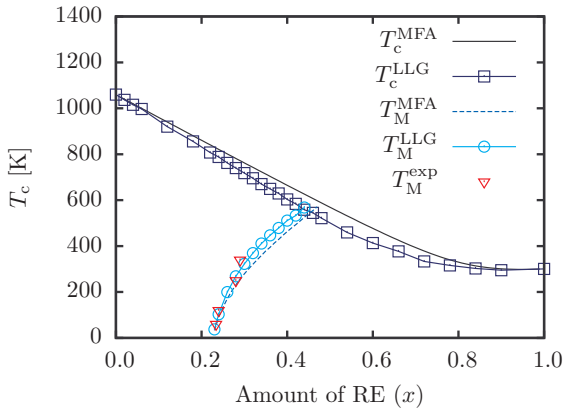

Figure 6.3: Compositional dependence of the Curie temperature (T_{C}) and magnetization compensation point (T_{M}). The Mean Field approximation (MFA) with renormalized exchange parameters is shown to agree very well (lines) with the Landau-Lifshitz-Gilbert (LLG) atomistic model (points). The compensation temperatures deduced from temperature dependent experimental hysteresis curves [128] show excellent agreement with the MFA and LLG models.

As can be seen in Figure 6.3 the LLG atomistic model agrees very well with the MFA predictions. The magnetization compensation point appears at the same composition in both models and disappears again at around the same point, showing the strength of the modified MFA model for predicting static properties. The composition range for which the magnetization compensation point exists is also in good agreement with the experimental data in Ref. [74, 128] .

These initial results act as a validation of the computational model and the MFA model.

The temperature dependence of the magnetization of each sublattice is different depending on the exchange strength acting on each moment in the MFA. Although the details of the exchange parameters are unknown, we can get an

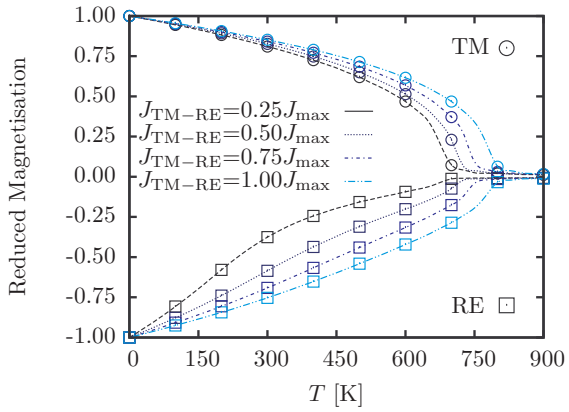

Figure 6.4: Reduced magnetization of the Fe and Gd sublattices as a function of the intersublattice exchange ($J_{\text{TM-RE}}$). Magnetization in each sublattice is normalized to its maximum value. The exchange leads to a polarization effect between the sublattices. Here $J_{\text{max}} = -2.18 \times 10^{-21}$ J.

insight into the strength of the exchange between the sublattices by comparing the results of our simulations with the XMCD experiments [128], which measure the magnetization of each sublattice separately. To get an insight into the strength of the exchange between the two sublattices, we employed the Langevin dynamics model of the TM-RE ferrimagnet to calculate the reduced static magnetization as a function of the intersublattice exchange parameter $J_{\text{TM-RE}}$. Other than the variable intersublattice exchange, the simulation details are the same as for the results in Fig. 6.3. The results are shown in Fig. 6.4, which shows the reduced magnetization of the Fe and Gd sublattices as a function of the intersublattice exchange coupling ($J_{\text{TM-RE}}$). Over the range of exchange coupling shown, the two sublattices share the same Curie temperature, suggesting that there is a polarization effect of one sublattice on the other. This polarization effect also changes the temperature dependence of the magnetization, as seen in Fig. 6.4. For weaker coupling (not shown here), the RE sublattice shows a reduced T_C. Comparison between the calculations and experimental results suggests a value of -1.09×10^{-21} J.

6.4 LLB equation for classical ferrimagnet

We consider a classical disordered ferrimagnet alloy described by the Hamiltonian (6.1). The dynamics of the mean magnetization can be obtained through the Fokker-Planck equation (FPE) (See Appendix C describing the LLB equation for a ferromagnet). The Fokker-Planck equation for the distribution function can be

derived in the same way as in the ferromagnetic case [64]. The FPE has as the static solution the distribution function $f_0(\{\mathbf{s}_i\}) \propto \exp[-\beta\mathcal{H}(\{\mathbf{s}_i\})]$, where $\mathcal{H}$ is given by Eq. (6.1) and $\beta = 1/(k_B T)$. Since the exact solution is impossible even in the simple ferromagnetic case, then, at this stage we again resort to the mean field approximation (MFA) with respect to spin-spin interactions and random average with respect to disorder configurations. In the MFA the distribution function is multiplicative and we can use the same strategy as in Ref. [64] by making the substitution $\mathbf{H} \Rightarrow \left\langle \mathbf{H}_\nu^{\mathrm{MFA}} \right\rangle^{\mathrm{conf}}$, where ν =TM or RE, and $\left\langle \mathbf{H}_\nu^{\mathrm{MFA}} \right\rangle^{\mathrm{conf}}$ is given by the equation (6.4). The solution of such FPE's leads to the set of coupled LLB equations for each $\mathbf{m}_\nu$

$$\dot{\mathbf{m}}_\nu = \gamma[\mathbf{m}_\nu \times \left\langle \mathbf{H}_\nu^{\mathrm{MFA}} \right\rangle^{\mathrm{conf}}] - \Gamma_{\nu,\parallel}\left(1 - \frac{\mathbf{m}_\nu \mathbf{m}_{\nu,0}}{m_\nu^2}\right)\mathbf{m}_\nu - \Gamma_{\nu,\perp}\frac{[\mathbf{m}_\nu \times [\mathbf{m}_\nu \times \mathbf{m}_{\nu,0}]]}{m_\nu^2} \quad (6.13)$$

where

$$\mathbf{m}_{\nu,0} = B(\xi_{\nu,0})\frac{\boldsymbol{\xi}_{\nu,0}}{\xi_{\nu,0}}, \quad \boldsymbol{\xi}_{\nu,0} \equiv \beta\mu_\nu \left\langle \mathbf{H}_\nu^{\mathrm{MFA}} \right\rangle^{\mathrm{conf}}, \quad (6.14)$$

$\Gamma_{\nu,\parallel} = \Lambda_{\nu,N}\frac{B(\xi_\nu)}{\xi_\nu B'(\xi_\nu)}$ and $\Gamma_{\nu,\perp} = \frac{\Lambda_{\nu,N}}{2}\left(\frac{\xi_\nu}{B(\xi_\nu)} - 1\right)$ describe parallel and perpendicular relaxation, respectively. Here $\Lambda_{\nu,N}$ is the characteristic diffusional relaxation rate or, for the thermo activation escape problem, the Neel attempt frequency given by $\Lambda_{\nu,N} = 2\gamma\lambda_\nu/\beta\mu_\nu$,

Eq. (6.13) has been derived in Ref. [64] (see also Appendix C) for a paramagnet and thus it is valid equally for the present purpose. Next step is to use in Eqs. (6.14) the MFA expressions (6.7) and (6.8). The resulting equation constitutes the LLB equation for a ferrimagnet and can be already used for numerical modeling at large scale since in what follows some strong approximations will be used. The use of these approximations is necessary for understanding the relaxation of a ferrimagnetic system from theoretical point of view. However, the resulting LLB equation will have less range of validity than that of the original Eq. (6.13).

We treat the most general case where the continuous approximation in each sub-lattice can be used. In order to simplify the problem we decompose the magnetization vector $\mathbf{m}_\nu$ into two components $\mathbf{m}_\nu = \boldsymbol{\Pi}_\nu + \boldsymbol{\tau}_\nu$, where $\boldsymbol{\Pi}_\nu$ is perpendicular to $\mathbf{m}_\kappa$, so that it can be expressed as $\boldsymbol{\Pi}_\nu = -[\mathbf{m}_\kappa \times [\mathbf{m}_\kappa \times \mathbf{m}_\nu]]/m_\kappa^2$, and $\boldsymbol{\tau}_\nu$ is parallel to $\mathbf{m}_\kappa$, and it can be expressed as $\boldsymbol{\tau}_\nu = \mathbf{m}_\kappa(\mathbf{m}_\nu \cdot \mathbf{m}_\kappa)/m_\kappa^2$, where $\kappa \neq \nu$, (see Fig. 6.5, as an example).

We can shorten the notation by definition of the following new variable $\Theta_{\nu\kappa}$

$$\Theta_{\nu\kappa} = \frac{\mathbf{m}_\nu \cdot \mathbf{m}_\kappa}{m_\kappa^2} \Longrightarrow \mathbf{m}_\nu = \boldsymbol{\Pi}_\nu + \Theta_{\nu\kappa}\mathbf{m}_\kappa. \quad (6.15)$$

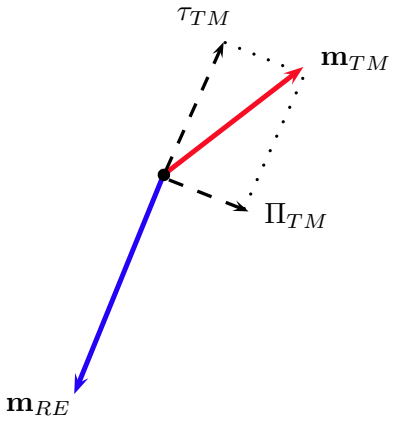

Figure 6.5: Schematic representation of the separation of the magnetization vector $\boldsymbol{m}_\nu = \boldsymbol{m}_{\mathrm{TM}}$ into the projection of the magnetization on the direction of the other sublattice $\boldsymbol{\tau}_{\mathrm{TM}}$ and the corresponding perpendicular component $\boldsymbol{\Pi}_\nu = \boldsymbol{\Pi}_{\mathrm{TM}}$.

As a consequence, the MFA exchange field $\langle \mathbf{H}^{\mathrm{MFA}}_{\mathrm{EX},\nu} \rangle^{\mathrm{conf}}$ in Eqs. (6.8) and (6.7) can be written as the sum of the exchange fields parallel and perpendicular to magnetization of the sublattice ν.

$$\begin{aligned} \langle \mathbf{H}^{\mathrm{MFA}}_{\mathrm{EX},\nu} \rangle^{\mathrm{conf}} &= \left(\frac{J_{0,\nu}}{\mu_\nu} + \frac{J_{0,\nu\kappa}}{\mu_\nu} \Theta_{\kappa\nu} \right) \mathbf{m}_\nu + \frac{J_{0,\nu\kappa}}{\mu_\nu} \mathbf{\Pi}_\kappa \\ &= \frac{\widetilde{J}_{0,\nu}}{\mu_\nu} \mathbf{m}_\nu + \frac{J_{0,\nu\kappa}}{\mu_\nu} \mathbf{\Pi}_\kappa \\ &= \mathbf{H}^{\parallel}_{\mathrm{EX},\nu} + \mathbf{H}^{\perp}_{\mathrm{EX},\nu} \end{aligned}$$

where we have defined a new function $\widetilde{J}_{0,\nu}\left(\mathbf{m}_\kappa, \mathbf{m}_\nu\right)$ as $\widetilde{J}_{0,\nu} = J_{0,\nu} + J_{0,\nu\kappa}\Theta_{\kappa\nu}\left(\mathbf{m}_\kappa, \mathbf{m}_\nu\right)$, we remark that $\widetilde{J}_{0,\nu}$ is not a constant but a function of both sublattices magnetizations. The exchange field is, therefore, separated in two contributions, a longitudinal one $\mathbf{H}^{\parallel}_{\mathrm{EX},\nu} = (\widetilde{J}_{0,\nu}/\mu_\nu)\mathbf{m}_\nu$ and a transverse one $\mathbf{H}^{\perp}_{\mathrm{EX},\nu} = (J_{0,\nu\kappa}/\mu_\nu)\mathbf{\Pi}_\kappa$.

In the following we will consider that the transverse contribution is small in comparison to longitudinal one, *i.e.* $|\mathbf{H}^{\parallel}_{\mathrm{EX},\nu}| \gg |\mathbf{H}^{\perp}_{\mathrm{EX},\nu}|$, so that we consider the case where the noncollinearities between sublattices are small. Finally, $\left\langle \mathbf{H}^{\mathrm{MFA}}_{\nu} \right\rangle^{\mathrm{conf}} \simeq \mathbf{H}^{\parallel}_{\mathrm{EX},\nu} + \mathbf{H}''_{\mathrm{eff},\nu}$ where $\mathbf{H}''_{\mathrm{eff},\nu} = \mathbf{H} + \mathbf{H}_{A,\mathrm{eff},\nu} + \mathbf{H}^{\perp}_{\mathrm{EX},\nu}$. Unfortu-

nately, in the opposite case no simplifications of the expressions seem to be possible. We now expand $\mathbf{m}_{\nu,0}$ up to the first order in $\mathbf{H}''_{\text{eff},\nu}$, under the assumption $\left|\mathbf{H}^{\parallel}_{\text{EX},\nu}\right| \gg |\mathbf{H}''_{\text{eff},\nu}|$. Similar to the ferromagnetic case (see formula (C.28) from the Appendix C), we get

$$\mathbf{m}_{\nu,0} \simeq \frac{B_\nu}{m_\nu}\mathbf{m}_\nu + B'_\nu \beta\mu_\nu \frac{\left(\mathbf{m}_\nu \cdot \mathbf{H}''_{\text{eff},\nu}\right)\mathbf{m}_\nu}{m_\nu^2} - \frac{B\mu_\nu}{m_\nu \widetilde{J}_{\nu,0}} \frac{\left[\left[\mathbf{H}''_{\text{eff},\nu} \times \mathbf{m}_\nu\right] \times \mathbf{m}_\nu\right]}{m_\nu^2} \quad (6.16)$$

Substituting this into Eq. (6.13) and repeating the same calculations as in the ferromagnetic case (see Appendix C), this leads to the equation of motion

$$\dot{\mathbf{m}}_\nu = \gamma[\mathbf{m}_\nu \times \mathbf{H}''_{\text{eff},\nu}] - \gamma_\nu \alpha^\nu_\parallel \left(\frac{1 - B_\nu/m_\nu}{\mu_\nu \beta B'_\nu} - \frac{\mathbf{m}_\nu \cdot \mathbf{H}''_{\text{eff},\nu}}{m_\nu^2}\right)\mathbf{m}_\nu \quad (6.17)$$

$$- \gamma_\nu \alpha^\nu_\perp \frac{\left[\mathbf{m}_\nu \times \left[\mathbf{m}_\nu \times \mathbf{H}''_{\text{eff},\nu}\right]\right]}{m_\nu^2} \quad (6.18)$$

where $B_\nu = B_\nu\left(\beta \widetilde{J}_{0,\nu}\left(\mathbf{m}_\nu, \mathbf{m}_\kappa\right) m_\nu\right)$ depends on the sublattice magnetizations $(\mathbf{m}_\nu, \mathbf{m}_\kappa)$ and the damping parameters are:

$$\alpha^\nu_\parallel = \frac{2\lambda_\nu}{\beta \widetilde{J}_{0,\nu}}, \qquad \alpha^\nu_\perp = \lambda_\nu \left(1 - \frac{1}{\beta \widetilde{J}_{0,\nu}}\right). \quad (6.19)$$

6.4.1 Temperature dependence of damping parameters

The temperature dependence of the damping parameters is obtained in the first order in deviations of magnetization from their equilibrium value. Note that in Eq. (6.18) all the terms are of the first order in the parameter $H''_{\text{eff},\nu}/H_{\text{EX},\nu}$ so that the damping parameters should be evaluated in the zero order in this parameter. In this case the effective damping parameters also depend on temperature T as for ferromagnets and $\widetilde{J}_{0,\nu}$ are evaluated at equilibrium:

$$\widetilde{J}_{0,\nu} \simeq \frac{J_{0,\nu} m_{e,\nu} + |J_{0,\nu\kappa}| m_{e,\kappa}}{m_{e,\nu}} \quad (6.20)$$

where the sign of the second term does not depend on the sign of the interlattice exchange interaction, $J_{0,\nu\kappa}$. The temperature dependence of (6.19) parameters are presented in Fig. 6.6 for a RE-TM ferromagnet and for various concentrations of RE impurities.

Let us consider some limiting cases for a transverse damping parameter. First we consider the simplest case of a completely symmetric antiferromagnet (AFM).

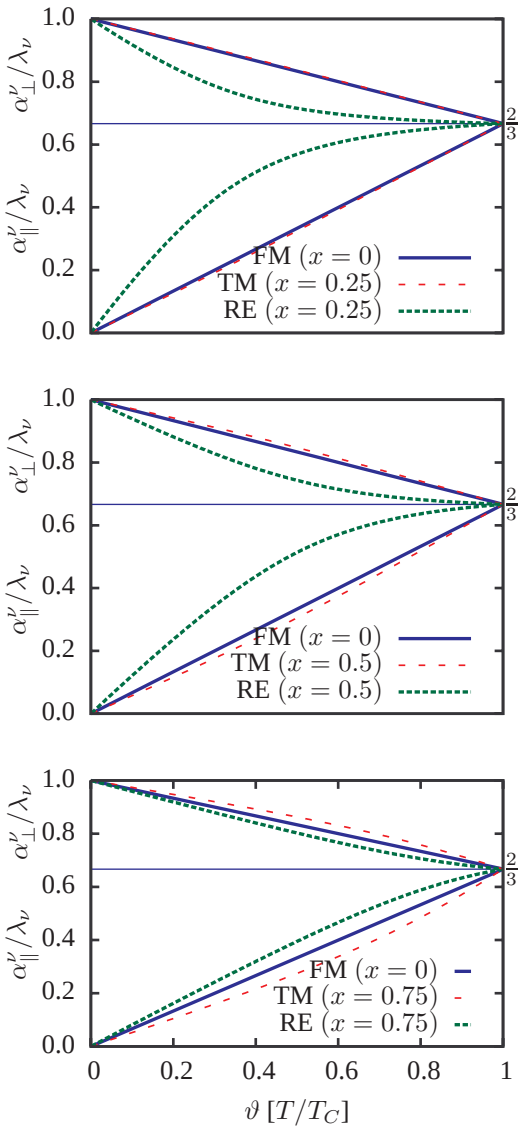

Figure 6.6: Damping parameters $\alpha^\nu_{\parallel(\perp)}(\vartheta)$ for a pure ferromagnet (FM), rare earth (RE) component in a ferrrimagnet and a transition metal (TM) in a ferrimagnet as a function of reduced temperature $\vartheta = T/T_C$ for three different rare earth (RE) concentrations x. (Up) The corresponding curves for a 25% concentration of RE. The blue line represents the $x = 0$ limit which corresponds to a pure ferromanget (FM). (Middle) The corresponding damping parameters for a 50% alloy. (Bottom) Damping values for 75% RE amount. It can be also seen as a RE doped with a 25% of transition metal (TM). The exchange parameters used in these representations correspond to the GdFeCo alloy presented in previous sections, see Table 6.1.

In such AFM all the relevant parameters are equal for both lattices, they have the same magnetic moments $\mu_1 = \mu_2$ and the same intra-lattice exchange parameters $J_{0,\nu}$, the inter-lattice exchange parameter is also the same $J_{0,\nu\kappa} = J_{0,\kappa\nu}$ in contrast to our disordered ferrimagnet. In this case the equilibrium magnetizations as a function of temperature are the same $m_{e,\nu}(T) = m_{e,\kappa}(T)$ and the effective exchange parameter reduces to $\widetilde{J}_{0,\nu} = J_{0,\nu} + J_{0,\nu\kappa}$, *i.e.* the sum of the two interaction coming from the intra-lattice and inter-lattice exchange. The Neel temperature in the MFA reads $k_B T_N = \widetilde{J}_{0,\nu}/3$ and the damping parameters recover the ferromagnetic type expression

$$\alpha_{\parallel}^{\nu(\mathrm{AFM})} = \lambda_\nu \frac{2T}{3T_N}, \qquad \alpha_{\perp}^{\nu(\mathrm{AFM})} = \lambda_\nu \left(1 - \frac{T}{3T_N}\right). \tag{6.21}$$

The use of the critical temperature provides an expression in which the damping parameters do not depend explicitly on the interlattice exchange , the implicit dependence comes form the change of the Neel temperature as the exchange parameter $J_{0,\nu\kappa}$ varies. There is a more simple AFM, when there is only interlattice exchange parameter $J_{0,\nu\kappa}$, it gives the same result as above and exactly the same as for a ferromagnet.

Now we study the case where one of the three exchange parameters can be neglected. We can consider for example a negligible exchange between the rare-earth magnetic moments, it is a good approximation if the impurity content is low. Then we can write the effective exchange as

$$\widetilde{J}_{0,\mathrm{TM}} = \frac{J_{0,\mathrm{TM}} m_{e,\mathrm{TM}} + |J_{0,\mathrm{TM\text{-}RE}}| m_{e,\mathrm{RE}}}{m_{e,\mathrm{TM}}} \simeq J_{0,\mathrm{TM}} \tag{6.22}$$

$$\widetilde{J}_{0,\mathrm{RE}} = |J_{0,\mathrm{RE\text{-}TM}}| \frac{m_{e,\mathrm{TM}}}{m_{e,\mathrm{RE}}}. \tag{6.23}$$

In this case the TM damping parameters can be approximately expressed with the ferromagnetic formula (6.21) because in the limit $x \to 0$ the Curie temperature is close to $k_B T_C = J_{0,\mathrm{TM}}/3$. The damping parameter for the the RE lattice differs from the FM limit. It strongly depends on the polarization effect of the TM lattice on the RE magnetization, see Fig. 6.4 (Up).

Close to T_C the polarization effect can be expressed using the expansion, $B \approx \xi/3$, which for this case reads $m_{e,\mathrm{RE}} \approx \beta J_{0,\mathrm{RE\text{-}TM}} m_{e,\mathrm{TM}}$, thus, $\widetilde{J}_{0,\mathrm{RE}} \approx 1/(3\beta)$.

Therefore, close to T_C we have the following expressions

$$\alpha_{\parallel}^{\mathrm{TM}} = \lambda_{\mathrm{TM}} \frac{2T}{3T_C}, \qquad \alpha_{\parallel}^{\mathrm{RE}} = \frac{2}{3}\lambda_{\mathrm{RE}} \tag{6.24}$$

$$\alpha_{\perp}^{\mathrm{TM}} = \lambda_{\mathrm{TM}} \left(1 - \frac{T}{3T_C}\right). \qquad \alpha_{\perp}^{\mathrm{RE}} = \frac{2}{3}\lambda_{\mathrm{RE}} \tag{6.25}$$

this relation becomes quite important above T_C. We observe in Fig. 6.4 that for amounts of RE of 25% and 50%, the above approximation holds quite well. We will use these relations to extend the LLB equation for temperatures above T_C.

If the inter-lattice exchange is quite large in comparison to the intra-lattice one then the equilibrium magnetization of both lattices is similar and the damping parameters behave similar to those of the FM damping parameters. That case corresponds to a concentration of 75% of RE. In figure 6.6 (down) we show the temperature dependence of the damping parameters for such concentration. We observe that the damping parameters are very similar for both sublattices, as predicted.

Note that these parameters should be distinguished from the damping parameters of normal modes, such as the ferromagnetic resonance and the antiferromagnetic exchange mode, which will be described in the next chapter.

6.4.2 Longitudinal relaxation parameters

The function $1 - B_\nu/m_\nu$ in Eq. (6.18) is a small quantity proportional to the deviation from the equilibrium in the both sublattices. It can be further simplified as a function of the equilibrium parameters after some algebra. Before we start to do it, we recall some definitions of susceptibilities which we will use in the following.

In order to calculate the longitudinal susceptibility, we have to solve Eq. (6.10) for the sublattice magnetization for $H_z \neq 0$ and then differentiate it with respect to H_z . Let us assume that in the absence of an external field, the sublattice magnetizations $\mathbf{m}_{\text{TM}}$ and $\mathbf{m}_{\text{RE}}$ are, respectively, parallel and antiparallel to the z-axis (under the above-mentioned assumption of smallness of the perpendicular component). The z-axis is chosen such that it is the "easy" axis of the magnetic crystal. To evaluate the longitudinal susceptibility, the field should be applied parallel to the easy direction, then the directions of $\mathbf{m}_{\text{RE}}$ and $\mathbf{m}_{\text{TM}}$ will not change but the magnitudes will. In order to calculate the susceptibility, we expand the right-hand side of Eq. (6.10) in terms of the external field:

$$m_\nu(T, h_z) = m_\nu(T, 0) + \mu_\nu H_z \beta B'_\nu \left(1 + \frac{\partial H^z_{\text{EX},\nu}}{\partial H_z}\right) + \mathcal{O}\left((H_z/H_{EX})^2\right), \quad (6.26)$$

where $B_\nu = B_\nu(\beta\mu_\nu H_{\text{EX},\nu})$ and $B'_\nu = B'_\nu(\beta\mu_\nu H_{\text{EX},\nu})$ are evaluated in absence of applied and anisotropy fields. Then,

$$\frac{m_\nu(T, h_z) - m_\nu(T, 0)}{H_z} = \left(\frac{\partial m_\nu(T, H_z)}{\partial H_z}\right)_{H_z=0} = \mu_\nu \beta B'_\nu \left(1 + \frac{\partial H^z_{\text{EX},\nu}}{\partial H_z}\right), \quad (6.27)$$

and we also use the relation

$$\frac{\partial H^z_{\mathrm{EX},\nu}}{\partial H_z} = \beta J_{0,\nu}\frac{\partial m_\nu}{\partial H_z} + \beta|J_{0,\nu\kappa}|\frac{\partial m_\kappa}{\partial H_z} = \beta J_{0,\nu}\widetilde{\chi}_{\nu,||} + \beta|J_{0,\nu\kappa}|\widetilde{\chi}_{\nu,||},$$

We easily get an expression for the longitudinal susceptibility,

$$\widetilde{\chi}_{\nu,||} = \left(\frac{\partial m_\nu(T,H_z)}{\partial H_z}\right)_{H_z=0} = \frac{\mu_\nu}{J_{0,\nu}}\frac{J_{0,\nu}\beta B'_\nu}{1-J_{0,\nu}\beta B'_\nu}\left[\frac{|J_{0,\nu\kappa}|}{\mu_\nu}\widetilde{\chi}_{\kappa,||}+1\right]. \quad (6.28)$$

We obtain two coupled equations for $\widetilde{\chi}_{\mathrm{RE},||}$ and $\widetilde{\chi}_{\mathrm{TM},||}$, solving them, we obtain the MFA expression for the susceptibilities

$$\widetilde{\chi}_{\nu,||} = \left(\frac{\mu_\kappa}{J_{0,\kappa\nu}}\right)\frac{J_{0,\kappa\nu}\beta B'_\nu\mu_\kappa J_{0,\nu\kappa}\beta B'_\kappa + (\mu_\nu/\mu_\kappa)J_{0,\kappa\nu}\beta B'_\nu\left(1-J_{0,\kappa}\beta B'_\kappa\right)}{\left(1-J_{0,\nu}\beta B'_\nu\right)\left(1-J_{0,\kappa}\beta B'_\nu\right)-\left(J_{0,\kappa\nu}\beta B'_\nu\right)\left(J_{0,\nu\kappa}\beta B'_\kappa\right)} = \left(\frac{\mu_\kappa}{J_{0,\kappa\nu}}\right)G_\nu(T) \quad (6.29)$$

The longitudinal susceptibility $\widetilde{\chi}_{\|,\nu}$ is then a function of temperature which we have called $G_\nu(T)$. It tends to zero at low temperature and diverges approaching Curie temperature T_C of the magnetic system, similar to the ferromagnetic case. The function $G_\nu = (|J_{0,\nu\kappa}|/\mu_\nu)\widetilde{\chi}_{\|,\nu}$ can be seen as a reduced longitudinal susceptibility.

Now it is time to calculate the small quantity $1 - B_\nu/m_\nu$, as promised. We will expand the function B_ν/m_ν near the equilibrium, as we did before for a ferromagnet (see Appendix C Eq. (C.35)). The function B_ν in the zero order in perpendicular field component, $H^\perp/H_{\mathrm{EX}}$ can be written as a function of m_ν and m_κ as follows

$$B_\nu \approx B_\nu\left(\beta[J_{0,\nu}m_\nu + |J_{0,\nu\kappa}|\tau_\kappa]\right) \quad (6.30)$$

where $\tau_\kappa = |(\mathbf{m}_\nu\cdot\mathbf{m}_\kappa)|/m_\nu$ is the length of the projection of the magnetization of the sublattice κ onto the sublattice ν. We expand the function B_ν/m_ν in the variables m_ν and m_κ near the equilibrium :

$$\begin{aligned}\frac{B_\nu}{m_\nu} &= \frac{B_{e,\nu}}{m_{e,\nu}} + \left[\frac{1}{m_\nu}\left(\frac{\partial B_\nu}{\partial m_\nu}\right) - \frac{1}{m_\nu^2}B_\nu\right]_{\mathrm{eq}}\delta m_\nu + \left[\frac{1}{m_\nu}\frac{\partial B_\nu}{\partial \tau_\kappa}\right]_{eq}\delta\tau_\kappa \\ &= 1 - \left[1-\beta J_{0,\nu}B'_\nu\right]_{eq}\frac{\delta m_\nu}{m_{e,\nu}} + \left[\beta|J_{0,\nu\kappa}|B'_\nu\right]_{eq}\frac{\delta\tau_\kappa}{m_{e,\nu}}\end{aligned}$$

here $\delta m_\nu = m_\nu - m_{e,\nu}$, with $m_{e,\nu} = B_\nu(\beta\mu_\nu H_{\mathrm{EX},\nu})$, and $\delta\tau_\kappa = \tau_\kappa - \tau_{e,\kappa}$, where $\tau_{e,\kappa} = |(\mathbf{m}_\nu\cdot\mathbf{m}_{e,\kappa})|/m_\nu$ and it corresponds to the projection of the equilibrium

magnetization state $\mathbf{m}_{e,\kappa}$ onto the other sublattice magnetization direction given by the unitary vector $\mathbf{u}_\nu = \mathbf{m}_\nu/m_\nu$. It is easy to show that $\partial\tau_\kappa/\partial m_\nu = 0$. This is because the projection does not depend on the modulus of m_ν but on its direction only. Similar to the ferromagnetic case, we want a nice expression as a function of sublattice susceptibilities. For this purpose, we divide the above expression by $\mu_\nu \beta B'_\nu$

$$\frac{1 - B_\nu/m_\nu}{\mu_\nu \beta B'_\nu} = \left[\frac{1 + \frac{|J_{0,\nu\kappa}|}{\mu_\nu}\widetilde{\chi}_{\kappa,||}}{\widetilde{\chi}_{\nu,||}}\right]\frac{\delta m_\nu}{m_{e,\nu}} - \left[\frac{\frac{|J_{0,\nu\kappa}|}{\mu_\nu}\widetilde{\chi}_{\kappa,||}}{\widetilde{\chi}_{\kappa,||}}\right]\frac{\delta\tau_\kappa}{m_{e,\nu}} \tag{6.31}$$

$$= \frac{1}{\widetilde{\chi}_{\nu,||}}\frac{\delta m_\nu}{m_{e,\nu}} + G_\kappa\left[\frac{1}{\widetilde{\chi}_{\nu,||}}\frac{\delta m_\nu}{m_{e,\nu}} - \frac{1}{\widetilde{\chi}_{\kappa,||}}\frac{\delta\tau_\kappa}{m_{e,\nu}}\right] \tag{6.32}$$

where we have used Eq. (6.28) and the function $G_\kappa = |J_{0,\nu\kappa}|\widetilde{\chi}_{\kappa,||}/\mu_\nu$ has now more sense. Thus, the contribution to the dynamical equation (6.13) of the exchange contribution given by Eq. (6.32) reads

$$\frac{\dot{\mathbf{m}}_\nu}{\gamma_\nu}|_{EX} = -\alpha_\parallel^\nu \frac{\left(1 + \frac{|J_{0,\nu\kappa}|}{\mu_\nu}\widetilde{\chi}_{\kappa,||}\right)}{\widetilde{\chi}_{\nu,||}}\left[\frac{\delta m_\nu}{m_{e,\nu}}\mathbf{m}_\nu\right] + \alpha_\parallel^\nu \frac{|J_{0,\nu\kappa}|}{\mu_\nu}\left[\frac{\delta\tau_\kappa}{m_{e,\nu}}\mathbf{m}_\nu\right] \tag{6.33}$$

$$= -\frac{\alpha_\parallel^\nu}{m_{e,\nu}}\left(\frac{1 + G_\kappa}{\widetilde{\chi}_{\nu,||}}\delta m_\nu - \frac{|J_{0,\nu\kappa}|}{\mu_\nu}\delta\tau_\kappa\right)\mathbf{m}_\nu = \widetilde{\Gamma}_\nu \mathbf{m}_\nu \tag{6.34}$$

Note that the first term defines the intralattice relaxation of the sub-lattice (for example, TM) to its own direction. This equation is the LLB equation with longitudinal relaxation only. It coincides with the complete LLB equation when the two sublattices remain antiparallel. The second term describes the angular momenta transfer between sublattices driven by coupling to the bath.

Compact form

In order to be consistent with the ferromagnetic LLB equation (Landau theory of phase transitions) we expand the deviations δm_ν ($\delta\tau_\kappa$) around $m_{e,\nu}^2$ ($\tau_{e,\nu}^2$). As we have already seen in FM (See Appendix C)

$$\frac{\delta m_\nu}{m_{\nu,e}} \approx \frac{1}{2m_{e,\nu}^2}\left(m_\nu^2 - m_{e,\nu}^2\right) \tag{6.35}$$

Therefore we can write the effective longitudinal fields as

$$\mathbf{H}^{\nu}_{\text{eff},||} = \left[\frac{1}{2\Lambda_{\nu\nu}}\left(\frac{m_\nu^2}{m_{e,\nu}^2}-1\right) - \frac{1}{2\Lambda_{\nu\kappa}}\left(\frac{\tau_\kappa^2}{\tau_{e,\kappa}^2}-1\right)\right]\mathbf{m}_\nu \tag{6.36}$$

where we have defined the longitudinal rates as (to shorten the notation):

$$\Lambda^{-1}_{\nu\nu} = \frac{1}{\widetilde{\chi}_{\nu,||}}\left(1+\alpha^{||}_{\nu\kappa}\right), \quad \Lambda^{-1}_{\nu\kappa} = \frac{\tau_{e,\kappa}}{m_{e,\nu}\widetilde{\chi}_{\kappa,||}}\alpha^{||}_{\nu\kappa} \text{ with } \nu \neq \kappa \tag{6.37}$$

Final forms of the LLB equation

Form 1

Finally, we collect all the above derived approximations and we finish up with the compact form of the LLB equation for the reduced magnetization vector, $\mathbf{m}_\nu = \mathbf{M}/M_\nu(T=0K)$

$$\dot{\mathbf{m}}_\nu = \gamma_\nu[\mathbf{m}_\nu \times \mathbf{H}_{\text{eff},\nu}] - \gamma_\nu\alpha^\nu_{||}\frac{(\mathbf{m}_\nu\cdot\mathbf{H}_{\text{eff},\nu})}{m_\nu^2}\mathbf{m}_\nu - \gamma_\nu\alpha^\nu_{\perp}\frac{[\mathbf{m}_\nu\times[\mathbf{m}_\nu\times\mathbf{H}_{\text{eff},\nu}]]}{m_\nu^2} \tag{6.38}$$

where the effective field $\mathbf{H}_{\text{eff},\nu}$ for sublattice ν is defined as

$$\mathbf{H}_{\text{eff},\nu} = \mathbf{H} + \frac{J_{0,\nu\kappa}}{\mu_\nu}\mathbf{\Pi}_\kappa + \left[\frac{1}{2\Lambda_{\nu\nu}}\left(\frac{m_\nu^2}{m_{e,\nu}^2}-1\right) - \frac{1}{2\Lambda_{\nu\kappa}}\left(\frac{\tau_\kappa^2}{\tau_{e,\kappa}^2}-1\right)\right]\mathbf{m}_\nu$$

and the relaxation parameters $\alpha^\nu_{||}$ and $\alpha^\nu_{\perp}$ are given by Eqs. (6.19).

Or in more explicit form, as a function of sub-lattice magnetizations $\mathbf{m}_\nu$ and its values at equilibrium $\mathbf{m}_{e,\nu}$

$$\dot{\mathbf{m}}_\nu = \gamma_\nu[\mathbf{m}_\nu \times \mathbf{H}_{\text{eff},\nu}] - \gamma_\nu\alpha^\nu_{||}\frac{\left(\mathbf{m}_\nu\cdot\mathbf{H}^{||}_{\text{eff},\nu}\right)}{m_\nu^2}\mathbf{m}_\nu - \gamma_\nu\alpha^\nu_{\perp}\frac{[\mathbf{m}_\nu\times[\mathbf{m}_\nu\times\mathbf{H}_{\text{eff},\nu}]]}{m_\nu^2} \tag{6.39}$$

where we have defined the "longitudinal field", $\mathbf{H}^{||}_{\text{eff},\nu}$, as

$$\mathbf{H}^{||}_{\text{eff},\nu} = \left[\frac{1}{2\Lambda_{\nu\nu}}\left(\frac{m_\nu^2}{m_{e,\nu}^2}-1\right) - \frac{1}{2\Lambda_{\nu\kappa}}\left(\left(\frac{\mathbf{m}_\nu\cdot\mathbf{m}_\kappa}{\mathbf{m}_\nu\cdot\mathbf{m}_{e,\kappa}}\right)^2-1\right)\right]\mathbf{m}_\nu$$

and the effective field, $\mathbf{H}_{\text{eff},\nu}$, reads

$$\mathbf{H}_{\text{eff},\nu} = \mathbf{H} + \frac{J_{0,\nu\kappa}}{\mu_\nu}\mathbf{m}_\kappa$$

In Eq. (6.39) also the temperature dependent damping parameters are given by Eqs. (6.19)

Form 2

It s also interesting to put the LLB equation in terms of macroscopic magnetization, $\mathbf{M}_\nu = x_\nu \mu_\nu \mathbf{m}_\nu / \upsilon_\nu$, where x_ν stands for the concentration of sites of type ν =TM or RE, μ_ν is the atomic magnetic moment of the lattice ν and υ_ν is the atomic volume. We multiply each sublattice LLB equation (6.39) by the corresponding factor, for example, in the case of TM by $q\mu_{\text{TM}}/\upsilon_{\text{TM}}$ and we obtain

$$\dot{\mathbf{M}}_\nu = \gamma_\nu [\mathbf{M}_\nu \times \mathbf{H}_{\text{eff},\nu}] - L_{\parallel,\nu} \frac{\left(\mathbf{M}_\nu \cdot \mathbf{H}^{\parallel}_{\text{eff},\nu}\right)}{M_\nu^2} \mathbf{M}_\nu - L_{\perp,\nu} \frac{[\mathbf{M}_\nu \times [\mathbf{M}_\nu \times \mathbf{H}_{\text{eff},\nu}]]}{M_\nu^2}$$

and the effective fields

$$\mathbf{H}^{\parallel}_{\text{eff},\nu} \;=\; \left[\frac{1}{2\widetilde{\Lambda}_{\nu\nu}} \left(\frac{M_\nu^2}{M_{e,\nu}^2} - 1 \right) - \frac{1}{2\widetilde{\Lambda}_{\nu\kappa}} \left(\left(\frac{\mathbf{M}_\nu \cdot \mathbf{M}_\kappa}{\mathbf{M}_\nu \cdot \mathbf{M}_{e,\kappa}} \right)^2 - 1 \right) \right] \mathbf{M}_\nu$$

where the rate parameters $\widetilde{\Lambda}_{\nu\kappa} = \upsilon_\nu \Lambda_{\nu\kappa} / \mu_\nu x_\nu$ and the effective field, $\mathbf{H}_{\text{eff},\nu}$, reads

$$\mathbf{H}_{\text{eff},\nu} \;=\; \mathbf{H} + A\mathbf{M}_\kappa$$

where $A = zJ_{\text{TM-RE}}/\mu_{\text{RE}}\mu_{\text{TM}}$. The damping coefficients $L_{\parallel,\nu}$ and $L_{\perp,\nu}$ read

$$L_{\parallel,\nu} = \gamma_\nu x_\nu \mu_\nu \alpha^\nu_\parallel / \upsilon_\nu, \quad L_{\perp,\nu} = \gamma_\nu x_\nu \mu_\nu \alpha^\nu_\perp / \upsilon_\nu$$

6.4.3 The LLB equation and the Baryakhtar equation

Finally we would like to mention the difference between the LLB equation and the equation derived by V. Baryakhtar *et al.* [16] and used in Ref. [122] to explain the transient ferromagnetic-like state in ferrimagnets and consequently the switching of magnetization in GdFeCo. This equation has the following form:

$$\frac{1}{\gamma_\nu} \frac{dM_\nu}{dt} = \lambda_e \left(H_\nu - H_\kappa \right) + \lambda_\nu H_\nu \tag{6.40}$$

Here λ_ν describes transfer of the angular momentum from sublattices $\nu = TM, RE$ to the environment. λ_e is of exchange origin and stems from spin-spin interactions, conserving the total angular momentum but allowing for the transfer of angular momentum between the sublattices. The effective fields defined as $H_\nu = -\delta W / \delta M_\nu$ are derived from the magnetic energy W. In Ref. [122] the authors used the Landau type free energy expansion near the critical temperature.

6. THE LANDAU-LIFSHITZ-BLOCH EQUATION FOR FERRIMAGNET

In our LLB equation we have 3 terms, the precession term which conserves the total angular momentum. The precession in the interlattice exchange field given by $[\mathbf{m}_{\mathrm{TM}} \times \mathbf{m}_{\mathrm{RE}}]$ allows the transfer of angular momentum between sublattices. The longitudinal and transverse relaxation terms which are related to the coupling to the heat bath are proportional to λ_ν. In principle different to ferromagnets the transverse motion given by precession and transverse relaxation terms are not negligible in comparison to longitudinal motion because in both cases the field acting on both motion is of exchange origin.

In the Baryakhtar's equation (6.40) a symmetry based term is phenomenologically added to the equation of motion to include longitudinal angular momentum transfer. However, in order to take into account the zero modes (ferromagnetic and exchange), the transverse terms (precession and relaxation) are needed. Additionally, the Baryakhtar equation does not have a term that transfer energy (momentum) from the longitudinal term to the transverse one.

We come back to our original equation (6.34) similar to the Baryakhtar equation, we restrict ourself to the case where both lattices are antiparallel. For the longitudinal relaxation we have the following expression

$$\frac{\dot{m}_\nu^z}{\gamma_\nu} = \alpha_\parallel^\nu H_\nu' + \alpha_{\nu\kappa}^\parallel \left(H_\nu' + H_\kappa'\right) \tag{6.41}$$

where $H_\nu' = -\frac{\delta m_\nu}{\widetilde{\chi}_{\nu,||}} m_\nu^z/m_\nu$, stands for the fields coming from interaction of each lattice with itself. The main difference between LLB type Eq. (6.41) with Eq. (6.40) is found in the sign of the effective field coming from the other sublattice. In order to ilustrate the differences between both equations we can compare them for the limiting case close to T_C, for Baryakhtar equation see Eq. (1.33) in Ref. [16] and it reads

$$\frac{\dot{m}_\nu^z}{\gamma_\nu} = -\lambda^\nu \frac{m_\nu^z}{\widetilde{\chi}_{\nu,||}} - \lambda_e \left(\frac{m_\nu^z}{\widetilde{\chi}_{\nu,||}} + \frac{m_\kappa^z}{\widetilde{\chi}_{\kappa,||}}\right) \tag{6.42}$$

and in the same limit and considering $m_{\mathrm{TM(RE)}} = m_{e,\mathrm{RE(TM)}} + \delta m_{\mathrm{RE(TM)}}$ and following Eq. (6.34) the LLB equation reads

$$\frac{\dot{m}_\nu^z}{\gamma_\nu} = -\alpha_\parallel^\nu \frac{m_\nu^z}{\widetilde{\chi}_{\nu,||}} - \alpha_\parallel^\nu \frac{|J_{0,\nu\kappa}|}{\mu_\nu} \left(\frac{\widetilde{\chi}_{\kappa,||}}{\widetilde{\chi}_{\nu,||}} m_\nu - m_\kappa^z\right) \tag{6.43}$$

both equations have a similar formal form but for the LLB equation the contribution of the other sublattice is negative and for the Baryakhtar equation is positive. The properties of Eq. (6.43) will be discussed in the next subsection.

Finally, we would like to note that because we have treated the spin-spin interaction in MFA we have lost this contribution. These two equations do not have a term responsible for the energy transfer from the uniform modes into non-linear spin waves and vice versa. In ferromagnets [66] this contribution is usually two or three orders of magnitude smaller than the contribution to relaxation of the coupling to the bath. At this stage we do not know how large will be this contribution in ferrimagnets. In Ref. [66] a random anisotropy was used to cause non-coliniarities, here we can see the small amount of RE as precursor of non-collinearity, but with an strength of the order of interlattice exchange parameter $J_{\text{TM-ER}}$. For completeness, a microscopic treatment of the spin wave contribution would be desirable, we let it for the future.

6.4.4 Relaxation of sublattices

The strength of the longitudinal relaxation of this mechanism is defined by the coupling parameter $\alpha^{\parallel}_{\nu\kappa}$ and it is temperature dependent through damping parameters $\alpha^{\nu}_{\parallel}$ (see Eqs. (6.19)) and the above defined function $G_\nu(T)$ [see Eq. (6.29]. The sign of the rate, $\widetilde{\Gamma}_\nu \lessgtr 0$, depends on the deviations from equilibrium δm_ν and $\delta\tau_\kappa$. In this case we have to draw the following lines separating different types of behaviour

$$\delta m_\nu = \frac{|J_{0,\nu\kappa}|}{\mu_\nu}\frac{\widetilde{\chi}_{\nu,||}}{G_\kappa + 1}\delta\tau_\kappa = \widetilde{\chi}_{\nu\kappa,||}\delta\tau_\kappa \tag{6.44}$$

where we have defined the dimensionless variable $\widetilde{\chi}_{\nu\kappa,||}$, which can be interpreted as the effect of the change in one sublattice on the other. Let us see

$$m_\nu(T,\delta m_\nu,\delta m_\kappa) = m_\nu(T,0,0)+\beta J_{0,\nu}B'_\nu\delta m_\nu+\beta|J_{0,\nu\kappa}|B'_\nu\delta m_\kappa+\mathcal{O}\left((\delta m_\nu)^2,(\delta m_\kappa)^2\right) \tag{6.45}$$

Now using that by definition $\delta m_\nu = m_\nu(T,\delta m_\nu,\delta m_\kappa) - m_\nu(T,0,0)$ we get

$$\widetilde{\chi}_{\nu\kappa,||} = \frac{\delta m_\nu}{\delta m_\kappa} \Longrightarrow \widetilde{\chi}_{\nu\kappa,||} = |J_{0,\nu\kappa}|\left(\frac{\beta B'_\nu}{1 - J_{0,\nu}\beta B'_\nu}\right) \tag{6.46}$$

Next, we substitute Eq. (6.28) into Eq. (6.46) and we get the following relation

$$\widetilde{\chi}_{\nu\kappa,||} = \frac{|J_{0,\nu\kappa}|}{\mu_\nu}\frac{\widetilde{\chi}_{\nu,||}}{\frac{|J_{0,\nu\kappa}|}{\mu_\nu}\widetilde{\chi}_{\kappa,||}+1} \tag{6.47}$$

We have then reduced the problem of the relaxation sign to the study of the sign of the function $g(\delta m_\nu,\delta\tau_\kappa,T) = \delta m_\nu - \widetilde{\chi}_{\nu\kappa,||}\delta\tau_\kappa$. Then the line separating both

behaviours is a straight line with the slope $\widetilde{\chi}_{\nu\kappa,||}(T)$ for each temperature. Fig. 6.7 shows three possible instantaneous rates depending on the relative state of both sublattice magnetization for a temperature close to T_C. In Eq. (6.44) we have assumed that equilibrium magnetizations are zero. For the region $m_{\text{RE}} \gg m_{\text{TM}}$ above the green line the rate for the TM , $\widetilde{\Gamma}_{\text{TM}} > 0$, is positive thus TM magnetization will increase and $\widetilde{\Gamma}_{\text{RE}} < 0$ decreasing the RE magnetization. In the central region, between green and red lines, both magnetizations go to equilibrium by decreasing their value. Finally, in the region below the red line the situation is that TM magnetization will decrease and the RE magnetization increase.

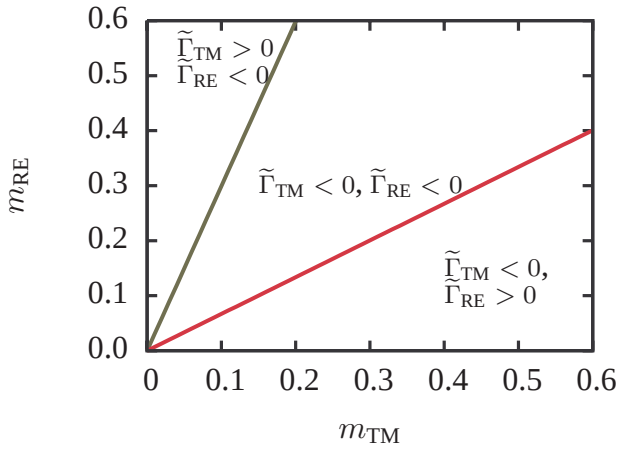

Figure 6.7: Different longitudinal relaxation regions for $T/T_C = 0.95$ for parameters of the GdFeCo alloy.

As a representative example, in GdFeCo near the magnetization reversal the situation is the following; the TM magnetization is almost zero, $m_{\text{TM}} = 0$ and the RE has finite magnetization value $m_{\text{TM}} > 0$. This situation corresponds to the left region in Fig. 6.7 where the rates are $\widetilde{\Gamma}_{\text{TM}} > 0$ and $\widetilde{\Gamma}_{\text{RE}} < 0$ Under this situation only the RE magnetization can polarize the TM sublattice magnetization through interlattice exchange interaction $H_{\text{EX,TM-RE}} \approx |J_{0,\text{TM-RE}}| m_{\text{RE}} > 0$. In this scenario then is easy to figure out that the RE sublattice order polarizes the TM lattice and the rate $\widetilde{\Gamma}_{\text{TM}}$ is positive. This means that its magnetization goes opposite to equilibrium position. This is not necessary a precursor of the ferromagnetic state in a ferrimagnetic material at high temperature, as has been reported in Ref. [134], since the TM magnetization can recover either to positive or to negative direction depending on the initial m^z_{TM}.

6.4.5 Ultrafast precessional switching

In this section we briefly describe the mechanism of the ultrafast magnetization switching in ferrimagnetic systems within the LLB equation model. We consider the same system parameters as for previous sections, $x = 0.25$ and exchange parameters of Table 6.1. For simplicity we perform the following theoretical experiment: the magnetization length of each sublattice at $t = 0$ is taken similar to experimental values after the femtosecond laser pulse excitation is gone. In our particular case at $t = 0$, $m_{z,\mathrm{TM}} = 0.1$ and $m_{z,\mathrm{RE}} = -0.5$. The temperature is taken constant during the process and equal to $T = 300$K. We also put a small angle, different to 180 degrees (antipararell configuration), between both sublattice magnetizations. This small angle can be viewed as product of the fluctuations introduced in the system by the laser heat excitation. Fig. 6.8 (Left) shows the result of the integration of the LLB equation. We observe that the magnetic orientation of both sublattices reverses in the timescale of the order of 1ps. In Fig. 6.8 (Right) a schematic representation of the precessional switching is presented. In ferrimagnet the exchange field coming from the magnetization of the other sublattice acts as dynamic field similar to the external applied field in precessional switching in ferromagnets. In the latter the timescale is determined by the precession frequency γH_Z ∼ns whereas, in the former is of $\gamma J_{0,\nu\kappa}/\mu_\nu$ ∼ps. Differently to proposed mechanisms in Ref. [122] where only the linear mode was discussed, the LLB theory suggest that the complete understanding of the mechanisms involved in the ultrafast switching of GdFeCo alloys should include the transverse terms and not only the longitudinal motion.

6.4.6 On the possibility to derive LLB equation above T_c

In the previous sections we have worked in a temperature range up to the Curie temperature T_C. The region just above T_C is also of interest because in the pump-probe experiments electron temperature can easily reach temperatures above T_C while the instantaneous magnetization is still finite. In order to correctly describe such experiments it is desirable to have an explicit expression for the LLB equation in the region above T_C.

In the LLB equation for ferromagnets the temperature dependent parameters were naturally extended from $T \lesssim T_C$ to $T \gtrsim T_C$. In that case, they only depended linearly on temperature ($\alpha_{\parallel(\perp)} \sim T$). However, in ferrimagnetic systems, they depend on the equilibrium magnetization of each sublattice $m_{e,\nu}$, as can be seen in Eq. (6.19). Fig. 6.6 shows both damping parameters as a function of temperature for $T \leqslant T_C$. The natural way to extend damping parameters, then, is to take the same temperature dependence below T_C and above T_C, *i.e.*

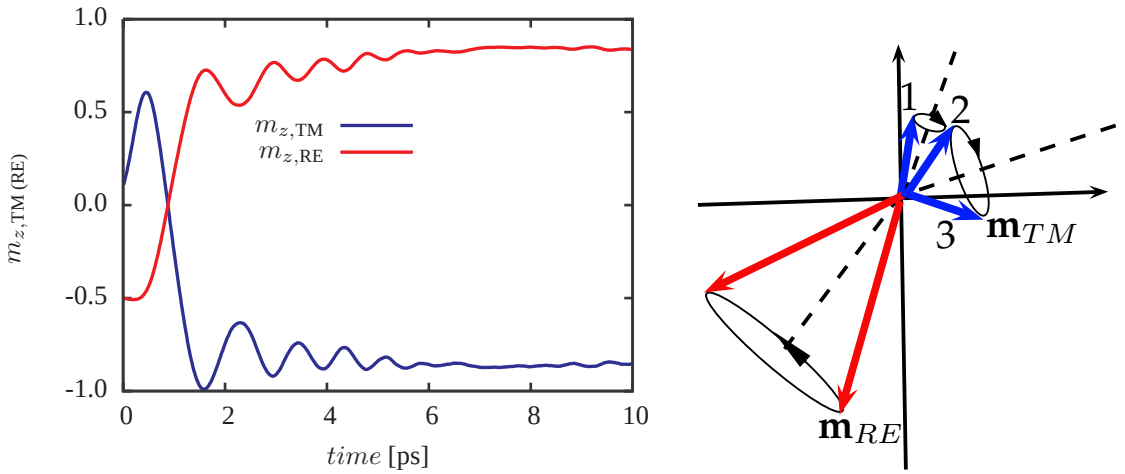

Figure 6.8: (Left) Ultrafast magnetization switching via ultrafast precessional path within the LLB model for ferrimagnets. (Right) Sketch of the precessional switching.

continuously extend the function $\alpha_{\parallel}$. We can see from Fig. 6.6 that the TM closely follows the ferromagnetic behaviour, as we have discussed previously in section 6.4.1. At the same time, RE damping parameter, $\alpha_{\parallel}^{\mathrm{RE}}$, is almost constant and equal to 2/3 (the value at T_C). We can infer from this behaviour, using the equation $\alpha_{\parallel}^{\nu} = 2\lambda_\nu/(\beta\widetilde{J}_{0,\nu})$, that the exchange should be $\widetilde{J}_{0,\mathrm{TM}} \approx T_C$, close to T_C. And for the RE latttice $\widetilde{J}_{0,\mathrm{RE}} \approx T$. In order to obtain an analytical expression we should study the expansion around T_C of "exchange" parameters $\widetilde{J}_{0,\nu}$ or more precisely, of $m_{e,\nu}/m_{e,\kappa}$. We let this study for the future.

Another point to work out above T_C is the corresponding expression for longitudinal relaxation parameters , see Eqs. (6.37). As for the ferromagnetic case we can use the well-know property [172] of the susceptibility close to T_C where we only have to change $2\widetilde{\chi}_{\parallel,\nu}(\varepsilon) \longrightarrow -\widetilde{\chi}_{\parallel,\nu}(-\varepsilon)$ where $\epsilon = 1 - T/T_C$. And we have to find a relation for equilibrium magnetization close to T_C as it is done for ferromagnets where $m_e = 5/3\varepsilon$. Therewith a full LLB equation valid above T_C can be found. We are in progress of solving this problem. Note also that the original equation (1.13) with the MFA fields can be used below and above T_C. Another solution could come from the multiscale modeling [95]. There the susceptibilities above T_C can easily be calculated from the LLG Langevin simulations.

6.5 Conclusions

We have derived the Landau-Lisfhitz-Bloch equation for a two-sublattice system such as a GdFeCo ferrimagnet for which an ultra-fast switching has been reported [134, 149]. This equation can serve in the future as a basis for multiscale modelling in two-component systems, the same way as the LLB equation for ferromagnet [47]. This equation correctly shows the possibility to reverse the sign of relaxation at high temperatures to the opposite sublattice and, therefore, is consistent with the existence of a recently reported ferromagnetic state in a ferrimagnet [134]. In the future, we preview the possibility to include a term taken the intrinsic spin-spin interactions phenomenologically firstly and from microscopic grounds in a future. The LLB equation is different from that derived by Baryakhtar and used recently to describe the GdFeCo switching [122].

Unfortunately, at the present time the compact derivation was possible only in the assumption of small perpendicular exchange field component. This assumption is sufficient to describe the normal modes such as ferromagnetic resonance and antiferromagnetic exchange precessional modes. The same way this approximation is sufficient to describe the switching of ferrimagnet if it occurs through a linear reversal path [122, 157]. However, our recent investigations with atomistic as well as with full LLB equations have shown that this switching may occur as a fast antiferromagnetic precessional switching. Weather the applied approximation completely describes the latter situation is an open question. Finally, up to now we were not able to derive a compact expression for the equation above T_C which is also a necessary step for a full modeling of the ultra-fast switching.

Conclusiones en español

En este capítulo hemos derivado teoricamente la ecuación de Landau-Lisfhitz-Bloch para un sistema magnético compuesto de dos redes, como por ejemplo, el GdFeCo para el cual se ha reportado una inversión ultrarrápida de la imanación [134, 149]. Esta ecuación puede servir como base para un futuro modelos multi-escala en sistemas magnético con dos componentes, del mismo modo que lo hace la ecuación de LLB en materiales ferromagnéticos [47]. Esta ecuación muestra la posibilidad de invertir el signo de la relajación a altas temperaturas hacia la dirección de la red opuesta, y por tanto, es consistente con la existencia de estado ferromagnético transitorio observado recientemente [134].

En el futuro, tenemos la intención de incluir un término que tenga en cuenta la interacción espín-espín, en un primer momento de manera fenomenologica y posteriormente a partir de consideraciones microscópicas. La ecuación de LLB

es diferente de la derivada recientemente por Mentink *et al.* [122] basada en las ecuaciones de Baryakhtar y que ha sido usada recientemente para describir la inversión de la imanación en GdFeCo [122].

7

Temperature-dependent Normal Modes in a Two-component Magnet

7.1 Introduction

The magnetization in solids reacts to external stimulus such as changes in external field or temperature. It is well-known that an external magnetic field can slightly get out of equilibrium the magnetization from its equilibrium position to a new one along spiral trajectories keeping the magnetization length constant. Usual external magnetic fields are not enough strong to induce substantial changes in magnetization length. Thus, magnetization motion is restricted to transverse components. In ferromagnets there is only one transverse homogeneous oscillation mode which is called **ferromagnetic resonance** (**FMR**) mode, and it can be excited experimentally by oscillating magnetic fields. The FMR mode can be viewed as an oscillation of the magnetization vector around the effective field H_{eff}, then the frequency value can be approximately expressed as $\Omega_{\text{FMR}} \simeq \gamma H_{\text{eff}}$. The value of the FMR frequency is usually determined by the anisotropy field H_A (whatever kind it is) and the Zeeman field H_Z (external magnetic applied field). The characteristic values of this frequency go up to 10 GHz (10^9s^{-1}) regime. Thus the timescale at which the magnetization precession moves is of the order of nanoseconds.

In systems with two (three,...,N) different coupled sublattices in addition to the ferromagnetic mode, there exist $N-1$ exchange modes. In two sublattice magnets this additional mode, the so called **exchange mode**, is well-know in the literature [73]. The characteristic timescale of the exchange mode is determined by the interlattice exchange coupling $H_{\nu,\text{ex}} \sim J_{\nu\kappa} M_\kappa$ included in the effective field

and it is usually several orders of magnitude bigger than the effective field around which the FMR precess.

In the literature [73, 168] the starting point in the study of the magnetization oscillations has been always the Landau-Lifshitz-Gilbert (LLG) equation for the macroscopic magnetization of each lattice. It is shown that the angular compensation temperature T_A strongly affects the magnetization dynamics leading to high-speed and strongly damped precession. In order to profit of these especial characteristics of ferrimagnetic systems a strong effort is done from the experimental point of view to control their properties. However, the interpretation of the experimental data is usually done by fitting them to the solution of the LLG equation. The problem comes when the temperature effects are important, for T approaching T_C, and the macroscopic LLG equation starts to fail.

Fig. 7.1 shows a typical frequency and damping values as a function of temperature from experimental measurements [150]. We can observe that predictions coming from the LLG equation (lines) close to T_A show that the frequency tends to increase dramatically. The micromagnetic LLG model also predicts a divergence of the damping close to T_A, not showed in Fig. 7.1, and also that the damping decreases to zero approaching T_C which is not physically correct. This discrepancy motivate us to present a more complete theoretical framework based on the Landau-Lifshitz-Bloch (LLB) equation to analyze the experimental results and get a better knowledge of the dynamical properties of ferrimagnetic systems.

Part of this chapter will be devoted to the study of the transverse oscillation modes that appears in a classical ferrimagnetic system basing on the derived ferrimagnetic LLB equation 6.39. The use of the LLB equation allows to include the temperature dependence of these modes in comparison to the standard LLG model.

In Ref. [139] we have carefully studied the differences between the consideration of the macroscopic LLG and LLB equations and the extensive atomistic LLG-Langevin simulations for an ordered ferrimagnet made by Frank Schlickeiser, a PhD. student in the Prof. U. Nowak's group in Konstanz University (Germany). Along this Chapter we will restrict ourselves to the derivation of analytical expressions for the frequency and damping values of the **precession modes**. In figure 7.2 we show a sketch of the two transverse oscillations modes; (a) the FMR mode and (b) the exchange mode. We will present in a brief section the main characteristics of the transverse motion, similar to the LLG description, see Ref. [73].

Finally, we will deal with the longitudinal relaxation motion of the magnetization, i.e. the change of magnetization modulus with time. We have seen

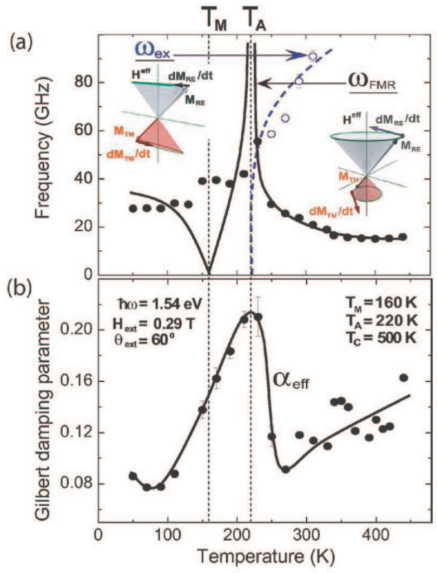

Figure 7.1: Experimental results of the frequencies (a) and effective damping parameters (b) of the resonance modes of ferrimagnetic amorphous GdFeCo [150]. Approaching the angular momentum compensation temperature, T_A, both parameters increase significantly. The line in (b) is the guideline.

throughout this thesis different features arising from the existence of longitudinal relaxation. This relaxation is included in the Landau-Lifshitz-Bloch equation.

We will study in detail the characteristic timescales of the longitudinal motion. This motion, in multilattice magnetic systems, has not been studied up to now within the classical LLB equation. The recent findings in ultra-fast magnetization dynamics experiments in GdFeCo alloys [134] show the importance of the longitudinal relaxation. These experiments use the time resolved X-ray Magnetic Circular Dichroism (XMCD) technique to get access to element specific magnetization dynamics and show that each sublattice magnetization evolves with different timescales. In such experiments the Fe sublattice magnetization dynamics is faster, of the order of hundreds of femtoseconds, than the Gd sublattice magnetization, of the order of a few picoseconds [134]. Although in these experiments magnetization magnitude changes under very high excitation conditions we analyze the characteristic times scales in the linear approximation which allows to get analytical solutions. We will show the importance of the initial

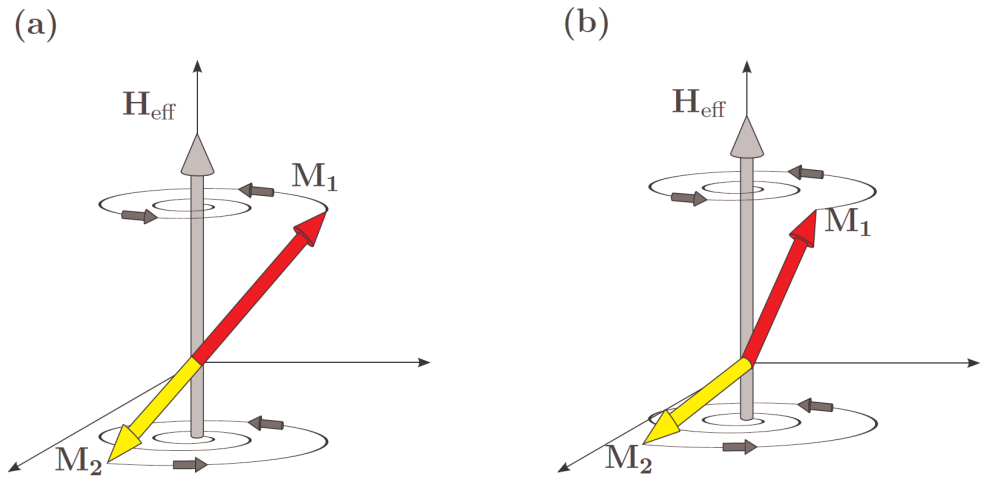

Figure 7.2: Schematic illustration of the two resonance modes in ferrimagnets. For the ferromagnetic mode (a), the sub-lattices stay anti-parallel to each other during the precession, while the angle between the sub-lattices is changing for the exchange mode (b). Taken from Ref. [139].

conditions and temperature for the longitudinal relaxation dynamics. Concrete example will include FeCoGd ferrimagnet.

Eigenvectors and eigenvalues

In the following sections we will reduce the problem of the characteristic times (frequencies or relaxation rates) to a system of first-order linear differential equations by properly linearizing the LLB equations. The solution of the corresponding system of linear equations reduces to the calculation of the eigenvalues and eigenvectors of the time-independent matrix $\mathcal{A} \equiv (a_{ij})$. The characteristic equation for eigenvectors and eigenvalues yields $(\mathcal{A} - \mathbf{\Omega} I)\,\delta\mathbf{u} = 0$ where I is the identity matrix of the same dimension as $\mathcal{A}$. This condition would be satisfied if the determinant $|\mathcal{A} - \mathbf{\Omega} I| = 0$. Thus

$$\Omega^2 - (a_{11} + a_{22})\,\Omega + (a_{11}a_{22} - a_{12}a_{21}) = 0 \tag{7.1}$$

this is called the *characteristic equation*, whose roots are the eigenvalues. Let Ω_1 and Ω_2 be the eigenvalues and $\mathbf{v}_1$ and $\mathbf{v}_2$ be the corresponding eigenvectors respectively , the general solution can be constructed as

$$\delta\mathbf{u} = c_1 e^{\Omega_1 t}\mathbf{v}_1 + c_2 e^{\Omega_2 t}\mathbf{v}_2 \tag{7.2}$$

the explicit expression Ω_i for different cases can be sometimes found. We start with the precession modes.

7.2 Precession modes in Ferrimagnets

In situations close to equilibrium it can be shown that in the linearized LLB equation the longitudinal and transverse components are decoupled. Because the system is composed of two different sublattices, it will have two different precession modes. These modes are associated to the transverse oscillations of the magnetization, therefore we only need that part of the equation.

LLB equation approach

Thus we start with the LLB equation without the longitudinal relaxation term which has the same mathematical expression as the LL equation, but with the temperature dependent parameters. It reads

$$\dot{\mathbf{m}}_\nu = \gamma_\nu[\mathbf{m}_\nu \times \mathbf{H}_{\text{eff},\nu}] - \frac{\gamma\alpha_\perp^\nu}{m_\nu^2}\left[\mathbf{m}_\nu \times [\mathbf{m}_\nu \times \mathbf{H}_{\text{eff},\nu}]\right], \qquad \mathbf{H}_{\text{eff},\nu} = \mathbf{H} + \frac{J_{0,\nu\kappa}}{\mu_\nu}\mathbf{\Pi}_\kappa$$

for $\nu, \kappa = 1, 2$, where we have to note that the transverse exchange field $\mathbf{H}_{\text{ex}}^\perp = J_{0,\nu\kappa}/\mu_\nu\mathbf{\Pi}_\kappa$ can be written as $\mathbf{H}_{\text{ex}}^\perp = J_{0,\nu\kappa}/\mu_\nu\mathbf{m}_\kappa$ if we recall that $[\mathbf{m}_\nu \times \mathbf{m}_\kappa] = [\mathbf{m}_\nu \times \mathbf{\Pi}_\kappa]$. Then, there is no difference with the usual interlattice exchange field used in the literature [73]. For simplicity we do not consider the anisotropy contribution to $\mathbf{H}_{\text{eff},\nu}$.

In the case of the LLB equation it is worth to change the variable $\mathbf{m}_\nu$ to $\mathbf{n}_\nu = \mathbf{m}_\nu/m_{e,\nu}$. In this case it reads

$$\dot{\mathbf{n}}_\nu = \gamma_\nu[\mathbf{n}_\nu \times \mathbf{H}_{\text{eff},\nu}] - \frac{\gamma_\nu\widetilde{\alpha}_\perp^\nu}{n_\nu^2}\left[\mathbf{n}_\nu \times [\mathbf{n}_\nu \times \mathbf{H}_{\text{eff},\nu}]\right], \qquad \mathbf{H}_{\text{eff},\nu} = \mathbf{H} + \frac{J_{0,\nu\kappa}m_{e,\kappa}}{\mu_\nu}\mathbf{n}_\kappa \quad (7.3)$$

where we have defined $\widetilde{\alpha}_\perp^\nu = \alpha_\perp^\nu/m_{e,\nu}$. We have expressed Eq. (7.3) in this way because this is the general form of the LLG micromagnetic equations and we can easily compare with the results coming from it. For the shake of simplicity we can assume that the external applied field is parallel to the z-axis. Now if we assume almost saturated state with $n_z \| H_z$ and $n_x, n_y \ll 1$, we can then linearize Eq. (7.3), and obtain a system of equations defined by a 2×2 matrix. Next, similar to the procedure employed for the LLG equation [73], we define the new variables $n_{\pm,1(2)} = n_{x,1(2)} \pm i n_{y,1(2)}$. We can now define the new variables to shorten the

notations $\mathbf{\Pi}^{+} = (n_1^{+}, n_2^{+})$ and $\mathbf{\Pi}^{-} = (n_1^{-}, n_2^{-})$. Then the dynamical equations reduce to $\partial_t \mathbf{\Pi}^{\pm} = \mathcal{A}_{\perp}^{\pm} \mathbf{\Pi}^{\pm}$ where

$$\mathcal{A}_{\perp}^{\pm} = \begin{pmatrix} -\gamma_{\mathrm{TM}} \left(H_0 + H_{\mathrm{EX}}^{\mathrm{RE}}\right)\left(1 \pm i\widetilde{\alpha}_{\mathrm{TM}}\right) & -\gamma_{\mathrm{TM}} H_{\mathrm{EX}}^{\mathrm{RE}}\left(1 \pm i\widetilde{\alpha}_{\mathrm{TM}}\right) \\ \\ \gamma_{\mathrm{RE}} H_{\mathrm{EX}}^{\mathrm{TM}}\left(1 \mp i\widetilde{\alpha}_{\mathrm{RE}}\right) & -\gamma_{\mathrm{RE}}\left(H_0 - H_{\mathrm{EX}}^{\mathrm{TM}}\right)\left(1 \mp i\widetilde{\alpha}_{\mathrm{RE}}\right), \end{pmatrix} \tag{7.4}$$

Here we have defined $H_{\mathrm{EX}}^{\kappa} = A_{\mathrm{ex}} M_{e,\kappa}$, where the micromagnetic exchange stiffness between sublattices is defined as

$$A_{\mathrm{ex}} = \widetilde{J}_{0,\text{TM-RE}} / (\mu_{\mathrm{RE}} \mu_{\mathrm{TM}}) \tag{7.5}$$

and $M_{e,\nu} = x_\nu \mu_\nu m_{e,\nu}$. Eigenfrequencies are then easily calculated by solving the characteristic equation $\left|\mathcal{A}_{\perp}^{\pm} - \mathbf{\Omega} I\right| = 0$ and eigenvectors for each eigenvalue as $\left(\mathcal{A}_{\perp}^{\pm} - \mathbf{\Omega}^{\pm} I\right) \mathbf{\Pi}^{\pm} = 0$.

7.2.1 Zero damping approximation

Before discussing the exact solution, we continue with a very common approximation done by Wangsness in 1953 [168]. Wangsness assumed that the damping parameter contribution should not contribute to the frequency calculation. The calculation within this approach is important since it is used as analytical expression for comparison to the experimental data in recent publications [150, 151] . In both approaches LLG and LLB the corresponding matrices $\mathcal{A}_{\perp}^{\pm}$ are equal and read

$$\mathcal{A}_{\perp}^{\pm} = \begin{pmatrix} \mp\gamma_{\mathrm{TM}} \left(H_0 + H_{\mathrm{EX}}^{\text{TM-RE}}\right) & -\gamma_{\mathrm{TM}} H_{\mathrm{EX}}^{\text{TM-RE}} \\ \\ \gamma_{\mathrm{RE}} H_{\mathrm{EX}}^{\text{RE-TM}} & \mp\gamma_{\mathrm{RE}}\left(H_0 - H_{\mathrm{EX}}^{\text{RE-TM}}\right) \end{pmatrix} \tag{7.6}$$

At this moment we make use of some approximations as $(H_{\mathrm{EX}}^{\text{TM-RE}} - H_{\mathrm{EX}}^{\text{RE-TM}}) \gg H_0$ and $H_{\mathrm{EX}}^{\text{TM-RE}}, H_{\mathrm{EX}}^{\text{RE-TM}} \gg H_0$ which are valid for almost all regions. Although they are not valid close to the more interesting ones, such as magnetization and angular compensation temperatures. Nevertheless, it is interesting to have simple expressions. The ferromagnetic mode frequency $\Omega_{\mathrm{FMR}}^{\alpha=0}$ reads

$$\Omega_{\mathrm{FMR}}^{\alpha=0} = \frac{\left(M_{e,\mathrm{TM}} - M_{e,\mathrm{RE}}\right)}{\frac{M_{e,\mathrm{TM}}}{\gamma_{\mathrm{TM}}} - \frac{M_{e,\mathrm{RE}}}{\gamma_{\mathrm{RE}}}} H_0 = \gamma_{\mathrm{eff}} H_0 \tag{7.7}$$

where the effective gyromagnetic ratio γ_{eff} is defined as the ratio between the total magnetization $M(T) = M_{e,\mathrm{TM}} - M_{e,\mathrm{RE}}$ and the total angular momentum defined as $A(T) = M_{e,\mathrm{TM}}/\gamma_{\mathrm{TM}} - M_{e,\mathrm{RE}}/\gamma_{\mathrm{RE}}$. The other solution gives the exchange mode frequency $\Omega_{\mathrm{EX}}^{\perp}$ given by

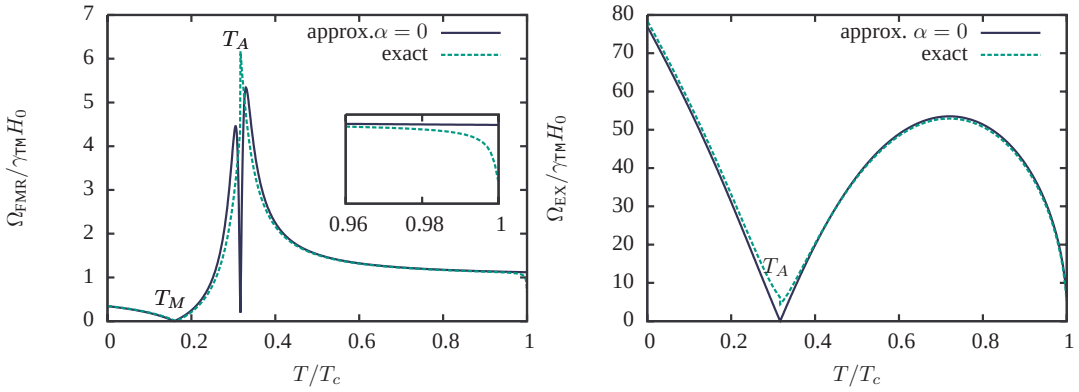

Figure 7.3: (Left) Ferromagnetic (FMR) mode frequency as a function of reduced temperature T/T_C. The solid line is calculated using the approximate solution given by Eq. (7.7). (Inset) FMR frequency close to T_C for approximated and exact solutions. (Right) Exchange mode as a function of reduced temperature T/T_C. Far from T_A both frequencies, approximated and exact solution, are similar.

$$\Omega_{\mathrm{EX}}^{\alpha=0} = A_{\mathrm{EX}}(\gamma_{\mathrm{RE}} M_{e,\mathrm{TM}} - \gamma_{\mathrm{TM}} M_{e,\mathrm{RE}}) = A_{\mathrm{EX}}\gamma_{\mathrm{RE}}\gamma_{\mathrm{TM}} A(T) \tag{7.8}$$

here A_{EX} is given by Eq. (7.5). As we have already mentioned, Eqs. (7.7) and (7.8) correspond to situations where an applied magnetic field is assumed to be sufficiently low and the system is far from the compensation points. Eqs. (7.7) and (7.8) indicate a divergence of the precession frequency of the FMR mode, $\Omega_{\mathrm{FMR}}^{\alpha=0}$, at the temperature T_A ("angular momentum compensation point") where $A(T)$ goes to zero, and $\Omega_{\mathrm{FMR}}^{\alpha=0}$ goes to zero close to temperature T_M ("magnetization compensation point"). On the other hand, approaching T_M the exchange mode frequency decreases, from usual THz regime to GHz region [73]. Therewith, we have seen that simple equations for precession frequency modes can be found. However, at critical temperatures T_A and T_M the validity of such approximations is quite bad.

Fig. 7.3 shows the approximated solution, Eqs. (7.7) and (7.8) of both FMR and exchange mode against the exact solution given by $|\mathcal{A}_{G,\perp}^{\pm,\alpha=0} - \Omega I| = 0$. In Fig. 7.3 we have considered concentration $x = 0.25$, this particular case contains both magnetization and angular momentum compensation temperatures, see Fig. 6.2. In Fig. 7.3 we can observe a substantial difference between approximated and exact solutions close to T_A as we have already pointed out. Nevertheless the approximated solution works quite well far from temperatures close to T_A. In the inset of Fig. 7.3 we have plotted the behavior of the FMR mode close to T_C where the exchange fields are of the order of the external applied field H_0, here we have used a large field of 5 Tesla in order to amplify the effect. The difference

between the approximated and the exact solution for the FMR mode is crucial when experimental data are compared with the theory predictions in order to extract information from the experiment [151]. Unfortunately, the approximated formula is often used in all temperature range. In the next section we will show that the inclusion of the damping contribution within the LLB equation gives also relevant differences near the critical temperatures. The inclusion of damping into calculations will give an effective damping for each precession mode. We will show that for the calculation of effective damping it is important what macroscopic model equation is used.

7.2.2 Damping contribution to transverse mode frequency

The Gilbert equation is the usual approach considered up to now in the literature and the results obtained from it are the standard ones widely used by the experimentalist to fit their results [150]. Fig. 7.1 shows frequency and effective damping calculated from experimental data fitted to the Gilbert equation in order to extract their values. In the Gilbert model the temperature dependence is only included as the temperature dependence of the magnetization. Here we will use the LLB equation which includes temperature dependence in the damping parameters, a different one for each sublattice equation of motion, see Eq. (6.19) and Fig. 6.6. We first present the Gilbert equation predictions and then we compare them with LLB equation ones.

We consider the full matrix $\mathcal{A}_{\perp}^{\pm}$ given by Eq. (7.4). We also consider the same approximations we used in the zero damping case, i.e. the exchange fields are always much larger than the external field, and terms of the second order in H_0 are neglected. We start with the LLG approach solution. Within this classical approach the FMR mode frequency can be easily written as

$$\Omega_{\mathrm{FMR}} = \frac{\gamma'_{\mathrm{eff}}}{1+\alpha_{\mathrm{eff}}^2} H_0 = \frac{\Omega_{\mathrm{FMR}}^{\alpha=0}}{1+\alpha_{\mathrm{eff}}^2} \tag{7.9}$$

Here the effective gyromagnetic ratio is redefined as $\gamma'_\nu = \gamma_\nu/(1+\alpha_\nu^2)$, where ν stands for sublattice labels and the effective damping parameter α_{eff} is introduced and defined as

$$\alpha_{\mathrm{eff}} = \frac{\alpha_{\mathrm{RE}} M_{\mathrm{RE}}/\gamma'_{\mathrm{RE}} + \alpha_{\mathrm{TM}}/M_{\mathrm{TM}}\gamma'_{\mathrm{TM}}}{M_{\mathrm{RE}}/\gamma'_{\mathrm{RE}} - M_{\mathrm{TM}}/\gamma'_{\mathrm{TM}}}. \tag{7.10}$$

This means that within the above presented approximation the ferrimagnetic system behaves as a simple ferromagnetic system described by a single LLG equation but now with an effective gyromagnetic ratio γ'_{eff} and an effective Gilbert

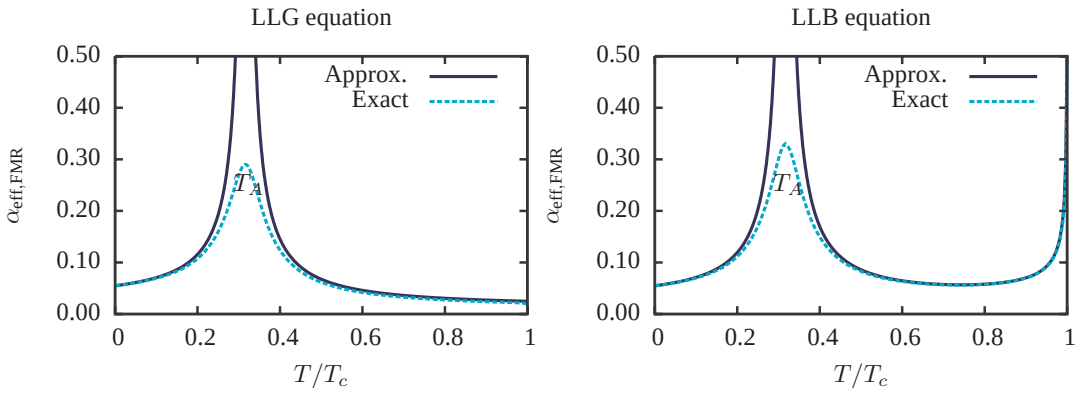

Figure 7.4: The effective damping parameter as a function of reduced temperature as defined by Eq. (7.13) using the LLG (left) and LLB (right) equation approaches. We plot both the approximate, see Eq. (7.10) and Eq. (7.12), solutions and the exact ones.

damping parameter α_{eff}. From Eq. (7.10), we see that α_{eff} diverges at temperature T_A where $A(T) = 0$. At this temperature FMR frequency also diverges, see Fig. 7.3. This fact has been used in order to explain all-optical magnetization reversal across the compensation point [151]. Close to T_A a high frequency FMR mode with a ultrahigh damping parameter will lead to a precession free magnetization reversal.

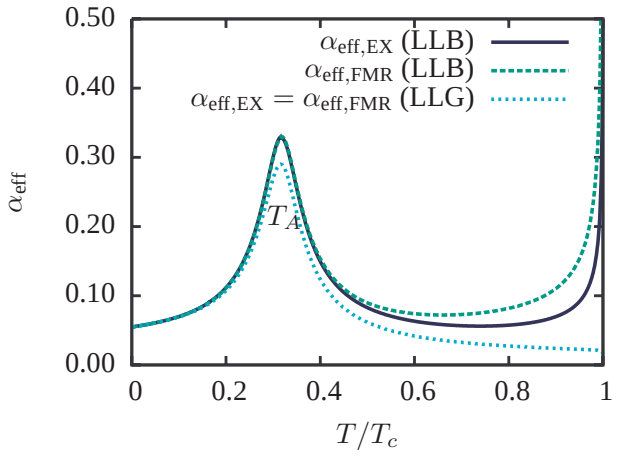

Figure 7.5: Comparison between FMR and exchange effective damping resulting from LLG and LLB approach. The LLG approach predicts the same effective damping as a function of temperature for both the exchange and the FMR modes. The LLB approach, however, predicts different temperature dependence for each mode.

Now we calculate the FMR frequency using the LLB equation. The main difference with the LLG frequency comes from the fact that now the damping parameters $\widetilde{\alpha}_\nu = \alpha_\nu(T)/m_{e,\nu}$ are temperature dependent. This gives a small contribution for low temperatures where the temperature dependence is not large. At high temperatures, close to T_C the differences are remarkable. More concretely, the FMR frequency reads

$$\Omega_{\text{FMR}}^{LLB} = H_0 \frac{\gamma_{\text{eff}}}{1+\widetilde{\alpha}_{\text{eff}}^2}\{1 + \left(\frac{\widetilde{\alpha}_{\text{TM}}^2 M_{\text{RE}}\gamma_{\text{TM}} - \widetilde{\alpha}_{\text{RE}}^2 M_{\text{TM}}\gamma_{\text{RE}}}{M_{\text{RE}}\gamma_{\text{TM}} - M_{\text{TM}}\gamma_{\text{RE}}}\right)\} \tag{7.11}$$

where the "effective damping" $\widetilde{\alpha}_{\text{eff}}$ is defined as

$$\widetilde{\alpha}_{\text{eff}} = \frac{\widetilde{\alpha}_{\text{RE}} M_{\text{RE}}/\gamma'_{\text{RE}} + \widetilde{\alpha}_{\text{TM}} M_{\text{TM}}/\gamma'_{\text{TM}}}{M_{\text{RE}}/\gamma'_{\text{RE}} - M_{\text{TM}}/\gamma'_{\text{TM}}}. \tag{7.12}$$

We note that this expression is the same as for the LLG one (7.10) but with temperature dependent damping parameters. The frequency in Eq. (7.11) is similar to Eq. (7.10) if we consider that the additional term is of second order in the damping parameter α_ν, and it is usually small at low temperatures.

For the exact solution, the effective damping is defined, as in the ferromagnetic case, as the ratio between the real and imaginary solutions of $|\mathcal{A}_\perp^\pm - \boldsymbol{\Omega} I| = 0$,

$$\alpha_{\text{eff,FMR(EX)}} = \frac{\text{Im}(\Omega_{\text{FMR(EX)}})}{\text{Re}(\Omega_{\text{FMR(EX)}})} \tag{7.13}$$

Fig. 7.4 (left) shows the effective damping for FMR mode considering the LLG approach; the approximate solution given by Eq. (7.10) and the exact one. It shows that this approximation is quite good far from the T_A point. Close to T_A, where approximations are no more valid, the effective damping does not diverge in the exact solution. Another interesting feature even for the exact solution, is the fact that at critical temperature T_C the relaxation does not diverge leading to a finite (non-zero) relaxation time at this temperature, which does not coincide with the experimental measurements in Ref. [150], see Fig. 7.1. Fig. 7.4 (right) shows the effective damping for FMR mode but using the LLB equation approach. In this case we also see the difference between approximate and exact solutions at T_A, in this temperature region LLB and LLG are similar. More interestingly, approaching the critical temperature T_C the effective damping diverges. In Ref. [139] we show that this description coincides with extensive atomistic simulations based in the LLG equation, as described in Sec. 6.2.

In Fig. 7.5 we compare the exact solution of effective damping parameter α_{eff} for the LLG and LLB approach. There are two main differences, first, the LLG approach gives the same effective damping for both modes, whereas the

LLB approach distinguishes between FMR and exchange modes. This distinction is more pronounced approaching the Curie temperature T_C and the effective damping diverges which is physically more correct.

7.3 Longitudinal modes in two-component systems

In this section we focus our attention on a very intriguing question about the different longitudinal magnetization dynamics of each sublattice in two component magnets. In measurements of ultrafast magnetization dynamics in FeCoGd alloys, provided by time dependent X-ray Magnetic Circular Dichroism (XMCD), the observed longitudinal relaxation in rare-earth (RE) Gd is reported to be 6 times slower than in FeCo sublattice. This distinct magnetization dynamics is sometimes called "decoupled dynamics" [87] in comparison with the expected "coupled dynamics", i.e. the same rate of demagnetization for both sublattices. We will use the LLB formalism for ferrimagnets to get some insights into this intriguing new topic.

Although the ultrafast magnetization dynamics induced by femtosecond laser pulses is a highly non equilibrium situation where the change of the magnetization can not be considered in the linear approximation, i.e. small deviations from equilibrium state, the understanding of the complex longitudinal dynamics given by the LLB equations (6.38) for a ferrimagnet is not straightforward. Thus, we will restrict to the linear approximation as a first step. This study is not useless as we will see along this section.

Fig. 7.11 shows a sketch of the simplistic modeling of the laser pulse as a step-like temperature increase of a duration of 1ps and the magnetization dynamics obtained from the integration of the LLB equations coupled to the temperature. As in the experimental observations in GdFeCo alloys [134] the LLB model describe correctly that the FeCo sublattice demagnetize faster than the Gd one.

7.3.1 Eigenproblem for longitudinal motion in ferrimagnets

Understanding different demagnetization rates of FeCo and Gd can be done considering the longitudinal term of the LLB equation for ferrimagnets. We will investigate the longitudinal relaxation time, i.e. the time that takes the non-equilibrium average spin polarization magnitude $m_{\mathrm{TM(RE)}} = \langle s_{\mathrm{TM(RE)}} \rangle$ of each lattice to come back to the equilibrium value $m_{e,\mathrm{TM(RE)}}$. The longitudinal term in the

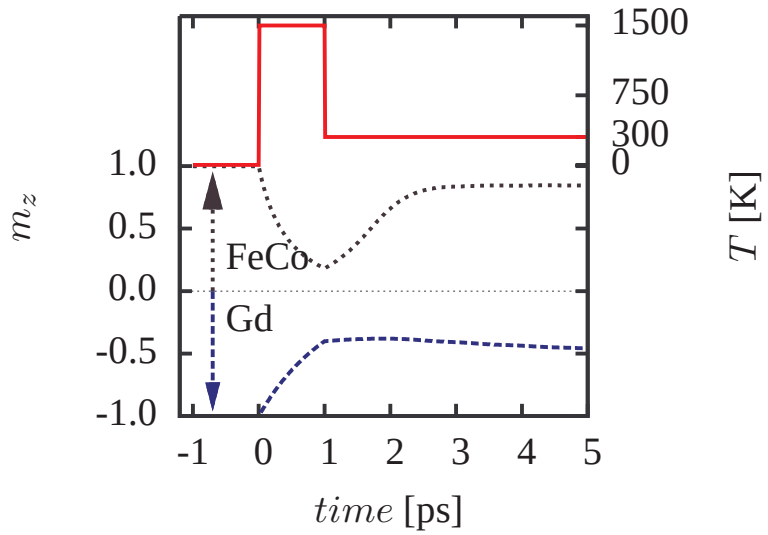

Figure 7.6: Schematic representation of the magnetic response of the two component ferrimagnet after the application of a step-like heat pulse. The dashed lines are obtained by the integration of the LLB equation.

LLB Eq. (6.38) can be linearized around the equilibrium values and the problem can be then reduced to a system of linear equations, as we have already obtained for the transverse modes problem (see Sec.7.1). Solving them we obtain their time dependence.

The system of coupled linearized LLB equations for a two-compound material gives a matrix $\mathcal{A}_\parallel$ which drives the dynamics of $\partial_t \delta\mathbf{m} = \mathcal{A}_\parallel \delta\mathbf{m}$, $\delta\mathbf{m} = (\delta m_{\mathrm{TM}}, \delta m_{\mathrm{RE}})$ where $m_{\mathrm{TM(RE)}} = m_{e,\mathrm{RE(TM)}} + \delta m_{\mathrm{TM(RE)}}$.

The matrix reads

$$\mathcal{A}_\parallel = \begin{pmatrix} -\gamma_{\mathrm{TM}}\alpha_\parallel^{\mathrm{TM}} \frac{1+\alpha^\parallel_{\text{TM-RE}}}{\widetilde{\chi}_{\parallel,\mathrm{TM}}} & +\gamma_{\mathrm{TM}}\alpha_\parallel^{\mathrm{TM}} \frac{\alpha^\parallel_{\text{TM-RE}}}{\widetilde{\chi}_{\parallel,\mathrm{RE}}} \\ +\gamma_{\mathrm{RE}}\alpha_\parallel^{\mathrm{RE}} \frac{\alpha^\parallel_{\text{RE-TM}}}{\widetilde{\chi}_{\parallel,\mathrm{TM}}} & -\gamma_{\mathrm{RE}}\alpha_\parallel^{\mathrm{RE}} \frac{1+\alpha^\parallel_{\text{RE-TM}}}{\widetilde{\chi}_{\parallel,\mathrm{RE}}} \end{pmatrix} = \begin{pmatrix} -\Gamma_{\mathrm{TT}} & +\Gamma_{\mathrm{TR}} \\ +\Gamma_{\mathrm{RT}} & -\Gamma_{\mathrm{RR}} \end{pmatrix}, \tag{7.14}$$

where we have defined matrix elements as $\Gamma_{\mathrm{TT}} = \gamma_{\mathrm{TM}}\alpha_\parallel^{\mathrm{TM}} \frac{1+\alpha^\parallel_{\text{TM-RE}}}{\widetilde{\chi}_{\parallel,\mathrm{TM}}}$, an so on. The exchange-coupling parameter $\alpha^\parallel_{\nu\kappa}$ is defined in Eq. (6.19) and longitudinal susceptibilities, $\widetilde{\chi}_{\parallel,\nu}$, in the MFA are given by Eq. (6.29).

Fig. 7.7 shows the temperature dependence of the matrix elements for a particular system parameters (the same as for the transverse modes problem).

From Fig. 7.7 we can see that at low temperatures the relaxation rates fulfill the conditions $\Gamma_{\mathrm{TT}} > \Gamma_{\mathrm{RR}}$ and $\Gamma_{\mathrm{RR}} \gg \Gamma_{\mathrm{RT(TR)}}$. Thus, the matrix (7.14) can be approximated by a diagonal one as follows

$$\mathcal{A}_{\parallel} \approx \begin{pmatrix} -\Gamma_{\mathrm{TT}} & 0 \\ \\ 0 & -\Gamma_{\mathrm{RR}} \end{pmatrix}, \tag{7.15}$$

meaning that the motion of each lattice is defined by the corresponding diagonal element, i.e. $\partial_t \delta m_{\mathrm{TM(RE)}} = -\Gamma_{\mathrm{TT(RR)}} \delta m_{\mathrm{TM(RE)}}$. This situation holds up to quite high temperatures, see Fig. 7.7, indeed, there is a temperature (in this particular case $T = 0.85 T_C$) where both diagonal relaxation rates have the same value $\Gamma_{\mathrm{TT}} = \Gamma_{\mathrm{RR}}$ and still $\Gamma_{\mathrm{TT}} \gg \Gamma_{\mathrm{RT(TR)}}$ holds, in this case the matrix (7.15) diagonal elements are the same and thus both sublattice magnetization relaxes at the same rate given by $\Gamma_{\mathrm{TT}} = \Gamma_{\mathrm{RR}}$. In this situation we can speak about "coupled" motion in the sense that both sublattices have the same relaxation rate. Therefore we call this temperature "coupling temperature" T_{co}. For $T > T_{\mathrm{co}}$, it happens that $\Gamma_{\mathrm{RR}} > \Gamma_{\mathrm{TT}}$ leading to a faster RE magnetization dynamics in comparison with the TM lattice. We conclude that T_{co} separates two temperature regions for the element specific magnetization dynamics. For $T < T_{\mathrm{co}}$ TM demagnetizes faster than RE while for $T > T_{\mathrm{co}}$ is the RE lattice magnetization which demagnetizes faster than TM. This is one of the main results of this section.

We note that the set of chosen system parameters have been demonstrated in Refs. [128, 134] that they describe well the static and dynamic magnetic properties of the experimental GdFeCo samples.

7.3.2 Eigenvalues for longitudinal motion in ferrimagnets

The solution of the characteristic equation $|\mathcal{A}_{\parallel} - \Gamma_{\parallel} I| = 0$ gives 2 different eigenvalues:

$$\Gamma_{\pm} = \frac{-(\Gamma_{\mathrm{TT}} + \Gamma_{\mathrm{RR}}) \pm \sqrt{(\Gamma_{\mathrm{TT}} - \Gamma_{\mathrm{RR}})^2 + 4\Gamma_{\mathrm{RT}}\Gamma_{\mathrm{TR}}}}{2} = \frac{-(\Gamma_{\mathrm{TT}} + \Gamma_{\mathrm{RR}}) \pm \sqrt{\Delta_D}}{2}. \tag{7.16}$$

It can be checked that the discriminant Δ_D is always positive. Thus, we do not have imaginary (oscillating) solutions. Now, we focus our attention to the sign of the eigenvalues. A negative sign means that deviations $\delta \mathbf{m}_{\mathrm{TM(RE)}}(t)$ decays to zero, i.e. the system goes to equilibrium. On the contrary, a positive eigenvalue corresponds to a non-stable situation, where deviations from the equilibrium increase. From Eq. (7.16) we can show that the values of $\Gamma_{\pm}$ are always negative.

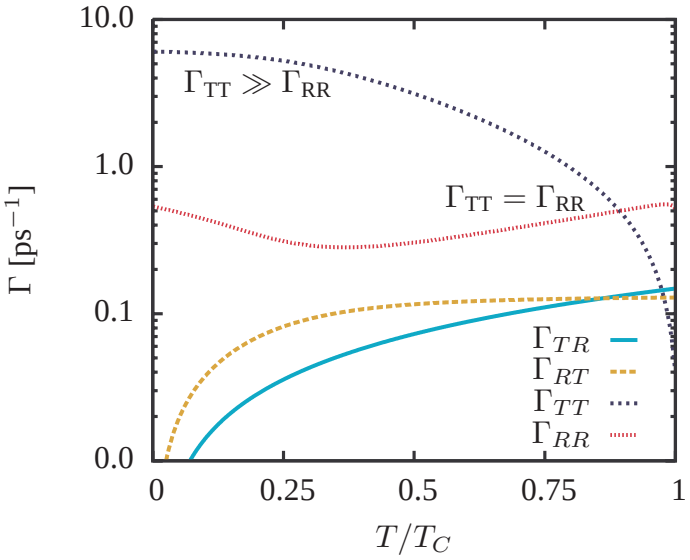

Figure 7.7: Matrix elements of the linearized LLB equations for ferrimagnets as a function of temperature.

The corresponding eigenvectors can be easily calculated using the relation

$$\mathbf{v}_{\pm} = (\Gamma_{\mathrm{TR}}, -(\Gamma_{\mathrm{TT}} + \Gamma_{\pm})). \tag{7.17}$$

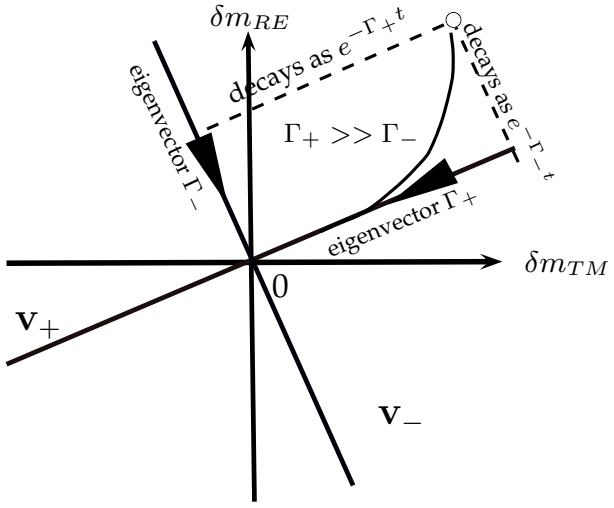

Figure 7.8: Sketch of the phase-space of deviations from equilibrium variables $\delta\mathbf{m} = (\delta m_{\mathrm{TM}}, \delta m_{\mathrm{RE}})$. The solid line from the initial position (dot) to origin represents the path followed by $\delta\mathbf{m}$ towards the origin $(0, 0)$, i.e. the equilibrium.

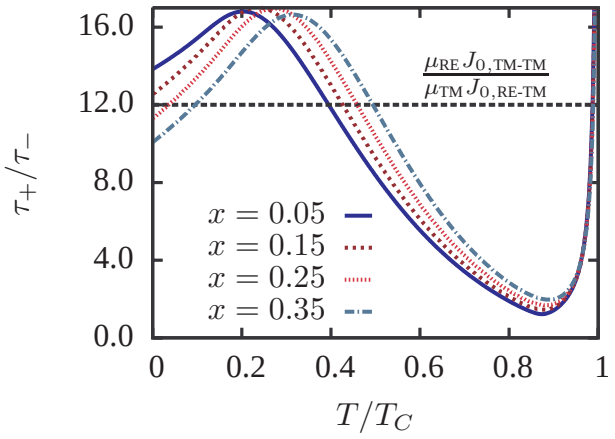

Figure 7.9: Ratio between demagnetization times as a function of reduced temperature for different RE concentrations in the TM bulk. Dashed black line stands for the predicted low temperature limit.

In ferrimagnets the longitudinal magnetization relaxation is more complicated than for ferromagnets but. at the same time, it can produce more interesting phenomena as we have seen in the previous Chapter. In ferromagnets we were interested in how fast the magnetic sample demagnetized but now in ferrimagnets there are two different magnetization variables ($m_{\rm TM(RE)}$) instead of only one, therefore a new question arises in ferrimagnets; how fast one sublattice demagnetizes in comparison with the other sublattice? To answer this question it is convenient to define the phase-space of the deviation from the equilibrium variables $\delta m_{\rm TM(RE)} = m_{\rm TM(RE)} - m_{e,\rm TM(RE)}$. Fig. 7.8 shows a sketch of the $\delta m_{\rm TM(RE)}$ phase space. There are two special directions given by the eigenvectors $\mathbf{v}_\pm$. If initially $\delta\mathbf{m}(t=0)$ lies along the straight line defined by one of the eigenvectors $\mathbf{v}_\pm$, then both sublattices will relax with the same rate, defined by the corresponding eigenvalue $\Gamma_\pm$ and $\delta\mathbf{m}$ will follow such straight line in the phase-space. Otherwise the magnetization will evolve as a combination of the two rates (timescales) Γ_+ and Γ_-. As we have sketched in Fig. 7.8 if the rate of demagnetization of one sublattice is larger (therefore faster than the other one), for instance $\Gamma_+ \gg \Gamma_-$, then the trajectory $\delta\mathbf{m}$ will be underneath the line connecting the starting point in the phase space, $\delta\mathbf{m}(t=0)$ and the origin $\delta\mathbf{m} = (0,0)$.

Pure ferromagnets

First we recall what happens in pure ferromagnetic systems in terms of our recent notations. If we consider two ferromagnetic systems without any exchange coupling, the problem is reduced to two pure ferromagnets. In that case we recover

the well-known formulae for the relaxation rates (times), the matrix $\mathcal{A}_{\parallel}$ becomes diagonal ($\Gamma_{\text{TR}} = \Gamma_{\text{RT}} = 0$) and the eigenvalues are directly the diagonal elements ($\Gamma_{ii} = \Gamma_i$). The eigenvectors are obviously the unitary vectors $\mathbf{e}_1 = (1, 0)$ and $\mathbf{e}_2 = (0, 1)$ and the solution is rather obvious:

$$\delta\mathbf{m}(t) \;=\; c_- e^{\Gamma_- t}\mathbf{e}_1 + c_+ e^{\Gamma_+ t}\mathbf{e}_2 \Longrightarrow \begin{cases} \delta m_{\text{TM}} = c_- e^{\Gamma_{\text{TM}} t} & ,\Gamma_{\text{TM}} = -\gamma_{\text{TM}}\alpha_{\parallel,\text{TM}}/\widetilde{\chi}_{\parallel,\text{TM}} \\ \delta m_{\text{RE}} = c_+ e^{\Gamma_{\text{RE}} t} & ,\Gamma_{\text{RE}} = -\gamma_{\text{RE}}\alpha_{\parallel,\text{RE}}/\widetilde{\chi}_{\parallel,\text{RE}}. \end{cases}$$

As we has been recently proposed by Koopmans [105] in pure ferromagnets the ratio between the magnetic moment and the Curie temperature, μ/T_C, is a good figure of merit of the "speed" of the magnetization. In that sense if we apply this simple relation to the pure Gd ($\mu_{Gd} = 7.63$ and $T_{C,Gd} \approx 300$ K) and Fe ($\mu_{Fe} = 2.21$ and $T_{C,Fe} \approx 1050$ K) we get a ratio between relaxation times of approximately 10 times. Ref. [105] also suggest that for ferrimagnets a similar relation should exist but for the net magnetization. Therefore no predictions for element specific dynamics were made. In the following we will see what happens with these systems.

Low temperature limit

At low temperatures $\Gamma_{\text{RT}}\Gamma_{\text{TR}} \ll |\Gamma_{\text{TT}} - \Gamma_{\text{RR}}|$ as it is shown in Fig. 7.7. In this case

$$\Gamma_- \;\approx\; -\Gamma_{\text{TT}} + \Gamma_{\text{TR}}\Gamma_{\text{RT}}/|\Gamma_{\text{TT}} - \Gamma_{\text{RR}}|, \quad \mathbf{v}_- \approx (1, 0) \tag{7.18}$$

$$\Gamma_+ \;\approx\; -\Gamma_{\text{RR}} - \Gamma_{\text{TR}}\Gamma_{\text{RT}}/|\Gamma_{\text{TT}} - \Gamma_{\text{RR}}|, \quad \mathbf{v}_+ \approx (0, 1) \tag{7.19}$$

which shows that the fast motion slows down and the slow one fastens, due to the mutual coupling. In this region the eigenvector corresponding to the rate $\Gamma_{+(-)}$ is close to the $y(x)$-axis which is associated to RE(TM) deviation variable $\delta m_{\text{RE(TM)}}$.

Here, we have to note that Γ_{TT} tends to the pure TM relaxation rate, Γ_{T}, as $x \to 0$ and $\Gamma_{\text{RR}} \to \Gamma_{\text{R}}$ as $x \to 1$. We should not confuse Γ_{RR} with its corresponding pure value. It is a common mistake to compare the pure RE relaxation time with that measured when RE is a dopant. In low concentration limit each RE moment is surrounded almost totally by TM moments, so that the mean exchange field that it feels is $J_{0,\text{RE-TM}}/\mu_{\text{RE}}$, therefore $\tau_{\parallel,\text{RE}} \sim \mu_{\text{RE}}/J_{0,\text{RE-TM}}$. In the same configuration $\tau_{\parallel,\text{TM}} \sim \mu_{\text{TM}}/J_{0,\text{TM-TM}}$. Thus, a simple phenomenological relation between both relaxation times can be found $\tau_{\parallel,\text{RE}}/\tau_{\parallel,\text{TM}} \approx (\mu_{\text{RE}}/\mu_{\text{TM}})(J_{0,\text{TM-TM}}/J_{0,\text{RE-TM}}) = 12$. Fig. 7.9 shows the ratio between longitudinal times at low concentrations ($x = 0.05, 0.15, 0.25$ and 0.35) as a function of temperature calculated from the solution of Eq. (7.16). We see in Fig. 7.9 that the ratio between relaxation times

at low temperatures is not far from the phenomenological estimation presented above. However for temperatures approaching the Curie temperature this crude estimation fails.

Next, we check the LLB model predictions against the LLG Langevin multispin simulations (see Sec. 6.2) performing the following simulation; at times $t < 0$, the magnetic system is in thermal equilibrium at a temperature of $T_{\text{initial}} =$ 300K, then for $t \geq 0$ bath temperature is instantaneously changed to $T_{\text{final}} = 0.75T_C = 600$K. Thus, the magnetization of the two lattices will evolve towards the new thermal equilibrium value given by $T_{\text{final}} = 0.75T_C = 600$K. Fig. 7.10 (Left) shows the magnetization normalized to the value at 2ps, $\Delta m(t)/\Delta m(0) = (m(t) - m(2ps))/(m(0) - m(2ps))$, for both sublattices and which is adequate to compare the magnetization rates. It can be clearly see that the TM magnetization relaxes faster than RE one. The inset of Fig. 7.10 (Left) represents the variable $\Delta m_{\text{TM}}(t)/\Delta m_{\text{TM}}(0)$ as a function of $\Delta m_{\text{RE}}(t)/\Delta m_{\text{RE}}(0)$. The dashed line represents the path of coupled motion. As expected the line (orange) joining the initial state $(1, 1)$ to equilibrium $(0, 0)$ lies above the line which represents the coupled motion, $\Gamma_{\text{TM}} = \Gamma_{\text{RE}}$.

We can conclude that at low temperatures the TM magnetization dynamics is faster than RE one as predicted by LLB model. In this case we can talk about "decoupled motion" in the sense that the rate that dominates the relaxation of each sublattice is different. In this limit the resulting characteristic relaxation time $\tau_{\text{RE}} = \Gamma_{-}^{-1}$ of Gd is of the order of $2 - 3$ ps. For FeCo lattice $\tau_{\text{TM}} = \Gamma_{-}^{-1}$ is of the order of $400 - 500$ fs. This is in a very good agreement with experimental results found recently using time dependent XMCD [134].

Transition to high T limit: coupled motion

In the temperature region around the coupling temperature T_{co} the diagonal relaxation rates has similar values by definition, $\Gamma_{\text{TT}} \approx \Gamma_{\text{RR}}$. In such a case the approximated solution of Eq. (7.16) reduces to

$$\Gamma_{\pm} \approx -(\Gamma_{\text{TT}} + \Gamma_{\text{RR}})/2 \pm \sqrt{\Gamma_{\text{TR}}\Gamma_{\text{RT}}}. \tag{7.20}$$

Under the assumption that $\Gamma_{\text{TT}} \gg \Gamma_{\text{TR(RT)}}$, see Fig. 7.7, both sublattice magnetization is relaxed at the same rate, Γ_{TT}, therefore we can say that the motion is coupled. The corresponding eigenvectors can be easily estimated using equation (7.17) with $\mathbf{v}_{\pm} \approx (\Gamma_{\text{TR}}, \mp\sqrt{\Gamma_{\text{TR}}\Gamma_{\text{RT}}}) = (1, \mp\sqrt{\Gamma_{\text{RT}}/\Gamma_{\text{RT}}})$. At this point the direction of $\mathbf{v}_{\pm}$ is not relevant because they have the same relaxation rate. We conclude that the key condition to speak about coupled motion is that both rates Γ_{TT} and Γ_{TT} should be similar.

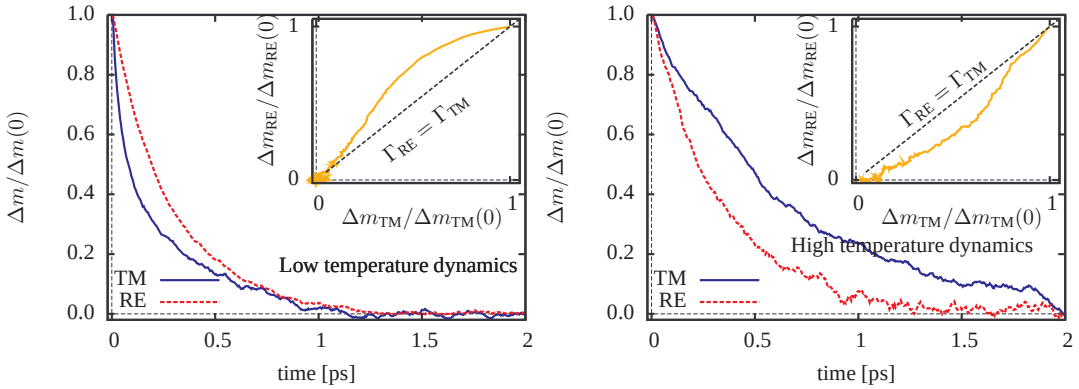

Figure 7.10: (Left) Normalized magnetization dynamics for TM and RE sublattice in the low temperature limit. (left inset) Path followed by $\delta\mathbf{m} = (\delta m_{\rm TM}, \delta m_{\rm RE})$ towards the equilibrium state $(0, 0)$. In this case TM magnetization is faster than RE. (Right) Normalized magnetization dynamics for TM and RE sublattice in the high temperature limit. (right inset) Path followed by $\delta\mathbf{m} = (\delta m_{\rm TM}, \delta m_{\rm RE})$ towards the equilibrium state $(0, 0)$. In this case RE magnetization is faster than TM.

Close to T_C limit

Above the coupling temperature, $T > T_{\rm co}$, the situation changes and the relaxation rate $\Gamma_{\rm RR}$ becomes larger than $\Gamma_{\rm TT}$, see Fig. 7.7. From Eq. (7.17) we calculate that the eigenvector directions are interchanged from $\mathbf{v}_+ \approx (0, 1)$ ($\mathbf{v}_- \approx (1, 0)$) to $\mathbf{v}_+ \approx (1, 0)$ ($\mathbf{v}_- \approx (0, 1)$). This means that the eigenvalue Γ_+ ($\mathbf{v}_+ \approx (1, 0)$) gives the rate along the $x-$axis, i.e. the TM relaxation rate. Equivalently, Γ_- describes the longitudinal relaxation rate of the RE sublattice.

From Eq. (7.16) we directly calculate the relaxation times $\tau_{\parallel,\pm} = \Gamma_\pm^{-1}$ as a function of temperature. We present the results in Fig. 7.11, there we can see that $\tau_{\parallel,+}$ is always larger (slower) than $\tau_{\parallel,-}$ (faster). For $T > T_{\rm co}$ the relaxation time $\tau_{\parallel,+}$ corresponds to TM lattice and therefore the TM magnetization will be slower that RE lattice magnetization relaxation.

As we did for the low temperature region we compare the LLB predictions and the LLG Langevin multispin simulations. At times $t < 0$, the magnetic system is taken in thermal equilibrium at a temperature of $T_{\rm initial} = 750$K, then for $t \geq 0$ the bath temperature is changed to $T_{\rm final} = 0.975 T_C = 780$K. Fig. 7.10 (Right) shows the path followed by $\Delta m_{\rm TM(RE)}(t)/\Delta m_{\rm TM(RE)}(0)$towards the origin $\delta\mathbf{m} = (0, 0)$. In this case RE magnetization is faster than TM one, in comparison with what happens at temperatures far from T_C, as predicted by our model.

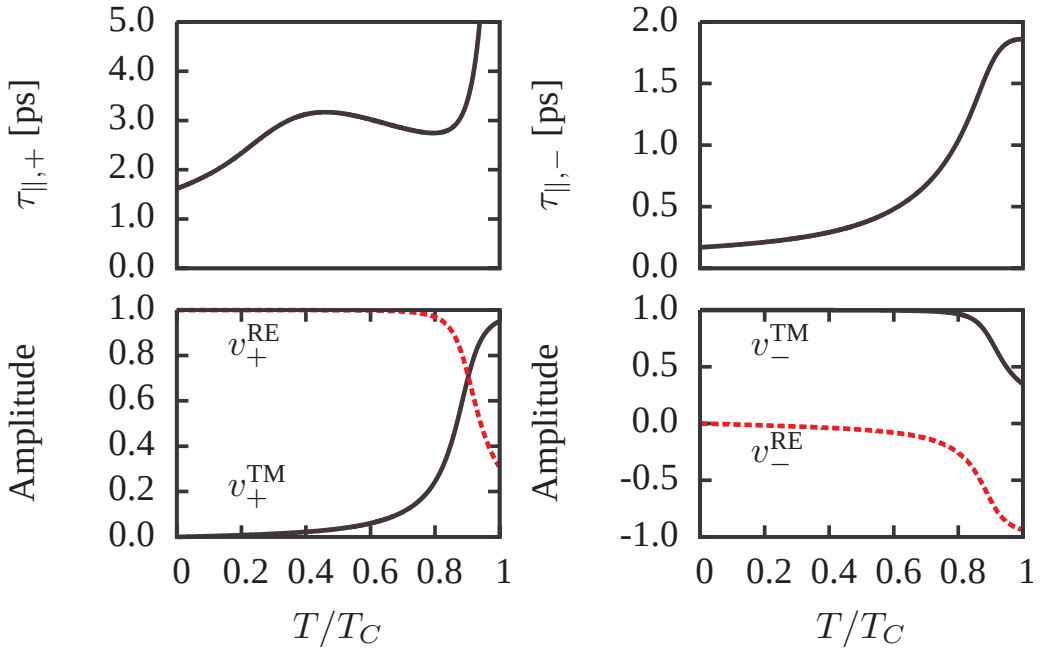

Figure 7.11: (Up) We present the temperature dependence of the relaxation time $\tau_\pm = \Gamma_\pm^{-1}$ along the eigenvector direction $\mathbf{v}_\pm = (v_\pm^{\mathrm{TM}}, v_\pm^{\mathrm{RE}})$ (Down) Eigenvector normalized amplitudes ($v_+^2 + v_-^2 = 1$) which in turn are also temperature dependent and their temperature dependece is ploted.

All temperatures

In ferrimagnetic systems as ours, the numerical solution of equations (7.16) and (7.17) will give access to the exact values of eigenvalues and eigenvector direction. Fig. 7.11 shows calculated eigenvalues and corresponding eigenvector amplitudes, here we have used unitary eigenvector, in such a way that $(v_\pm^{\mathrm{TM}})^2 + (v_\pm^{\mathrm{RE}})^2 = 1$, where $v_\pm^{\mathrm{TM\ (RE)}}$ corresponds to the projection of the eigenvector $\mathbf{v}_\pm$ onto the $\delta m_{\mathrm{TM(RE)}}$ axis. Figs. 7.11 summarizes all the features of the relaxation times of each sublattice and whose we have extensively discussed above.

7.3.3 Comparison with atomistic simulations

In this section we compare the large-scale atomistic simulation using the LLG Langevin approach and the LLB equation. In principle the LLB equations represents the dynamics of the average magnetization of the system. However, in the derivation of the LLB equation some approximations were made and no-exact comparison is expected. Thus, we will take this section as a test of our derivation.

Longitudinal relaxation

Longitudinal relaxation time is usually calculated in ferromagnetic systems by putting the system in thermal equilibrium at a given initial temperature T_{initial} and then suddenly, at $t = 0$, raising the temperature to T_{final} (it can be done by lowering the temperature). When the deviation from equilibrium are sufficiently small the relaxation to equilibrium can be described by a simple linear equation which solution is an exponential decay function. The demagnetization curve obtained from atomistic simulations can be fitted to this exponential function and extract the longitudinal relaxation time. Thus, it is similar to the procedure we have used to analytically derive the relaxation times of a ferrimagnet. Nevertheless, for ferrimagnetic systems a bi-exponential decaying function should be used to fit the data, as it is suggested by the solution of the system of linear equations describing the normal modes. We test the FeCoGd ferrimagnetic alloy ($x = 0.25$)

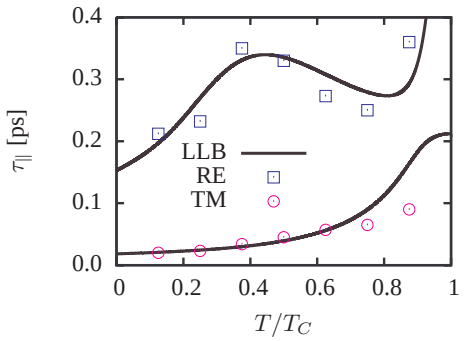

Figure 7.12: Comparison between longitudinal relaxation times from the LLB theory (lines) and the LLG atomistic simulations (symbols) for both sublatttices.

longitudinal relaxation times. We note that for an accurate calculation of the relaxation times from this impurity model, an average over disorder configurations has to be done. However, in this section we are interested in the comparison

between the analytical results and simulations than in the accurate calculation of these relaxation times.

The atomistic simulations are done as follows: we thermalize the spin system for $t < 0$ for a temperature T_{initial} slightly lower than final temperature T_{final}. At $t = 0$ we change the temperature to T_{final} thereafter the system evolve to a new equilibrium configuration. When the relaxation curves are fitted to one exponential function the two exponential decaying function defining the relaxation are artificially averaged out into only one, in such case the relaxation time of the faster sublattice slows and the slow is fasten. In order to avoid this artifact we fit the relaxation curves to a bi-exponential function. Being one of the relaxation times amplitude dominant we can neglect in our analysis the second fitted relaxation time. Therefore for each lattice magnetization dynamics we keep only the relaxation time obtained from the fitting function which gives the main contribution (amplitude). In Fig. 7.12 we compare calculated relaxation times from atomistic simulations against the predictions of the LLB model. The agreement between theory (LLB) and simulations (LLG-Langevin) is very good.

Rapid heat calculations

As a next step we simulate the response of the magnetization to a heat pulse with the atomistic model and the LLB for GdFeCo. We start our simulation at $T = 0$K and at $t = 0$ we apply a pulse of temperature T. Later on, the system cools down to $T = 300$ K. We simplify the temperature profile by a step function, the peak and duration of which can be varied. This rectangularly shaped temperature pulse is a simplification of the electron temperature profile as they occur in the pump-probe experiments.

Fig. 7.13 shows the dynamics of the magnetization in response to the step-shaped heat-pulse with a peak temperature of $T = 500$K and a duration of 3 ps, calculated with the atomistic (symbols) as well as the macroscopic LLB model (solid lines). The dynamics of both models are in good agreement.

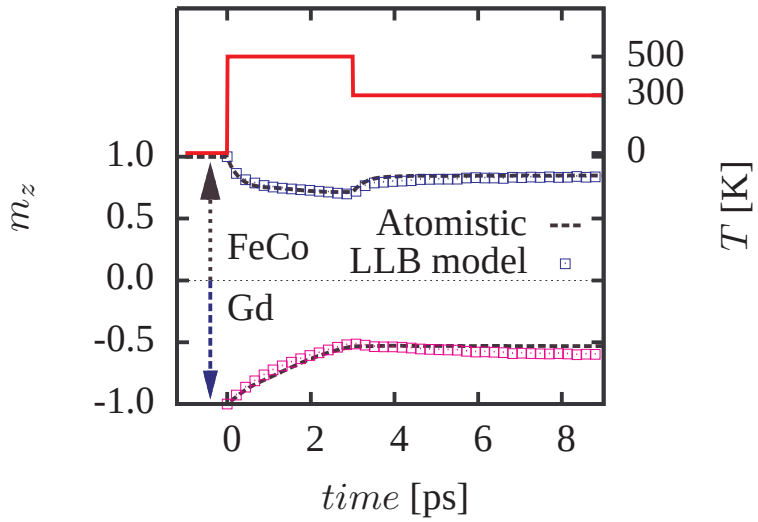

Figure 7.13: Comparison of rapid heating simulations between atomistic (symbols) and macro-spin LLB model (lines). The graph shows the z-component of the magnetization of each sublattice vs. time for a pulse heights 500K and a pulse duration of 3 ps..

7.4 Conclusions

In this chapter we have studied the times that characterized the transverse and longitudinal relaxation motion in two-component magnets using the previously (see Chapter 6) derived LLB equation. We have analytically calculate the normal modes of such magnets. Firstly, we have analyzed the well-known transverse modes of oscillations [73] under the LLB equation. We point out the main differences between the LLG approach used up to now and the LLB approach. We show that the LLB equation based transverse oscillations modes, the so-called FMR and exchange modes, have the correct temperature dependence approaching the Curie temperature. Far away from the critical temperature T_C both approaches behaves similarly as expected. We have applied the derived expression to the calculation of the frequency and effective damping of GdFeCo alloy for which these parameters are important for the control of the magnetization switching by a polarized light pulse.

Secondly, we have dealt with the longitudinal relaxation motion in two-component magnets. In this case, we have applied the analytical results to the parameters corresponding to ferrimagnetic alloy GdFeCo. We have found that the characteristic relaxation times of each magnetic lattice are in agreement with experimental findings [134]. Finally, we have predicted that for temperatures close to T_C the transition metal magnetization becomes slower than rare-earth Gd magnetization.

Conclusiones en espaõl

En este capítulo hemos estudiado los tiempos caracaterísticos de las relajaciones longitudinal y transversal en materiales magnéticos de dos componentes usando la ecuación de LLB derivada en el capítulo precedente. Hemos calculado analíticamente los modos normales, primero los modos transversales de oscilación, poniendo de manifiesto las diferencias con el modelo de LLG que ha sido usado hasta ahora. Demostramos que la dependencia con la temperatura de estos modos es la correcta cerca de la temperatura de Curie. A bajas temperaturas ambos enfoques coinciden. Hemos aplicado nuestros resultados teoricos al calculo de damping en GdFeCo. Segundo, hemos estudiado la relajacion longitudinal analiticamente para encontrar los tiempos de relajacion de cada componente, y gracias a ello podemos predecir que cerca de la temperatura critica la imanacion de la red FeCo se hace mas lenta que la del Gd.

7. TEMPERATURE-DEPENDENT NORMAL MODES IN A TWO-COMPONENT MAGNET

8

Ultrafast spin dynamics: the effect of colored noise

Atomistic spin models have proved to be a powerful approach to model ultrafast magnetization dynamics [96, 97]. The basis of these models is the stochastic Landau-Lifshitz-Gilbert (LLG) equation for each localized (at lattice site i) magnetic moment $\mathbf{s}_i$:

$$\dot{\mathbf{s}}_i = \gamma[\mathbf{s}_i \times \mathbf{H}_i] - \gamma\alpha[\mathbf{s}_i \times [\mathbf{s}_i \times \mathbf{H}_i]]. \tag{8.1}$$

Here $\mathbf{H}_i$ is the local effective field which includes Zeeman, exchange, anisotropy and magnetostatic contribution, augmented with a stochastic field $\boldsymbol{\xi}_i(t)$ with the well-known following properties for both components and different spin sites:

$$\langle \xi_i(t) \rangle = 0, \quad \langle \xi_i(t)\xi_j(t') \rangle = \frac{2\alpha k_B T}{\gamma\mu_0}\delta(t-t')\delta_{ij}. \tag{8.2}$$

Here T is the temperature, γ is the gyro-magnetic ratio, μ_0 is the magnetic moment and α is the parameter describing the coupling to the bath system. The coefficient in front of the delta function is determined by the fluctuation-dissipation theorem [31]. The basis of this equation is the separation of timescales, assuming that the bath (phonon or electron system) is much faster than the spin system. In this case, the bath degrees of freedom can be averaged out and replaced by a stochastic field with white noise correlation functions. As the fluctuating fields are being caused by a large number of weakly coupled microscopic events they are because of the central limit theorem described by a Gaussian distribution [163]. In principle the noise can be correlated both in ordinary space and in spin space. The assumption of white noise is therefore invalid for magnetization dynamics occurring on a timescale comparable to the the relaxation time of the electron system. The typical correlation time for the electron system in metals is

$\lesssim 10fs$ [153]. Such magnetization dynamics time scale is now commonly achieved by applying femtosecond laser pulses. A further limitation of this approach comes from the fact that characteristic frequencies, THz spin wave emission [53, 112], of the magnetization process are now also of the order of the timescale of the noise (electron) variable. Therefore, for modeling the ultra-fast magnetization experiments the approach (8.1) could break down. The aim of the present Chapter is to present a classical formalism beyond the white noise approximation to form a strong physical basis for models of ultra-fast magnetization dynamics in the new extreme conditions. We first introduce the formalism for a single spin and show that this approach is consistent with the equilibrium Boltzmann distribution and coincides with the previous atomistic approach for small correlation times for the bath variable. We then show that the approach can be generalized to a set of coupled spins under the assumption of localized coupling to the heat bath. We also discuss the influence of noise correlations on the most relevant characteristics of magnetization dynamics: the longitudinal and transverse relaxation times. Finally, similar to the Landau-Lisfhitz-Bloch (LLB) equation for withe noise, we analytically derive a dynamical equation for the average spin-polarization under color noise approach. Within this macrospin approach the observed correlation time dependence of the longitudinal and transverse relaxation times is simply explained.

8.1 Ornstein-Uhlenbeck process

The standard generalization of the white noise to include correlations is the Ornstein-Uhlenbeck stochastic process [137]. In this approach the set of Eqs. (8.1) is augmented with the following equation for the noise variables

$$\frac{d\xi_i}{dt} = (-\xi_i + \sqrt{2D}G_i)/\tau_c, \tag{8.3}$$

where G_i is a white-noise Gaussian stochastic variable with zero mean and variance 1. The solution of Eq. (8.3) gives noise with exponentially correlated properties

$$\langle \xi_i(t) \rangle = 0, \quad \langle \xi_i(t)\xi_j(t') \rangle = \frac{D}{\tau_c} \exp(-|t-t'|/\tau_c)\delta_{ij}, \tag{8.4}$$

where τ_c is the **correlation time**. In the limit $\tau_c \to 0$ the correlation function approaches a δ-function with variance $\langle \xi^2 \rangle = 2D$. In principle, for non-equilibrium processes, the strength of the noise does not need to be connected with the damping by means of the fluctuation-dissipation theorem. In equilibrium, however, one has to recover the Boltzmann distribution, leading to the relation $D = \alpha k_B T/\gamma\mu_0$.

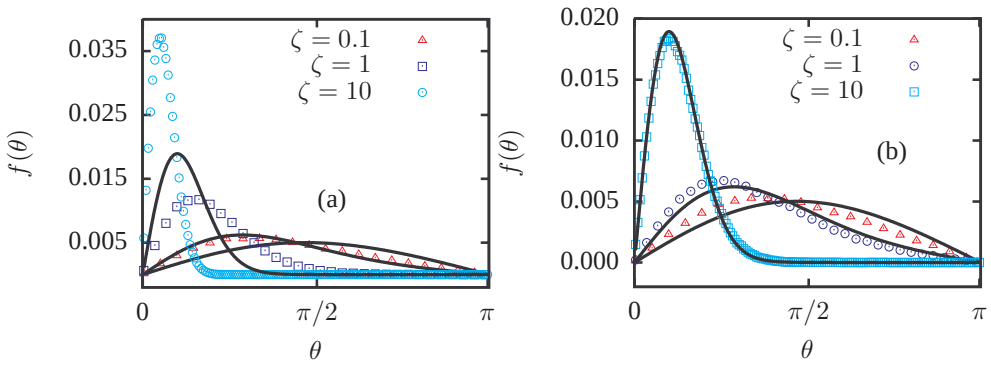

Figure 8.1: (a) Equilibrium distribution function for spin system under Ornstein-Uhlenbeck noise for different values of the reduced field $\zeta = 0.1, 1, 10$. (b) Distribution function after the renormalization of the noise strength. The correlation time used is $\tau_c = 10$fs. The solid line represents Boltzmann distribution function.

We first investigate the equilibrium properties of the model by calculating the azimuthal angle distribution function of an ensemble of atomistic non-interacting magnetic moments with the set of Eqs. (8.1)) and 8.3, and compare it with equilibrium Boltzmann distribution $f(\mathbf{s}) \sim \exp(-\beta E(\mathbf{s}))$, $\beta = (k_B T)^{-1}$. We restrict ourselves to the special case where we only consider an external magnetic field $\mathbf{H} = H\mathbf{e}_z$, in this case the energy reads $E(\mathbf{s}) = \mu_0 H \cos\theta$. Then, the Boltzmann distribution as function of angle θ reads $f(\theta) = \zeta \exp(\zeta \cos\theta)/2 \sinh\zeta$, where the reduced field ζ is given by $\zeta = \mu_0 H/k_B T$. Fig. 8.1 shows the angle distribution function in three temperature regimes, defined by the values of ζ, we choose the values $\zeta = 0.1, 1$ and 10. It can be seen that the Boltzmann distribution at equilibrium is not recovered for magnetization dynamics with correlated noise. The deviations invariably correspond to precession frequencies of the order of the inverse correlation time. These findings are in agreement with the general theory for a Newtonian particle under the influence of colored noise [75], which demonstrates that under the influence of additive noise the diffusion coefficient is re-normalized, whereas multiplicative noise leads to non-Boltzmann stationary distribution functions. It is known that stochastic magnetization dynamics governed by the linearized form of Eq. (8.1) involves additive noise [40]. Consequently, for small temperatures where linearization of the LLG equation is appropriate, the dynamics is governed by the LLG equation with re-normalized diffusion coefficient $\widetilde{D} = D[1 + (\omega_p \tau_c)^2]$, where $\omega_p = \gamma H$ is the precession frequency (see Fig. 1(b)).

At high temperatures, the noise is strictly multiplicative and the distribution function does not have the Boltzmann form. The colored noise approach

based on the Ornstein-Uhlenbeck process may provide a reasonable description in some situations when the system goes to a stationary condition not necessary coinciding with the equilibrium one (an example of this could be the spin-torque pumping into a magnetic system). However, in experiments such as those corresponding to laser-pulsed induced dynamics, a stochastic approach giving the correct equilibrium magnetization long after the laser pulse is gone, is necessary.

8.2 Atomistic colored noise approach

A suitable approach has been found in the work of Miyazaki and Seki [123] who generalized the Langevin equation for one spin to a non-Markovian case. The approach has been introduced for one spin at high temperatures, neglecting the interactions with other spins and assuming that their role is to provide the bath environment. In the present Chapter we generalize this approach to a many spin case, similar to the standard way of Eq. (8.1) where the applied field is substituted by the local field. We assume that the bath variable is due to external sources such as electrons. The other assumption made in this approach is that the spin is connected locally to the bath. Consequently, the set of equations for magnetization dynamics (in the following called Landau-Lifshitz-Miyazaki-Seki (LLMS)) reads:

$$\begin{aligned} \dot{\mathbf{s}}_i &= \gamma[\mathbf{s}_i \times (\mathbf{H}_i + \boldsymbol{\eta}_i)], \\ \dot{\boldsymbol{\eta}}_i &= -\frac{1}{\tau_c}(\boldsymbol{\eta}_i - \chi \mathbf{s}_i) + \mathbf{R}_i, \end{aligned} \tag{8.5}$$

with the fluctuation-dissipation theorem for the bath variable:

$$\langle \mathbf{R}_i(t) \rangle = 0, \quad \langle \mathbf{R}_i(t) \mathbf{R}_j(t') \rangle = (2\chi k_B T/\tau_c)\delta_{ij}\delta(t-t'). \tag{8.6}$$

The parameter χ describes the coupling of the bath variable to the spin. The precession term in the first equation of the set (8.5) has the same form as in the Eq. (8.1). However, the damping is now described by the second equation in this set. In comparison to Eq. (8.3), in the second equation in Eqs. (8.5) the bath variable adjusts to the direction of the spin due to the interaction with it. In the limit $\tau_c \to 0$ the stochastic LLG equation (8.1) is recovered. This also provides a relation between the damping and the coupling constants as $\alpha = \gamma\chi\tau_c$, giving a more precise physical sense to the LLG damping constant at atomistic level.

Onsager kinetic coefficient

Now we turn to the multi-spin system. First of all, we prove that the stochastic Eqs. (8.5) for a multi-spin system are consistent with the standard equilibrium properties. For this purpose we use the formalism of the Onsager kinetic coefficient method applied in Ref. [40] for the LLG multispin system (8.1). The system (8.5) is linearized near equilibrium and represented in a general form of the Langevin equation:

$$\begin{aligned} \frac{dx_i}{dt} &= -\sum_j \gamma_{ij} X_j + r_i \\ \langle r_i(t)\rangle &= 0; \;\; \langle r_i(0) r_j(t)\rangle = \mu_{ij}\delta(t). \end{aligned} \tag{8.7}$$

Here x_i stands for small deviations of the stochastic variables $\mathbf{s}_i$ or η_i from their equilibrium values, $\mu_{ij} = \gamma_{ij} + \gamma_{ji}$, and X_i represent the thermodynamically conjugate variables. For the spin variable we have: $X_j = -(\mu_s/k_B T)H_j$, where H_j is the internal field corresponding to a particular lattice site and spin component. Unlike Eq. (8.1), the first equation in Eqs. (8.5) contains only a precession term and, therefore, the corresponding kinetic coefficients are antisymmetric in spin components, giving for this equation $\mu_{ij} = 0$. Taking into account the generalization of the internal energy to include the bath variable as

$$F(\{\mathbf{s}_i\}, \{\eta_i\}) = F_0(\{\mathbf{s}_i\}) + \sum_i [\eta_i^2/(2\chi) - \eta_i \mathbf{s}_i], \tag{8.8}$$

where $F_0(\{\mathbf{s}_i\})$ is the internal energy without the bath variable, the conjugate variable to the bath one is $\mathbf{X}_j = (\eta_j - \chi \mathbf{s}_j)/(k_B T \chi)$. Therefore, the corresponding matrix of the kinetic coefficients is diagonal and for the second equation we obtain $\mu_{ij} = (2k_B T\chi/T_c)\delta_{ij}$. Consequently, we have proven that, under the supposition of local coupling of the spin to the bath variables, the set of multi-spin equations (8.5) is consistent with the equilibrium properties.

Equilibrium properties

For integration of Eqs. (8.5), we first change the thermal field variable $\boldsymbol{\eta}$ by a more convenient variable $\mathbf{H}_{\rm th} = \boldsymbol{\eta} - \chi \mathbf{s}$. We use it to rewrite the LLMS equations (8.5) as

$$\begin{aligned} \frac{d\mathbf{s}_i}{dt} &= \gamma \mathbf{s}_i \times (\mathbf{H}_i + \mathbf{H}_{i,\rm th}) \\ \frac{d\mathbf{H}_{i,\rm th}}{dt} &= -\chi\gamma \mathbf{s}_i \times (\mathbf{H}_i + \mathbf{H}_{i,\rm th}) - \frac{1}{\tau_c}\mathbf{H}_{i,\rm th} + \mathbf{R}. \end{aligned} \tag{8.9}$$

The integration of Eqs. (8.9) is more stable using the new noise variable $\mathbf{H}_{i,\mathrm{th}}$ that the old one. We use the Heun integration scheme [67] to solve Eqs. (8.9). First of all we investigated the equilibrium properties of Eqs. (8.5) for an ensemble of non-interacting spins using the same values of the parameters as in Fig. 8.1. In all cases of large fields, temperatures and correlation times, the correct Boltzmann distribution is obtained at equilibrium (see Fig. 8.2).

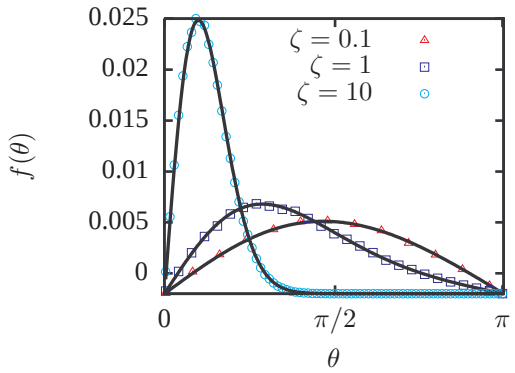

Figure 8.2: The figure shows distribution functions for non-interacting spin system modeled within the LLMS approach for different values of the reduced field and correlation time $\tau_c = 10$fs. The solid line represents the Boltzmann distribution.

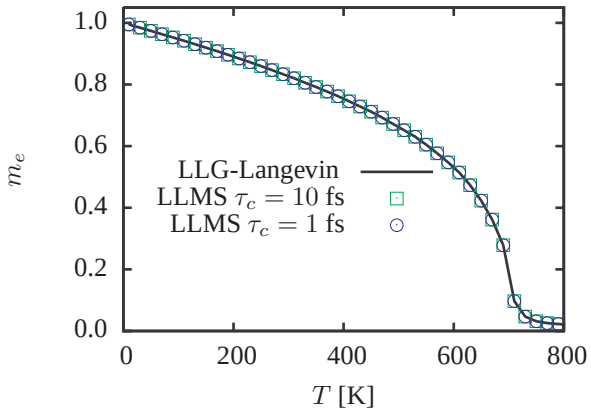

Figure 8.3: Equilibrium magnetization as a function of temperature for a system of $\mathcal{N} = 32^3$ interacting spins, integrating the LLMS equation with different correlation times and integrating the LLG equation.

In Fig. 8.3 we present calculations of the equilibrium magnetization as a function of temperature for spin systems with different values of the correlation

times. Independence of the equilibrium properties on the correlation time, and the agreement with calculations using the LLG equation with uncorrelated noise demonstrates our generalization of the LLMS equation to multi-spin systems. Consequently, the LLMS equation provides a basis for the phenomenological description of magnetization dynamics in extreme situations of high temperatures, and large and rapidly varying external fields. The advantage of the approach is also that the fluctuation-dissipation theorem is not applied directly to the spin variable. Therefore, the bath variable (for example electrons) and the spin system need not be in equilibrium with each other.

8.3 Relaxation times

Next we discuss the most important implications of this new approach to the ultra-fast dynamics. It is known that during the excitation with spatially inhomogeneous fields in the TeraHertz range [153, 156] and also during laser-induced magnetization dynamics [19, 107], strong local disordering of the spin system occurs. The dynamics in these cases is governed by field or temperature excited high-frequency spin waves which are responsible for the effective damping. The important dynamical feature then is the rate of magnetization recovery. During these processes two types of relaxation could be distinguished. The first one known as longitudinal relaxation is responsible for linear magnetization recovery, i.e. the magnetization magnitude. During the laser-induced demagnetization, the longitudinal relaxation is responsible for the femtosecond demagnetization. The second one is the transverse relaxation when the magnetization vector relaxes to the direction parallel to the internal field via magnetization precession. The longitudinal relaxation time increases with the temperature while the transverse relaxation time has minimum at T_C [41], see also Chapter 3. The transverse processes are normally much slower than the longitudinal ones. In our simulations we use a cubic system of 32^3 magnetic moments with $\mu_0 = 1.45\mu_B$ and the Curie temperature $T_C = 700$K ($k_B T_C \approx 1.44$J for the simple cubic structure Heisenberg model used here). The coupling parameter χ was chosen to give the LLG damping parameter $\alpha = 0.01$. To simulate the **longitudinal relaxation**, we start with the initial condition $\{s_i^z\} = 1.0$ and observe the system to relax at given temperature T. The obtained relaxation curves are then fitted to exponential decay to extract the longitudinal relaxation rate. The longitudinal relaxation time, normalized to the uncorrelated case, is presented in Fig. 8.4 as a function of the noise correlation time. The longitudinal time calculated by means of the LLG approach (8.1) is of the order of 10fs ($\tau_{||}^0 = 28$fs at $T = 300$K).

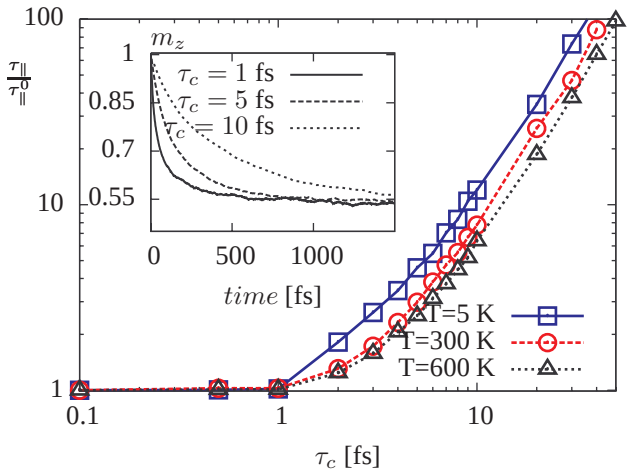

Figure 8.4: Longitudinal relaxation time (normalized to the uncorrelated case) as a function of the correlation time for various temperatures calculated within LLMS approach. The inset shows longitudinal relaxation for various correlation times and $T = 600$K.

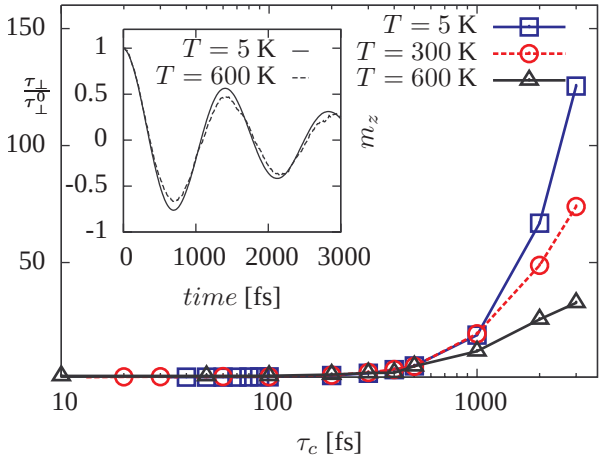

Figure 8.5: Transverse relaxation time (normalized to the uncorrelated case) as a function of the correlation time for various temperatures calculated within LLMS approach. The insert shows transverse relaxation for two temperatures $T = 5$K and $T = 600$K and $\tau_c = 10$fs.

For correlation time $\tau_c \lesssim 1$fs the uncorrelated approach gives the same results as the LLMS one. However, one can see that $\tau_c \simeq 10 - 100$fs gives a dramatic increment of the longitudinal relaxation time. The effect is less pronounced at higher temperature since in this case the temperature contributes to the loss of

correlations.

Next, we investigate the **transverse relaxation** in Fig. 8.5. In this case, the spin system was first equilibrated at given temperature and applied field $H = 24.85$T. After that the whole system was rotated to an angle 30^o and the relaxation to the direction parallel to the applied field was observed. The transverse relaxation time is much longer than the longitudinal one. Consequently, much longer correlation times are necessary in order to see the influence on the longitudinal relaxation.

8.4 Generalized macroscopic equation

Equations (8.5) shows that the fluctuating magnetic field $\boldsymbol{\eta}$ has a tendency to adjust to the direction of the spin due to the interactions with the noise. This contribution has been neglected in most theories where the fluctuating field is supposed to be independent of the spin, and therefore they are uncorrelated. This assumption has been very advantageous to handle with the analytical solutions of the average spin-polarization $\langle \mathbf{s} \rangle$ for the withe noise Landau-Lifshitz-Gilbert (LLG) equation as, for example, the Landau-Lifshitz-Bloch (LLB) equation, see Appendix C. However, the exact analytical solution for the dynamics of $\langle \mathbf{s} \rangle$ of these LLMS equations is a formidable task. We are not going to exactly solve these equations. We will follow the same idea as in the withe noise LLB equation calculation. First of all we need the Fokker-Planck equation (FPE) corresponding to Eqs. (8.5) which contains the magnetization and noise variables [123]. This FPE containing both variables is not useful to analytical calculations, then some approximations have to be made to get rid of the noise variable. In Ref. [123] two approximations were made. First, it was assumed that the fluctuation field is rather weak and stay in second order in $\chi k_b T/\tau_c$. Then the noise and spin variable can be factorize as $\langle R(t)R(t')s(t')\rangle \approx \langle R(t)R(t')\rangle\langle s(t')\rangle$ as the spin change only weakly over time scale τ_c of the fluctuation field. And the second assumption was that the spin s varies only slowly on the time scale of τ_c over which the correlation of the fluctuating field is significant, thus, it can be assumed that that $\langle R(t)R(t')\rangle\langle s(t')\rangle \approx \langle R(t)R(t')\rangle\langle s(t)\rangle$. Under these approximations the Fokker-Planck equation which describes the temporal evolution of the distribution function $f(\mathbf{N}, t)$ was derived [123]

$$\frac{\partial f}{\partial t} = -\frac{\partial}{\partial \mathbf{N}}\left\{\gamma\left(1+\delta\right)\left[\mathbf{N}\times\mathbf{H}\right]+\gamma\widetilde{\eta}_2(\mathbf{N}\cdot\mathbf{H})[\mathbf{N}\times\mathbf{H}]-\widetilde{\eta}_1[\mathbf{N}\times[\mathbf{N}\times\mathbf{H}]]\right\}f$$
$$-\frac{\partial}{\partial \mathbf{N}}\left\{\mathcal{D}\left[\mathbf{N}\times\left[\mathbf{N}\times\frac{\partial}{\partial \mathbf{N}}\right]\right]\right\}f, \tag{8.10}$$

here $\widetilde{\eta}_1 = \gamma\alpha/\kappa$, $\widetilde{\eta}_2 = \widetilde{\eta}_1\tau_c$, $\delta = \widetilde{\eta}_2/(\beta\mu_0)$, and $\mathcal{D} = \Lambda_N/(2\kappa)$, where $\kappa = 1 + (\omega_0\tau_c)^2$. In the Markovian limit $\tau_c = 0$ and from Eq. (8.10) the withe noise FPE is recovered, see Appendix C Eq. (C.2). The equation of motion for the mean average spin polarization, $\mathbf{m} = \langle\mathbf{s}\rangle$ (see Appendix B) of an assembly of magnetic moments can be derived from Eq. (8.10) and has the form

$$\frac{d\mathbf{m}}{dt} = \gamma\left(1+\delta\right)\left[\mathbf{m}\times\mathbf{H}\right]-2\mathcal{D}'\mathbf{m}-\widetilde{\eta}_1\left\langle[\mathbf{s}\times[\mathbf{s}\times\mathbf{H}]]\right\rangle-\gamma\widetilde{\eta}_2\left\langle(\mathbf{s}\cdot\mathbf{H})[\mathbf{s}\times\mathbf{H}]\right\rangle, \tag{8.11}$$

where

$$\mathcal{D}' = \frac{\Lambda_N}{2\kappa}\begin{pmatrix}\kappa+1 & 0 & 0\\ 0 & \kappa+1 & 0\\ 0 & 0 & 1\end{pmatrix}. \tag{8.12}$$

From this equation we can directly see three main effects:

1. The precession *frequency is shifted* from $\omega_0 = \gamma H$ to $\omega' = \omega_0(1+\delta)$.
2. The *longitudinal relaxation* time $\tau_\parallel$ is related to the $\mathcal{D}'_{zz}$ element of the matrix $\mathcal{D}$' which is proportional to $\kappa = 1 + (\omega_0\tau_c)^2$.
3. The *transverse relaxation* time is approximately given by $\tau_\perp = \kappa/\left(\gamma\alpha H\right) = \tau_\perp^0\kappa$, where $\tau_\perp^0$ is the transverse relaxation time calculated from the white noise LLB approach.

The results of the longitudinal relaxation time using the LLMS multispin atomistic simulations presented in Fig. 8.4 shows that $\tau_\parallel$ starts to deviate form the white noise limit, $\tau_\parallel^0$, for correlation times much more shorter than for the transverse relaxation time as shown in Fig. 8.5.

Bloch equation

Here, we consider the case where the damping parameter, $\chi = 0$ is set to zero in the equations of motion (8.5). In this particular case the equations reduces

$$\begin{aligned}\dot{\mathbf{s}}_i &= \gamma[\mathbf{s}_i\times(\mathbf{H}_i+\boldsymbol{\eta}_i)],\\ \dot{\boldsymbol{\eta}}_i &= -\frac{1}{\tau_c}\boldsymbol{\eta}_i+\mathbf{R}_i.\end{aligned} \tag{8.13}$$

These equations are the starting point in the derivation of the Bloch equations of motion [**?**]. From Eq. (8.11) it is easy to get the Bloch equation by putting $\chi = 0$. Thus,

$$\frac{d\mathbf{m}}{dt} = \gamma\,(1+\delta)\,[\mathbf{m}\times\mathbf{H}] - 2\mathcal{D}'\mathbf{m}. \tag{8.14}$$

If we decompose it in cartesian components, we get a more familiar expression of the Bloch equation

$$\begin{aligned}
\frac{dm_x}{dt} &= -\omega' m_y - \frac{m_x}{T_2}, \\
\frac{dm_y}{dt} &= -\omega' m_x - \frac{m_y}{T_2}, \quad \text{where} \quad \frac{1}{T_2} = \frac{D(1+\kappa)}{\kappa}\tau_c \\
\frac{dm_z}{dt} &= -\frac{m_z}{T_1} \quad \text{where} \quad \frac{1}{T_1} = \frac{D}{\kappa}\tau_c,
\end{aligned} \tag{8.15}$$

where the longitudinal relaxation time T_1 is usually called the *spin relaxation time* and the transverse relaxation T_2 is called *spin dephasing time*. From this equation we can see that for $\omega_p\tau_c \ll 1$ ($\kappa \approx 1$) both times are equal and inversely proportional to correlation time, $T_1 = T_2 = D/\tau_c$. It is at first sight surprising that the spin relaxation time is inversely proportional to the correlation time.

Landau-Lifshitz-Bloch equation

We now consider that the coupling of the spin variable to the noise is not zero, $\chi \neq 0$. Then the complete Eq. (8.11) has to be considered which is not closed but coupled to the second moments of the distribution function, $\langle s_i s_j\rangle$, in its last two terms. Here we use the same decoupling procedure of the $\langle s_i s_j\rangle$ used in the derivation of the ferromagnetic LLB equation (see Appendix C), for example, the term $\langle(\mathbf{s}\cdot\mathbf{H})[\mathbf{s}\times\mathbf{H}]\rangle$ is written as

$$\langle(\mathbf{s}\cdot\mathbf{H})[\mathbf{s}\times\mathbf{H}]\rangle = \left(1 - \frac{3m}{\xi}\right)\frac{(\mathbf{H}\cdot\mathbf{m})\,[\mathbf{m}\times\mathbf{H}]}{m^2}. \tag{8.16}$$

This term is responsible for an additional frequency shift that we can sum up to the frequency shift given by δ. We can define a renormalize gyromagnetic ratio

$$\frac{\gamma'}{\gamma} = 1 + \left(\Gamma_2 - \frac{\Lambda_N}{2}\right)\frac{\tau_c}{\kappa}, \tag{8.17}$$

where we have calculated it using close to equilibrium conditions. Finally, we can write Eq. (8.11) as

$$\frac{d\mathbf{m}}{dt} = \gamma'[\mathbf{m}\times\mathbf{H}] - \overleftrightarrow{\Lambda}\mathbf{m} - \widetilde{\Gamma}_2\frac{[\mathbf{m}\times[\mathbf{m}\times\mathbf{m}_0]]}{m^2}, \tag{8.18}$$

where $\widetilde{\Gamma}_2 = \Gamma_2/\kappa$ and the longitudinal relaxation matrix $\overleftrightarrow{\Lambda}$ is defined as

$$\overleftrightarrow{\Lambda} = \widetilde{\Gamma}_1\left(1 - \frac{\mathbf{m}\mathbf{m}_0}{m^2}\right)\overleftrightarrow{I} + \begin{pmatrix} \Lambda_N & 0 & 0 \\ 0 & \Lambda_N & 0 \\ 0 & 0 & 0 \end{pmatrix}, \tag{8.19}$$

where $\overleftrightarrow{I}$ is the unitary matrix. The longitudinal relaxation term can be separated into two contribution; (i) one coming from the interaction of magnetization parallel to the field, and (ii) one from the interaction with transverse to the field magnetization. In an exchange coupled ferromagnet the transverse contribution can be neglected in comparison with the exchange field $\mu_0\mathbf{H}_{\text{EX}} = J_0\mathbf{m}$. Thus, for ferromagnets the macroscopic equation for the $\mathbf{m}$ is quite similar to that derived by Garanin [47] but with renormalized relaxation parameters as well as a shift in the precession frequency. The macroscopic equation for magnetization dynamics of a ferromagnet is then written

$$\frac{d\mathbf{m}}{dt} = \gamma'[\mathbf{m}\times\mathbf{H}_{\text{eff}}] - \gamma\widetilde{\alpha}_\parallel\frac{(\mathbf{m}\cdot\mathbf{H}_{\text{eff}})}{m^2}\mathbf{m} - \gamma\widetilde{\alpha}_\perp\frac{[\mathbf{m}\times[\mathbf{m}\times\mathbf{H}_{\text{eff}}]]}{m^2}, \tag{8.20}$$

where $\widetilde{\alpha}_\parallel = \alpha_\parallel/\kappa_\parallel$, $\widetilde{\alpha}_\perp = \alpha_\perp/\kappa_\perp$, $\kappa_\perp = 1 + (\omega_p\tau_c)^2$, $\kappa_\parallel = 1 + (\omega_{\text{ex}}\tau_c)^2$ and $\omega_{\text{ex}}(T) = \gamma(J_0/\mu_0)m_e(T)$. We recall that the relaxation times derived from the white noise LLB type equation read

$$\tau_\parallel = \frac{\widetilde{\chi}_\parallel(H,T)}{\gamma\alpha_\parallel}, \quad \tau_\perp = \frac{\widetilde{\chi}_\perp(H,T)}{\gamma\alpha_\perp}, \tag{8.21}$$

Then the ratio between colored and withe noise relaxation times is given by the functions $\tau_\parallel/\tau_\parallel^0 = \kappa_\parallel$ and $\tau_\perp/\tau_\perp^0 = \kappa_\perp$.

Figure 8.6 (Right) shows the function $\kappa_\parallel = \tau_\parallel/\tau_\parallel^0$ as a function of temperature for the same parameters as for the atomistic simulations used in Fig. 8.4. The qualitative behaviour of the relaxation times as a function of correlation time for both cases is similar. For low temperature, $T = 5$K in Fig. 8.6 (Right) we can see that the deviation from the uncorrelated case starts to be appreciable for $\tau_c \approx 1$ fs. As we have mentioned for longitudinal motion the characteristic frequency is given by the exchange field around which the local spins precess. The characteristic frequency is given by $\omega_{\text{ex}} = \gamma(J_0/\mu_0)m$. At low temperatures the mean magnetization value m can be taken as 1, and for high temperatures

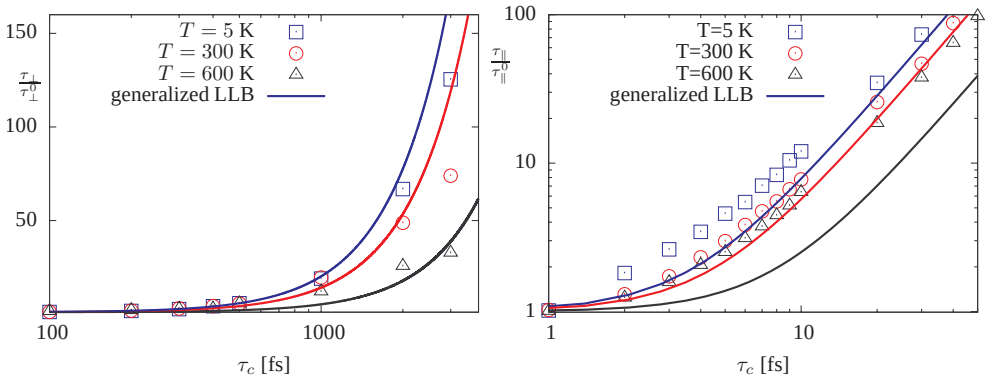

Figure 8.6: Comparison between simulation (points) and the LLB theory (lines) of (Left) the transverse relaxation time normalized to the uncorrelated case as as a function of τ_c for $T = 5, 300$ and 600K, and (Right) the longitudinal relaxation time normalized to the uncorrelated case as a function of τ_c for $T = 5, 300$ and 600K.

the mean value m can be taken as the equilibrium magnetization at final temperature. In Fig. 8.6 (Right) we have used these values in the determination of $\kappa_\parallel = 1 + (\gamma(J_0/\mu_0)m_e\tau_c)^2$. There is a shift between atomistic simulations and the generalized LLB equation predictions. We think that this shift could be caused by all the approximations that we have done, for example, the approximation $m \approx m_e$ in the calculation of exchange frequency. As we can see in the inset of Fig. 8.4 for τ_c large enough the system magnetization is quite far from equilibrium value for long time, therefore the approximation $m \approx m_e$ seems to be not enough precise. We can improve our estimation if we use the mean average magnetization value during the process better than the equilibrium value at final temperature $\langle m \rangle_t = \int m(t)dt$. A more accurate equation should include the dynamical exchange field, $(J_0/\mu_0)m(t)$ into $\kappa_\parallel$.

Figure 8.6 (Left) shows the function $\kappa_\perp = \tau_\perp/\tau_\perp^0$ as a function of temperature for the same parameters as for the atomistic simulations used in Fig. 8.5. Here the agreement is very good in comparison with the longitudinal problem. We argue that this is because in the transverse relaxation problem the magnetization length is constant during the relaxation, thus, there are not dynamical variable into the relaxation rates that should be approximated.

8.5 Conclusions

In conclusion, the standard phenomenological approach to model spin dynamics has been generalized to the non-Markovian case. This approach is necessary in the extreme situations of large characteristic frequencies occurring during ultra-fast magnetization processes. The advantages of the new approach are the following: (i) the memory (correlation) effects arising from the fact that the bath variable responds to the spin direction are taken into account, this corresponds to the situation when the bath variable is not in equilibrium with the spin system, (ii) the fluctuation-dissipation theorem is not applied to the spin systems as in the standard LLG approach, and (iii) in equilibrium the Boltzmann distribution is recovered. The price for this new approach is the use of two phenomenological constants: the phenomenological damping parameter α for the LLG approach is substituted by two phenomenological parameters in the LLMS approach: the correlation time τ_c and the coupling constant χ. Several processes may be important in determining these constants, as for example, the spin-orbit coupling, momentum relaxation, scattering rate and dephasing time of conduction electrons. As in the LLG approach, these parameters will be material-specific and their physical origins should be clarified on the basis of first-principle approaches. We have shown that the magnetization relaxation processes are strongly influenced by these parameters which stresses the necessity of first-principle models, capable to clarify their physical origins.

An open question is the problem of doped permalloy where an attempt to systematically change the damping parameter by doping with rare-earth impurities was undertaken [170] in order to clarify the relation between the LLG damping and the ultra-fast demagnetization rate [133, 166]. The results are not in agreement with the withe noise LLB model. However in this case we think that the hypothesis of the slow relaxing impurities presented in Ref. [133] might be a plausible explanation. Indeed, if the relaxation time of the rare earth impurities is high, the standard LLB model is not valid since it assumes an uncorrelated thermal bath. The above derived color noise LLB equation shows that the correlation time of the order of 10 fs slows down the longitudinal relaxation independently on the transverse relaxation.

Conclusiones

En conclusión, hemos generalizado el modelo estándard de la dinámica de espín al caso no Markoviano. Este enfoque es necesario en situaciones extremas durante los procesos ultrarrápidos de la imanación a altas frecuencias. Las ventajas de este nuevo modelo son las siguientes: (i) los efectos de memoria (correlaciones

temporales) debido a la respuesta del baño a la interacción con el espín son tenidos en cuenta, esto sucede en situaciones de no equilibrio entre baño y sistema de espines, (ii) el teorema de fluctuación-disipación no se aplica al sistema de espines del mismo modo que al modelo LLG estándard, y (iii) en equilibrio se obtiene la distribución de Boltzmann.

El precio a pagar por este nuevo enfoque es la aparición de dos parámetros fenomenologicos; la constante de relajación λ en el modelo LLG es sustituida por dos nuevos parámetros en el modelo LLMS, el tiempo de correlación τ_c y la constante de acoplo χ. Muchos procesos pueden ser importantes en la determinación de dichas constantes, como por ejemplo, el acoplo espín-órbita, la relajación de momento, ratio de *scattering* y el tiempo de desfase de los electrones de conducción. Del mismo modo que en el modelo LLG, estos parámetros serán específicos de cada material y sus orígenes físicos deberían ser clarificados en base a cálculos de primeros principios. Hemos demostrado que los procesos de relajación están fuertemente influenciados por estos parámetros lo que enfatiza la necesidad de modelos de primeros principios capaces de clarificar sus orígenes físicos.

Una cuestión abierta es el problema de Permalloy dopado donde se intento variar de manera sistematica el parametero de relajacion mediante la inclusion de dopaje de tierras raras [170] para clarificar la relacion entre el parámetro de relajación y la desimanción ultrarrápida [133, 166]. Estos resultados no están en acuerdo con el modelo LLB de ruido blanco. Sin embargo, creemos que la hipótesis de impurezas lentas propuesto en la referencia [133] is una explicacion plausible. De hecho, si el tiempo de relajación de la impurezas de tierras raras es alto, el modelo estándard de LLB no es válido ya que este asume un baño térmico no correlacionado. La ecuación LLB para ruido coloreado muestra que para tiempos de correlación del orden de 10 fs desacelera la relajación longitudinal independientemente de la relajación longitudinal.

8. ULTRAFAST SPIN DYNAMICS: THE EFFECT OF COLORED NOISE

Appendix A

Heisenberg Hamiltonian and the mean field approximation

A.1 Heisenberg Magnetic Hamiltonian

The magnetic order in ferromagnets and antiferromagnets is the result of correlation between the directions of the electron spins on individual atoms. This correlation is in turn due to the fact that the space symmetry of the wave function depends on the magnitude of the resultant spin of the system of electrons. This dependence is a consequence of the principle of indistinguishableness of identical particles. Thus, it is a purely quantum-mechanical effect which results from the fact that electrons obey Fermi-Dirac statistics. This explanation of the magnetic state has been suggested by Heisenberg [77] and further developed by Dirac [51] and Van Vleck [161] was that the combined effect of the Coulomb inter-electronic interactions and Pauli's exclusion principle between two atoms with spins $\mathbf{S}_i$ and $\mathbf{S}_j$ would produce an effective interaction potential that can be written on the following Hamiltonian form

$$\mathcal{H}_{\text{ex}} = -\frac{1}{2}\sum_{i,j} J(R_{ij})\mathbf{S}_i \cdot \mathbf{S}_j, \tag{A.1}$$

where $J(R_{ij})$ is the exchange energy, a function of the inter-atomic distance R_{ij}. Therewith the spins $\mathbf{S}_i$ represent the magnetic moments, $\boldsymbol{\mu}_i$, which are normalized to $\mathbf{S}_i = \boldsymbol{\mu}_i/\mu_s$ with $\mu_s = |\boldsymbol{\mu}_i|$. Therefore the magnitude of $\mathbf{S}_i$ is constantly equal 1. Usually, the **exchange interaction** decays rapidly with distance and thus affect mainly nearest neighbours [59]. In this case only one exchange constant is needed to define the Hamiltonian (A.1). The sign of this exchange constant defines the type of order; a positive exchange constant $J > 0$ leads to the parallel

alignment of spins as observed in ferromagnets, while $J < 0$ leads to an anti-parallel alignment as in antiferromagnets.

As the overlap of wave functions in general is not isotropic in space due the quantum mechanical spin-orbit coupling, the magnetization of magnetic materials often is pointed in a certain direction along a crystal axis, which is called easy axis. In the simplest case of the so-called **magneto-crystalline anisotropy** with an uniaxial anisotropy the corresponding Hamiltonian reads:

$$\mathcal{H}_{\mathrm{K}} = -K \sum_i (S_i^z)^2 \,. \tag{A.2}$$

Thus, in axial symmetry, only the K parameter is needed to express the energies level splitting due to spin-orbit coupling. K can be positive or negative; negative K corresponds to easy-plane magnetic anisotropy, the spins prefer any perpendicular direction and $z-$axis is the hard axis. However for positive K the spins lower the energy by being parallel to the $z-$axis, in which case the $z-$axis is called easy axis.

Finally, the Hamiltonian also contains a term which describes the interaction with applied magnetic field. This interaction is described by the **Zeeman** term and is given by

$$\mathcal{H}_{\mathrm{Z}} = -\mu_s \sum_i \mathbf{H} \cdot \mathbf{S}_i. \tag{A.3}$$

According with this term, magnetic moments tend to be parallel to the applied magnetic field.

General Heisenberg Hamiltonian

Finally, the energetics of a ferromagnetic body can be quite well described by the Heisenberg Hamiltonian [77]. It is made by adding up all the contribution (A.1), (A.2) and (A.3) of each lattice site. It reads

$$\mathcal{H} = -J \sum_{i<j} \mathbf{S}_i \cdot \mathbf{S}_j - K \sum_i (S_i^z)^2 - \mu_0 \sum_i \mathbf{H} \cdot \mathbf{S}_i. \tag{A.4}$$

A.2 Mean-Field Approximation for the Heisenberg model

In the Heisenberg model (A.4), each spin interacts both with the external magnetic field and the one created by neighbor spins. The magnetic field created by the spins is obviously a dynamical variable, which cannot be controlled, for its

value changes with the fluctuations of the configurations. The mean field approximation (MFA) consists of replacing the magnetic field created by the spins by its thermal average.

Consider the Heisenberg Hamiltonian described in Eq. (A.4) with $\mathcal{N}$ spins. We define the reduced mean magnetization calculated as a thermal average over all possible states and all spins,

$$\mathbf{m} = \frac{1}{\mathcal{N}} \sum_i \langle \mathbf{S}_i \rangle. \tag{A.5}$$

Within the MFA we assume that a deviation of the magnetic moment, $\mathbf{S}_i$, from the mean magnetic moment, $\langle \mathbf{S}_i \rangle$, is quite small, $\mathbf{S}_i - \langle \mathbf{S}_i \rangle$. and we can express the product of the spins as

$$\mathbf{S}_i \cdot \mathbf{S}_j = \langle \mathbf{S}_i \rangle \langle \mathbf{S}_j \rangle + \mathbf{S}_i(\langle \mathbf{S}_j \rangle - \langle \mathbf{S}_j \rangle) + \mathbf{S}_j(\langle \mathbf{S}_i \rangle - \langle \mathbf{S}_i \rangle) + (\mathbf{S}_i - \langle \mathbf{S}_i \rangle)(\mathbf{S}_j - \langle \mathbf{S}_j \rangle). \tag{A.6}$$

The mean field approximation consists of completely neglecting the last term which is quadratic in small deviation of spin value. Furthermore, if we assume that the mean magnetization is identical in the whole lattice, $\mathbf{m} = \langle \mathbf{S}_i \rangle$, then the Hamiltonian (see Eq. (A.4)) with exchange, anisotropy and Zeeman interaction terms in MFA is given by

$$\mathcal{H} \Rightarrow \mathcal{H}^{\text{MFA}} = \mathcal{H}_{00} - \mu_0 \sum_i \mathbf{H}^{\text{MFA}} \cdot \mathbf{S}_i, \tag{A.7}$$

where $\mathcal{H}_{00} = -zJ\mathcal{N}\mathbf{m} \cdot \mathbf{m} - \mathcal{N}Km_z^2$ does not depend on spin operators and the molecular field $\mathbf{H}_i^{\text{MFA}}$ is given by

$$\mu_0 \mathbf{H}^{\text{MFA}} = \mu_0 \mathbf{H} + 2Km_z \mathbf{e}_z + zJ\mathbf{m}, \tag{A.8}$$

then the solution of one-spin problem in Eq. (A.7) leads to the following free energy general expression $F = \mathcal{H}_{00} - \mathcal{N}k_BT \ln(4\pi) - k_BT\mathcal{N}\Lambda(\xi)$ where $\Lambda(\xi) = \ln(\sinh(\xi)/\xi)$ with the effective field defined as $\boldsymbol{\xi} = \beta \mathbf{H}^{\text{MFA}}$, $(\xi = |\boldsymbol{\xi}|)$.

Mean field equilibrium magnetization

The free MFA energy can be minimized with respect to the average magnetization $\mathbf{m}$ to find the equilibrium distribution. The minimum condition for the free energy, $\partial F/\partial \mathbf{m} = 0$, leads to Curie-Weiss equation

$$\mathbf{m} = B(\xi) \frac{\boldsymbol{\xi}}{\xi}, \tag{A.9}$$

where $B(\xi) = \coth(\xi) - 1/\xi$ is the Langevin function. This expression is a so called self consistency equation, because the unknown variable **m** is on both sides of the equation. Therewith, this equation poses a root finding problem.

Mean field susceptibility

In the paramagnetic regime, $T > T_C$, the zero field susceptibility is isotropic: the longitudinal and transverse components are equal. The longitudinal susceptibility is defined as $\widetilde{\chi}_{\parallel} = (\partial m/\partial H)_{H=0}$. In the MFA the Eq. (A.9) is used to obtain the following relation for the longitudinal susceptibility

$$\widetilde{\chi}_{\parallel} = \frac{\mu_0}{J_0} \frac{B' \beta J_0}{1 - B' \beta J_0}, \tag{A.10}$$

where μ_0 stand for atomic magnetic moment. $B' \equiv dB/d\xi$ is evaluated at equilibrium and $H = 0$. In vicinity of T_C the parallel susceptibility increases within the mean-field model with the critical exponent 1, i.e. $\chi_{\parallel} \sim (\varepsilon)^{-}1$. We note that for $T \nearrow T_C$, the proportionality coefficient for the critical expression of the longitudinal susceptibility is a half of this for $T \searrow T_C$ [117].

The MFA is then proved to be and easy method to describe the magnetic systems at elevated temperatures and it will be useful along this work but this model only deliver the equilibrium description of a magnetic body only.

Appendix B

Stochastic Methods

B.1 General case

A general ***stochastic differential equation*** (SDE) for a multi-component process $\mathbf{y} = (y_1, \ldots, y_n)$ has the form

$$\frac{dy_i}{dt} = A_i(\mathbf{y}, t) + B_{ik}(\mathbf{y}, t)\xi_k(t) \tag{B.1}$$

where the $\xi_k(t)$ are white noise terms. The statistical properties of the $\xi_k(t)$ are

$$\langle \xi_k(t) \rangle = 0 \quad \text{and} \quad \langle \xi_k(t)\xi_l(t') \rangle = 2D\delta_{kl}\delta(t - t')$$

The successive coefficients occurring in the ***Kramers-Moyal expansion*** can be calculated by using advanced stochastic methods

$$\frac{\partial P(y,t)}{\partial t} = \sum_{m=1}^{\infty} \frac{(-1)^m}{m!} \sum_{j_1,\ldots,j_m} \frac{\partial^m}{\partial y_{j_1} \ldots \partial y_{j_m}} \left[a^{(m)}_{j_1,\ldots,j_m}(\mathbf{y}, t) P(y,t) \right] \quad \text{Kramers} - \text{Moyal} \tag{B.2}$$

it is not easy to handle but, under certain conditions, one may break off after a suitable number of terms. When this is done after the second-order terms one gets a partial differential equation of second order for $P(y,t)$ called the ***Fokker-Planck equation*** (FPE):

$$\frac{\partial P}{\partial t} = -\sum_i \frac{\partial}{\partial y_i} \left[a^{(1)}_i(\mathbf{y}, t) P \right] + \frac{1}{2} \sum_{ij} \frac{\partial^2}{\partial y_i \partial y_j} \left[a^{(2)}_{ij}(\mathbf{y}, t) P \right] \tag{B.3}$$

The successive coefficients occurring in the Kramers-Moyal expansion can be calculated. On doing so, one gets the following expressions

$$
\begin{aligned}
a_i^{(1)}(\mathbf{y},t) &= A_i(\mathbf{y},t) + D_{jk}B_{jk}(\mathbf{y},t)\frac{\partial B_{ik}(\mathbf{y},t)}{\partial y_j} \\
a_i^{(2)}(\mathbf{y},t) &= 2DB_{ik}(\mathbf{y},t)B_{jk}(\mathbf{y},t) \\
a^{(m)}_{j_1,\ldots,j_m} &= 0, \quad \text{for } m \geq 3
\end{aligned}
$$

introducing them into the Kramers-Moyal expansion the probability distribution obeys a Fokker-Plank equation

$$
\begin{aligned}
\frac{\partial P}{\partial t} &= -\frac{\partial}{\partial y_i}\left\{\left[A_i(\mathbf{y},t) + DB_{jk}(\mathbf{y},t)\frac{\partial B_{ik}(\mathbf{y},t)}{\partial y_j}\right]P\right\} \\
&+ D\frac{\partial^2}{\partial y_i \partial y_j}\left\{\left[B_{ik}(\mathbf{y},t)B_{jk}(\mathbf{y},t)\right]P\right\}
\end{aligned}
\tag{B.4}
$$

which is entirely determined by the coefficients of the Langevin equation.

B.2 Dynamical equations for the averages: macroscopic equation

From the master equation one can derive the dynamical equations for the averages of a Markov stochastic process. Let us first write the equation for the time evolution of an arbitrary function $\langle f(\mathbf{y})\rangle$. First, one has ,

$$
\frac{d}{dt}\langle f(\mathbf{y})\rangle = \frac{d}{dt}\int d\mathbf{y} f(\mathbf{y})P(\mathbf{y},t) = \int d\mathbf{y} f(\mathbf{y})\frac{\partial}{\partial t}P(\mathbf{y},t) \tag{B.5}
$$

Applying the stochastic methods for the function $f(\mathbf{y}) = y_i$, we obtain

$$
\frac{d}{dt}\langle y_i\rangle = \left\langle a_i^{(1)}(\mathbf{y},t)\right\rangle \tag{B.6}
$$

Note that when $a_i^{(1)}$ is *linear* function of $\mathbf{y}$ one has $\left\langle a_i^{(1)}(\mathbf{y},t)\right\rangle = a_i^{(1)}(\langle\mathbf{y}\rangle,t)$, whence

$$
\frac{d}{dt}\langle y_i\rangle = a_i^{(1)}(\langle\mathbf{y}\rangle,t) \tag{B.7}
$$

which is a system of ordinary differential equations for $\langle\mathbf{y}\rangle$ and can be identified with the macroscopic equation of the system. On the other hand, when $a_i^{(1)}$ is

non-linear function of $\mathbf{y}$, Eq. (B.6) is not a differential equation for $\langle y_i \rangle$. Then Eq. (B.6) is not a closed equation for $\langle y_i \rangle$ but higher-order moments enter as well. Thus, the evolution of $\langle y_i \rangle$ in the course of time is not determined by $\langle y_i \rangle$ itself, but is also influenced by the fluctuations around this average. For instance, for $\langle y_i y_j \rangle$, on has

$$\frac{d}{dt}\langle y_i y_j \rangle = \left\langle a_{ij}^{(2)}(\mathbf{y},t) \right\rangle + \left\langle y_i a_j^{(1)}(\mathbf{y},t) \right\rangle + \left\langle y_j a_i^{(1)}(\mathbf{y},t) \right\rangle \tag{B.8}$$

However, if $a_{ij}^{(2)}$ is a non-linear function of $\mathbf{y}$, the equation involves even higher order moments, so what we have is an infinite hierarchy of coupled equations for the moments.

B.3 FPE for the classical LL Langevin equation.

For classical spins the stochastic Landau-Lifshitz is a Langevin equation which reads

$$\frac{d\mathbf{s}}{dt} = \gamma \left[\mathbf{s} \times (\mathbf{H} + \boldsymbol{\xi})\right] - \gamma\alpha \left[\mathbf{s} \times [\mathbf{s} \times \mathbf{H}]\right] \tag{B.9}$$

we rewrite the latter in components upon rewriting the vector products using the Levi-Civita fully antisymmetric unit tensor ϵ_{ijk}

$$\frac{ds_i}{dt} = \gamma\epsilon_{ijk}s_j H_k - \gamma\alpha\epsilon_{ijk}\epsilon_{lmn}s_j s_m H_n + \gamma\epsilon_{ijk}s_j\xi_k \tag{B.10}$$

Now, the stochastic Landau-Lifshitz equation, can be cast into the form of the general system of Langevin equations (B.1), by identifying

$$A_i(\mathbf{s},t) = \gamma\epsilon_{ijk}s_j H_k - \gamma\alpha\epsilon_{ijk}\epsilon_{lmn}s_j s_m H_n, \quad B_{ik}(\mathbf{s},t) = \gamma\epsilon_{ijk}s_j \tag{B.11}$$

To calculate the noise-induced drift coefficient of the FPE (the term accompanying A_i in (B.4) we need the derivative of the diffusion coefficient

$$\frac{\partial B_{ik}}{\partial s_j} = \gamma\epsilon_{ijk} \tag{B.12}$$

and, finally using the contraction property of Levi-Civita unit tensor $\epsilon_{jlk}\epsilon_{ijk} = -2\delta_{il}$

$$B_{jk}\frac{\partial B_{ik}}{\partial s_j} = \epsilon_{jlk}\epsilon_{ijk}s_l = -2\gamma^2\delta_{il}s_l \tag{B.13}$$

First of all, we calculate $a_i^{(1)}(\mathbf{s},t)$,

$$a_i^{(1)}(\mathbf{s},t) = \gamma\epsilon_{ijk}s_jH_k - \gamma\alpha\epsilon_{ijk}\epsilon_{lmn}s_js_mH_n - 2\gamma^2D\delta_{il}s_l \tag{B.14}$$

then $a_{ij}^{(2)}(\mathbf{s},t)$,

$$a_{ij}^{(2)}(\mathbf{s},t) = 2DB_{ik}(\mathbf{s},t)B_{jk}(\mathbf{s},t) = 2D\left(s^2\delta_{ij} - s_is_j\right) \tag{B.15}$$

Now we can write down the FPE for LL-Langevin equation (B.10) as

$$\begin{aligned}\frac{\partial P}{\partial t} &= -\frac{\partial}{\partial y_i}\left\{\left[\gamma\epsilon_{ijk}s_jH_k - \gamma\alpha\epsilon_{ijk}\epsilon_{lmn}s_js_mH_n - 2\gamma^2D\delta_{il}s_l\right]P\right\} \\ &+ D\frac{\partial^2}{\partial y_i\partial y_j}\left\{\left[2\left(s^2\delta_{ij} - s_is_j\right)\right]P\right\}\end{aligned} \tag{B.16}$$

which can be written in vectorial form as Eq. (C.2):

$$\frac{\partial f}{\partial t} + \frac{\partial}{\partial \mathbf{N}}\left\{\gamma[\mathbf{N}\times\mathbf{H}] - \gamma\lambda[\mathbf{N}\times[\mathbf{N}\times\mathbf{H}]] + \frac{\gamma\lambda T}{\mu_0}\left[\mathbf{N}\times\left[\mathbf{N}\times\frac{\partial}{\partial\mathbf{N}}\right]\right]\right\}f = 0 \tag{B.17}$$

at this moment we can derive the equation of motion for the spin polarization of an assembly of magnetic moments using (B.6). then, the time evolution of the average $\langle\mathbf{s}\rangle$ reads

$$\frac{d\langle\mathbf{s}\rangle_i}{dt} = \gamma\epsilon_{ijk}\langle s_j\rangle H_k - \gamma\alpha\epsilon_{ijk}\epsilon_{lmn}\langle s_js_m\rangle H_n - 2D\gamma^2\langle s_i\rangle \tag{B.18}$$

where $\Lambda_N = 2\gamma\alpha k_BT/\mu_0$ is the characteristic diffusional relaxation rate. It is more convenient to write Eq. (B.18) in vectorial form

$$\frac{d\mathbf{m}}{dt} = \gamma[\mathbf{m}\times\mathbf{H}] - \Lambda_N\mathbf{m} - \gamma\lambda\langle[\mathbf{s}\times[\mathbf{s}\times\mathbf{H}]]\rangle \tag{B.19}$$

Appendix C

One Spin LLB equation

We develop Garanin's derivation of the LLB equation. In the case of a weak coupling with the bath the dynamics of the vector $\mathbf{s}$ can be described with the help of the stochastic Landau-Lifshitz equation

$$\frac{d\mathbf{s}}{dt} = \gamma\left[\mathbf{s}\times(\mathbf{H}+\boldsymbol{\zeta})\right] - \gamma\lambda\left[\mathbf{s}\times[\mathbf{s}\times\mathbf{H}]\right], \tag{C.1}$$

to date, the correlators of the $\alpha,\beta = x,y,z$ components of the Langevin field $\boldsymbol{\zeta}(t)$ are given by

$$\langle\boldsymbol{\zeta}(t)\rangle = 0 \quad \text{and} \quad \langle\zeta(t)\zeta(t)\rangle = 2\frac{\lambda k_B T}{\gamma\mu_0}\delta(t-t').$$

The Fokker-Plank equation corresponding to Eq. (C.1) is formulated for the distribution function $f(\mathbf{N},t) = \langle\delta(\mathbf{N}-\mathbf{s}(t))\rangle$ in the sphere $|\mathbf{N}| = 1$ where the average is taken over the realization of $\boldsymbol{\zeta}$. Differentiating f over t with the use of Eq. (C.1) and calculating the right part with the methods of stochastic theory (see Appendix B), one comes to the Fokker-Planck equation

$$\frac{\partial f}{\partial t} + \frac{\partial}{\partial\mathbf{N}}\left\{\gamma[\mathbf{N}\times\mathbf{H}] - \gamma\lambda[\mathbf{N}\times[\mathbf{N}\times\mathbf{H}]] + \frac{\gamma\lambda T}{\mu_0}\left[\mathbf{N}\times\left[\mathbf{N}\times\frac{\partial}{\partial\mathbf{N}}\right]\right]\right\} f = 0. \tag{C.2}$$

One can easily see that the distribution function

$$f_0(\mathbf{N}) \propto \exp[-\mathcal{H}/k_B T], \quad \mathcal{H}(\mathbf{s}) = -\mu_0\mathbf{H}\mathbf{s}, \tag{C.3}$$

satisfies Eq. (C.2) at an equilibrium. The equation of motion for the spin polarization (the first moment of the distribution function)

$$\mathbf{m} \equiv \langle \mathbf{s} \rangle = \int d^3N \, \mathbf{N} f(\mathbf{N}, t), \tag{C.4}$$

of an assembly of magnetic atoms can be derived from Eq. (C.2) and has the form (see Appendix B)

$$\frac{d\mathbf{m}}{dt} = \gamma[\mathbf{m} \times \mathbf{H}] - \Lambda_N \mathbf{m} - \gamma\lambda \left\langle [\mathbf{s} \times [\mathbf{s} \times \mathbf{H}]] \right\rangle . \tag{C.5}$$

It can be seen that Eq. (C.5) is not closed but coupled to the second moments of the distribution function, $\langle s_i s_j \rangle$, in its last term. In the next paragraphs we will focus in this term and how to approximate it for a non-equilibrium situation. For an isolated magnetic moment the dynamical behaviour is determined by the reduced field $\boldsymbol{\xi}_0 = \frac{\mu_0 \mathbf{H}}{k_B T}$

Paramagnet

One can obtain an *isolated* equation of motion for the spin polarization of an assembly of magnetic atoms choosing the distribution function in a form

$$f(\mathbf{N}) = \frac{\exp\left[\boldsymbol{\xi_0} \cdot \mathbf{N}\right]}{\mathcal{Z}(\xi_0)}, \quad \mathcal{Z} = 4\pi \frac{\sinh \xi_0}{\xi_0}. \tag{C.6}$$

Let us consider the distribution function $f = \exp(\boldsymbol{\xi} \cdot \mathbf{N})/\mathcal{Z}(\xi)$, where $\boldsymbol{\xi}$ is a non-equilibrium reduced field. We can use the fact that

$$\mathcal{Z}(\xi) = \int d^3N \, \exp(\boldsymbol{\xi} \cdot \mathbf{N}) \quad \widetilde{m}_i = \int d^3N \, N_i f(\mathbf{N}, t) = B(\xi) \frac{\xi_i}{\xi}. \tag{C.7}$$

We derive the partition function $\mathcal{Z}(\xi)$ with respect to ξ_i and obtain

$$\frac{\partial \mathcal{Z}(\xi)}{\partial \xi_i} = \frac{\partial}{\partial \xi_i} \int d^3N \, \exp(\boldsymbol{\xi} \cdot \mathbf{N}) = \mathcal{Z}(\xi) \widetilde{m}_i \tag{C.8}$$

Now, we derive the obtained $\frac{\partial \mathcal{Z}(\xi)}{\partial \xi_i}$ with respect to the component ξ_k

$$\frac{\partial}{\partial \xi_k} \frac{\partial \mathcal{Z}(\xi)}{\partial \xi_i} = \frac{\partial}{\partial \xi_k} \mathcal{Z}(\xi) \widetilde{m}_i = \mathcal{Z}(\xi) \left\{ \widetilde{m}_k \widetilde{m}_i + \int d^3N \, N_i \frac{\partial}{\partial \xi_k} f(\mathbf{N}, t) \right\} \tag{C.9}$$

we also calculate the expression for $\frac{\partial}{\partial \xi_k} f(\mathbf{N}, t)$

$$\frac{\partial}{\partial \xi_k} f(\mathbf{N},t) = \frac{\partial}{\partial \xi_k} \exp(\boldsymbol{\xi}\cdot\mathbf{N})/\mathcal{Z}(\xi) = N_k f(\mathbf{N},t) - f(\mathbf{N},t)\widetilde{m}_k, \tag{C.10}$$

we put this result into Eq. (C.9) and we obtain the second moment distribution $\langle s_i s_k\rangle$ as a function of the partition function

$$\langle s_i s_k\rangle = \frac{1}{\mathcal{Z}(\xi)} \frac{\partial}{\partial \xi_k} \frac{\partial \mathcal{Z}(\xi)}{\partial \xi_i} \tag{C.11}$$

We now calculate explicitly $\langle s_i s_k\rangle$ via partition function

$$\frac{\partial}{\partial \xi_k}\frac{\partial \mathcal{Z}(\xi)}{\partial \xi_i} = \frac{\partial}{\partial \xi_k}\mathcal{Z}(\xi)B(\xi)\frac{\xi_i}{\xi} = \mathcal{Z}(\xi)\frac{\partial}{\partial \xi_k}B(\xi)\frac{\xi_i}{\xi} + \widetilde{m}_i \frac{\partial}{\partial \xi_k}\mathcal{Z}(\xi) = \mathcal{Z}(\xi)\left\{\frac{\partial}{\partial \xi_k}B(\xi)\frac{\xi_i}{\xi} + \widetilde{m}_i\widetilde{m}_k\right\}, \tag{C.12}$$

and we make use of the following relations

$$\frac{\partial}{\partial \xi_k} \quad B(\xi)\tfrac{\xi_i}{\xi} = \quad \left(B'(\xi) - \frac{B(\xi)}{\xi}\right)\frac{\xi_k\xi_i}{\xi^2} + \frac{B(\xi)}{\xi}\delta_{ik}$$

and the property of the Langevin function, $B^2 = 1 - B' - 2B/\xi$, we arrive to

$$\begin{aligned} \langle s_i s_k\rangle &= \left\{\frac{\partial}{\partial \xi_k}B(\xi)\frac{\xi_i}{\xi} + \widetilde{m}_i\widetilde{m}_k\right\} && \text{(C.13)} \\ &= \frac{B(\xi)}{\xi}\left\{\left(\frac{\xi}{B(\xi)} - 3\right)\frac{\xi_k\xi_i}{\xi^2} + \delta_{ik}\right\}. && \text{(C.14)} \end{aligned}$$

We write Eq. (C.5) in a compact form

$$\frac{dm_i}{dt} = \gamma\epsilon_{ijk}\langle s_j\rangle H_k - \frac{\Lambda_N}{2}\epsilon_{ijn}\epsilon_{lmn}\langle s_j s_m\rangle \xi_{0n} - \Lambda_N\langle s_i\rangle \tag{C.15}$$

where Λ_N=$2\gamma\lambda k_B T/\mu_0$ and $\xi_{\mathbf{0}} = \mu_0\mathbf{H}/k_B T$. We use the Eq. (C.14) to write Eq. (C.15)

$$\frac{dm_i}{dt} = \gamma\epsilon_{ijk}m_j H_k - \Lambda_N m_i - \frac{m}{\xi}\frac{\Lambda_N}{2}\epsilon_{ijn}\epsilon_{lmn}\xi_{0n}\delta_{ik} - \frac{\Lambda_N}{2}\epsilon_{ijn}\epsilon_{lmn}\left(1 - \frac{3m}{\xi}\right)\frac{m_j m_m}{m^2}\xi_{0n} \tag{C.16}$$

using the mathematical relation $\epsilon_{ijn}\epsilon_{lmn}\delta_{jm} = 2\delta_{il}$ and the relation $-\epsilon_{ijn}\epsilon_{lmn}\xi_m\xi_j\xi_{0n} = \xi^2\xi_{0i} - (\xi_j\xi_{0j})\,\xi_i$ which can be transformed into

$$\xi_{0i} = \frac{(\xi_j\xi_{0j})}{\xi^2}\xi_i - \epsilon_{ijn}\epsilon_{lmn}\frac{\xi_m\xi_j}{\xi^2}\xi_{0n} \tag{C.17}$$

$$= \frac{(\mathbf{m}\boldsymbol{\xi}_0)}{m^2}m_i - \epsilon_{ijn}\epsilon_{lmn}\frac{m_m m_j}{m^2}\xi_{0n} \tag{C.18}$$

where we have used that $\xi_j/\xi = m_j/m$. We carefully arrange Eq. (C.16)

$$\frac{dm_i}{dt} = \gamma\epsilon_{ijk}m_jH_k - \Lambda_N\left(1 - \frac{\mathbf{m}\boldsymbol{\xi}_0}{m\xi}\right)m_i - \gamma\lambda\left(1 - \frac{m}{\xi}\right)\epsilon_{ijn}\epsilon_{lmn}\frac{m_m m_j}{m^2}H_n$$

which in vectorial notation reads

$$\frac{d\mathbf{m}}{dt} = \gamma[\mathbf{m}\times\mathbf{H}] - \Lambda_N\left(1 - \frac{\mathbf{m}\boldsymbol{\xi}_0}{m\xi}\right)\mathbf{m} - \gamma\lambda\left(1 - \frac{m}{\xi}\right)\frac{[\mathbf{m}\times[\mathbf{m}\times\mathbf{H}]]}{m^2} \tag{C.19}$$

For small deviations from equilibrium, where $\boldsymbol{\xi} \cong \boldsymbol{\xi}_0$ and, accordingly, $\mathbf{m} \cong \mathbf{m}_0 \equiv B(\xi_0)\boldsymbol{\xi}_0/\xi_0$, one can put the LLB equation into the form $\mathbf{H} = k_BT\boldsymbol{\xi}_0/\mu_0$

$$\mathbf{m} - \mathbf{m}_0 \approx B'(\xi_0)(\boldsymbol{\xi} - \boldsymbol{\xi}_0) \tag{C.20}$$

therefore we can write the longitudinal term in Eq. (C.19) as

$$\Lambda_N\left(1 - \frac{\mathbf{m}\boldsymbol{\xi}_0}{m\xi}\right) = \Lambda_N\left(\frac{\mathbf{m}(\boldsymbol{\xi} - \boldsymbol{\xi}_0)}{m\xi}\right) = \frac{\Lambda_N}{B'}\frac{B}{\xi}\left(\frac{m^2 - \mathbf{m}\mathbf{m}_0}{m\xi}\right) = \Gamma_1\left(1 - \frac{\mathbf{m}\mathbf{m}_0}{m^2}\right),$$

where $\Gamma_1 = \frac{\Lambda_N}{\xi B'}B$. The transverse part can be calculated directly

$$\frac{\gamma\lambda k_BT}{\mu_0}\left(1 - \frac{m}{\xi}\right)\frac{\xi_0}{B(\xi_0)}\frac{[\mathbf{m}\times[\mathbf{m}\times\mathbf{m}_0]]}{m^2} = \Gamma_2\frac{[\mathbf{m}\times[\mathbf{m}\times\mathbf{m}_0]]}{m^2} \tag{C.21}$$

where $\Gamma_2 = \frac{\Lambda_N}{2}\left(\frac{\xi_0}{B(\xi_0)} - 1\right)$. Finally, we get the following expression

$$\frac{d\mathbf{m}}{dt} = \gamma[\mathbf{m}\times\mathbf{H}] - \Gamma_1\left(1 - \frac{\mathbf{m}\mathbf{m}_0}{m^2}\right) - \Gamma_2\frac{[\mathbf{m}\times[\mathbf{m}\times\mathbf{m}_0]]}{m^2}. \tag{C.22}$$

Ferromagnet

We now consider the case where the magnetic moment are not isolated but exchange coupled. The interaction will be assumed to be as an isotropic interaction to first nearest neighbours. For shake of the simplicity we will consider the simple case where only and external field is applied. Then the Hamiltonian reads

$$\mathcal{H} = -\mu_0 \sum_i \mathbf{H}\mathbf{s}_i - \sum_{\langle ij \rangle} J\mathbf{s}_i \cdot \mathbf{s}_j \tag{C.23}$$

The exact treatment of the spin-spin correlations in Hamiltonian (C.23) is impossible, thus, Garanin made use of the mean-field approximation (MFA) for the description of each lattice site effective field. Then, the problem simplifies to the substitution of $\mathbf{H}$ by the corresponding MFA field. In the continuous approximation ($J_0 = zJ$) is given by

$$\mathbf{H}^{\mathrm{MFA}}(\mathbf{r}) \cong \mathbf{H}_E + \mathbf{H} = \frac{J_0}{\mu_0}\mathbf{m} + \mathbf{H} \tag{C.24}$$

The most important for ferromagnets is the case of the strong homogeneous exchange field, $|\mathbf{H}_E| \gg |\mathbf{H}|$, which is realized below $T_C = (1/3)J_0$ where there is a spontaneous magnetization, and also in the region just above T_C, thus we can consider the external field $\mathbf{H}$ as a perturbative term

$$\mathbf{H}^{\mathrm{MFA}}(\mathbf{r}) \cong \mathbf{H}_E \left(1 + \frac{\mathbf{H}_E \cdot \mathbf{H}}{H_E^2}\right). \tag{C.25}$$

The magnetization $\mathbf{m}_0$ in MFA reads

$$\mathbf{m}_0 = B(\xi_0)\frac{\boldsymbol{\xi}_0}{\xi_0}, \quad \boldsymbol{\xi}_0 \equiv \beta\mu_0\mathbf{H}^{\mathrm{MFA}} \tag{C.26}$$

we expand $B(\xi_0)$ up to the first order on $\mathbf{H}$

$$B(\xi_0) \cong B(\beta\mu_0\mathbf{H}_E) + B'(\beta\mu_0\mathbf{H}_E)\frac{\mathbf{H}_E \cdot \mathbf{H}}{H_E^2} \tag{C.27}$$

thereby

$$\mathbf{m}_0 = \left[B + B'\frac{\mathbf{H}_E \cdot \mathbf{H}}{H_E^2}\right]\frac{\mathbf{H}^{\mathrm{MFA}}}{H^{\mathrm{MFA}}}. \tag{C.28}$$

We make use of the fact that the inverse of the MFA field modulus can be written as

$$\frac{1}{H^{\mathrm{MFA}}} \cong \frac{1}{H_E}\left(1 - \frac{\mathbf{H}_E \cdot \mathbf{H}}{H_E^2}\right) \tag{C.29}$$

and we substitute Eq. (C.29) into Eq. (C.28)), and we use that $\mathbf{H}_E = J_0/\mu_0\mathbf{m}$ to finish up with

$$\mathbf{m}_0 \cong \frac{B}{m}\mathbf{m} + B'\beta\mu_0\frac{(\mathbf{m}\cdot\mathbf{H})\mathbf{m}}{m^2} - \frac{B\mu_0}{mJ_0}\frac{[[\mathbf{H}\times\mathbf{m}]\times\mathbf{m}]}{m^2}. \tag{C.30}$$

Transverse relaxation term

We work out the transverse relaxation rate given by Γ_2:

$$\Gamma_2 = \gamma\left[\lambda\left(1-\frac{B}{\xi}\right)\right]\left(\frac{m}{B}\right)\frac{J_0}{\mu_0}. \tag{C.31}$$

We define $\alpha_\perp = \lambda(1-\frac{B}{\xi})$ and substitute Eq. (C.30) into the transverse term in Eq. (C.21) to get

$$\Gamma_2\frac{[\mathbf{m}\times[\mathbf{m}\times\mathbf{m}_0]]}{m^2} = \gamma\alpha_\perp\frac{[\mathbf{m}\times[\mathbf{m}\times\mathbf{H}]]}{m^2}. \tag{C.32}$$

We calculate B/ξ appearing in both relaxation terms in Eq. (C.22). It can be easily approximated considering the fact that $\xi_0 = \beta\mu_0 H^{\mathrm{MFA}} \approx \beta J_0 m_0$, and using that $B(\xi_0) = m_0$ to obtain $B/\xi = \beta J_0$. In the MFA the following relation holds $J_0 = 3k_B T_C$, then it follows that $B/\xi = 3T_C/T$

Longitudinal relaxation term

We work out the longitudinal rate given by Γ_1. We insert $\mathbf{m}_0$ given by Eq. (C.30) into Eq. (C.21)

$$\Gamma_1\left(1-\frac{\mathbf{m}\mathbf{m}_0}{m^2}\right) = \gamma\alpha_\parallel\left(\frac{1-\frac{B}{m}}{\beta\mu_0 B'} - \frac{\mathbf{m}\cdot\mathbf{H}}{m^2}\right) \tag{C.33}$$

where $\alpha_\parallel = \lambda\xi/B = \lambda T/(3T_C)$. Next, we estimate the difference $1-B/m$ which is a small quantity proportional to the deviation from the equilibrium. We develop the function B around the equilibrium magnetization m_e up to the first order in $\delta m = m - m_e$

$$B(\xi) \cong B(\xi_e) + \beta J_0 B'(\xi_e)\delta m \tag{C.34}$$

dividing by m and subtracting it to 1

$$1 - \frac{B(\xi)}{m} \;\cong\; \frac{\delta m}{m}\left(1-\beta J_0 B'(\xi_e)\right) \tag{C.35}$$

where we have used $m_e = B(\xi_e)$. Now we develop around m_e^2 the function $\delta m/m$

$$\frac{\delta m}{m} \approx \frac{1}{2}\frac{(m^2 - m_e^2)}{m_e^2} \tag{C.36}$$

finally, the term $(1 - B/m)/\beta\mu_0 B'$ reads

$$\frac{1 - B/m}{\beta\mu_0 B'} \approx \frac{(1 - \beta J_0 B'(\xi_e))}{\beta\mu_0 B'}\frac{1}{2}\frac{(m^2 - m_e^2)}{m_e^2} = \frac{1}{2\widetilde{\chi_{||}}}\frac{(m^2 - m_e^2)}{m_e^2} \tag{C.37}$$

Eq. (C.33) can be now written as

$$\gamma\alpha_{\|}\left(\frac{1 - \frac{B}{m}}{\beta\mu_0 B'} - \frac{\mathbf{m}\cdot\mathbf{H}}{m^2}\right) = -\gamma\alpha_{\|}\left(\frac{\mathbf{m}\cdot\left(\frac{1}{2\widetilde{\chi}_{||}}\left(1 - \frac{m^2}{m_e^2}\right) + \mathbf{H}\right)\mathbf{m}}{m^2}\right) \tag{C.38}$$

Above T_C

Above Curie temperature we use the expansion $B(\xi) \simeq (\xi/3)(1 - \xi^2/15)$ and the fact that $\xi^2 \simeq 15\epsilon$ to obtain

$$\frac{B}{\xi} = \frac{\xi}{3}\frac{1 - \epsilon}{\xi} = \frac{T}{3T_C} \tag{C.39}$$

therefore we can write both relaxation parameters as

$$\alpha_{\|} = \alpha_{\perp} = 2\lambda\frac{T}{3T_C}. \tag{C.40}$$

On the other hand, close to T_C the longitudinal susceptibility can be approximated by $\widetilde{\chi}_{\|} \simeq (2\epsilon)^{-1}$ and equilibrium magnetization by $m_e^2 \simeq (5/3)\varepsilon$, where $\varepsilon = 1 - T/T_C$ then,

$$\frac{1 - B/m}{\beta\mu_0 B'} \approx \frac{J_0}{\mu_0}\left(\frac{3}{5}m^2 - \varepsilon\right) \tag{C.41}$$

The LLB equation for ferromagnets

Replacing the above derived expressions for the transverse and longitudinal relaxation, Eqs. (C.32) and (C.38), respectively, into Eq. C.22 we end up with the well-known LLB equation for ferromagnets:

$$\dot{\mathbf{m}} = \gamma[\mathbf{m} \times \mathbf{H}_{\text{eff}}] + \gamma\alpha_{\parallel}\frac{[\mathbf{m} \cdot \mathbf{H}_{\text{eff}}]\,\mathbf{m}}{m^2} - \gamma\alpha_{\perp}\frac{[\mathbf{m} \times [\mathbf{m} \times \mathbf{H}_{\text{eff}}]]}{m^2}. \tag{C.42}$$

The effective field has two different forms below and above T_C,

$$\mathbf{H}_{\text{eff}} = \mathbf{H} + \mathbf{H}_A + \begin{cases} \frac{1}{2\tilde{\chi}_{\parallel}}\left(1 - \frac{m^2}{m_e^2}\right)\mathbf{m} & T \lesssim T_C \\ -\frac{J_0}{\mu_0}\left(\frac{T}{T_C} - 1 + \frac{3}{5}m^2\right)\mathbf{m} & T \gtrsim T_C \end{cases} \tag{C.43}$$

The damping parameters below T_C reads

$$\alpha_{\parallel} = \frac{2}{3}\frac{T}{T_C}\lambda \quad \text{and} \quad \alpha_{\perp} = \lambda\left(1 - \frac{T}{3T_C}\right) \tag{C.44}$$

and at temperatures above Curie temperature, $T > T_C$, both damping parameters coincides

$$\alpha_{\perp} = \alpha_{\parallel} = \frac{2}{3}\frac{T}{T_C}\lambda. \tag{C.45}$$

Appendix D

Micromagnetic exchange stiffness

The micromagnetic exchange stiffness A calculation is quite tricky. In the work [12] we have calculated in detail the temperature dependence of the micromagnetic exchange parameter using both numerical (LLG-Langevin) and analytical techniques. As analytical technique we have used the so-called classical spectral density method (CSDM) [35]. In order to extract $A(T)$ from the LLG-Langevin simulations two methods were used. First, a domain wall into the system was forced assuming the well-known equations for the domain-wall width,

$$\delta(T) = \pi\sqrt{\frac{A(T)}{K(T)}} \tag{D.1}$$

and the free energy

$$\Delta F = 4\sqrt{A(T)K(T)} \tag{D.2}$$

hold even at finite temperature. Therefore, we calculated both $\delta(T)$ and $\Delta F(T)$ using the LLG-Langevin technique. From Eqs. (D.1) and (D.2) the micromagnetic exchange stiffness $A(T)$ as well as the anisotropy energy constant $K(T)$ were obtained. For a more detailed description of the applied methods see Refs. [81] and [78]. Interestingly, a scaling behaviour $A(m) \sim m^{\kappa}$ (see Table D.1) was found at low temperatures.

Secondly, we evaluated $A(T)$ via LLG-Langevin dynamics simulation of thermally excited spin waves (SW). The random thermal field introduces correlated magnetization fluctuations. These can be analyzed via a Fourier analysis, both in space and time, by transforming the magnetization fluctuations around the equilibrium direction. The power spectral density $F(\mathbf{q}, \omega)$ is presented in Fig. D.2 for four different characteristic temperature region and for a fixed wave vector $\mathbf{q} = [0, 0, \pi/4]$. The mode intensities were fitted by the Lorentzian profile from which the resonance frequency of each mode is extracted and finally the dispersion

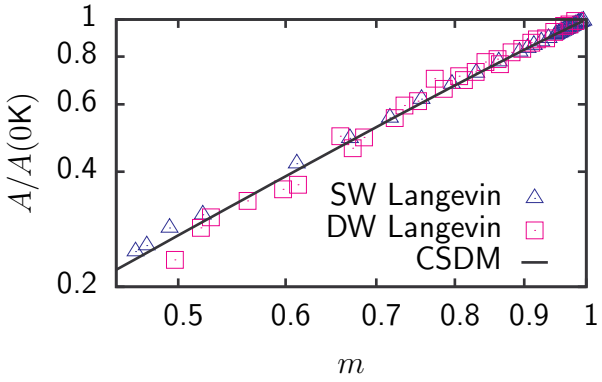

Figure D.1: Scaling behaviour of the exchange stiffness (DW Langevin) as obtained from the domain-wall free energy. The solid line is the solution of the analytical CSDM [12]. The SW Langevin points are obtained from the SW stiffness approach based on the atomistic LLG-Langevin simulations.

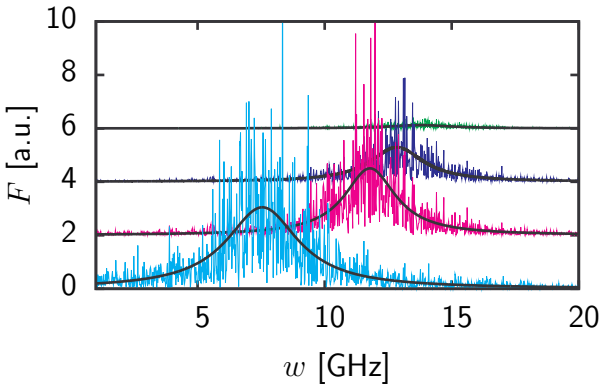

Figure D.2: Power spectrum density as a function of frequency for thermally excited SW of a Heisenberg Hamiltonian for various temperatures $T = T_C/70$, $T = T_C/4$, $T = T_C/2$ and $T = 0.9T_C$ for a fixed wave vector $\mathbf{q} = [0, 0, \pi/4]$.

relation $\omega_{\mathbf{q}}$ was constructed. We assumed the following temperature-dependent dispersion relation for the LLG Langevin simulated SWs,

$$\frac{\omega_{\mathbf{q}(T)}}{\gamma} = H + \frac{A(T)}{M_s(T)a^2}\left(1 - \gamma_{\mathbf{q}}\right). \tag{D.3}$$

By fitting our numerical dispersion relation to this expression, we were able to extract $A(T)$. The results are presented in Fig. D.1 as a function of the equilibrium magnetization $m(T)$. Once again, a scaling behaviour $A(m) \sim m^{\kappa}$ (see Table D.1) was found, coinciding with the results based on the numerical evaluation of the domain-wall stiffness.

	W	G	ε	κ
sc	1.5164	0.52	0.343	1.66
bcc	1.393	0.3965	0.2847	1.715
fcc	1.3446	0.343	0.255	1.745
FePt	1.317	0.3175	0.24	1.76

Table D.1: Geometrical factors and values of the scaling exponents ε and $\kappa = 2 - \varepsilon$ for different lattice structures and for the particular case of the full *ab initio* parametrized FePt Hamiltonian.

Finally, the theoretical formalism known as the CSDM [35] was used to analytically calculate the dispersion relation of the thermally excited SWs [12]. After some algebra the dispersion relation reduced to

$$\omega_{\mathbf{q}} = \omega_0 + m\mathcal{Q}(m)J_0\left(1 - \gamma_{\mathbf{q}}\right) \tag{D.4}$$

where the function $\mathcal{Q}(m)$ can be approximated at low enough temperatures as $\mathcal{Q}(m) = m^{-\epsilon}$ where $\epsilon = G(\varsigma)/W(\varsigma)$. The lattice sums $W(\varsigma)$ and $G(\varsigma)$ are defined according to

$$W(\varsigma) = \frac{1}{\mathcal{N}}\sum_{\mathbf{q}}\frac{1}{1-\varsigma\gamma_{\mathbf{q}}}, \quad G(\varsigma) = \frac{1}{\mathcal{N}}\sum_{\mathbf{q}}\frac{\gamma_{\mathbf{q}}}{1-\varsigma\gamma_{\mathbf{q}}} \tag{D.5}$$

where $\varsigma = J_0/(\omega_0 + J_0)$. For usual materials $\omega_0 \ll J_0$ and $\varsigma \approx 1$. Analogously to the SW Langevin approach the micromagnetic exchange stiffness at low temperatures is defined by

$$A(T) \propto \mathcal{Q}(m)m^2 \propto m^{2-\epsilon} \tag{D.6}$$

Thus, the scaling exponent dependent on the lattice structure. The values of W, G and scaling exponents, ϵ and κ, are presented in Table D.1 for sc, bcc, fcc and FePt structures. A complete study can be found in Ref. [12].

References

[1] **http://math.nist.gov/oommf/**. 12

[2] Y. Acremann, J. P. Strachan, V. Chembrolu, S. D. Andrews, T. Tyliszczak, J. A. Katine, M. J. Carey, B. M. Clemens, H. C. Siegmann, and J. Stöhr. **Time-Resolved Imaging of Spin Transfer Switching: Beyond the Macrospin Concept**. *Phys. Rev. Lett.*, **96**:217202, May 2006. 95

[3] M. Aeschlimann, M. Bauer, S. Pawlik, W. Weber, R. Burgermeister, D. Oberli, and H. C. Siegmann. **Ultrafast spin-dependent electron dynamics in fcc Co**. *Phys. Rev. Lett.*, **79**:5158, 1997. 2, 4

[4] M. Aeschlimann, A. Vaterlaus, M. Lutz, M. Stampanoni, and F. Meier. **Ultrafast thermomagnetic writing processes in rareearth transition-metal thin films**. *Journal of Applied Physics*, **67**:4438, 1990. 9

[5] M. B. Agranat, S. I. Ashitkov, A. B. Granovski, and G. I. Rukman. *Zh. Exp. Teor. Fiz.*, **86**:1376, 1984. 3

[6] P. B. Allen. **Theory of thermal relaxation of electrons in metals**. *Phys. Rev. Lett.*, **59**:1460, 1987. 16, 22, 47

[7] N. W. Ashcroft and N. D. Mermin. *Solid State Physics*. Brooks Cole;, 1976. 21

[8] A. Aspelmeier, F. Gerhardter, and K. Baberschke. **Magnetism and structure of ultrathin Gd films**. *J. Magn. Magn. Mat.*, **132**(1):22, Apr 1994. 75

[9] P. Asselin, R. F. L. Evans, J. Barker, R. W. Chantrell, R. Yanes, O. Chubykalo-Fesenko, D. Hinzke, and U. Nowak. **Constrained Monte Carlo method and calculation of the temperature dependence of magnetic anisotropy**. *Phys. Rev. B*, **82**:054415, Aug 2010. 35

[10] U. Atxitia, O. Chubykalo-Fesenko, N. Kazantseva, D. Hinzke, U. Nowak, and R. W. Chantrell. **LLB-Micromagnetic modelling of**

laser-induced magnetisation dynamics. *Appl. Phys. Lett.* , **91**:232507, 2007. 4, 12, 16, 33, 37, 58, 60, 62, 96

[11] U. Atxitia, O. Chubykalo-Fesenko, J. Walowski, A. Mann, and M. Münzenberg. **Evidence for thermal mechanisms in laser-induced femtosecond spin dynamics**. *Phys. Rev. B*, **81**(17):174401, May 2010. 4, 6, 24, 39, 57, 62, 66, 67, 68, 69, 73

[12] U. Atxitia, D. Hinzke, O. Chubykalo-Fesenko, U. Nowak, H. Kachkachi, O. N. Mryasov, R. F. Evans, and R. W. Chantrell. **Multiscale modeling of magnetic materials: Temperature dependence of the exchange stiffness**. *Phys. Rev. B*, **82**:134440, Oct 2010. 35, 37, 175, 176, 177

[13] C. H. Back, R. Allenspach, W. Weber, S. S. P. Parkin, D. Weller, E. L. Garwin, and H. C. Siegmann. **Minimum Field Strength in Precessional Magnetization Reversal**. *Science*, **285**:864, 1999. 95

[14] C. H. Back, D. Weller, J. Heodmann, D. Mauri, D. Guarisco, E. L. Garwin, and H. C. Siegmann. **Magnetization reversal in ultrashort magnetic field pulses**. *Phys. Rev. Lett.*, **81**:3251, 1998. 2

[15] T. Balashov, A. F. Takács, M. Däne, A. Ernst, P. Bruno, and W. Wulfhekel. **Inelastic electron-magnon interaction and spin transfer torque**. *Phys. Rev. B*, **78**(17):174404, Nov 2008. 6, 57

[16] V. G. Baryakhtar. **Crystal symmetry and structure of relaxation terms in the dynamic equations of motion for antiferromagnetics**. *Zhurnal Eksperimentalnoi i Teoreticheskoi Fiziki*, **94**:196, 1988. 113, 114

[17] R. Bastardis, U. Atxitia, O. Chubykalo-Fesenko, and H. Kachkachi. **Unified decoupling scheme for exchange and anisotropy contributions and temperature-dependent spectral properties of anisotropic spin systems**. sumitted. 32, 36

[18] M. Battiato, K. Carva, and P. M. Oppeneer. **Superdiffusive Spin Transport as a Mechanism of Ultrafast Demagnetization**. *Phys. Rev. Lett.*, **105**(2):027203, Jul 2010. 5, 7, 18, 41, 71, 73, 75

[19] E. Beaurepaire, J.-C. Merle, A. Daunois, and J. Y. Bigot. **Ultrafast spins dynamics in ferromagnetic nickel**. *Phys. Rev. Lett.*, **76**:4250, 1996. ii, iii, 2, 3, 4, 5, 16, 21, 22, 41, 95, 149

[20] L. Berger. **Emission of spin waves by a magnetic multilayer traversed by a current**. *Phys. Rev. B*, **54**:9353–9358, Oct 1996. 2, 8

[21] D. Berkov. **Theory of thermal fluctuations and fluctuation/dissipation theorem**. In H. Kronmüller and S. Parkin, editors, *The Handbook of Magnetism and Advanced Magnetic Materials*. John Wiley & Sons Ltd., Sussex, 2006. 26

[22] S. M. Bhagat and P. Lubitz. **Temperature variation of ferromagnetic relaxation in the 3*d* transition metals**. *Phys. Rev. B*, **10**(1):179–185, Jul 1974. 30, 69

[23] J.-Y. Bigot, V. Mircea, and E. Beaurepaire. **Coherent ultrafast magnetism induced by femtosecond laser pulses**. *Nat. Phys.*, **5**:515–520, 2009. 15, 16, 17, 41

[24] J.-Y. Bigot, M. Vomir, L.H.F. Andrade, and E. Beaurepaire. **Ultrafast magnetization dynamics in ferromagnetic cobalt: The role of the anisotropy**. *Chemical Physics*, **318**:137, 2005. 3, 9, 16

[25] C. Boeglin, E. Beaurepaire, V. Halté, V. López-Flores, N. Pontius C. Stamm, H. A. Drr, and J.-Y. Bigot. **Distinguishing the ultrafast dynamics of spin and orbital moments in solids**. *Nature*, **465**:458, 2010. 15

[26] U. Bovensiepen. **Coherent and incoherent excitations of the Gd(0001) surface on ultrafast timescales**. *J. Phys.: Condens. Mat.*, **19**:083201, 2007. 4, 16, 17, 18, 74, 75, 78, 80

[27] R. M. Bozorth. *Ferromagnetism*. IEEE Press, New York, 2003. 100

[28] M. Braun, R. Kohlhaas, and O. Vollmer. **High Temperature Calorimetry of Metals**. *Z. Angew. Phys.*, **25**:365, 1968. 47

[29] S. D. Brorson, J. G. Fujimoto, and E. P. Ippen. **Femtosecond electronic heat-transport dynamics in thin gold films**. *Phys. Rev. Lett.*, **59**:1962–1965, Oct 1987. 18

[30] W. F. Brown. *Micromagnetics*. Wiley, New York, 1963. 11

[31] W. F. Brown. **Thermal Fluctuations of a single-domain particle**. *Phys. Rev.*, **130**:1677, 1963. 12, 25, 26, 143

[32] K. H. J. Buschow and F. R. de Boer. *Physics of Magnetism and Magnetic Materials*. Kluwer Academic, New York, 2003. 98

[33] A. P. Caffrey, P. E. Hopkins, J. M. Klopf, and P. M. Norris. **Thin film non-noble transition metal thermophysical properties**. *Microscale Thermophysics. Eng.*, **9**:365, 2005. 48

[34] H. Callen and E. Callen. **The present status of the temperature dependence of magnetocrystalline anisotropy, and the l(l+1)/2 law**. *J. Phys. Chem. Solids*, **27**:1271, 1966. 36, 38

[35] L. S. Campana, A. Caramico D'Auria, M. D'Ambrosio, U. Esposito, L. De Cesare, and G. Kamieniarz. **Spectral-density method for classical systems: Heisenberg ferromagnet**. *Phys. Rev. B*, **30**:2769–2775, Sep 1984. 175, 177

[36] E. Carpene, E. Mancini, C. Dallera, M. Brenna, E. Puppin, and S. De Silvestri. **Dynamics of electron-magnon interaction and ultrafast demagnetization in thin iron films**. *Phys. Rev. B*, **78**:174422, 2008. 2, 53, 68, 69

[37] R. W. Chantrell, M. Wongsam, T. Schrefl, and J. Fidler. **Micromagnetics I: Basic principles**. In K. H. J. Buschow, R. W. Cahn, M. C. Flemings, B. Ilschner, E. J. Kramer, and S. Mahajan, editors, *Encyclopedia of Materials: Science and Technology*. Elsevier, Amsterdam, 2001. 11

[38] Kun Chen and D. P. Landau. **Spin-dynamics study of the dynamic critical behavior of the three-dimensional classical Heisenberg ferromagnet**. *Phys. Rev. B*, **49**(5):3266–3274, Feb 1994. 53

[39] O. Chubykalo, J. D. Hannay, M. A. Wongsam, R. W. Chantrell, and J. M. González. **Langevin dynamic simulation of spin waves in a micromagnetic model**. *Phys. Rev. B*, **65**:184428, 2002. 26

[40] O. Chubykalo, R. Smirnov-Rueda, M. A. Wongsam, R. W. Chantrell, U. Nowak, and J. M. González. **Brownian dynamics approach to interacting magnetic moments**. *J. Magn. Magn. Mat.*, **266**:28, 2003. 12, 26, 145, 147

[41] O. Chubykalo-Fesenko, U. Nowak, R. W. Chantrell, and D. Garanin. **Dynamic approach for micromagnetics close to the Curie temperature**. *Phys. Rev. B*, **74**:094436, 2006. 12, 28, 29, 30, 53, 58, 60, 61, 91, 149

[42] M. Cinchetti, M. Snchez Albaneda, D. Hoffmann, T. Roth, J.-P. Wstenberg, M. Krauss, O. Andreyev, H. C. Schneider, M. Bauer, and M. Aeschlimann. **Spin-Flip Processes and Ultrafast Magnetization Dynamics in Co: Unifying the Microscopic and Macroscopic View of Femtosecond Magnetism**. *Phys. Rev. Lett.*, **97**:177201, 2006. 53

[43] B. D. Cullity. *Introduction to Magnetic Materials*. Addison-Wesley, Menlo Park, California, 1972. 68

[44] C. W. Gardiner. *Handbook of Stochastic Methods*. Springer, Berlin, 1990. 26

[45] Łukasz Cywiński and L. J. Sham. **Ultrafast demagnetization in the $sp-d$ model: A theoretical study**. *Phys. Rev. B*, **76**(4):045205, Jul 2007. 80, 84, 85, 88

[46] D. A. Garanin. **Generalized Equation of Motion for a Ferromagnet**. *Physica A*, **172**:470, 1991. 28, 58, 59, 81, 82, 83

[47] D. A. Garanin. **Fokker - Planck and Landau - Lifshitz - Bloch equation for classical ferromagnets**. *Phys. Rev. B*, **55**:3050, 1997. 12, 53, 119, 154

[48] F. Dalla Longa, J. T. Kohlhepp, W. J. M. de Jonge, and B. Koopmans. **Influence of photon angular momentum on ultrafast demagnetization in nickel**. *Phys. Rev. B*, **75**(22):224431, Jun 2007. 51

[49] T. Devolder, A. Tulapurkar, Y. Suzuki, C. Chappert, P Crozat, and K Yagami. **Temperature study of the spin-transfer switching speed from dc to 100 ps**. *J. Appl. Phys.*, **98**:053904, 2005. 95

[50] G. Dewar, B. Heinrich, and J. F. Cochran. **Ferromagnetic antiresonance transmission of 24GHz radiation through Nickel**. *Can. J. Phys.*, **55**:821, 1977. 69

[51] P. A. M. Dirac. **On the theory of quantum mechanics.** *Proc. Roy. Soc.*, **112A**:661, 1926. 159

[52] M. Djordjevic, M. Lüttich, P. Moschkau, P. Guderian, T. Kampfrath, R. G. Ulbrich, M. Münzenberg, W. Felsch, and J. S. Moodera. **Comprehensive view on ultrafast dynamics of ferromagnetic films**. *Phys. Status Solidi C*, **3**:1347, 2006. 47, 49, 50

[53] Marija Djordjevic and Markus Münzenberg. **Connecting the timescales in picosecond remagnetization experiments**. *Phys. Rev. B*, **75**:012404, Jan 2007. 144

[54] S. M. Harrel M. C. Beard J.-Y. Bigot E. Beaurepaire, G. M. Turner and C. A. Schmuttenmaer. **Coherent terahertz emission from ferromagnetic films excited by femtosecond laser pulses**. *App. Phys. Lett.*, **84**, 2004. 57

[55] D. M: Edwards and F. A. Hertz. *J. Phys. F. Met. Phys.*, **3**:2191, 1973. 6

[56] R. J. Elliott. **Theory of the Effect of Spin-Orbit Coupling on Magnetic Resonance in Some Semiconductors**. *Phys. Rev.*, **96**(2):266–279, Oct 1954. 5

[57] M. Sultan et al. **unpublished**. 90

[58] R. F. L. Evans, D. Hinzke, U. Atxitia, U. Nowak, R. W. Chantrell, and O. Chubykalo-Fesenko. **Stochastic form of the Landau-Lifshitz-Bloch equation**. *Phys. Rev. B*, **85**:014433, Jan 2012. 33

[59] F. Bloch. **Zur Theorie des Austauschproblems und der Remanenzerscheinung der Ferromagnetika**. *Z. Physik*, **74**:295, 1932. 159

[60] M. Fähnle and C. Illg. **Electron theory of fast and ultrafast dissipative magnetization dynamics**. *Journal of Physics: Condensed Matter*, **23**:493201, 2011. 15

[61] Manfred Fähnle, Jonas Seib, and Christian Illg. **Relating Gilbert damping and ultrafast laser-induced demagnetization**. *Phys. Rev. B*, **82**:144405, Oct 2010. 70

[62] J. Fidler and T. Schrefl. **Micromagnetic modelling — the current state of the art**. *J. Phys. D: Appl. Phys.*, **33**:R135, 2000. 11

[63] M. Djordjevic G. X. Miao A. Gupta-A. V. Ramos K. Gehrke Moshnyaga K. Samwer J. Schmalhorst A. Thomas A. Hütten G. Reiss J. S. Moodera G. M. Müller, J. Walowski and M. Münzenberg. **Spin polarization in half-metals probed by femtosecond spin excitation**. *Nature Mat.*, **8**:56, 2009. 2, 66, 71

[64] D. A. Garanin. **Fokker-Planck and Landau-Lifshitz-Bloch equations for classical ferromagnets**. *Phys. Rev. B*, **55**:3050–3057, February 1997. iii, 28, 30, 31, 95, 104

[65] D. A. Garanin and O. Chubykalo-Fesenko. **Thermal fluctuations and longitudinal relaxation of single-domain magnetic particles at elevated temperatures**. *Phys. Rev. B*, **70**:212409, 2004. 32, 59, 60

[66] D. A. Garanin and H. Kachkachi. **Magnetization reversal via internal spin waves in magnetic nanoparticles**. *Phys. Rev. B*, **80**:014420, Jul 2009. 115

[67] J. L. García-Palacios and F. J. Lázaro. **Langevin-dynamics study of the dynamical properties of small magnetic particles**. *Phys. Rev. B*, **58**:14937, 1998. 26, 148

[68] T. Gilbert. **A phenomenological Theory of Damping in Ferromagnetic Materials**. *IEEE Trans. Magn.*, **40**:6, 2004. 12

[69] K. Gilmore, Y. U. Idzerda, and M. D. Stiles. **Identification of the Dominant Precession-Damping Mechanism in Fe, Co, and Ni by First-Principles Calculations**. *Phys. Rev. Lett.*, **99**(2):027204, Jul 2007. 55, 56, 60

[70] G. Grimvall. *The Electron-Phonon Interaction.* North-Holland Publishing Co., 1981. 16

[71] G. Grinstein and R. H. Koch. **Coarse Graining in Micromagnetics**. *Phys. Rev. Lett.*, **90**:207201, May 2003. 12, 27

[72] J. Güdde, U. Conrad, V. Jähnke, J. Hohlfeld, and E. Matthias. **Magnetization dynamics of Ni and Co films on Cu(001) and of bulk nickel surfaces**. *Phys. Rev. B*, **59**:R6608–R6611, Mar 1999. 3

[73] A. G. Gurevich and G. A. Melkov. *Magnetization Oscillations and Waves.* CRC Press, Boca Raton, Florida, 1996. 121, 122, 125, 127, 142

[74] P. Hansen, C. Clausen, G. Much, and M. Rosenkranz. **Magnetic and Magneto-optical properties of rare-earth transition-metal alloys containing Gd, Tb, Fe, Co**. *J. Appl. Phys.*, **66**:756–766, 1989. 102

[75] H. Hasegawa. **Dynamics of the Langevin model subjected to colored noise: Functional-integral method**. *Physica A*, **387**:1404, 2008. 145

[76] B. Heinrich, J. F. Cochran, M. Kowalewski, J. Kirschner, Z. Celinski, A. S. Arrott, and K. Myrtle. **Magnetic anisotropies and exchange coupling in ultrathin fcc Co(001) structures**. *Phys. Rev. B*, **44**:9348–9361, Nov 1991. 69

[77] W. Heisenberg. **Zur Theorie des Ferromagnetismus**. *Z. Physik*, **49**:619, 1928. 159, 160

[78] D. Hinzke, N. Kazantseva, U. Nowak, O. N. Mryasov, P. Asselin, and R. W. Chantrell. **Domain wall properties of FePt: from Bloch to lonear walls**. *Phys. Rev. B*, 2008. 175

[79] D. Hinzke and U. Nowak. **Domain Wall Motion by the Magnonic Spin Seebeck Effect**. *Phys. Rev. Lett.*, **107**:027205, Jul 2011. 81

[80] D. Hinzke, U. Nowak, and D. A. Garanin. **Uniform susceptibility of classical antiferromagnets in one and two dimensions in a magnetic field**. *Euro. Phys. J. B*, **16**:435, 2000. 36, 37

[81] D. Hinzke, U. Nowak, O. N. Mryasov, and R. W. Chantrell. **Orientation and Temperature Dependence of Domain Wall Properties in FePt**. *Appl. Phys. Lett.*, **90**:082507, 2007. 175

[82] J. Hohlfeld, E. Matthias, R. Knorren, and K. H. Bennemann. **Nonequilibrium magnetization dynamics of nickel**. *Phys. Rev. Lett.*, **78**:4861, 1997. 2, 3, 95

[83] J. Hohlfeld, S. S. Wellershoff, J. Gudde, U .Conrad, V. Jahnke, and E. Matthias. **Electron and Lattice Dynamics Following Optical Excitation of Metals**. *Chemical Physics*, **251**:237–258, 2000. 16

[84] J. Hohlfeld, S.-S. Wellershoff, J. Güdde, U. Conrad, V. Jahnke, and E. Matthias. **Electron and lattice dynamics following optical excitation of metals**. *Chem. Phys.*, **251**:237, 2000. 18, 47

[85] Jisang Hong and D. L. Mills. **Spin dependence of the inelastic electron mean free path in Fe and Ni: Explicit calculations and implications**. *Phys. Rev. B*, **62**(9):5589–5600, Sep 2000. 6, 41

[86] W. Hübner and K. H. Bennemann. **Simple theory for spin-lattice relaxation in metallic rare-earth ferromagnets**. *Phys. Rev. B*, **53**(6):3422–3427, Feb 1996. 3, 7, 73, 81, 83

[87] A. Eschenlohr K. Vahaplar T. Kachel N. Pontius-R. Mitzner K. Holldack A. Fhlish F. Radu R. F. L. Evans T. A. Ostler J. Mentink R. W. Chantrell A. Tsukamoto A. Itoh A. Kirilyuk A.V. Kimel I. Radu, C. Stamm and Th. Rasing. **Ultrafast Distinct Spin Dynamics in Multi-component Magnetic Alloys and Heterostructures**. 131

[88] J. Jensen and Allan. R. Mackintosh. *Rare Earth Magnetism: Structures and Excitations*. Clarendon Press, Oxford, 1991. 100

[89] Ganping Ju, Julius Hohlfeld, Bastiaan Bergman, René J. M. van de Veerdonk, Oleg N. Mryasov, Jai-Young Kim, Xiaowei Wu, Dieter Weller, and Bert Koopmans. **Ultrafast Generation of Ferromagnetic Order via a Laser-Induced Phase Transformation in FeRh Thin Films**. *Phys. Rev. Lett.*, **93**:197403, Nov 2004. 9

[90] Ganping Ju, A. V. Nurmikko, R. F. C. Farrow, R. F. Marks, M. J. Carey, and B. A. Gurney. **Ultrafast optical modulation of an exchange biased ferromagnetic/antiferromagnetic bilayer**. *Phys. Rev. B*, **58**:R11857–R11860, Nov 1998. 8

[91] H. Kachkachi and D.A. Garanin. **Magnetic free energy at elevated temperatures and hysteresis of magnetic particles**. *Physica A*, **291**:485–500, 2001. 99, 100

[92] M. I. Kaganov, I. M. Lifshitz, and L. V. Tanatarov. **Relaxation between electrons and the crystalline lattice**. *Sov. Phys. JETP*, **4**:173, 1957. 16, 19, 21, 47

[93] T. Kaneyoshi. **Critical temperatures and the compensation temperatures of disordered and amorphous ferrimagnetic Ising systems**. *Phys. Rev. B*, **33**:7688–7699, Jun 1986. 97, 99

[94] N. Kazantseva, D. Hinzke, R.W. Chantrell, and U. Nowak. **Linear and elliptical magnetization reversal close to the Curie temperature**. *Europhys. Lett.*, **86**:27006, 2009. 62, 65, 73, 91, 95

[95] N. Kazantseva, D. Hinzke, U. Nowak, R. W. Chantrell, U. Atxitia, and O. Chubykalo-Fesenko. **Towards multiscale modelling of magnetic materials: Simulations of FePt**. *Phys. Rev. B*, **77**:184428, 2008. iii, 4, 11, 16, 28, 29, 32, 33, 37, 53, 58, 60, 62, 70, 71, 96, 102, 118

[96] N. Kazantseva, D. Hinzke, U. Nowak, R. W. Chantrell, and O. Chubykalo-Fesenko. **Atomistic models of ultrafast reversal**. *Phys. Stat. Sol.*, **244**:4389, 2007. 4, 11, 27, 37, 38, 45, 62, 143

[97] N. Kazantseva, U. Nowak, R. W. Chantrell, J. Hohlfeld, and A. Rebei. **Slow recovery of the magnetisation after a sub-picosecond heat-pulse**. *Europhys. Lett.*, **81**:27004, 2008. 4, 5, 11, 38, 62, 143

[98] N. Kazantseva, R. Wieser, and U. Nowak. **Transition to Linear Domain Walls in Nanoconstrictions**. *Phys. Rev. Lett.*, **94**:37206, 2005. 29

[99] J. W. Kim, K. D. Lee, J. W. Jeong, and . S. C. Shin. **Ultrafast spin demagnetization by nonthermal electrons of TbFe alloy film**. *Appl. Phys. Lett*, **94**:192506, 2009. 66

[100] A. V. Kimel, A. Kirilyuk, A. Tsvetkov, R. V. Pisarev, and Th. Rasing. **Laser-induced ultrafast spin reorientation in the antiferromagnet** $TmFeO_3$. *Nature*, **429**:850–853, 2004. 9

[101] A. V. Kimel, R. V. Pisarev, J. Hohlfeld, and Th. Rasing. **Ultrafast Quenching of the Antiferromagnetic Order in** $FeBO_3$**: Direct Optical Probing of the Phonon-Magnon Coupling**. *Phys. Rev. Lett.*, **89**:287401, Dec 2002. 2

[102] Andrei Kirilyuk, Alexey V. Kimel, and Theo Rasing. **Ultrafast optical manipulation of magnetic order**. *Rev. Mod. Phys.*, **82**:2731–2784, Sep 2010. 3, 4, 95

[103] C. Kittel. *Introduction to Solid State Physics*. Wiley, New York, 1996. 19

[104] B. Koopmans. **Laser-induced magnetization dynamics**. In B. Hillebrands and K. Ounadjela, editors, *Spin Dynamics in Confined Magnetic Structures II*, page 245. Springer-Verlag, Berlin Heidelberg New York, 2003. 42

[105] B. Koopmans, G. Malinowski, F. Dalla Longa, D. Steiauf, M. Fhnle, T. Roth, M. Cinchetti, and M. Aeschlimann. **Explaining the paradoxical diversity of ultrafast laser-induced demagnetization**. *Nat. Mat.*,

9:259265, 2010. 4, 7, 16, 29, 41, 42, 49, 53, 59, 62, 65, 66, 68, 69, 70, 71, 73, 75, 90, 136

[106] B. Koopmans, J. J. M. Ruigrok, F. Dalla Longa, and W. J. M. de Jonge. **Unifying ultrafast magnetization dynamics**. *Phys. Rev. Lett.*, **95**:267207, 2005. 7, 53, 57

[107] B. Koopmans, M. van Kampen, J. T. Kohlhepp, and W. J. M. de Jonge. **Ultrafast Magneto-Optics in Nickel: Magnetism or Optics?** *Phys. Rev. Lett.*, **85**:844, 2000. 149

[108] J. Kötzler, D. A. Garanin, M. Hartl, and L. Jahn. **Evidence for Critical Fluctuations in Bloch Walls near Their Disordering Temperature**. *Phys. Rev. Lett.*, **71**:177, 1993. 29

[109] Michael Krauss, Tobias Roth, Sabine Alebrand, Daniel Steil, Mirko Cinchetti, Martin Aeschlimann, and Hans Christian Schneider. **Ultrafast demagnetization of ferromagnetic transition metals: The role of the Coulomb interaction**. *Phys. Rev. B*, **80**(18):180407, Nov 2009. 4, 5, 41

[110] J. Kuneš and V. Kamberský. **First-principles investigation of the damping of fast magnetization precession in ferromagnetic** $3d$ **metals**. *Phys. Rev. B*, **65**(21):212411, Jun 2002. 55, 56, 60

[111] D. L. Landau and E. Lifshitz. **On the theory of the dispersion of magnetic permeability in ferromagnetic bodies**. *Phys. Z. Sowjetunion*, **8**:153, 1935. 12, 24

[112] Benjamin Lenk, Gerrit Eilers, Jaroslav Hamrle, and Markus Münzenberg. **Spin-wave population in nickel after femtosecond laser pulse excitation**. *Phys. Rev. B*, **82**:134443, Oct 2010. 144

[113] Yi Li, K. Baberschke, and M. Farle. **Critical spin fluctuations of Ni monolayers at the Curie temperature: A magnetic resonance study in UHV (invited)**. *Journal of Applied Physics*, **69**:4992, 1991. 30

[114] J. Lindner, I. Barsukov, C. Raeder, C. Hassel, O. Posth, R. Meckenstock, P. Landeros, and D. L. Mills. **Two-magnon damping in thin films in case of canted magnetization: Theory versus experiment**. *Phys. Rev. B*, **80**:224421, Dec 2009. 69

[115] M. Lisowski, P. A. Loukakos, A. Melnikov, I. Radu, L. Ungureanu, M. Wolf, and U. Bovensiepen. **Femtosecond Electron and Spin Dynamics in Gd(0001) Studied by Time-Resolved Photoemission and Magneto-optics**. *Phys. Rev. Lett.*, **95**:137402, Sep 2005. 80

[116] A. Lyberatos and R. W. Chantrell. **Thermal Fluctuations in a pair of magnetostatistically coupled particles**. *J. Appl. Phys.*, **73**:6501, 1993. 26

[117] N. Majlis. *The Quantum Theory of Magnetism*. World Scientific, London, 2007. 162

[118] M. Mansuripur. **Mean-Field Analysis of Amorphous Rare Earth-Transition Metal Alloys for Thermomagnetic Recording**. *IEEE Trans. Magn.*, **22**:1, 1986. 97, 98

[119] M. Mansuripur. *The Physical Principles of Magneto-optical Recording*. Cambridge University Press, Cambrige, UK, 1995. 97, 98

[120] R. D. Mattuck and M. W. P. Strandberg. **Spin-Phonon Interaction in Paramagnetic Crystals**. *Phys. Rev.*, **119**:1204–1217, Aug 1960. 81

[121] Alexey Melnikov, Ilya Razdolski, Tim O. Wehling, Evangelos Th. Papaioannou, Vladimir Roddatis, Paul Fumagalli, Oleg Aktsipetrov, Alexander I. Lichtenstein, and Uwe Bovensiepen. **Ultrafast Transport of Laser-Excited Spin-Polarized Carriers in** Au/Fe/MgO(001). *Phys. Rev. Lett.*, **107**:076601, Aug 2011. 5

[122] J. H. Mentink, J. Hellsvik, D. V. Afanasiev, B. A. Ivanov, A. Kirilyuk, A. V. Kimel, O. Eriksson, M. I. Katsnelson, and Th. Rasing. **Ultrafast Spin Dynamics in Multisublattice Magnets**. Jan 2012. 113, 117, 119, 120

[123] K. Miyazaki and K. Seki. **Brownian motion of spins revisited**. *J. Chem. Phys.*, **108**:7052, 1998. 146, 151

[124] O. N. Mryasov, U. Nowak, K. Guslienko, and R. W. Chantrell. **Temperature dependent magnetic properties of FePt: effective spin Hamiltonian model**. *Europhys. Lett.*, **69**:805, 2005. 35

[125] G. M. Müller, M. Djordjevic, G.-X. Miao, A. Gupta, A. V. Ramos, K. Gehrke, V. Moshnyaga, K. Samwer, J. Schmalhorst, A. Thomas, A. Hütten, G. Reiss, J. S. Moodera, and M. Münzenberg. **Spin polarization in half-metals probed by femtosecond spin excitation.** *Nat. Mat.*, **8**:56, 2009. 45, 53

[126] Y. Nakatani, Y. Uesaka, N. Hayashi, and H. Fukushima. **Computer simulation of thermal fluctuation of fine particle magnetization based on Langevin equation**. *J. Magn. Magn. Mat.*, **168**:347, 1997. 26

[127] U. Nowak. *Classical Spin Models*. John Wiley & Sons Ltd., Chichester, 2007. 27

[128] Thomas A. Ostler, Richard F. L. Evans, Roy W. Chantrell, Unai Atxitia, Oksana Chubykalo-Fesenko, Ilie Radu, Radu Abrudan, Florin Radu, Arata Tsukamoto, A. Itoh, Andrei Kirilyuk, Theo Rasing, and Alexey Kimel. **Crystallographically amorphous ferrimagnetic alloys: Comparing a localized atomistic spin model with experiments**. *Phys. Rev. B*, **84**:024407, Jul 2011. 96, 98, 100, 101, 102, 103, 133

[129] R.E. Pawel and E.E. Stansbury. **Specific heat contributions of the ferromagnetic transition in nickel and nickel-copper alloys**. *Journal of Physics and Chemistry of Solids*, **26**(4):757 – 765, 1965. 20

[130] M. Pickel, A. B. Schmidt, F. Giesen, J. Braun, J. Minár, H. Ebert, M. Donath, and M. Weinelt. **Spin-Orbit Hybridization Points in the Face-Centered-Cubic Cobalt Band Structure**. *Phys. Rev. Lett.*, **101**:066402, Aug 2008. 4

[131] D. Pines. *Elementary excitations in Solids*. Westview Press, 1999. 16, 17, 21

[132] M. Plihal, D. L. Mills, and J. Kirschner. **Spin Wave Signature in the Spin Polarized Electron Energy Loss Spectrum of Ultrathin Fe Films: Theory and Experiment**. *Phys. Rev. Lett.*, **82**(12):2579–2582, Mar 1999. 6

[133] I. Radu, G. Woltersdorf, M. Kiessling, A. Melnikov, U. Bovensiepen, J.-U. Thiele, and C. H. Back. **Laser-Induced Magnetisation Dynamics of Lanthanide-Doped Permalloy Thin Films**. *Phys. Rev. Lett.*, **103**:117201, 2009. 57, 70, 156, 157

[134] K. Stamm C. Kachel T. Pontius N. Durr H. A. Ostler T. A. Barker J. Evans R. F. L. Chantrell R. W. Tsukamoto A. Itoh A. Kirilyuk A. Rasing Th. Kimel A. V. Radu, I. Vahaplar. **Transient ferromagnetic-like state mediating ultrafast reversal of antiferromagnetically coupled spins**. *Nature*, **472**:205, 2011. ii, 11, 96, 116, 119, 123, 131, 133, 137, 142

[135] H. Regensburger, R. Vollmer, and J. Kirschner. **Time-resolved magnetization-induced second-harmonic generation from the** Ni(110) **surface**. *Phys. Rev. B*, **61**:14716, 2000. 4

[136] G. S. Rushbrooke, J. G. A. Baker, and P. J. Wood. *Phase Transitions and Critical Phenomena*. Academic Press, New York, 1974. 102

[137] J. M. Sancho, M. San Miguel, S. L. Katz, and J. D. Gunton. **Analytical and numerical studies of multiplicative noise**. *Phys. Rev. A*, **26**:1589–1609, Sep 1982. 144

[138] C. Schieback, D. Hinzke, M. Kläui, U. Nowak, and P. Nielaba. **Temperature dependence of the current-induced domain wall motion from**

a modified Landau-Lifshitz-Bloch equation. *Phys. Rev. B*, **80**:214403, Dec 2009. 81

[139] Frank Schlickeiser. *Computer Simulation of the Dynamics of Ferrimagnets*. Master's thesis, University of Konstanz, 2011. 122, 124, 130

[140] A. B. Schmidt, M. Pickel, M. Donath, P. Buczek, A. Ernst, V. P. Zhukov, P. M. Echenique, L. M. Sandratskii, E. V. Chulkov, and M. Weinelt. **Ultrafast Magnon Generation in an Fe Film on Cu(100)**. *Phys. Rev. Lett.*, **105**:197401, Nov 2010. 4

[141] R. W. Schoenlein, W. Z. Lin, J. G. Fujimoto, and G. L. Eesley. **Femtosecond studies of nonequilibrium electronic processes in metals**. *Phys. Rev. Lett.*, **58**(16):1680–1683, Apr 1987. 47

[142] A. Scholl, L. Baumgarten, R. Jacquemin, and W. Eberhardt. **Ultrafast spin dynamics of ferromagnetic thin films observed by fs spin-resolved two-photon photoemisson**. *Phys. Rev. Lett.*, **79**:5146, 1997. 2, 4, 95

[143] W. Scholz, T. Schrefl, and J. Fidler. **Micromagnetic simulation of thermally activated switching in fine particles**. *J. Magn. Magn. Mat.*, **233**:296, 2001. 26

[144] Jonas Seib and Manfred Fähnle. **Calculation of the Gilbert damping matrix at low scattering rates in Gd**. *Phys. Rev. B*, **82**:064401, Aug 2010. 93

[145] J. C. Slonczewski. **Current-driven excitation of magnetic multilayers**. *J. Magn. Magn. Mat.*, **159**:L1, 1996. 2, 8, 95

[146] Neil Smith. **Comment on "Fluctuation-dissipation considerations and damping models for ferromagnetic materials"**. *Phys. Rev. B*, **74**:026401, Jul 2006. 26

[147] S.Mizukami, H.Abe, D.Watanabe, M.Oogane, Y.Ando, and T.Miyazaki. **Laser-Induced Fast Magnetization Precession and Gilbert Damping for CoCrPt Alloy Thin Films with Perpendicular Magnetic Anisotropy**. *Appl. Phys. Expr.*, **3**:123001, 2010. 7, 39, 68

[148] C. Stamm, T. Kachel, N. Pontius, R. Mitzner, T. Quast, K. Holldack, S. Khan, C. Lupulescu, E. F. Aziz, M. Wietstruk, H. A. Drr, and W. Eberhardt. **Femtosecond modification of electron localization and transfer of angular momentum in nickel**. *Nature Mater.*, **6**:740, 2007. 4, 15

[149] C. D. Stanciu, F. Hansteen, A. V. Kimel, A. Kirilyuk, A. Tsukamoto, A. Itoh, and Th. Rasing. **All-Optical Magnetic Recording with Circularly Polarized Light**. *Phys. Rev. Lett.*, page 047601, 2007. 9, 10, 119

[150] C. D. Stanciu, A. V. Kimel, F. Hansteen, A. Tsukamoto, A. Itoh, A. Kirilyuk, and Th. Rasing. **Ultrafast spin dynamics across compensation points in ferrimagnetic GdFeCo: The role of angular momentum compensation**. *Phys. Rev. B*, **73**:220402(R), 2006. 10, 122, 123, 126, 128, 130

[151] C. D. Stanciu, A. Tsukamoto, A. V. Kimel, F. Hansteen, A. Kirilyuk, A. Itoh, and Th. Rasing. **Subpicosecond Magnetization Reversal across Ferrimagnetic Compensation Points**. *Phys. Rev. Lett.*, **99**:217204, 2007. 10, 126, 128, 129

[152] D. Steiauf and M. Fähnle. **Elliott-Yafet mechanism and the discussion of femtosecond magnetization dynamics**. *Phys. Rev. B*, **79**(14):140401, Apr 2009. 5, 41, 62, 65

[153] J. Stöhr and H.C. Siegmann. *Magnetism*. Springer-Verlag, Berlin, 2006. 2, 4, 15, 144, 149

[154] M. Sultan, U. Atxitia, O. Chubykalo-Fesenko, A. Melnikov, and U. Bovensiepen. **Electron- and phonon-mediated ultrafast magnetization dynamics of Gd(0001)**. *Phys. Rev. B*, **in press**:004400, 2012. 21

[155] M. Sultan, A. Melnikov, and U. Bovensiepen. **Ultra-fast magnetization dynamics of Gd(0001): Bulk vs surface**. *submitted*, 2011. 76

[156] I. Tudosa, C. Stamm, A. B. Kashuba, F. King, H. C. Siegmann, J. Sthr, G. Ju, B. Lu, and D. Weller. **The ultimate speed of magnetic switching in granular recording media**. *Nature*, **428**:831–833, 2004. ii, 2, 95, 149

[157] K. Vahaplar, A. M. Kalashnikova, A.V. Kimel, D. Hinzke, U. Nowak, R. Chantrell, A. Tsukamoto, A. Itoh, A. Kirilyuk, and Th. Rasing. **Ultrafast Path for Optical Magnetization Reversal via a Strongly Nonequilibrium State**. *Phys. Rev. Lett.*, **102**:117201, 2009. ii, iv, 10, 33, 57, 62, 95, 119

[158] M. van Kampen, C. Jozsa, J. T. Kohlhepp, P. LeClair, L. Lagae, W. J. M. de Jonge, and B. Koopmans. **All-Optical Probe of Coherent Spin Waves**. *Phys. Rev. Lett.*, **88**:227201, May 2002. 3, 7, 8, 16

[159] J. H. Van Vleck. **Paramagnetic Relaxation Times for Titanium and Chrome Alum**. *Phys. Rev.*, **57**:426–447, Mar 1940. 81

[160] A. Vaterlaus, T. Beutler, and F. Meier. **Spin-lattice relaxation time of ferromagnetic gadolinium determined with time-resolved spin-polarized photoemission**. *Phys. Rev. Lett.*, **67**:3314–3317, Dec 1991. 3, 6, 73

[161] J. H. Van Vleck. *The theory of electric and magnetic susceptibility.* Universisty Press Oxford, 1932. 159

[162] M. Vomir, L. H. F. Andrade, L. Guidoni, E. Beaurepaire, and J.-Y. Bigot. **Real Space Trajectory of the Ultrafast Magnetization Dynamics in Ferromagnetic Metals**. *Phys. Rev. Lett.*, **94**:237601, Jun 2005. 2, 3, 29

[163] Yu P Kalmykov W T Coffey and J T Waldron. *The Langevin equation.* World Scientific, Singapore, 2004. 26, 143

[164] J. Walowski. Master's thesis, University of Gottingen, 2009. 40

[165] J. Walowski, M. Djordjevic, M. D. Kauffman, B. Lenk, C. Hamann, J. McCord, and M. Münzenberg. **Intrinsic and non-local Gilbert damping in polycrystalline nickel studied by Ti : sapphire laser fs spectroscopy**. *J. Phys. D: Appl. Phys.*, **41**:164016, 2008. 7, 8, 39, 68

[166] J. Walowski, G. Müller, M. Djordjevic, M. Münzenberg, M. Kläui, C. A. F. Vaz, and J. A. C. Bland. **Energy Equilibration Processes of Electrons, Magnons, and Phonons at the Femtosecond Time Scale**. *Phys. Rev. Lett.*, **101**(23):237401, Dec 2008. 4, 41, 51, 55, 56, 57, 70, 156, 157

[167] J. Wang, Ł. Cywinski, C. Sun, J. Kono, H. Munekata, and L. J. Sham. **Femtosecond demagnetization and hot-hole relaxation in ferromagnetic $\mathbf{Ga_{1-x}Mn_xAs}$**. *Phys. Rev. B*, **77**:235308, Jun 2008. 2

[168] Roald K. Wangsness. **Sublattice Effects in Magnetic Resonance**. *Phys. Rev.*, **91**:1085–1091, Sep 1953. 9, 122, 126

[169] Marko Wietstruk, Alexey Melnikov, Christian Stamm, Torsten Kachel, Niko Pontius, Muhammad Sultan, Cornelius Gahl, Martin Weinelt, Hermann A. Dürr, and Uwe Bovensiepen. **Hot-Electron-Driven Enhancement of Spin-Lattice Coupling in Gd and Tb $4f$ Ferromagnets Observed by Femtosecond X-Ray Magnetic Circular Dichroism**. *Phys. Rev. Lett.*, **106**(12):127401, Mar 2011. iii, 6, 7, 66, 73, 75, 76, 91

[170] G. Woltersdorf, M. Kiessling, G. Meyer, J.-U. Thiele, and C. H. Back. **Damping by Slow Relaxing Rare Earth Impurities in $Ni_{80}Fe_{20}$**. *Phys. Rev. Lett.*, **102**(25):257602, Jun 2009. 57, 69, 70, 156, 157

[171] Y. Yafet. **g Factors and Spin-Lattice Relaxation of Conduction Electrons**. **14**:1 – 98, 1963. 5

[172] C. J. Yeomans. *Statistical Mechanics of Phase Transitions*. Oxford University Press, Oxford, UK, 1995. 118

[173] G. P. Zhang and W. Hübner. **Laser-Induced Ultrafast Demagnetization in Ferromagnetic Metals**. *Phys. Rev. Lett.*, **85**(14):3025–3028. 2, 11, 15

List of Publications of U. Atxitia

[1] **U. Atxitia**, O. Chubykalo-Fesenko, N. Kazantseva, D. Hinzke, U. Nowak and R. W. Chantrell.
Micromagnetic modelling of laser-induced magnetisation dynamics using the Landau-Lifshitz-Bloch equation."
Appl. Phys. Lett. **91**, 232507 (2007)

[2] N. Kazantseva, D. Hinzke, U. Nowak, R. W. Chantrell, **U. Atxitia**, O. Chubykalo-Fesenko.
"*Towards multiscale modelling of magnetic materials: Simulations of FePt*"
Phys. Rev. B, **77**, 184428 (2008).

[3] **U. Atxitia**, O. Chubykalo-Fesenko , U. Nowak, R. W. Chantrell and A.Rebei.
"*Ultrafast Spin Dynamics: The Effect of Colored Noise* "
Phys. Rev. Lett. **102**, 057203 (2009).

[4] **U. Atxitia**, O. Chubykalo-Fesenko, J. Walowski, A. Mann and M. Munzenberg
"*Evidence for thermal mechanisms in laser-induced femtosecond spin dynamics* "
Phys. Rev. B, **81** , 174401 (2010).

[5] Yu. P. Kalmykov, W. T. Coffey, **U. Atxitia**, O. Chubykalo-Fesenko, P-M. Djardin and R. W. Chantrell
"*Damping dependence of the reversal time of the magnetization of single-domain ferromagnetic particles for the Nel-Brown model: Langevin dynamics simulations versus analytic results* "
Phys. Rev. B, **82** , 024412 (2010).

[6] **U. Atxitia**, D. Hinzke, O. Chubykalo-Fesenko, U. Nowak, H. Kachkachi, O. N. Mryasov, R. F. Evans and R. W. Chantrell
"*Multiscale modeling of magnetic materials: Temperature dependence of exchange stiffness* "
Phys. Rev. B, **82** , 134440 (2010).

[7] T. A. Ostler, R. F. L. Evans, R. W. Chantrell, **U. Atxitia**, O. Chubykalo-Fesenko, I. Radu, R. Abrudan, F. Radu, A. Tsukamoto, A. Itoh, A. Kirilyuk, Th. Rasing and A. Kimel
"*Crystallographically Amorphous Ferrimagnetic Alloys: Comparing a Localized Atomistic Spin Model with Experiments* "
Phys. Rev. B, **84** , 024407 (2011).

[8] **U. Atxitia**, and O. Chubykalo-Fesenko.
"*Ultra-fast magnetisation rates within the Landau-Lifshitz-Bloch model* "
Phys. Rev. B, **84** , 144414 (2011).

[9] R. F. L. Evans, D. Hinzke,**U. Atxitia**, U. Nowak, R. W. Chantrell, and O. Chubykalo-Fesenko.
"*The stochastic form of the Landau-Lifshitz-Bloch equation.*."
Physical Review B 84, 014433 (2012)

[10] T. A. Ostler , J. Barker, R. F. L. Evans, R. Chantrell, **U. Atxitia**, O. Chubykalo-Fesenko, S. El Moussaoui, L. Le Guyader, E. Mengotti, L. J. Heyderman, F. Nolting, A. Tsukamoto, A. Itoh, D. Afanasiev, B. A. Ivanov, A. M. Kalashnikova, K. Vahaplar, J. Mentink, A. Kirilyuk, Th. Rasing and A. V. Kimel
"*Ultrafast Heating as a Sufficient Stimulus for Magnetization Reversal in a Ferrimagnet.*"
Nature Communications 3, 666 (2012)

[11] M. Sultan, **U. Atxitia**, O. Chubykalo-Fesenko , A. Melnikov, and U. Bovensiepen.
"*Electron- and phonon-mediated ultrafast magnetization dynamics of Gd(0001).*"
Phys. Rev. B, in press

[12] R. Bastardis, **U. Atxitia**, O. Chubykalo-Fesenko, and H. Kachkachi.
"*Unified decoupling scheme for exchange and anisotropy contributions and spectral properties of anisotropic spin systems.*"
submitted to Phys. Rev. B

In preparation:

[13] F. Schlickeiser, **U. Atxitia**, S. Wienholdt, D. Hinzke, O. Chubykalo-Fesenko, and U. Nowak
"*Temperature dependence of normal modes of ferrimagnets.*"
in preparation

[14] **U. Atxitia**, T. Ostler, J. Barker, R. F. L. Evans, R. W. Chantrell, and O. Chubykalo-Fesenko
"*Ultrafast dynamical path for the switching of a ferrimagnet after femtosecond heating.*"
in preparation

[15] **U. Atxitia**, P. Nieves-Cordones, and O. Chubykalo-Fesenko
"*The Landau-Lifshitz-Bloch equation for ferrimagnetic materials.*"
in preparation

Acknowledgements

I would like to acknowledge ....